Universidade de Aveiro Departamento de Engenharia Cerâmica e do Vidro
2008

Cristina Maria da Silva Fernandes

A pulverização catódica na produção de compósitos de carboneto de tungsténio

Universidade de Aveiro Departamento de Engenharia Cerâmica e do Vidro
2008

Cristina Maria da Silva Fernandes

Sputtering on the production of tungsten carbide based composites

tese apresentada à Universidade de Aveiro para cumprimento dos requisitos necessários à obtenção do grau de Doutor em Ciência e Engenharia de Materiais, realizada sob a orientação científica da Doutora Ana Maria de Oliveira e Rocha Senos, Professora Auxiliar do Departamento de Engenharia Cerâmica e do Vidro da Universidade de Aveiro.

Apoio financeiro da FCT e do FSE no âmbito do III Quadro Comunitário de Apoio.

Dedico este trabalho à minha filha Catarina pelo tempo que a privei da minha presença, ao meu marido pelo incansável apoio e aos meus pais pelo seu esforço e dedicação durante toda a minha formação.

o júri

presidente

Prof. Dr. Jorge Carvalho Arroteia
professor catedrático do Departamento de Ciências da Educação da Universidade de Aveiro

Prof. Dr. José Manuel Torralba Castelló
professor catedrático da Escola Politécnica Superior do Departamento de Ciência e Engenharia de Materiais da Universidade Carlos III de Madrid

Prof. Dr. Rui Ramos Ferreira e Silva
professor associado do Departamento de Eng. Cerâmica e do Vidro da Universidade de Aveiro

Prof. Dr.ª Maria Teresa Freire Vieira
professora catedrática do Departamento de Engenharia Mecânica da Faculdade de Ciências e Tecnologia da Universidade de Coimbra

Doutor Fernando de Almeida Costa Oliveira
investigador principal do Departamento de Materiais e Tecnologias de Produção do Instituto Nacional de Engenharia, Tecnologia e Inovação (INETI)

Prof. Dr.ª Ana Maria de Oliveira e Rocha Senos
professora auxiliar do Departamento de Eng. Cerâmica e do Vidro da Universidade de Aveiro

agradecimentos

O presente trabalho de investigação envolveu um número significativo de instituições e pessoas que directamente ou indirectamente contribuíram para a obtenção desta tese.
Começo desta forma por agradecer à Fundação para a Ciência e a Tecnologia como entidade financiadora de uma bolsa de doutoramento, concedida durante a condição de aluna de pós-graduação. Seguidamente, expresso o meu agradecimento à Universidade de Aveiro, como instituição de acolhimento facultando todos os meios físicos disponíveis para a realização do trabalho de investigação. Finalmente, a última instituição a que presto o meu grato agradecimento é ao Departamento de Engenharia Mecânica, da Universidade de Coimbra pela parceria na realização de uma parte da investigação.

Agradeço de forma muito especial à Doutora Ana Senos, pela sua orientação, incentivo, apoio e confiança concedidos durante toda a minha pós-graduação.
À Doutora Teresa Vieira agradeço sinceramente a forma como me recebeu na sua instituição facultando todos os meios técnicos de análise. Agradeço também a sua orientação e sugestões durante a realização dos artigos científicos. Ao Doutor Valdemar Fernandes agradeço a seu contributo na caracterização mecânica das amostras.

Por todas as análises efectuadas no decurso do trabalho, agradeço a disponibilidade dispensada pelos técnicos do Departamento de Engenharia Cerâmica e do Vidro, da Universidade de Aveiro e também de algumas pessoas do departamento de Engenharia Mecânica da Universidade de Coimbra, nomeadamente à Doutora Paula Piedade e à Eng.ª Mariana Matos.

Aos meus colegas do departamento de Engenharia Cerâmica e do Vidro, especialmente aos do laboratório, particularmente à Catarina, agradeço a amizade, apoio e incentivo manifestados durante este período.

Finalmente, a minha sincera gratidão a todas as pessoas ligadas a mim afectivamente, especialmente ao meu marido, pelo seu constante apoio e estímulo durante este percurso.

palavras-chave

carboneto de tungsténio, aço inoxidável, metal duro, pulverização catódica, revestimentos, microestrutura, propriedades mecânicas

resumo

O principal objectivo deste trabalho é estudar a viabilidade do revestimento de partículas de carboneto de tungsténio (WC), como etapa alternativa à mistura convencional de componentes. Para tal, revestiram-se pós de WC com aço inoxidável 304 (AISI), por uma técnica de deposição física em fase de vapor, denominada pulverização catódica. O outro objectivo deste trabalho incide na investigação das potencialidades das ligas de Fe/Cr/Ni como ligantes nos compósitos à base de WC.

Para estudar a viabilidade da técnica de deposição como alternativa à mistura de componentes, depositaram-se quantidades variáveis de aço inoxidável (entre 1 e 10%) nas partículas de pó de WC. Alternativamente, e para efeitos de comparação, prepararam-se composições similares por mistura convencional.

Os resultados da caracterização de pós revestidos foram motivadores, uma vez que indicaram que as partículas de WC possuíam revestimentos nanocristalinos bastante uniformes e que todos os elementos constituintes do aço foram depositados nas proporções existentes no alvo. Estes pós apresentam ainda boa escoabilidade e prensabilidade, uma resistência à oxidação acrescida e elevada estabilidade em soluções aquosas a pH ácido e neutro.

A investigação do aço inoxidável como ligante de sinterização mostrou que os elementos constituintes do aço são eficazes na promoção da densificação dos compactos à base de WC. Os pós revestidos apresentaram uma sinterabilidade e reactividade superiores às das misturas convencionais. Atingiram-se valores superiores de densificação nos pós revestidos, sobretudo com as perdas de peso controladas através do ciclo térmico ou atmosfera de sinterização. A cinética de formação de fases, designadamente de M_6C, é mais rápida nestes pós, mas a quantidade formada pode ser reduzida ou mesmo eliminada, aumentando o teor de níquel no ligante e com pequenas adições de carbono.

Os resultados da caracterização mecânica de compósitos preparados com os pós revestidos evidenciaram um bom compromisso entre a tenacidade e dureza, superior ao observado em amostras preparadas convencionalmente. Por outro lado, os ligantes à base de aço inoxidável mostraram uma relação de tenacidade versus dureza superior à existente em dados publicados para compósitos de Co. A presença de M_6C aumentou a dureza dos compósitos, sem degradar a sua tenacidade, enquanto que o aumento do teor de níquel reduziu substancialmente a dureza do material.

keywords

Tungsten carbide, stainless steel, hardmetal, sputtering, coatings, microstructure, mechanical properties

abstract

The main objective of this work is to study the feasibility of the tungsten carbide (WC) particle covering as an alternative to the conventional mixture of components. For such purpose, WC powders were coated with stainless steel 304 (AISI) by a physical vapour deposition technique, called sputtering. The other objective of this work is to study the potentiality of Fe/Cr/Ni alloys as binders in WC based composites.

To study the viability of the deposition technique as an alternative to the mixture process, different amounts of stainless steel (between 1 and 10 wt.%) were deposited on WC powder particles. Alternatively, similar compositions have been prepared by conventional mixture, for comparison. The results of the characterization of coated powders are very promising, since they indicated that the WC particles have very uniform nanocrystalline coatings and that all the elements were deposited in the same proportions of the target. These powders present good flowability and prensability, an increased oxidation resistance and high stability in aqueous solutions, at acid and neutral pH values.

The study of the stainless steel as a sintering binder demonstrated that the steel constituent elements are efficient in the promotion of densification of the WC based composites. Coated powders present higher reactivity and sinterability than conventional mixtures, especially when weight losses are controlled through the thermal cycle or sintering atmosphere. The kinetic of phase formation, namely M_6C, is faster in these powders, but the amount formed can be reduced, or eliminated, by increasing the Ni amount in the binder and by small carbon additions.

The results of the mechanical characterization of composites prepared with coated powders evidenced a good compromise between hardness and toughness, higher than the one observed in conventionally prepared composites. On the other hand, the composites with stainless steel based binders show superior values of toughness versus hardness than the ones reported in literature for composites with cobalt. The presence of M_6C increases the composites hardness, without degrading its toughness, while the increase of Ni substantially reduces the hardness of the material.

Abbreviations List

BCC – Body centred cubic

BET – Brunauer-Emmett-Teller

CS – Compressive Strength

CVD – Chemical Vapour Deposition

DIL – Dilatometry

DSC – Differential Scanning Calorimetry

EDS – Energy Dispersive Spectroscopy

EGA – Mass Spectroscopy Gas Analysis

EPMA – Electron Probe Microanalysis

FCC – Face centred cubic

HCP – Hexagonal compact

HIP – Hot Isostatic Pressing

HM - Hardmetals

LPS – Liquid Phase Sintering

MVHP – Monoaxial Vacuum Hot Pressing

PAS – Plasma Activated Sintering

PIM – Powder Injection Molding

P^2C – Plasma Pressure Compaction

PVD – Physical Vapour Deposition

SEM – Scanning Electron Microscopy

SLS – Selective Laser Sintering

SPS – Spark Plasma Sintering

TG – Termogravimetry

TRS – Transverse Rupture Strength

XRD – X-ray Diffraction

Symbols List

$\dot{\varepsilon}$- Shrinkage rate

ε -Plastic strain

ε(HCP) – Martensitic phase

γ - Surface tension

γ(FCC) – Austenitic phase

λ_m – Mean free path

ν - Poisson's ratio

σ_y - Yield stress

ξ - Zeta potential

Ω - Average atomic volume

a – Indent half diagonal

C – Contiguity

c –Median crack length

d – Average grain size

D - Density

Dv – Volume diffusion coefficient

E – Young's Modulus

G – Grain size

H - Hardness

Hv – Vickers Hardness

H^0 - Entalpy

K_{IC} – Fracture toughness

$\overline{l}$ - Arithmetic mean linear intercept

L – Length of test line

<L> - Mean centre-to centre distance

l – Palmqvist crack length

n - Hardening coefficient

N_L – Average number of intercepts per unit length of test line

P – Load

S –Area of contact per unit volume

S_V – Specific area per unit volume

T – Temperature

V – Volume fraction

<x> - Mean radius

Index

Introduction

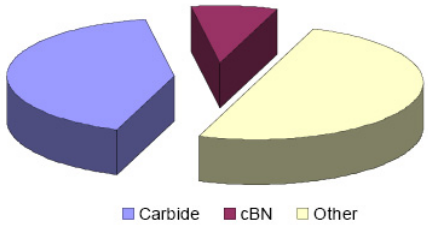

Cutting Tool Market

Worldwide market for machine tool metal cutting tools (estimated 2003 data):

- Total market size: $ 12 billion
- Carbide tools: $ 5 billion
- cBN tools: $ 1 billion & growing

The history of tungsten goes back to the end of the Middle Ages. The miners in the Erz Mountains of Saxony noticed that certain ores disturbed the reduction of cassiterite and induced slagging. "They tear away the tin and devour it like a wolf devours a sheep", a contemporary wrote in the symbolic language of the Middle Ages. The miners gave these annoying ore German nicknames like "wolfart", "wolfrahm" or "wolframite".

In 1758 the Swedish chemist A. Cronstedt discovered an unusually heavy mineral that he called "tungsten", which is Swedish for heavy stone. Tungsten is usually found in the form of tungstates in nature. The most important minerals are wolframite ($(Fe, Mn)WO_4$) and scheelite ($CaWO_4$) [1]. China has the world's largest deposits of tungsten, followed by Canada, United States, Australia, Korea, Turkey, Bolivia and Burma. The largest European reserves are in Portugal, France, Austria, Sweden and southern England; smaller deposits are found in the Erz Mountains, near Reichstein and also Baden-Württemberg, Germany. In World War II, the tungsten played a role of enormous importance in the diplomatical relations. Portugal, as the main source of this element in the Europe, was placed under great pressure of both sides in the dispute, since this element was essential for the wolfram production as a material in the armament industry.

The discovery of tungsten is credited to the brothers José Elhuyar and Fausto Elhuyar in Spain during 1783. They had found an acid in wolframite that was similar to tungstic acid and by the reduction of that acid with vegetal coal they isolate the tungsten. In 1898, P. Williams, working at Moissan's laboratory at the School of Pharmacy at the University of Paris, treated a mixture of tungstic acid, pretroleum coke and iron in a carbon crucible for one hour [1,2]. The melted button was chemically treated and a new tungsten carbide (WC) was isolated. The first sintered tungsten carbide was produced in 1914 for use in drawing dies and rock drills [3].

The year 1923 represents an important milestone in the tungsten chronology (see Fig. 1). It marks the invention of the first hardmetal tool by Karl Schröter and the corresponding application for a patent granted by Krupp in German in 1926. The two inventions claimed by the patent were [3]:

- A unique hardmetal alloy composition, namely the combination of the very hard tungsten carbide, WC, with small amounts of a metal of the iron group (Fe, Ni and Co);

- The manufacture of the hardmetal alloys by the application of the process of Powder Metallurgy (PM), namely the pressing and sintering of mixed powders of tungsten carbide and binder metal.

The name «WIDIA-N» (WC-6%Co) was choose by Krupp for this hardmetal, a trademark that was created from the German words "Wie" and "Diamond", meaning "like a diamond" [1,3]. Other proprietary names known are Wimet and Ardoloy (Great Britain) and Carboloy (USA).

The next developments arose only two years later with the discovery by Schwarzkopf that solid solutions of carbides, particularly TiC, TaC, NbC and Mo_2C, are superior to the individual carbide WC (see Fig. 1). An important advance in the development of hard metals happens in the late 1960s and early 1970s with the application of coatings like TiC, TiN, TiCN and Al_2O_3 which are extremely hard and thus very abrasion resistant [3].

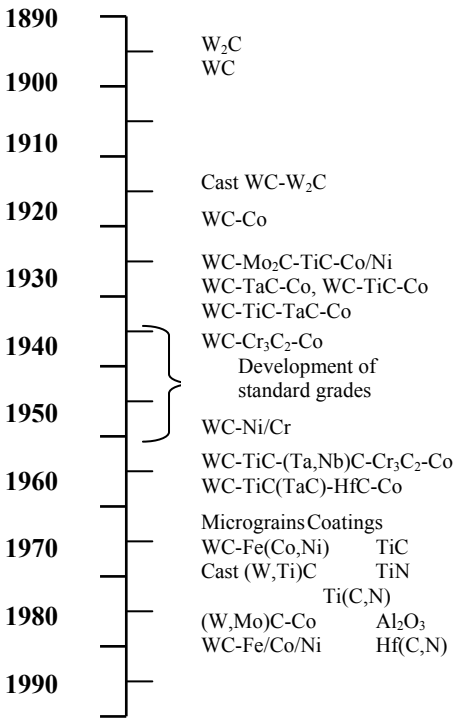

Fig. 1. Historical development of the materials for cutting tools during the last century [1].

The development of metal cutting tools, which are suitable to cut a variety of materials such as gray cast iron, ductile nodular iron, austenitic stainless steel, nickel-base alloys, titanium alloys, aluminium, free-machining steels, plain carbon steels, alloy steels, and martensitic and ferrite stainless steels, has been very rapid over the last four decades,

having been greatly stimulated by much improved design and manufacturing techniques (Fig. 1) [2]. However, the development of new coatings and improved design are only one side of the coin. Continuous improvement of intermediates and manufacturing techniques led to improve the performance of hardmetals and opened new areas of applications. Nowadays, almost 50% of the total production of cemented carbides is used for non-metal cutting applications such as drill bits and components for mining, oil and gas drilling, transportation and construction, metalforming, structural and fluid-handling components, and forestry tools [4]. New applications are constantly being identified for carbides, largely because of their excellent combinations of abrasion resistance, mechanical impact strength, compressive strength, high elastic modulus, thermal shock resistance and corrosion resistance.

Althought other metal carbides, such as TiC, are also used in cutting tools, around 95% of all cemented carbide cutting tools are tungsten carbide-based [2]. In 2005, 60% of metallic tungsten produced went into WC cemented carbides, only 25% went into steels and superalloys, lamp filaments, heating element, with most of the remainder used in mill products [2,5]. In all these applications, there has been a continuous expansion in the consumption of cemented carbide from an annual world total of 10 tons in 1930; to 100 tons around 1935; 1 000 tons in the early 1940's; through 10 000 tons in the early 1960's and up to nearly 30 000 tons at present [6].

Annual production of tungsten for use in tungsten carbide worldwide was about 25.000 metric tons in 1991/92. Nowadays the world wide cemented carbide industry is estimated to be more than 10 billion € [7].

Future developments in the field of hard materials are mainly related with: the raw materials supply and its scarcity resulting in high prices owing to the main ore deposits being in areas less accessible to the "industrial world", economic factors, the general objective to save energy and with the increasing demand to have special materials with defined and optimized properties. Besides that, chronic inhalation of hard metal particles can produce an interstitial lung disease (hard metal disease). Recent studies have demonstrated that this disorder can be explained by an interaction between cobalt metal (Co) and tungsten carbide (WC) particles, which represent the main constituents of hard metal [8]. The inhalation effects of both particles (WC-Co) are more severe than those

induced by Co metal particles alone, while WC particles could be considered as innocuous [8].

The actual investigation on WC cemented carbides could be oriented in different directions, like:

1. the development of a new material with superior properties;
2. the processing improvement of current materials;
3. the development of new processing methods;
4. the modification of the existing materials with additions of new elements.

The work developed and presented in this thesis was focused on the two last scopes. The replacement of the traditional cobalt binder in WC cemented carbides by a new binder material, stainless steels based and the use of a new processing method for composite powders preparation were investigated.

The binder material used as coating was a stainless steel AISI 304. This steel belongs to the group of the austenitic stainless steel, which is essentially a ternary alloy of iron-chromium-nickel. The austenitic definition for these alloys is related to the austenitic structure (FCC – face centred cubic) that remains at normal temperatures of thermal treatments. This structure is in fact known for having better properties than the ferritic structure (BCC – body centred cubic), in particular as regards resistance to corrosion, and for not being magnetic. The modification of the binder composition through the increase of the nickel content was also investigated. The increase of nickel reduces the carbon necessary to keep the alloy in the region free of second phases, like carbon and η-phase [9,10].

The addition of the binder to WC was performed through a sputtering technique, here innovatively used to coat powders particles, i.e., to coat WC powder particles with the binder material.

The main objectives of the present work is the investigation of the sputtering technique in the preparation of WC composite powders, applied to a very few explored system of WC-stainless steel. For such purpose the coated powders have been first characterized in order to evaluate the morphology and structure of the coating layer, the behaviour in dry and humid atmospheres and the flowability. The thermal performance of the coated powders during the sintering process and the comparison with composites conventionally

prepared constituted the next step. The influence of the coating nanostructure in the thermal reactivity of the system was also evaluated. Finally, the mechanical properties have been investigated.

The dissertation is organized according to the following scheme. The current section (Introduction) provides a brief introduction into the research topic and a statement of the motivation and objectives of the research. In Chapter I, a theoretical background of the research area is provided through a survey of the literature on tungsten carbide cemented carbides. The details of the experimental procedures performed in this work can be found in Chapter II. The results and discussion are divided in three chapters, which are formed by papers already published or submitted during this investigation. Chapter III is concerned with the coated powder characterization and is constituted by 3 papers. In Chapter IV, sintering and reactivity of coated powders is discussed and compared with conventional mixtures (3 papers). Chapter V, formed by two papers, is related with the mechanical characterization. The dissertation ends with Chapter VI, which contains the conclusions on the sputter deposition of tungsten carbide with Fe/Ni/Cr binders.

References

[1] Pastor H. 1996: Centenaire de la découverte du carbure de tungstène par Henri moissan; historique du développement de ce matériau. La Revue de Métallurgie-CIT/Science et Génie des Matériaux 1997: 1537-1552.

[2] Yao Z, Stiglich JJ, Sudarshan TS. Nano-grained tungsten carbide-cobalt (WC/Co). Materials Modification 1999: 1-27.

[3] Cornwall RG, German RM WC-Co enjoys proud history and bright future. Metall Powder Report J-A 1998; 53 (7-8): 32-33.

[4] Santhanam AT, Tierney P, Hunt JL. Cemented Carbides. In *ASM Handbook*. Edited by ASM Int. 1992: 588-592.

[5] PM takes pole position in tungsten heavy alloy production. Metal Powder 2005.

[6] Itia - Cemented Carbides. Information on http://www.itia.org.uk 2008.

[7] Cornwall RG, German RM. Think bigger! the future is bright for MIM. Metal Powder Report 2004; 59(11): 8-11.

[8] Lison D, Lauwerys R. The interaction of cobalt metal with different carbides and other mineral particles on mouse peritoneal macrophages. Toxic.in Vitro 1995; 9(3): 341-347.

[9] Meredith B, Milner DR. Densification Mechanisms in the Tungsten Carbide-Cobalt system. Powder Metallurgy 1976; 1: 38-45.

[10] Upadhyaya GS, Bhaumik SK. Sintering of submicron WC-10 wt.% Co hard metals containing nickel and iron. Materials Science and Engineering A-(Structural Materials Properties Microstructure and Processing) 1988; A105-106: 249-256.

Chapter I

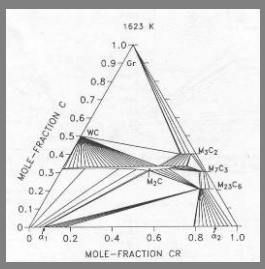

Literature Review

"Mister Tungsten" is the nickname given to Hermann C. Starck due to his worldwide reputation as an expert for tungsten raw materials.

German, 1956

1.1. Tungsten Carbide

1.1.1. General Characteristics

Refractory carbides are useful materials with numerous industrial applications and a promising future, in addition to being materials of great interest to the scientific community. Although most of their applications are recent, the refractory carbides have been known for over one hundred years, they are hard and wear resistant, have high melting points, and are chemically inert at low temperatures. In a relatively short time, they have become major industrial materials with numerous applications such as cutting and grinding tools, bearings, textile-machinery components, oxidation-resistant gas burners, and many others.

The term *refractory* means a material with a high melting point, normally greater than 1800 ºC, and with a high degree of chemical stability [1]. The element carbon forms compounds with most other elements (i.e., CO_2, CCl_4) but, by convention, the term *carbide* is only applied to those compounds formed by carbon and other elements of lower or about equal electronegativity [1]. Three general and interrelated atomic characteristics play an essential part in the formation of carbides, i.e. [1]:

a. the difference in electronegativity between carbon and the other element;
b. the difference in size of the respective atoms;
c. the bonding characteristics of these atoms.

The carbides, as defined above, can be classified in four general categories which are commonly identified as [1]:

a) *Interstitial carbides* (formed by the elements of Box A of Fig. 1.1) – the difference in electronegativity between the two elements of the interstitial carbides is large. The carbon atom has a much smaller size than the other atom, allowing it to nest in the interstices of the lattice (hence the name intersticial). The bonding is partly covalent and ionic, but mostly metallic.
b) *Covalent carbides* (formed by the elements of Box B of Fig. 1.1) – the difference in electronegativity between the two elements of the covalent carbides is small. The carbon atom is only slightly smaller than the other atom and the bonding is essentially covalent.

c) *Intermediate carbides* (formed by the transition metals such as manganese, iron, cobalt, and nickel, as well as chromium) – their atomic radii are too small to accommodate the carbon atom in interstitial positions without severe distortion of the lattice. These carbides are not generally chemically stable.

d) *Salt-like carbides* (formed by the elements of Group 1, 2 and 3 of the Periodic Table) – these elements have an electronegativity difference of about two or more, which corresponds to an atomic bond that is at least 50% ionic. These compounds have the characteristics of a salt, that is, fixed composition, generally transparent to optical radiation and good electrical insulators.

1																
H 2.1	***2***											***13***	***14***	***15***	***16***	***17***
											Box B					
Li 1.9	**Be** 1.5	***3***	***4***	***5***	***6***	***7***	***8***	***9***	***10***	***11***	***12***	**B** 2.0	**C** 2.5	**N** 3.0	**O** 3.5	**F** 4.0
Na 0.9	**Mg** 1.2			**Box A**								**Al** 1.5	**Si** 1.8	**P** 2.1	**S** 2.5	**Cl** 3.0
K 0.9	**Ca** 1.0	**Sc** 1.3	**Ti** 1.5	**V** 1.6	**Cr** 1.6	**Mn** 1.5	**Fe** 1.8	**Co** 1.8	**Ni** 1.8	**Cu** 1.0	**Zn** 1.6	**Ga** 1.6	**Ge** 1.8	**As** 2.0	**Se** 2.4	**Br** 2.8
Rb 0.8	**Sr** 1.0	**Y** 1.2	**Zr** 1.4	**Nb** 1.6	**Mo** 1.8	**Tc** 1.9	**Ru** 2.2	**Rh** 2.2	**Pd** 2.2	**Ag** 1.9	**Cd** 1.7	**In** 1.7	**Sn** 1.8	**Sb** 1.9	**Te** 2.1	**I** 2.5
Cs 0.7	**Ba** 0.9	**La** 1.1	**Hf** 1.3	**Ta** 1.5	**W** 1.7	**Re** 1.9	**Os** 2.2	**Ir** 2.2	**Pt** 2.2	**Au** 2.4	**Hg** 1.9	**Tl** 1.8	**Pb** 1.8	**Bi** 1.9	**Po** 2.0	**At** 2.2

Fig. 1.1. Periodic table of the elements showing their electronegativities. The elements in Box A form interstitial carbides and in Box B form covalent carbides.

Hägg [1] observed that the metals of the nine early-transition elements (Box A in Fig. 1.1) fit the criteria for size and site availability and form intersticial carbides, inside this the elements of Group 6 (Cr, Mo, W) earn special attention. These three carbide systems have similar atomic bonding, composition, and crystallography and their properties and characteristics are also similar. These types of carbides, particularly tungsten carbide and chromium carbide, are important industrial materials due to their properties. The structural characteristics of these carbides can be summarized as follows [1]:

- they have several compositions, i.e.

- $Cr_{23}C_6$ Mo_2C W_2C
- Cr_7C_3 Mo_3C_2 WC
- Cr_3C_2 MoC_{1-x}

- they have two major crystalline structures: hexagonal and orthorhombic;
- the carbon atoms in MoC_{1-x} and WC occupy the more spacious trigonal prismatic sites (hexagonal structure);
- the metal-to-metal bonds are strong and the metal-to-carbon bonds are weak;
- high melting points, above 1800 ºC, and good chemical resistance;
- good thermal conductors, due to their metallic character;
- relatively low thermal expansion coefficient which varies with temperature.

1.1.2. **P**roduction of **T**ungsten **C**arbide

Tungsten carbide composites are the aim of this thesis, so a special attention will be focused on the processing and main properties of this carbide. The first commercial tungsten carbide products were melted cast wire-drawing dies. Unfortunately, the cast of pure WC is quite impractical because the stoichiometric compound WC, with 6.13 wt.% carbon, does not melt congruently; it decomposes to a brittle mixture of W_2C, WC and graphite upon cooling. However, at lower carbon contents, mixtures of WC and W_2C are formed on cooling, which melt at a relatively moderate temperature, around 2750 ºC, and result in a cast product which is very hard, although by nature quite brittle, but nevertheless usable for some applications, such as dies [2].

Tungsten carbide finds large application in powder form to be manufactured by powder metallurgy process. There are two methods by which tungsten carbide powders are produced from the tungsten-bearing ores [3]. Traditionally, tungsten ore is chemically processed to ammonium paratungstate and tungsten oxides [4]. These compounds are then hydrogen-reduced to tungsten metal powder. The fine tungsten powders are blended with carbon, such as lamp black or graphite and heated in hydrogen or vacuum atmosphere between 1400 and 2000 ºC to produce tungsten carbide particles with sizes varying from 0.5 to 30 μm [1]. Each particle is composed of numerous tungsten carbide crystals. Small amounts (0.25 to 3.0 wt.%) of vanadium, chromium or tantalum are sometimes added to

tungsten and carbon powders before carburization to produce very fine (<1 μm) WC powders [5].

In a more recently developed and patented process, tungsten carbide is produced in the form of single crystals through the direct reduction of tungsten ore (sheelite). The ore is mixed with iron oxide, aluminium, carbon and calcium carbide. A high-temperature exothermic reaction ($2Al + 3FeO \leftrightarrow Al_2O_3 + 3Fe$) at about 2500 ºC produces a molten mass that, when cooled, consists of tungsten carbide crystals dispersed in iron and a slag containing impurities [4]. The crystalline WC is then chemically separated from the iron matrix [5]. Other tungsten carbide synthesis methods have been explored, for example ball milling of tungsten and activated carbon powders [6]. However, the production of WC itself during milling results in enhanced iron contamination from the steel mill and balls on extended milling.

1.1.3. **P**roperties and **S**tructure

The monocarbide, WC, is formed by a simple hexagonal crystal structure where the metal-atom layers are stacked directly over one another forming a sequence of layers *AA* or *BB* [1,7]. The structure has two atoms per unit cell and a c/a ratio of 0.976, as presented in Table 1.1 [1]. These structures are not close-packed, not forming octahedral sites, and the available interstitial sites are trigonal prisms as shown in Fig. 1.2. In the primitive hexagonal lattice, half of the six-fold coordinated carbon positions are unoccupied. The structure unit of the hexagonal phase is thus the M_6C triangular prism with carbon in the center, or the C_6M with a six-fold coordinated metal atom. The advantage enjoyed by this WC structure, relative to the NaCl-type, is a lower energy for the electrons in the *dd* M-M bonding states [2].

The WC, also called δ-WC [8], is a line compound with insignificant deviation from stoichiometric composition, in contrast to the cubic MC carbides which exist over a wide composition range MC_x, where $1>x>0.5$ [7]. Tungsten also forms two other carbides: $WC_{0.5}$ (normally named β-W_2C) with a hexagonal compact (HCP) metal sublattice with the C atoms partly filling the octahedral intersticies; the second form is almost imperceptibly at high temperatures and is a cubic NaCl type composition γ-WC_{1-x}, where $x \approx 0.4$, in

which the faced centred cubic (FCC) interstitial sublattice is partly occupied by C [7,9]. The β-W_2C crystallizes in three types: PbO_2, Fe_2N and CdI_2 types, denoted by β, β' and β'', respectively. These carbides have several polymorphic compositions, stable in different temperature and compositions range. Recently [8] a phase diagram in the W-C system was proposed in order to a more accurately assessing of this system (Figure 1.3).

Table 1.1.

Characteristics and properties of tungsten carbides [1].

Phases	WC (also called δ-WC) W_2C (subcarbide β-WC) γ-WC_{1-x} (unstable, forming only above 2510 ºC)
Crystal structure and lattice parameters (nm)	WC: hexagonal, a = 0.2907, c = 0.2837, c/a = 0.976 W_2C: hexagonal, a = 0.3001, c = 0.4736, c/a = 1.578
Composition	Narrow range of homogeneity, δ-$WC_{0.98}$-$WC_{1.00}$
Molecular weight	WC: 195.86 g/mol W_2C: 379.71 g/mol
Colour	WC: Gray
X-ray density	WC: 15.8 g/cm^3 W_2C: 17.2 g/cm^3
Melting point	WC: 2785ºC W_2C: 2715ºC
Specific Heat (C_p)	WC: 39.8 J/mol K
Heat of Formation ($-\Delta H^o_f$)	WC: 37.7 kJ/g-atom metal at 298 K
Thermal expansion	WC: a = 5.2×10^{-6} ºC^{-1}, c = 7.3×10^{-6} ºC^{-1}
Vickers Hardness **Young´s Modulus of Elasticity** **Poisson´s Ratio** **Transverse rupture strength**	WC: 22 GPa WC: 620-720 GPa WC: 0.18 WC: 550 MPa
Oxidation resistance	WC: Oxidation in air starts at 500-600 ºC
Chemical resistance	WC is resistant to acids and not attacked at room temperature by mistures of HF and HNO_3, but attacked by these acids at elevated temperature. Attacked by chlorine above 400 ºC and by fluorine at room temperature. Stable in dry hydrogen until the melting point. W_2C is less stable than WC and reacts with Murakami's♣ reagent.

Test temperature is 20 ºC unless otherwise is stated. ♣(10g NaOH: 10g $K_3Fe(CN)_6$: 100 ml H_2O)

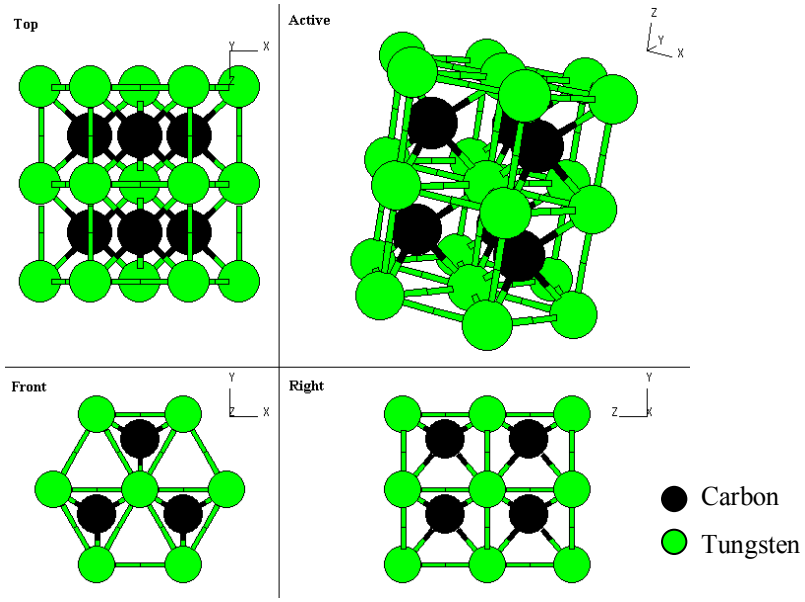

Fig. 1.2. Representation of the simple hexagonal structure of the tungsten carbide crystal [10].

The W_2C phase originates from a eutectoidal reaction between elemental W and δ-WC at 1250 ºC and melts congruently with the W solid solution at 2715±5 ºC and γ-WC_{1-x} at approximately 2758 ºC [8]. Phases of W_2C stoichiometry are obtained as intermediate products during WC production. The γ-phase results from a eutectoidal reaction between β and δ at 2516 ºC and melts at approximately 2785 ºC. δ-WC is the only binary phase stable at room temperature and has almost no solid solubility up to 2384 ºC but may become carbon deficient between this temperature and its incongruent melting point.

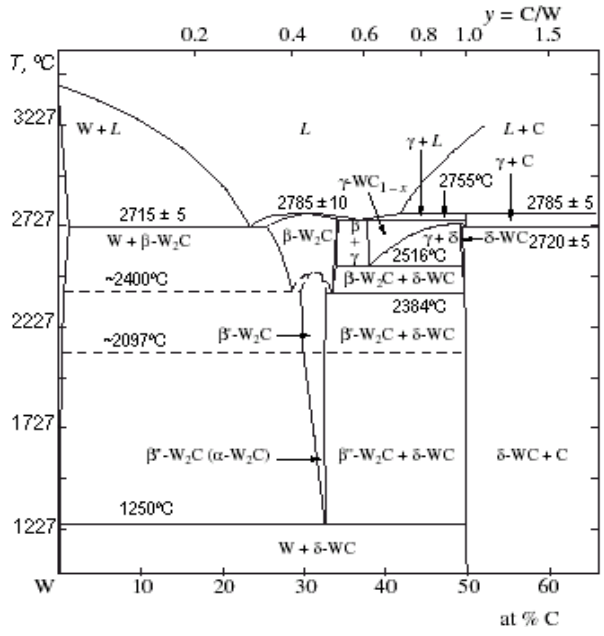

Fig. 1.3. Phase diagram of the W-C system, adapted from Kurlov [8].

Tungsten carbide has good wear resistance, high strength and high hardness but poor resistance to cracking and fracture [11,12]. At high temperatures, most cubic carbides rapidly loose their hardness, whereas the hardness of the WC is quite stable. In addition, WC has a factor of 1.5-2.0 higher elastic modulus and a factor of 1.5-2.0 smaller thermal expansion coefficient in comparison with other transition metal carbides [8]. These properties and other characteristics of the tungsten carbides are summarised in Table 1.1.

The high-temperature enthalpy data from 298 until 1600 K, for tungsten carbide are provided by the equation [1]:

$$H^0_T - H^0_{298K} = A + BT + CT^2 + DT^3 + (E/T) \quad (1.1)$$

were $A = -2.7595\times10^3$; $B = 8.5025$; $C = 2.0550\times10^{-3}$; $D = -2.4625\times10^{-7}$; $E = 144249\times10^5$ (for H in cal/mol).

The oxidation resistance of WC in air is good at room temperature, but at temperatures higher than 500 ºC an oxide layer is formed [13,14,15]. Two stable tungsten oxides, WO_2 and WO_3 exist. Of these, the WO_3 is the most thermodynamically stable at low temperatures and atmospheric pressures and forms by the following equation [13,16]:

$$WC\,(s) + \frac{5}{2}O_2\,(g) \rightarrow WO_3\,(s) + CO_2\,(g) \quad (1.2)$$

The oxidation resistance of WC in water was reported [14] to be good, and even with preoxidation exposure the WC is resistant to further oxidation in aqueous media. The main product of reaction from WC and water is WO_3 [16]:

$$WC\,(s) + 3H_2O\,(l) \rightarrow WO_3\,(s) + CH_4\,(g) + H_2\,(g) \quad (1.3)$$

It is this combination of technological properties and the thermal stability which underlie the wide use of tungsten carbide in the production of wear-resistant hard alloys, which are basic components of tool materials. These considerations, lead one to believe that at least for the short term, WC will be the principal hard phase in new cemented carbide systems under consideration for further development.

1.2. WC Cemented Carbides

1.2.1. Classification

Cemented carbides are one of the two types of materials constituted by metal and ceramic composites. The other category encloses cermet, which is used worldwide to designate "a heterogeneous combination of metal(s) or alloy(s) with one or more ceramic phases and in which there is relatively little solubility between metallic and ceramic phases at the preparation temperature" [5]. Although the term cemented carbide is widely used in the United States, these materials are better known as hardmetals.

Cemented carbides can be classified as tungsten carbide/cobalt grades or alloyed tungsten carbides. The first grades are also often referred as unalloyed grades, straight tungsten carbides, cast iron cutting grades or edge wear-resistant grades of cemented carbides. They consist of fine angular particles of tungsten carbide bonded with metallic cobalt, although nickel can also be used as a binder material. Cobalt may vary from 3 to 13 wt.% for cutting tool grades and up to 30 wt.% for wear-resistant parts [17].

The alloyed tungsten carbides are often referred as steel cutting or crater-resistant grades. These materials, in which cobalt is usually the binder phase and tungsten carbide is the major constituent of the carbide phase, also contain titanium carbide and/or tantalum carbide. The basic compositions of the grades contain 3 to 12 wt.% cobalt, 60 to 85 wt.% tungsten carbide, 4 to 25 wt.% titanium carbide and up to 25 wt.% tantalum carbide [18].

Another classification of WC composites is related to the particle size distribution (Table 1.2). This classification is accepted both for the hard metal industry and for the research world.

Table 1.2.

Classification of WC composites based on the particle size distribution.

Definition	Grain size (μm)
Nano	< 0.2
Ultrafine	0.2 – 0.5
Submicron	0.5 – 0.8
Fine	0.8 – 1.3
Medium	1.3 – 2.5
Coarse	2.5 – 6.0
Extracoarse	> 6.0

The first systematic experiments to bind powdered tungsten carbide with iron, nickel or cobalt were carried out from 1918 to 1923 in Germany by Karl Schröter, who used tungsten monocarbide (6.13% C) [18]. The tests performed in sintered cemented carbide dies showed cobalt to be the best additive. These composites are essentially aggregates of particles of tungsten carbide bonded with cobalt via liquid-phase sintering, which results in a strong binder/carbide interface without anomalous growth of the carbide [19]. The properties of these materials, usually named cemented carbides, are derived from those of the constituents – namely the hard and brittle carbide and the softer, more ductile binder. The cutting tool and wear part applications arise because of their unique combination of mechanical, physical, and chemical properties. The importance of the invention is confirmed by nothing that today, eighty years later, the same compositions, made by essentially the same process, are still a very significant product of tool materials industry. Cemented tungsten carbides find now a wide range of applications especially where combinations of high hardness and fracture toughness are required and ceramics or metals alone will not serve.

1.2.2. **P**hase **D**iagrams

The knowledge of the phase equilibria diagram of cemented carbides is an important tool to predict the phases after the sintering step and the adequate sintering temperature. The phase equilibria of cemented carbides are characterized by the existence of a two phase region between the carbide phase and the binder metal phase (Fig. 1.4, grey region).

The best properties are obtained within the two phase's region. The carbide-binder metal sections are eutectic systems and the special character of the WC-based materials is due partly to the constitution of this system. The systems of WC with Fe, Co or Ni show eutectic compositions richer in the carbide component (see Fig. 1.5) than other systems, namely TiC-based materials. The sintering temperature of the hardmetals lies above the eutectic temperature and the relatively high carbide content in solution leads to good densification by solution-precipitation processes and contributes to obtain the desired microstructure.

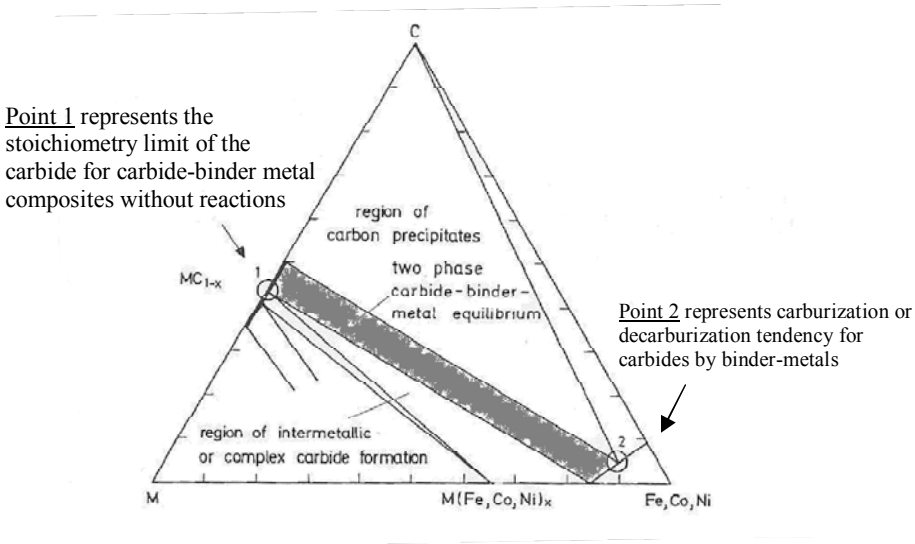

Fig. 1.4. Hard metal phase equilibria schematically [20].

Since the hard metal compacts are densified predominantly by liquid phase sintering, the sintering temperature must be selected high enough that at least one phase of the systems is in liquid state. Besides that, satisfactory combinations of hardness and transverse rupture strength of the cemented carbides are achieved when precipitation of other phases besides FCC and WC (e.g. graphite or the M_6C carbide) on cooling from the sintering temperature is avoided.

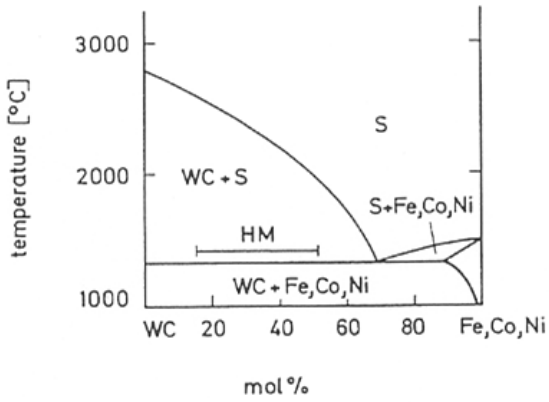

Fig. 1.5. Phase relations for the sections WC-Fe,Co,Ni. HM indicates the composition of commercial hardmetals [20].

1.2.2.1. System W-C-Co

More than 90% of all WC-hardmetals utilize Co as the preferred binder metal with contents between 3 and 30 wt.%. The reasons for the dominant role of Co are some unique properties of Co and the W-C-Co ternary system.

Over the last century, there have been several investigations concerning the W-C-Co system. The investigations have shifted from using only classic metallography toward combining experimental information with theoretical descriptions to define equilibrium phase boundaries. Guillermet [21] has made the most through CALPHAD (i.e. CALculation of PHAse Diagrams) method of the W-C-Co system. The analysis was based on experimental information on the lower-order systems with interpolations and extrapolations based on thermodynamic-model calculations. This method has been used extensively to calculate phase equilibria in cemented carbides [22]. However, tradition and experience are a strong tool too and most cemented carbide producers can make high quality cemented carbides without a detailed knowledge of the phase diagrams. This is particularly true for the W-C-Co system which is a very straightforward ideal system for cemented carbides, with a eutectic at 1280 ºC which is well below cobalt's melting point of 1490 ºC.

Fig. 1.6 shows a calculated isothermal section through the W-C-Co system at 1400 ºC, that represents a common sintering temperature [21,23]. From this figure it is obvious that WC is in stable equilibrium with liquid cobalt only within a rather narrow region of compositions. The solubility of tungsten carbide in cobalt at the sintering temperature is high but decreases during cooling with reprecipitation on existing carbide grains. In order to follow the changes during cooling, vertical sections through the system are useful.

Gruter [24] constructed a pseudobinary WC-Co phase diagram with a eutectic temperature at 1280 ºC (Fig. 1.7(a)). This author proposed that the η-phase remains in equilibrium with WC and liquid, even at stoichiometric compositions, at temperatures ranging from approximately 1280 to 1450 ºC.

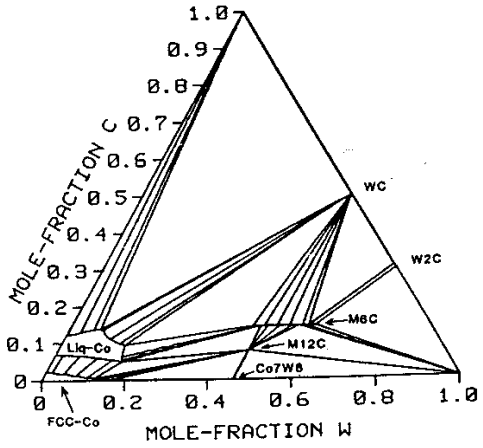

Fig. 1.6. Isothermal section of the W-C-Co phase diagram at 1400 ºC [21,23].

Fig. 1.7(b) shows a vertical section of the W-C-Co phase diagram calculated at 10 wt.% Co, which allows to easily follow what occurs at each temperature during cooling. The filled symbol on the composition axis represents the carbon content of the system corresponding to contents of W and C in the stoichiometric proportion for WC. Two other compositions are indicated by **a** and **b**. They correspond to the minimum and maximum carbon contents of alloys which will consist, just after solidification, of a mixture of only FCC+WC, assuming that there is no segregation. Regarding the previous considerations of the effect of the precipitation of graphite or M_6C, **a** and **b** are considered as the limits of the region of favourable carbon contents.

Regarding the Fig. 1.7(b) the precipitation of graphite will not occur during solidification of a stoichiometric alloy made from pure cobalt and WC. However, increasing the carbon content to an excess of 0.05 wt.% will cause graphite precipitation during the cooling of the liquid. The effect of Co content in the extension of the critical carbon range was investigated by Guillermet, too [21]. This author reported that the change of Co content from 6 to 10 wt.% induces an increase of about 70% in the range of favourable carbon amounts.

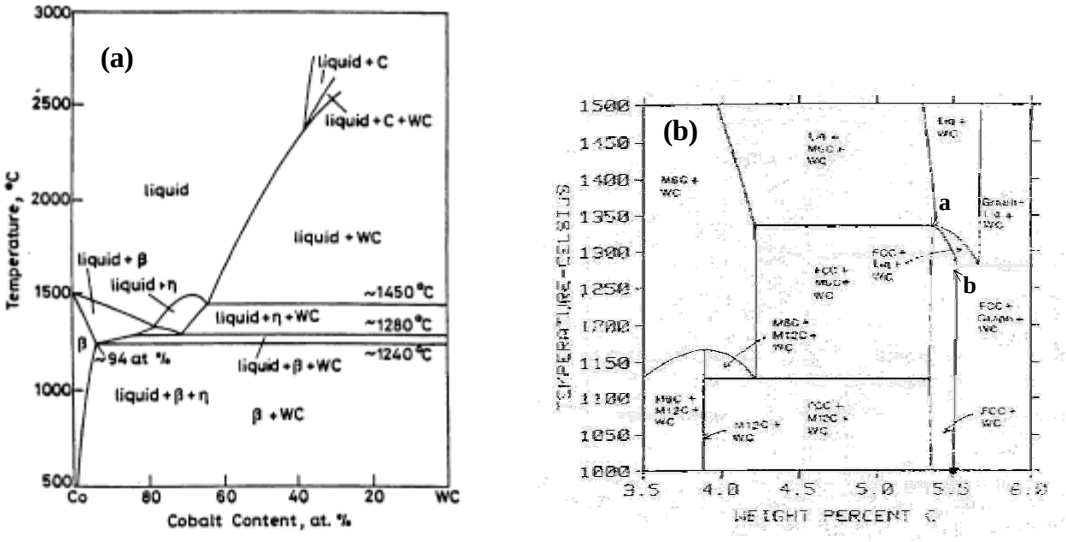

Fig. 1.7. Vertical section of the W-C-Co phase diagram **(a)** between stoichiometric WC and Co [24]; **(b)** calculated at 10 wt.% Co [25,21,23]. The solid symbol on the composition axis indicates the stoichiometric composition (5.5 wt.% C). The points denoted by **a** and **b** define, respectively, minimum and maximum carbon contents of alloys which are in two-phase state of FCC+WC just after the equilibrium solidification.

The solubility of WC in Co is not only high but also strongly varies depending upon the temperature. The solubility of tungsten in cobalt increases with decreasing the carbon content and has been reported to vary, accordingly, between 0 and 15 wt.% at around 1250 ºC [26,27]. The solubility of tungsten at ambient temperature has been reported to be 3.5 wt.% in cobalt binder [19]. The solubility of cobalt in tungsten carbide is very small and can be neglected. With regard to carbon in the binder, a typical range reported for WC-Co was 0-0.2 wt.% at elevated temperatures, with the higher values at the lower tungsten levels. Tungsten and carbon in cobalt binders are inversely related [19].

1.2.2.2 System **W-C-Fe**

The W-C-Fe system has been subjected to many experimental and theoretical investigations over the years [9,28], because iron forms a ternary eutectic melting at only 1143 ºC (see Fig. 1.8) and is also a possible substitute for Co [19]. However, iron dissolves

a much lower quantity of WC at the eutectic temperature (1143 ºC) than cobalt at the eutectic temperature of 1280 ºC [29].

In Fig. 1.8 is a calculated section performed by Guillermet [25] for the phase diagram of Fe-W-C with 10 wt.% Fe. Comparing with Fig. 1.7(b), corresponding to W-C-Co phase diagram for 10 wt.% Co, is now noted a decrease in the solid/liquid equilibrium temperatures, and a displacement of the favourable region towards values higher than the stoichiometric composition. On the other hand, the calculations suggest that the favourable effect of Fe additions on decreasing the solid/liquid equilibrium temperatures is coupled with an unfavourable reduction in the extent of the region of favourable carbon contents (between a and b). After descriptions of each element rich part, four ternary carbide phases have been reported in the ternary W-C-Fe system, M_4C, M_6C, $M_{12}C$ and $M_{23}C_6$ [9].

The sintering of an alloy with stoichiometric composition and 10 wt.% of iron binder, can be possible within the two-phase field WC+liquid if the temperature is above 1400 ºC, see Fig. 1.8. However, on cooling, the stoichoimetric composition is within the three-phase field WC+M_6C+Fe (FCC) and the embrittling η-phase (M_6C) will form. In addition, iron is a carbide former as WC bonded with Fe results in the double carbide Fe_3W_3C [30,31]. However, additions of free carbon to Fe-WC alloys, exceeding the stoichiometric amount required for the tungsten carbide, can inhibit the formation of large grains of the brittle η-phase [30,31].

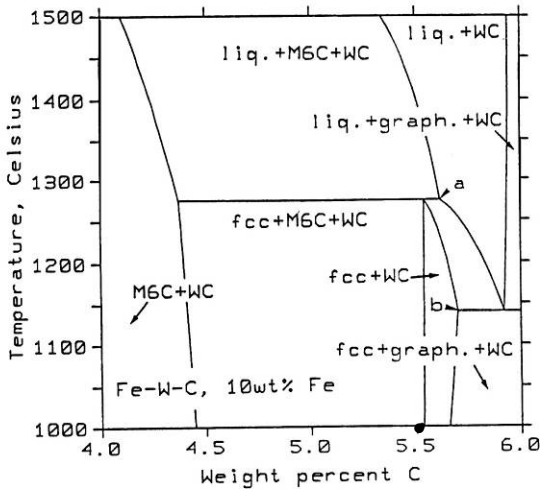

Fig. 1.8. Vertical section of the Fe-W-C phase diagram, calculated at 10 wt.% Fe [25]. The solid symbol on the composition axis indicates the stoichiometric composition (5.5% C). The points denoted by "a" and "b" define, respectively, minimum and maximum carbon contents of alloys which are in two-phase state of FCC+WC just after the equilibrium solidification.

The solubility of Fe in the WC carbide is reported [28] to be very limited about 0.6 wt.% at 1250 ºC, while the solubility of W in ferrite phase was found to be about 4.5 wt.% at 700ºC and 5.0 wt.% at 1250 ºC [28]. Uhrenius [32] reported the solubility of W and C in the liquid phase at 1350 ºC to be about 9.0 and 4.7 wt.%, respectively.

1.2.2.3. System **W-C-Ni**

Nickel has received the most attention as an alternative binder to cobalt. Its structure and properties are similar and the lattice parameter of FCC nickel is only slightly less than FCC cobalt. The principal differences are (i) FCC cobalt is metastable and can transform to HCP and (ii) cobalt is much more strongly magnetic [19].

The melting point of nickel at 1455 ºC is appreciably lower than cobalt at 1495 ºC, however to obtain satisfactory densification it is necessary to use increased sinter time and temperature [33,34]. This leads to a tendency to pick-up carbon from the graphite vacuum furnaces leading to graphite precipitation. The higher vapour pressure of nickel (ten times that of cobalt) at sintering temperature also causes considerable loss of the nickel binder and it is, therefore, necessary to control the working pressure [34]. The loss of nickel in practice has been reported to be 10 wt.% or more at sintering temperatures [34].

Nickel is a binder material almost exclusively used in die and wear parts because of its good corrosion resistance and non-magnetic behaviour [35]. Comparing the W-C-Ni phase diagram, Fig. 1.9(b), with the corresponding section of W-C-Co, Fig. 1.9(a), it is possible to examine the consequences of a full substitution of Co by Ni. The width of the FCC/WC region remains essentially unchanged, but the range of favourable carbon contents moves towards lower values as can be seen by comparison with the stoichoimetric composition [25]. Besides that, the change W-C-Co to W-C-Ni involves an appreciable increase in the equilibrium temperatures of eutectic and peritectic points. The partial substitution of Co by Ni induces an increase in the as referred equilibrium temperatures [25] that depends on the Co;Ni ratio. However, according to Guillermet [25] conclusions, the predicted effects on the solid/liquid equilibrium temperature remain relatively small, until the full substitution of Co by Ni.

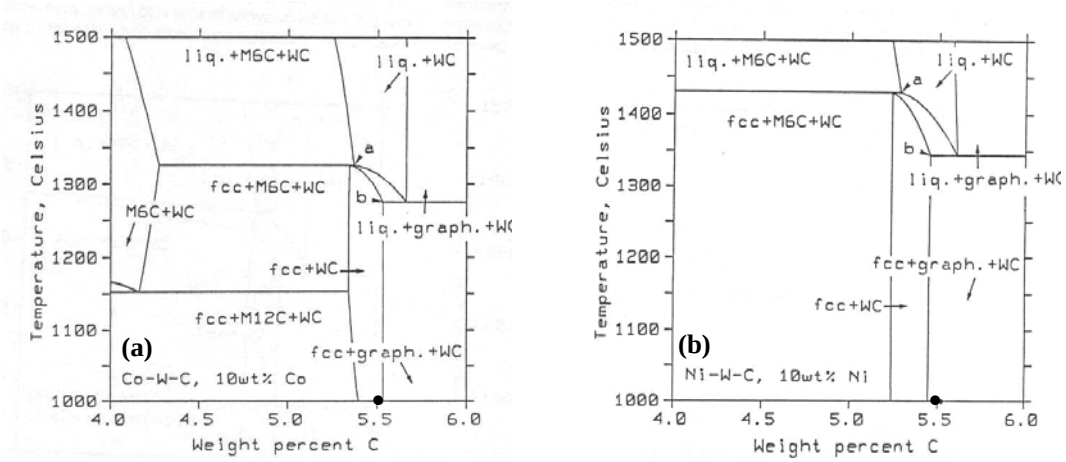

Fig. 1.9. (a) Vertical section of the W-C-Co phase diagram, calculated at 10 wt.% Co [25]. **(b)** Vertical section of the W-C-Ni phase diagram, calculated at 10 wt.% Ni [25]. The solid symbol (•) on the composition axis indicates the stoichiometric composition (5.5 wt.% C). The points denoted by **a** and **b** define, respectively, minimum and maximum carbon contents of alloys which are in two-phase state of FCC+WC just after the equilibrium solidification.

At sintering temperatures, the stoichiometric composition is within the two-phase field WC+liquid, but on cooling, graphite will precipitate as indicated in the section of the phase diagram shown in Fig. 1.9(b). This situation is opposite of iron, so attempts have been made in using Fe-Ni binders with more favourable conditions to stoichiometric composition.

The tungsten solubility in nickel has been reported to be of the same order of cobalt, but with the inclination to be somewhat higher [33,19]. The solubility of W and C in the liquid phase of the ternary W-C-Ni system was reported by Uhrenius [32] to be about 5.0 and 2.0 wt.%, respectively at 1350 ºC. At ambient temperature the solubility of tungsten in nickel has been reported to be 5.4 wt.% [19].

1.2.2.4. System **W-C-Fe-Ni**

The satisfactory properties of Fe-Ni bonded WC carbide tools are associated with an accurate control of the composition, in order to guarantee the absence of M_6C and graphite in the sintered alloy [36,37,38,39,40]. This means that the global composition of the system at the sintering temperature should fall inside the WC+liquid region of the respective phase diagram. During cooling, the composition should fall within the FCC+WC region and not precipitate graphite or M_6C. So, in order to achieve satisfactory results one should be able to accurately define the region of critical carbon contents once the Fe:Ni ratio has been selected. An assessment based upon the use of thermodynamic models has been attempted by Guillermet [41,42].

Guillermet [41,42] calculated sections of temperature and composition from the W-C-Fe-Ni system, for Fe+Ni=20 wt.% and Fe:Ni ratios of 3:1, 1:1 and 1:3. For comparison between the graphs, it is observed a general increase in the temperatures of the solid-liquid equilibria when the Ni content increases. Simultaneously, the two-phase field FCC+WC moves towards lower carbon contents with respect to the stoichiometric composition. It is also observed, that the width of the two-phase field varies with the content of Ni, diminishing first, but increasing again when it become closer to the ratio Fe:Ni 0:1.

In order to exemplify the previously interpretation, it is represented in Fig. 1.10(a) the calculation of a vertical section of the W-C-Fe-Ni diagram from the work carried out by Guillermet [41,42]. The calculation was performed for an alloy containing 20 wt.% of binder and Fe:Ni ratio equal to 3:1. It can be seen from that figure that the stoichiometric mixture of WC would precipitate M_6C during sintering at 1350 ºC. Even though the alloy after cooling would arrive at a stable two-phase field of FeNi-binder (FCC) and WC at temperatures below 1300 ºC, the precipitates of M_6C formed at sintering temperature, would not dissolve during cooling and will stay in a metastable form at lower temperatures. The calculated section shows that it would be better to increase the carbon content of the alloy to a value between 5.0 and 5.1 wt.% in order to avoid either M_6C precipitation or the graphite precipitation which would occur if the carbon content exceeded 5.1 wt.% [23,43].

The positions of these points change with the Fe+Ni content and the Fe:Ni ratio, but the lines defined by their displacement in the temperature-composition space can be directly

calculated. The temperature projection of the areas in the Fe-Ni-W-C system which would give graphite or M_6C phase in equilibrium with the liquid phase during sintering or subsequent cooling was calculated by Guillermet [41,42]. The zone in the middle, in Fig. 1.10(b), shows the most favourable compositions where none of these two phases will precipitate. The temperature projection presented in Fig. 1.10(b) correspond to an amount of Fe+Ni equal to 20 wt.%. From the figure it is observed that stoichiometric mixtures of WC and the pure metals will give WC+FCC-metal only if the ratio Ni/(Ni+Fe) falls in the region between 45 and 65%.

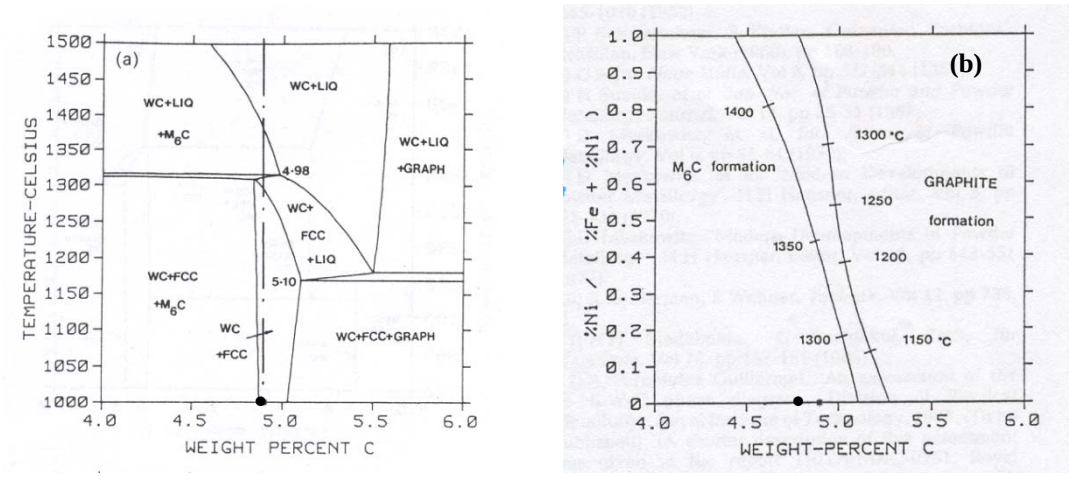

Fig. 1.10. (a) Vertical section of the Fe-Ni-W-C phase diagram calculated at Fe+Ni = 20 wt.% and %Fe:%Ni=3:1 [41,42]. The stoichiometric composition is represented by the traced line. **(b)** Temperature projection calculated at Fe+Ni=20 wt.%. The lines describe the compositions of a mixture of WC + liquid in equilibrium with FCC+M_6C (left) or FCC+graphite (right). The solid symbol on the composition axis indicates the stoichiometric composition [41].

When the (Fe+Ni) content is decreased, the region of interest gets considerably narrow. This is illustrated in Fig. 1.11(a) and (b) were the results concerned to the calculation of Fe+Ni=10% are presented. The analysis of these figures and Fig. 1.10(b), may offer a simple explanation of an empirical observation reported by Agte [44] and more recently by Moskowitz [45]. They observed that:

a) satisfactory properties may be obtained if the carbon content of the Fe-Ni-W-C alloy exceed the stoichiometric composition;

b) the increase of the Ni content in the initial composition, decreases the necessary carbon excess.

These observations can be explained by the position of the two-phase region and by the displacement of both lines in Fig. 1.10(b) and 1.11(b) to lower carbon contents when the Ni content is increased. In particular, a low excess carbon content is required if a Fe:Ni ratio 3:1 is adopted. This may explain the satisfactory results obtained by adopting this ratio in early attempts [45,44] to substitute Co by Fe:Ni.

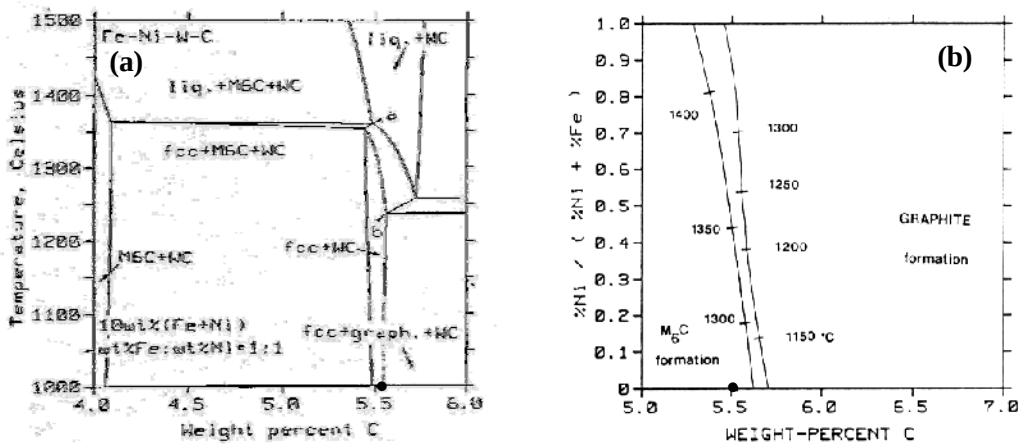

Fig. 1.11. (a) Vertical section of the Fe-Ni-W-C phase diagram calculated at Fe+Ni = 10 wt.% and %Fe:%Ni=1:1 [41]. **(b)** Temperature projection calculated at Fe+Ni=10 wt.%. The lines describe the compositions of a mixture of WC + liquid in equilibrium with FCC+M_6C (left) or FCC+graphite (right) [41]. The solid symbol on the composition axis indicates the stoichiometric composition.

It should be emphasized that due to scarcity of information in this quaternary system some carbide phases are not enclosed in the curves calculated by Guillermet [41]. However, they had been detected in Fe-W-C and Ni-W-C systems, namely the $M_{12}C$ carbide which may form at low values of the carbon activity and high Ni contents, the M_4C and M_2C carbides [41].

Uhrenius [32] reported the solubility of W and C in the liquid phase at 1350 ºC depending on the Fe:Ni ratio. Its investigation concluded that the solubility of W and C increase up to 9.0 and 4.7 wt.%, respectively, as the Fe:Ni ratio increases until 1:0. The solubility of these elements is more limited when the liquid phase is constituted only by Ni.

Among the interesting findings of Guillermet [41,25] the following are emphasized:

a) the substitution of cobalt by nickel does not alter the width of the two phase region but shifts it to an area of lower carbon content;
b) there is an appreciable increase in the four phase equilibrium temperature;
c) adding iron instead of nickel displaces the favourable region to higher carbon contents, lowers the liquidus temperature and narrows the width of the two phase region;
d) by the addition of iron and nickel together it is possible to arrange for the favourable zone to remain centred roughly on the stoichiometric composition.

1.2.2.5. System **W-C-Co-Fe-Ni**

It is represented in Fig. 1.12 a section calculated by Guillermet [25] for a composition of WC with 10 wt.% of binder, containing 5 wt.% of Fe and equal parts of nickel and cobalt. The effect of Fe additions depends on the Ni:Co ratio [25]. For example, keeping the same percentage of Fe (5 wt.%) and modifying the Ni:Co ratio between 1:4 and 1:1, a decrease in the width of the favourable zone is observed, being approximately 50% of the width observed in the W-C-Co-Ni diagram, for the same Ni:Co ratio and binder percentage. This effect is more pronounced when the iron addition is made to the alloy with the highest Ni:Co ratio, where reductions of about 70% of the width of the favourable zone in the diagram W-C-Co-Ni are observed [25].

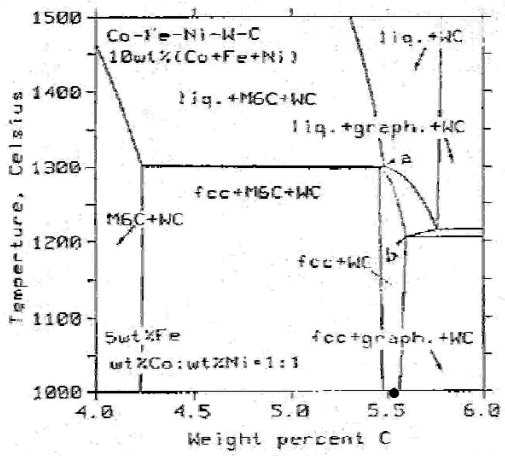

Fig. 1.12. Vertical section of the W-C-Co-Fe-Ni phase diagram calculated at 5 Fe, 2.5 Ni and 2.5 wt.% Co: the stoichiometric composition is indicated by the solid symbol (•) at 5.5 wt.% C; the alloys with carbon amount between **a** and **b** solidified with the formation of only WC+FCC [25].

1.2.2.6. System **W-C-Cr**

Chromium carbide (Cr_3C_2) is normally added to WC-Co system as a grain-growth inhibitor, but it also improves corrosion and oxidation resistance, because it forms a tough, self-repairing film [35]. Besides that, hardmetals with chromium in the binder are reported to have increasing hardness and work hardening rate and a marked improvement in abrasion resistance [34,46]. However, chromium is also a strong carbide former and the solubility of chromium in the Co binder is thus very much limited by the formation of carbides. Chromium restricted the solution/re-precipitation stage and as a result higher temperatures and longer times were required to sinter these materials [47].

The information in the literature is restricted to the ternary W-C-Cr system. Isothermal sections at temperatures higher than 1300 ºC, give the same kind of phase diagram even, tough details differ [48,49]. No information on the system at lower temperatures has been found in the literature.

Fig. 1.13 shows a calculated section at 1350 ºC in the ternary W-C-Cr system calculated by Gustafson [50]. A maximum solubility of 8.6 at.% W in $M_{23}C_6$ was determined, whereas the other stable Cr carbides, M_7C_3 and M_3C_2, also dissolve low amounts of W, about 3.8 and 8.8 at.%, respectively [50]. The C-rich side is dominated by the two-phase equilibrium WC+M_3C_2. The temperature for the invariant four-phase equilibrium WC+M_2C+M_3C_2+graphite was placed at 1498 ºC [50].

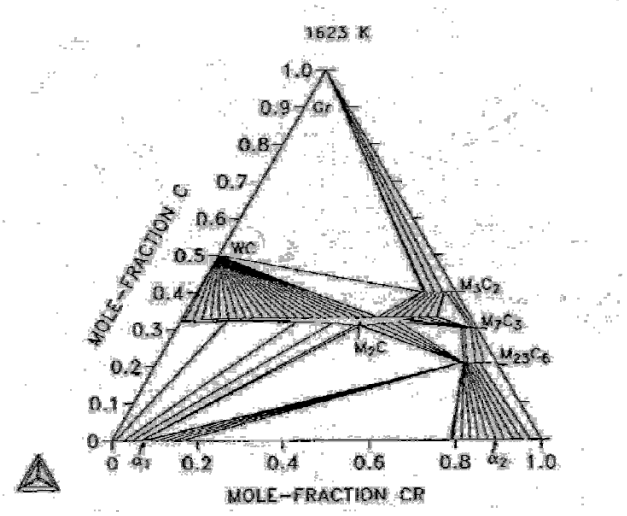

Fig. 1.13. The calculated isothermal section of the W-C-Cr system at 1350 ºC. The Greek letters α1 and α2 are used to denote the W and Cr-rich side of the BCC phase [50].

1.2.2.7. System W-C-Cr-Fe

There is relatively little experimental information available on the quaternary system W-C-Cr-Fe in the literature. Both Cr and W form carbides and many different types of carbide may form in steels containing these elements. The first schematic diagram of the quaternary W-C-Cr-Fe system was presented by Goldschmidt [51] in the early 1950's. Only one new carbide, not present in any of the binary systems, was included in that diagram. The ternary M_6C carbide, also stable in the W-C-Fe system, was shown to possess a limited solid solubility for Cr. The diagram also indicated that all Cr in the $Cr_{23}C_6$ carbide can be replaced by Fe and some W to attain the composition $Fe_{21}W_2C_6$.

Uhrenius et al. [52] presented experimental data on equilibria between Fe-rich FCC phase (austenite) and carbides in the W-C-Cr-Fe system at 900, 1000 and 1100 ºC. Their work was mainly concerned with equilibria involving $M_{23}C_6$, but some results on M_6C and cementite were also presented. The solid solubility for Fe in the $M_{23}C_6$ carbide is always less than 50% in the ternary C-Cr-Fe system, but the Fe content in the quaternary $M_{23}C_6$ carbide can be higher than 75% [50].

The region of existence of the M_6C carbide has been studied by Bergström [53]. He reported the existence of two additional carbides, $M_{12}C$ and M_4C, also found on the ternary C-W-Fe. The M_6C and $M_{12}C$ carbides were found to dissolve up to 8 and 4 at.% Cr, respectively at 1250 ºC. The maximum solubility at 1250 ºC of Cr in other phases, like Fe and W, were reported to be 10 at.% and 2 at.%, respectively. In Figs. 1.14 are represented the isothermal sections at 1250 ºC of the W-C-Fe and W-C-Fe-Cr at Cr levels of 2 and 10 at.% constructed by Bergström.[53] The isopleth W-C-Fe-2Cr (Fig. 1.14(b)) contains the same regions as the isopleth Fe-W-C-0Cr (Fig. 1.14(a)) since no phase, except WC has a Cr solubility limit below this section. The isopleth W-C-Fe-10Cr (Fig. 1.14(c)) is positioned above the maximum Cr solubilities of all phases. The maximum solubility of Cr in Fe lies on this level, which implies that the four-phase tetrahedron, $M_6C+M_{12}C+\mu(Fe_3W_2)+Fe$, the three-phase volume, $M_6C+M_{12}C+Fe$, and the two-phases volumes M_6C+Fe and $M_{12}C+Fe$, touch the section only in one corner [53].

The existence of an additional phase not covered in any of the above-mentioned papers has been reported by Goldschmit [54]. He found a new intermetallic phase, possessing the beta-manganese structure, at high temperatures. The phase occurred over an appreciable composition range in the W-C-Cr-Fe system, a representative composition being $Fe_{10}Cr_9W_2C$. The phase was stable only above about 1350 ºC and it is decomposed into a mixture of Fe-rich BCC and chi phases (iron tungstites) on cooling.

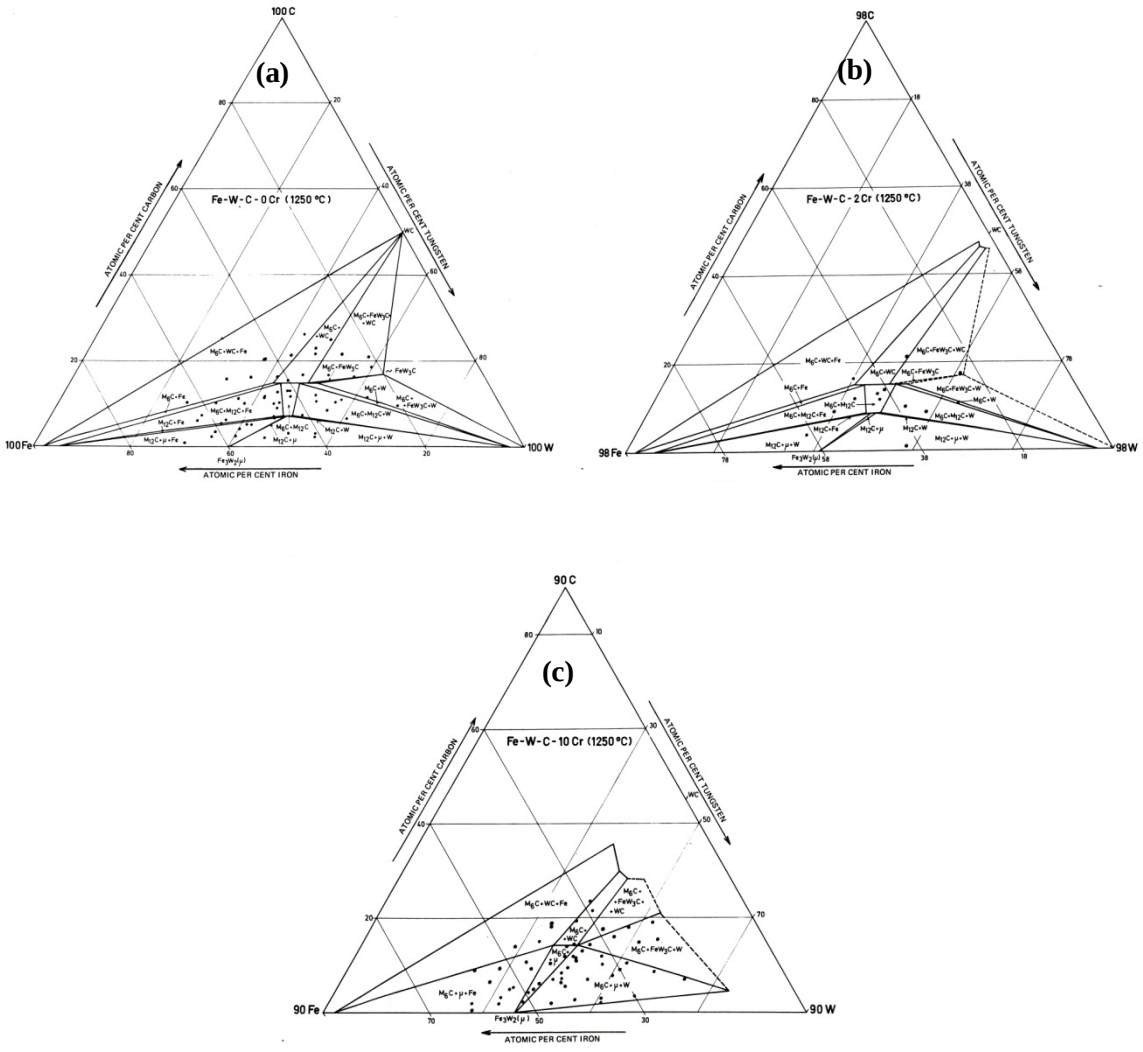

Fig. 1.14. (a) Isopleth W-C-Fe-0Cr (1250 ºC) [53]; **(b)** Isopleth W-C-Fe-2Cr (1250 ºC) [53]; **(c)** Isopleth W-C-Fe-10Cr (1250 ºC) [53].

1.2.3. **P**hase **S**tructures

The properties of sintered cemented carbides are critically dependent on their final composition and structure [2]. On the other hand, as discussed in the section before, slight deviations from the stoichiometric carbon content bring about the occurrence of either graphite or η-phase [23,43]. Therefore, the crystal structures of the principal phases that can be present in WC composites are WC, binder phase, η-phase and graphite, which will be described in this chapter. The hexagonal WC structure was already described in section 1.1.3.

1.2.3.1. **B**inder **P**hase

The metallic binder phase can consist of a variety of elements, alone or in combination such as cobalt, nickel, iron, chromium, molybdenum and tungsten; it can also contain other materials, such as stainless steel, superalloys, titanium, zirconium or some of the lower-melting copper or aluminium alloys [5].

Cobalt has been the traditional choice for a binder metal, since Schröter in his patent application of 1923 in Germany proposed to bond tungsten carbide with cobalt. The apparent superiority of cobalt relatively to other binders is related to its best comminution characteristics in milling, superior wettability for WC, higher solubility of WC in cobalt at sintering temperatures and excellent properties [34]. Because of the relatively high cost of cobalt and its scarcity of supply, attempts have been made to design alternate materials, with nickel and iron as the predominant cobalt substitutes. In Table 1.3 it is listed some physical and mechanical characteristics of Co, Ni and Fe, the most used elements for WC binders.

Cobalt is a ferromagnetic metal with a HCP structure as the most stable phase at room temperature. It undergoes a phase transition from HCP into a FCC structure at 450 ºC (Table 1.3). Nickel presents a FCC structure with a lattice parameter very close to the FCC Co. Similar properties at room temperature can be found in Ni and Co, with exception of hardness that is much lower for Ni, Table 1.3. Iron presents a magnetic BCC crystal structure, also known as α-Fe (ferrite), with the properties listed in Table. 1.3. It is, like Ni,

a soft metal that can dissolve only a small concentration of carbon (0.021 wt.% at 910 ºC). In the presence of higher amount of C, at temperatures above 912 ºC and up to 1400 ºC, α-Fe undergoes a phase transition from BCC to FCC, also called γ-Fe (austenite). This phase is metallic and non-magnetic and can dissolve considerably more carbon (2.04 wt.% at 1146 ºC). There are also some elements called austenite stabilizers, like Mn and Ni, that alloyed with Fe are effective in stabilizing the austenite phase down to room temperature. Fe-Ni-C binders can impart martensitic transformations, depending on the carbon content of the binder, that can influence the final mechanical properties depending on the binder structure (austenitic or martensitic) [55,56]. Other workers [57] reported that the iron-manganese (Fe-Mn) alloys show characteristics similar to Co with regard to the melting temperature, crystal structure, and γ(FCC)→ε(HCP) phase transformation on cooling. So, the interest in iron-rich binders is increasing, because in spite of being a carbide former, iron is an efficient binder candidate provided that the range of WC solubility in it could be increased.

Table 1.3.

Physical and mechanical characteristics of Co, Ni and Fe [58].

Property	**Cobalt**	**Nickel**	**Iron**
Crystal structure	Cubic (FCC) T>450 ºC Hexagonal (HCP)	Cubic (FCC)	Cubic (BCC)
Lattice parameter (nm)	a = 0.354 (FCC) a = 0.251, c= 0.407	a = 0.352	a = 0.387
Melting temperature (ºC)	1495	1455	1535
Theoretical density (g/cm^3)	8.9	8.9	7.9
Thermal expansion (10^{-6}/ºC)	12.5	13.4	12.3
Modulus of elasticity (GPa)	209	200	211
Hardness Vickers (MN/m^2)	1043	638	608

The binder phase that will be more investigated in this thesis is a stainless steel (Fe, Ni, Cr). The structure of this steel is normally austenitic (FCC) at room temperature but, after sputter-deposition, the most stable structure is ferrite with a BCC structure. It is presented in Fig. 1.15 a ferrite structure, for a prototype of $Cr_9Fe_{16}Ni_7$ with a cubic lattice parameter of a = 1.1109 nm, representing a possible ordering which may be found in Fe-Ni-Cr steels.

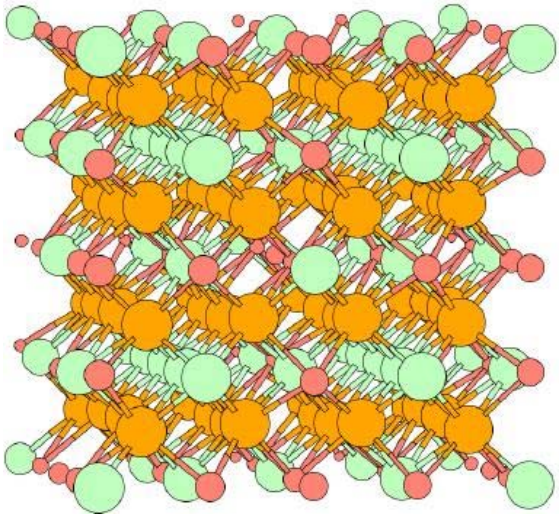

Fig. 1.15. Crystal structure of ferrite $Cr_9Fe_{16}Ni_7$; ○Chromium ○Iron ○Nickel [59].

1.2.3.2. η-Phase

Decarburization of WC leads to the formation of W_2C. This compound reacts with the matrix material and forms complex carbides (η phase), which consists of both tungsten and the matrix material. It is now well established that two types of η phase can be obtained – $M_{12}C$ of substantially constant composition and M_6C in which the composition can vary within the range of $M_{3.2}W_{2.8}C$ and M_2W_4C (M = Co, Fe). The M_6C type of η phase is in equilibrium with the liquid phase and can nucleate and grow during the sintering process. The $M_{12}C$ type is formed in the solid state (during cooling) with small grains distributed throughout the matrix and is therefore effectively less embrittling [60] than M_6C. However, Pollock [61] reported that the most high-temperature stable η-carbide is M_6C.

The M_6C carbide, which has many isomorphs among ternary carbides, contains at least two types of metal atoms. Its formation is favoured by the combination of one weak and other strong carbide formers, e.g. Fe and W. The $M_{12}C$ composition is a carbon poor η-carbide and its crystal structure differs from that of M_6C only by the absence of carbon atoms from half the carbon sites [28]. The structure of the carbide phase is represented by a formula with different sublattices. The M_6C carbide has a face centred cubic structure (cF112) containing 96 atoms per unit cell. The carbide is stoichiometric with respect to C

but has a measurable range of existence with respect to Fe and W. Experimentally, the carbide has been found for compositions within the range Fe_2W_4C and Fe_4W_2C [61,28,51]. The atoms are distributed among four sublattices with 48, 16, 32 and 16 atoms per sublattice, where the last sublattice contains only C (16 atoms). The standard chemical formulae are A_3B_3C, A_4B_2C and A_2B_4C where A stands for Co, Cr, Fe, Mn, Ni, etc., and B stands for Ta, Ti, W, etc. Sometimes, A_3B_3C and A_4B_2C are called η_1-carbide and A_2B_4C η_2-carbide [62]. For the representation of the Fe_3W_3C crystal structure (Fig. 1.16) the first sublattice is occupied by 48 W, the second and third by Fe and by C, respectively. Therefore, each C (16c) atom has two neighboring Fe (32e) atoms at a distance of 0.96 Å. The second Fe (16d) is shown with a different colour in Fig. 1.16, because all of the carbon atoms are on the edge of the cubic cell [63].

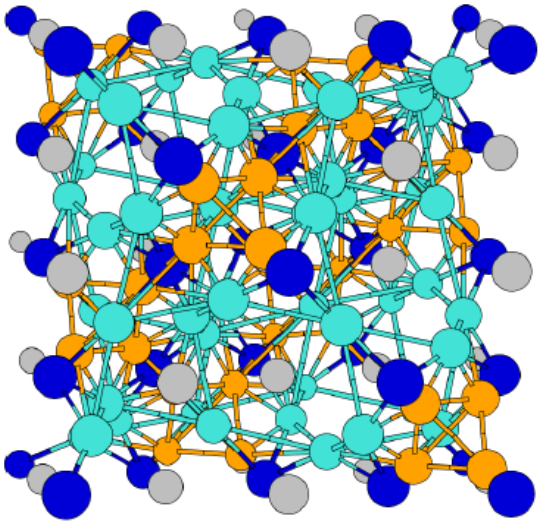

Fig. 1.16. Crystal structure of Fe_3W_3C; Carbon Tungsten Iron [63].

The crystallographic data for the M_6C carbide in the Fe-W-C system show that mixing of Fe and W atoms needs to be introduced in two sublattices, but considering the limited amount of experimental information the model was approximated by a simpler formula: $Fe_2(Fe, W)_2W_2C$ [9]. When extended this formula to systems with more elements we must decide on what sublattice to add the new element. When this description was extended to the quaternary W-C-Cr-Fe system Cr was placed on sublattice 2 [50], and M_6C is thus described by the formula, $Fe_2(Cr, Fe, W)_2W_2C$. In extending the models, Ni was added on the second sublattice [50] and also included into the first sublattice together with Fe, giving, $(Fe, Ni)_2$ $(Cr, Fe, Ni, W)_2W_2C$.

Moskowitz et al. [30,31] reported on the investigation of 25Fe-75WC compositions with different carbon contents, that WC is not stable in the presence of low-carbon austenite at elevated temperatures. Consequently, under these conditions, the more stable carbon-saturated austenite would be obtained by solution of carbon resulting from dissociation of WC to W_2C+C, subsequently producing Fe_3W_3C on cooling. This phase nucleates and grows due to the constant dissolution of tungsten carbide in the liquid binder; its presence is controlled by the amount of carbon present in the binder [64].

The morphology of η-phase can be determined by the sintering temperature, initial level of carbon deficiency and decarburizing during sintering. Cho et al. [65] investigated the influence of these factors on WC-Co alloys, concluding that the η-phase formed during sintering in a region of WC+L+η shows irregular shape, but η-phase developed from the WC+L region during cooling shows dendritic growth behaviour and huge octahedron shape when fully developed.

1.2.3.3. Graphite

The two known forms of graphite, *alpha* (hexagonal) and *beta* (rhombohedral), have identical physical properties (except for their crystal structure). Graphites that naturally occur have been found to contain up to 30% of the *beta* form, when synthetically-produced, as the case of WC composites, graphite only contains the alpha form. The crystal structure of graphite consists of carbon atoms. The carbon atoms within a graphite layer plane form a regular hexagonal network with a C-C distance of 1.421 Å (see Fig. 1.17). The layer planes are stacked parallel to each other at 3.354 Å apart. The hexagonal unit cell (Fig. 1.17) is represented with stacking sequence ABAB- (hexagonal system) with lattice parameters a = 0.2456 nm and c = 0.6696 nm. Another alternating stacking sequence (ABCABC-) results in a rhombohedral unit cell (rhombohedral system).

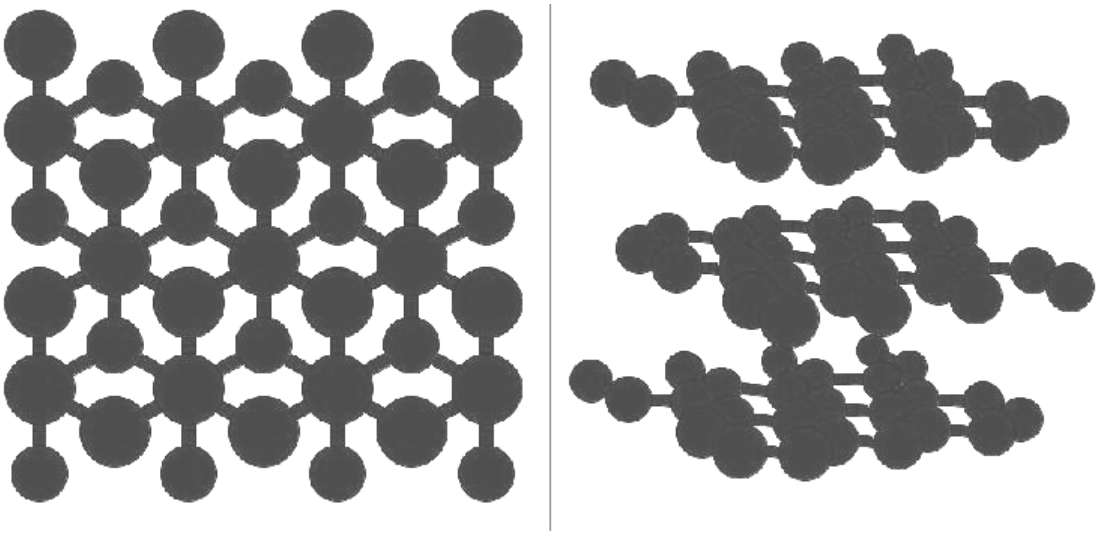

Fig. 1.17. Crystal structure of graphite [66].

1.3. **P**rocessing of **WC C**emented **C**arbides

Most cemented carbides are manufactured by a powder metallurgy process consisting of powder mixture, powder consolidation, sintering, and post-sinter forming (Fig. 1.18). WC powder, generated by a carburization process, is mixed with a relatively ductile matrix material (cobalt, nickel, or iron) and paraffin wax in either an atrittor or ball mill to produce a "composite" powder. The milled powder is consolidated into net- and near-net-shape green compacts and billets by pressing or extrusion. The usual applied process is cold pressing with pressures of about 200 MPa. Higher pressures have little effect on the further packing of the compact and cause increased die wear. Lower pressures induce greater shrinkage during final sintering, which increased distortion and porosity. Density of the green compacts ranges 45 to 65% of theoretical. Other consolidation methods used more restrictedly are powder injection moulding and slip casting.

Another method normally used for larger pieces is isostatic pressing. Powders are charged into a closed, flexible container that is pressed to the point where the powders become properly compacted. This system is advantageous for pressing large pieces, because the pressure acting on the powder operates equally from all directions, resulting in a compact of uniform pressed density.

The green parts are presintered at a low-temperature heat treatment (between 600 and 900 ºC), carried out in hydrogen or vacuum, to remove die lubricant and to impart adequate strength to the compact enabling preforming or machining operations, if required. The parts are subsequently vacuum or hydrogen sintered just above liquidus temperature of the alloy/composite (between 1350 and 1600 ºC, depending on the composition) which results in a fully dense, virtually pore-free part. The compact shrinks approximately 16% linearly, or 40% volumetrically. The exact amount of shrinkage depends on the particle size of the powders, green density and the composition of the grade. Hot isostatic pressing (HIP) eliminates the residual porosity (see Fig. 1.18). An alternative technology is a combination sinter-HIP process that combines dewaxing, presintering, vacuum sintering and low-pressure HIP, to speed up the overall cycle time.

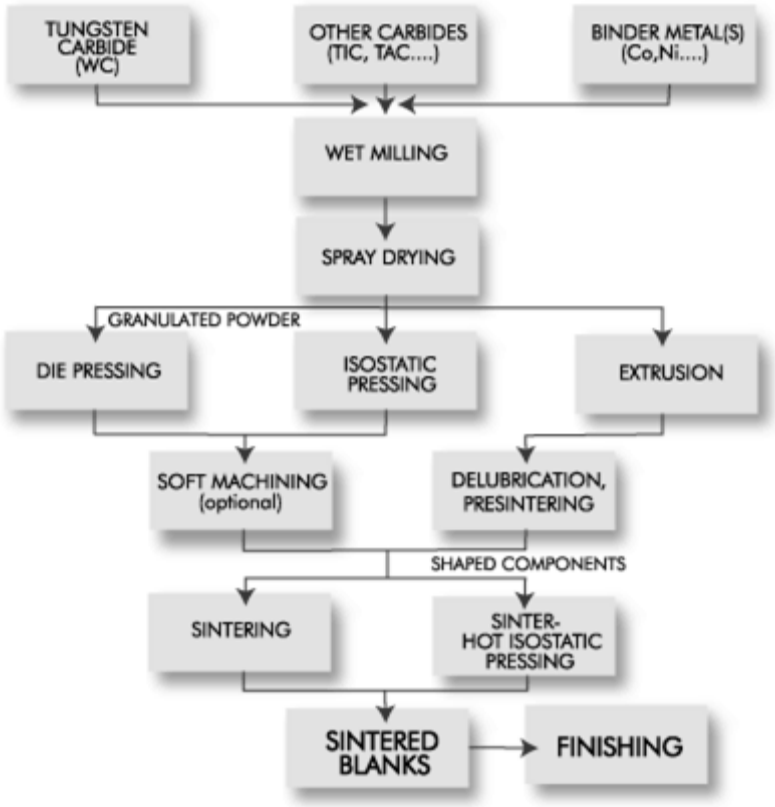

Fig. 1.18. Consolidation of powders hardmetal (cemented carbide) [67].

The worldwide tungsten carbide industry generates large quantities of scrap due to the rejected parts at various stages of production. The greater environmental concerns have led to the development of recycling carbide inserts. The most basic recycling approach would

be to break down the scrap pieces into powders and then fabricate more WC base cutting tools. However, this approach would cause severe equipment wear due to the abrasive nature of the cutting tool materials and therefore is not used. As a result, the recycling is done by chemical means, such as the zinc recovery process, electrolytic recovery and extraction by oxidation [2,4].

In this section a particular attention will be focused on the sintering stage, where the full density of green parts is attained and the final properties are defined. The sintering process of the system WC-Co will be described in more detail, since this system is the most investigated. The influence of other binders in the sintering process will be boarded, too. A small description of the new rapid consolidation techniques will also be performed.

1.3.1. **S**intering

.

After cold compaction of WC/binder mixed powders containing a pressing lubricant, such as paraffin (1 to 2 wt.%) in a high-pressure hydraulic press, the powder compact is heated to a temperature above the eutectic point in order to attain dense materials. Two basic methods are used to sinter cemented carbides [68,69]:

- Hydrogen sintering uses a hydrogen-based atmosphere at atmospheric pressure to dynamically control composition;
- Vacuum sintering uses a vacuum or reduced-pressure environment for the same effect.

Vacuum sintering is the predominant industrial process for sintering cemented carbides. Compared to hydrogen atmosphere sintering, vacuum sintering has several major advantages: (i) it allows superior control of product composition; (ii) the rate of carbon and oxygen exchange between the atmosphere and the cemented carbides is very low and (iii) the main factor controlling composition is the oxygen content of the carbide powder, not the rate of reaction with the atmosphere [68,69,70,71].

Sintering of cemented carbides consists of removal of pressing lubricant, densification and microstructure development. Commonly used lubricants, such as paraffin, evaporate

readily in vacuum from 100 to 250 ºC. Consequently, heating rate should be controlled in this temperature range to prevent excessive pressure within the compact, due to evolving lubricant vapours [70].

The compatibility of the melted binder with the refractory carbide at the sintering temperature is an essential prerequisite to a successful liquid phase sintering. Iron group transition metals have excellent wettability to WC, group VI metal carbide, compared to other transition metal carbides of group IV or V [19].

1.3.1.1. System **WC-C**o

The phenomena that occur during the sintering of WC-cobalt systems have been investigated thoroughly over a long period of time. Sintering in the WC-Co system is usually regarded as liquid phase sintering (LPS). However, during the heating period a considerable part of the changes in density, carbon content and cobalt distribution takes place in the solid state sintering [72,73,74]. Therefore, the sintering process must involve a solid state sintering mechanism, too.

1.3.1.1.1. Solid **S**tate **S**intering

There are some theories presented in the literature for the explanation of the solid sate sintering mechanism, including the one given by Meredith and Milner [72]. These authors reported that the rapid densification of the carbide particles, which takes place at the early stage of sintering (stage I in Fig. 1.19), is due to enhanced and interfacial diffusion forming close packed boundaries. These boundaries first occur in Co-rich regions around the cobalt particles, leading to localised densification, or aggregation of carbide particles. The initial size of such aggregates depends on the size and distribution of cobalt [72].

The stages II and III in Fig. 1.19 occur during liquid phase sintering (LPS) and correspond to collapse and filling of voids at the eutectic temperature when the Co dissolves carbide and forms eutectic liquid that flows into the void space (stage II). Further sintering occurs more slowly by diffusion leading to densification of the aggregates formed in stage I (stage III) [72].

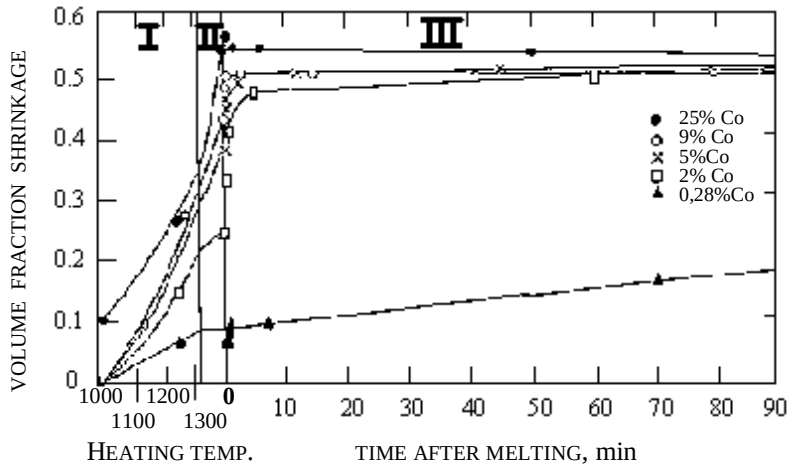

Fig. 1.19. Stages of densification of a range of WC-Co alloys. Stage I below eutectic temperature; Stage II densification at eutectic temperature; Stage III subsequent densification [72].

To analyse the densification kinetics during solid state sintering of either a single phase material, or a binary mixture of a hard phase with a minor soft phase a general model was proposed by Missiaen & Roure [75]. In the WC-Co case, the shrinkage rate, $\dot{\varepsilon}$, can be expressed as a function of temperature, physical parameters of the material, and geometrical parameters of the microstructure, when the dominant mechanism for densification is the volume diffusion in the cobalt binder phase:

$$\dot{\varepsilon} \approx \frac{8\gamma\Omega_{Co}D_V}{KT}\frac{S_V(\mathrm{P:Co})}{S_V(\mathrm{WC:Co})}\frac{2}{<L>}\frac{1}{<x>}\left(\frac{1}{<x>}+<H(\mathrm{P:Co})>\right) \qquad (1.4)$$

were γ is the cobalt surface tension, Ω_{Co} the average atomic volume in the binder phase, D_V the volume diffusion coefficient of the diffusion-limiting atom in the binder phase, and T the temperature. S_V(WC:Co) and S_V(P:Co) are, respectively, the WC_Co and pore-Co specific surface areas per unit volume. <H(P:Co)> is the mean curvature of the pore-Co surfaces. <L> is the mean centre-to-centre distance between WC particles which are bounded by the binder phase, and <x> is the mean radius of a slice of the binder phase (see Fig. 1.20). The geometrical parameters in Eq. 1.4 are determined from image analysis results.

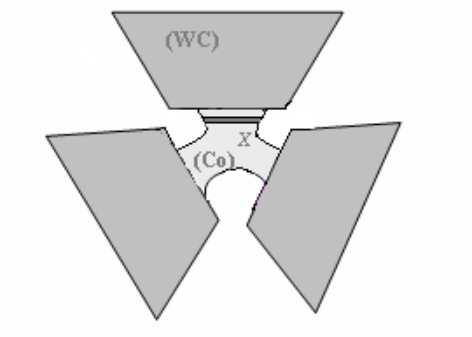

Fig. 1.20. Schematic representation in R^2 of WC particles bounded by the Co binder phase [75].

The evolution of stereological parameters with densification during solid state sintering was reported by those authors [75]. The decrease of the pore surface area with density is practically linear. The pore-Co surface area variation is homothetic, with a proportionality constant equal to the Co-volume fraction in the solid mixture, which indicates a uniform repartition of the two solid phases around pores. The WC-Co surface area evolution corresponds to a minimization of the surface energy by solid state "wetting" of WC grains by the binder phase. This surface area first increases rapidly, then slowly, as WC grains are gradually covered. The total mean pore curvature is the sum of the pore-WC and pore-Co curvatures. It remains negative over the whole density range, due to the convex shape of grains of the major WC phase. On the contrary, the pore-Co mean curvature is positive over the whole density range, which is evidence of a good "wetting" of WC grains by the Co-binder phase.

1.3.1.1.2. Liquid **P**hase **S**intering

The liquid phase sintering (LPS) process occurs above the pseudo-binary WC-Co eutectic (1300-1500 ºC) in order to attain the required liquid phase. From the technical point of view, LPS is very attractive as it provides faster sintering and complete densification without the need of any external pressure. Higher sinterability is due to the enhanced atomic diffusion in the presence of liquid phase which ultimately facilitates material transport. The criteria for successful LPS include these principal features [5,29,71]:

- The binder should have high solubility for the hard phase in the liquid-phase during sintering rather than vice versa.
- The liquid binder must provide a good wetting of the solid grains.
- The temperature difference between the hard phase melting point and the eutectic should be as high as possible.
- The sintering temperature must be high enough so that an appreciable amount of liquid phase is present. When these conditions are met, densification takes place.
- The finer the particle size of the hard phase is the more rapid and complete the densification of the compact is.

At the beginning of peak temperature holding, i.e. in first stage of liquid phase sintering, the microstructure can be nearly fully dense, for higher binder amounts and the carbide particles are nearly unchanged in size and shape from the original milled powder state. The good densification characteristics of WC-Co are due to the initial solution of the carbide by cobalt, which results in an extensive densification even before the first liquid is formed. Once the liquid is formed, further formation and spreading over the grains is fast due to surface energy reasons. As soon as the liquid penetrates the particle boundaries, a capillary force is developed which leads to particle rearrangement for closer packing in the presence of liquid phase. Although solution and reprecipitation of solid occurs concurrently with rearrangement, the rearrangement events dominate the early stage of densification [71,76]. The maximum amount of densification attainable due to rearrangement is influenced by some important factors, such as the amount of liquid present, particle size, solubility of the solid in liquid, contact angle, etc. [76].

The main purpose of the final stage of sintering operation is to develop the microstructure by holding at a temperature above the cobalt eutectic point for a time sufficient to develop a more uniform carbide structure with good binder phase distribution and minimal residual porosity. The microstructure will show grain growth when compared to the particle size of the original hard-phase powder. This grain growth can be appreciable and is dependent on the sintering time and temperature. Unusual microstructures can be present due to under or oversintering. For example, oversintering can lead to discontinuous carbide grain growth and correspondingly nonuniform microstructures [47,77].

During the liquid phase sintering of WC-Co the liquid cobalt rich phase flows from a region with higher cobalt content or finer grain sizes to a region with lower cobalt content or coarser grain sizes. The binder has fair amounts of tungsten and carbon in solid solution. Both tungsten and carbon stabilize the FCC phase of Co, which is the high temperature form, by impeding the martensitic transformation [27]. In the three-phase region with a large liquid fraction, a binder film is often detected between WC and η grains, whereas graphite and WC seem in contact. This indicates that the interface energy is higher between WC and η than between WC and liquid, and WC and graphite [78]. During cooling, after sintering, the tungsten and carbon elements precipitate on neighbouring carbide grains; as a result there is a gradient of tungsten concentration in the binder phase [27]. Irregular distribution of a binder phase leads to formation of large volumes of the binder phase in the hardmetal microstructure, resulting in the appearance of fields with lower hardness [79].

Leitner [80], with the help of thermoanalytical methods, such as dilatometry (DIL), thermogravimetry (TG), differential scanning calorimetry (DSC) and mass spectrometry gas analysis (EGA), summarise the characteristic processes taking place in a conventional WC/6Co hardmetal during debinding, outgassing and sintering (Table 1.4). These analytical techniques could be useful to check model calculations and process simulations and to optimise time, temperature and atmosphere in practical sintering cycles.

Table 1.4.

Processes occurring in different temperature ranges during sintering of WC-6Co [80].

Temperature range (ºC)	**Code**	**Processes**
20-200	TG	Humidity, residual organic solvents
	DSC	Melting of paraffin
200-600	TG	Paraffin debinding
	DSC	Decomposition of paraffin, reduction of oxidic impurities (Co)
	EGA	Decomposition and reduction products hydrocarbons, CO, CO_2
600-1100	TG/DSC	Reduction of oxidic impurities (WC)
	EGA	Formation of CO, CO_2
	DIL	Beginning of shrinkage
1100-1450	DIL	Shrinkage
	DSC	Formation of eutectic

Complete densification is readily accomplished for typical cemented carbide compositions that contain about 3 to 25 wt.% Co. Complete densification is more difficult to achieve for cobalt contents less than 3 wt.%. For cobalt contents greater than about 25 wt.%, part shape is difficult to maintain due to the presence of high liquid phase fraction, which allows the part to sag [70].

1.3.1.1.3. Grain **G**rowth

The mechanical properties of sintered hardmetal are largely dependent upon grain size distribution, and so the production of a consistent grain size distribution in the finished sintered product is of major concern. The final grain size distribution of the sintered product is affected at almost every stage in the production from the purchase of the original ore concentrate to the final sintering of the material [81]. During the sintering step some of the processing parameters that influence the final grain size distribution are: initial grain size distribution; binder content, sintering time and temperature and C/W ratio in the binder phase.

The use of finer grain powders in order to obtain microstructure refinement and increased hardness is frequent. However, during sintering, materials prepared from submicron size WC powders undergo abnormal grain growth, and so grain growth inhibitors like vanadium and chromium carbides are added to control microstructure [77,78]. Stereometric analysis of the particle size of WC [82] shows that the mean grain size increases with increasing of sintering time.

The growth rate and the morphology of the WC grains are also affected by the C/W ratio in the binder phase [77,78]. The growth rate of the WC grains is observed [77] to increase with the C content in the field {WC + liquid} in phase diagrams, this trend is not significantly modified in the domains where graphite or M_6C are present [77]. Several authors report that the WC average grain size is larger in the C-rich side [83,78]. When the binder is enriched in C, WC grains are faceted. In W-rich binder some WC grains appear slightly rounded [77,78]. Grain growth is slightly smaller in alloys with W-rich binder, and significantly reduced in alloys containing η-phase and/or V or Cr. The growth rate and the morphology of the WC/interfaces, different in C-rich or W-rich alloys, suggest that the

steps controlling the WC nucleation and growth should change with the binder composition [77,78].

Rüdiger et al. [82] reported that at low cobalt content, the average grain size of WC increases linearly as a function of the sintering time, while in the case of high Co-contents a faster grain growth can be observed. They also observed that with increasing sintering time, the W-content of the binder phase increases.

In spite of the control of WC grain size is of main importance, the grain size distribution of the binder-phase in WC-Co alloy was also investigated by Suzuki et al. [84], and the main conclusions are:

1) the average grain size of γ-phase increased with increasing the cobalt contents, the mean grain size of WC and with decreasing cooling rates;
2) the grain morphology of γ-phase consisted of equiaxed grains regardless of cooling rates or cobalt contents;
3) a region deficient in cobalt contents (or excess in W/C contents) existed near γ-phase grain boundary;
4) the strength of the alloy increased, in particular in high cobalt alloy, with decreasing the grain size of γ-phase.

1.3.1.1.4. Inhibitors

The initial WC particle size that determines the driving force for grain growth is the major parameter influencing the grain growth. The presence of coarse WC particles in an initial WC powder whose dimensions exceed the double of the average grain size is supposed to be a major reason for formation of large grains in the hardmetal microstructure [79,85].

The driving force for the growth of WC grains in a Co-based liquid is the overall interface energy decrease. Obviously, the smaller the initial WC grain size, the larger the interface area and the larger the driving force [78]. The contributions of the WC/Co and WC/WC interfaces for the several WC crystal planes could vary and could induce a slightly different growth process depending on the C content [77]. WC grain growth during

liquid phase sintering of WC-Co alloys is phenomenologically treated as an Ostwald ripening process (dissolution/reprecipitation processes) [86,87]. Smaller grains dissolve due to their higher dissolution potential (increased chemical potential), while coarser ones grow by material re-precipitation, thereby reducing the interface area of the system.

The addition of appropriate grain growth inhibitors is one of the essential factors in preventing WC grain growth during sintering. Growth inhibition was more pronounced with increasing amounts of inhibitor carbide, but reached a saturation limit, above which neither a higher hardness nor a finer microstructure was obtained. This level is believed to correspond to the maximum solubility of the carbide phase in liquid binder.

The nature of the binder (Co, Ni, Fe) contributes to determining the growth behaviour by influencing the metal-to-carbon bond relationship. For example, iron has the highest affinity to carbon, followed by cobalt and nickel. This affinity can also be interpreted as the ability to form stable metal-carbon bonds (also in the liquid phase), the iron masking the carbon, and impeding carbon transport and precipitation by increasing the activation energies of the nucleation and growth processes (i.e. increases the resistance against growth). A decrease in the interface energy of the WC/binder interface might also be a possible explanation for the extremely low coarsening rate of the WC in case of the iron binder (through bond formation), compared with the WC-Co and WC-Ni systems.

VC has been found to be the most effective grain growth inhibitor [83,78]. The content of VC in WC-Co is usually kept at 0.7 wt.%, which is regarded as the practical upper limit, in order to avoid embrittlement due to (V,W) C precipitation at the interface of WC-Co [83]. VC proved to be also the most effective grain growth inhibitor in WC-Ni hardmetals, followed by TaC, Cr_3C_2, TiC and ZrC [86]. It was also reported [86] for WC-Ni alloys a significant growth inhibition in low carbon (tungsten-rich binder environment), in particular in alloys with η-phase.

1.3.1.1.5. Nanocrystalline **WC-C**o

When the powder of WC becomes finer there are some interrelations between powder properties and the sintering behaviour which become more pronounced. In particular, the densification which is obtained in the stage of solid state-sintering increases and is intensified considerably with decreasing WC grain size and increasing interfaces between WC particles and Co binder. Gille et al. [88] investigated the sintering of WC (0.1 μm)-10 wt.% Co and compared with sintering of WC (0.6 μm)-10 wt.% Co. The most important findings are:

- Shrinkage starts at a lower temperature and the maximum of shrinkage rate is shifted from 1260 to 1200 ºC, when the WC grain size is reduced from 0.6 to 0.1 μm.
- The shrinkage rate curve for 0.1 μm is wider and more flat than that of the 0.6 μm.
- The mass loss is higher for the WC (0.1 μm) hardmetal due to the higher content of oxygen and oxides which have to be released as CO_2 and CO.

The decrease of the melting temperature in nanosize hardmetal powder was experimentally revealed by Harmat et al. [89]. They observed a decrease of 130 ºC for hardmetal powders WC-Co with 30 nm average grain size, comparatively with micrometer size powders. In addition, they noted that at the beginning of the heating up process, the relevant characteristic size is much smaller than 30 nm, i.e. the Co layers between two WC powder particles can be very thin (≈3 nm thick). According to theoretical extrapolations developed by the authors [89], the melting of a 3 nm thick layer of Co can be expected 400ºC below the WC-Co eutectic melting temperature.

In spite of the reported advantages of fine-grained hardmetal manufacture, very fine WC grains (50-200 nm) show a strong tendency to coarse, due to their high interface energies as well as differences in individual grain sizes, constituting the driving force for the growth process [90,91]. Many researchers have developed novel approaches to control the rapid grain growth, such as adding grain growth inhibitors or conducting the sintering at lower temperatures with the aid of rapid consolidation techniques, such as plasma pressure compaction (P^2C), spark plasma sintering (SPS), plasma activated sintering (PAS), pulse current process, microwave process and hot isostatic pressing (HIP). These new sintering techniques will be described in more detail in the following section.

1.3.1.2. Other Systems

Meredith and Milner [72] investigated the effect in densification of several metal additives to tungsten carbide. These authors reported high degree of densification when small amounts (1 vol.%) of iron-group metals (Co, Fe, Ni) are added to WC (see Fig. 1.21). Chromium and Molybdenum are carbide-forming elements so they react and form a mixed carbide with the base carbide, WC, not leading to significant densification, Fig. 1.21. Manganese, as an element between Cr and Fe in the Periodic Table, show a slight improvement of the densification.

Iron-group binders activate the sintering process, due to enhanced surface and interfacial diffusion and therefore are the most effective binders in the market. WC forms low-energy prismatic interfaces in the presence of Co or other Fe-group metals. This process takes place rapidly, because the segments of low-energy interfaces set up activity/diffusion gradients which bring about a rapid flux of material to take up, and expand, these low-energy boundaries [72].

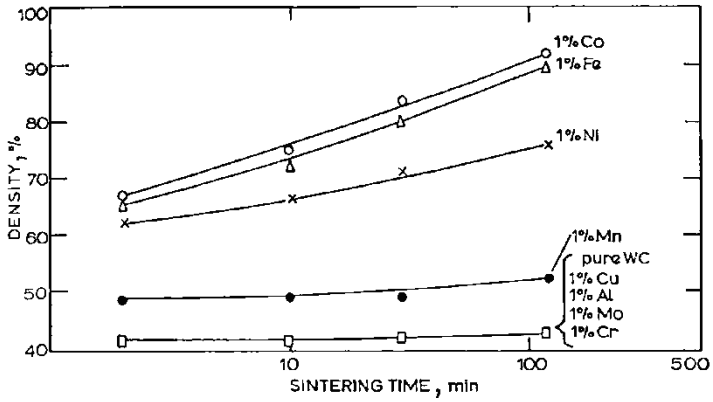

Fig. 1.21. Densification effects of the addition of 1 vol.% of metal powders to WC at 1400 ºC [72].

Other additions, like carbon to Fe-Ni binder also aids densification due to its effect in decreasing the liquidus temperature of the binder [36,30]. The C content in the binder is itself much lower after sintering than that added, since C is lost during sintering, by reduction of oxides and evaporation of the binder phase constituents at temperatures above 1250ºC [36].

The sintering process of WC hardmetals with iron group metals is comparable to the already exposed WC-Co system, since the structural characteristics of this type of binder are similar to cobalt.

1.3.2. **O**ther **T**hermal **C**onsolidation **P**rocesses

Other consolidation processes also applied in the manufacture of hardmetals, besides the vacuum sintering, involve the hot pressing and hot isostatic pressing. Rapid consolidation technologies have also been recently emerged due to the development of nanocrystalline WC-Co composites, namely spark plasma sintering (SPS), selective laser sintering (SLS) and others. More details on P^2C, SPS and PAS are provided in section 1.5.

1.3.2.1. **H**ot **P**ressing

Hot pressing is a consolidation method to produce simple geometry parts in which the pressure and temperature are applied simultaneously. The powder mixtures are either compacted directly in the hot press mold or prepressed cold in graphite dies and then transferred to the hot press tools of the pressure-sintering furnace. The densification effect of conventional static hot pressing is more pronounced than the effect that can be achieved by cold pressing and subsequent sintering. Heating the cermet powder mixture increases its plasticity and produces larger areas of inter-particle contact. The surface nearing action that occurs during the process mechanically disrupts surface oxide films and generates clean bonding surfaces. Because the graphite dies are expensive, this method generally is used only when the part to be produced is too large for cold pressing and sintering.

1.3.2.2. **H**ot **I**sostatic **P**ressing

Hot isostatic pressing (HIP) is an improvement over static hot pressing in that it eliminates the need for costly and highly perishable molds [92]. However, before compacts are submitted to isostatic pressing, they need to have a sufficiently high dense structure to inhibit gas penetration. Compacts with lower density and interconnecting pores require a gas-tight encapsulation of some sort before being treated [5]. HIP of cemented carbides is becoming a standard process for certain applications and is being more and more widely applied to the carbide industry. The main reason for its use is to eliminate flaws either in pre sintered parts that will be subjected to extensive grinding and polishing or in finished parts to avoid premature failure during service [92].

1.4. **T**echnological **P**roperties

The assessment of the final properties of cemented carbides is very important, since the performance and sometimes the life time of a tool can be estimated. In this chapter the mechanical properties, namely hardness, transverse rupture strength, fracture toughness and abrasion resistance will be described in terms of measurement methods and the most used expressions to describe the dependence of the properties on the microstructural parameters. Other properties like corrosion and oxidation resistance will be presented, too. The related microstructure parameters are first listed, in the following section.

1.4.1. **M**icrostructural **P**arameters

After sintering, the final microstructure of hardmetal is developed and the microstructural parameters that influence the final technological properties are characterized. Grain size distribution, volume fraction of all the phases including porosity, contiguity, C, and mean free path, λ_m, constituted the most important ones. Some of them could be assessed with parameters directly obtained from a linear intercept technique, using established relations, as those presented in Table 1.5.

The Eq. 1.5 of Table 1.5 is used to calculate the average grain size of WC, d_{WC}, taking the parameters obtained with the line intercept technique, while the average diameter of Co, d_{Co}, can be calculated from the contiguity, *C*, volume fraction of Co and d_{WC}. The contiguity, *C*, is the quantitative measure of the contact between grains of the WC phase. The contiguity depends essentially on the binder volume fraction, but the grain size distribution and the uniformity of the binder distribution also influences this value. The contiguity can be calculated using three different expressions, which are presented in Table 1.5. The Eq.s 1.7 and 1.8 depend on the parameters obtained from the line intercept technique, while Eq. 1.9 relates the contiguity to the coefficient of variation of WC grain size distribution. The mean free path of the binder phase, λ_m, is the average distance between WC particles and depends on the binder volume fraction and the contiguity. Two expressions can be used to calculate λ_m (Table 1.5). The Eq. 1.10 is related to parameters obtained in the line intercept technique, while Eq. 1.11 uses parameters previously calculated, such as contiguity.

Table 1.5.

Expressions for the microstructural parameters.

Expressions	Eq.	Parameters	Ref.
$d_{WC} = \frac{2V_{WC}}{2(N_L)_{WC/WC} + (N_L)_{WC/Co}}$	(1.5)	d_{WC} – WC average grain size V_{WC} – WC volume fraction $(N_L)_{WC/WC}$ - average number of intercepts per unit length of the test line with carbide/carbide boundaries $(N_L)_{WC/Co}$ - the same for carbide/cobalt interface	[93]
$d_{Co} = \frac{1}{1-C} d_{WC} \frac{V_{Co}}{V_{WC}}$	(1.6)	d_{Co} – Co average grain size V_{Co} – volume fraction of Co C – contiguity	[47]
$C = \frac{S_{WC/WC}}{S_{WC/WC} + S_{WC/Co}}$	(1.7)	$S_{WC/WC}$ – area of contact per unit volume between adjacent WC grains $S_{WC/Co}$ - area of contact per unit volume between WC grains and Co regions	[47]
$C = \frac{2(N_L)_{WC/WC}}{2(N_L)_{WC/WC} + (N_L)_{WC/Co}}$	(1.8)		[93]
$C = 1 - V_{Co}^{0.644} \exp(0.391 \times V)$	(1.9)	V – coefficient of variation of WC grain size distribution $V = \sigma_{WC} / \overline{d}_{WC}$ (σ_{WC} - standard deviation $\overline{d}_{WC}$ - mean carbide grain size)	[94]
$\lambda_m = \frac{2V_{binder}}{(N_L)_{WC/Co}}$	(1.10)	λ_m – mean free path V_{binder} – volume fraction of binder	[93]
$\lambda_m = \frac{d_{WC}(1 - V_{WC})}{V_{WC}(1-C)}$	(1.11)		[36]

1.4.2. Hardness

Hardness is related to the manner in which the material flows and work-hardens beneath the indenter. It is well established that the cobalt-rich binder phase in WC-Co composites is not as free to deform with loading as its bulk form; the binder is highly constrained by the WC grains, this increases its yield strength and makes the hardness of the composites dependent on the binder mean free path in addition to the binder content [27]. The ability of WC grains to accommodate substantial plastic deformation without the occurrence of brittle fracture is probably the most important property underlying the success of WC-based hardmetals.

Hardness, because of its close relationship with resistance to abrasion and wear, is a critical requirement in most applications involving carbide materials. The value of hardness provides a measure of the resistance of the ceramic to deformation, densification, and cracking or fracture. Sintered carbide hardness is generally measured using either Vickers diamond pyramid indentation, HV, or the Rockwell A-scale (HRA) diamond-cone indentation [95]. Hardness can be affected by composition (i.e., volume fraction of binder), and microstructural parameters, such as, porosity, carbide grain size and contiguity/binder mean free path [95,96]. The qualitative dependence of hardness in some of these microstructural parameters is presented in Table 1.6, a resume based on published literature results [11,95,18,27]. The increase of the binder content leads to decreasing hardness values, because, by increasing binder content in the composition of the specimens, a part of the hard WC phase is replaced by the ductile binder phase (Table 1.6 and Fig. 1.22). The hardness of cemented carbides increases with decreasing the carbide grain size and the binder mean free path, increasing the contiguity of the carbide phase (Table 1.6) [27].

Table 1.6.

Qualitative variation of some mechanical properties with related microstructural parameters, assuming two phases (WC + FCC).

Property	**Binder content** ⇧	**WC grain size** ⇧	**Contiguity** ⇧	**Mean free path** ⇧
Hardness	⇩	⇩	⇧	⇩
TRS	⇧	⇩	⇩	⇩
Young's modulus	⇩	—	—	—
Fracture toughness	⇧	⇧	⇩	⇧

⇧ - Increase; ⇩ - Decrease

The ability to retain hardness at high temperatures is a function of the tungsten carbide/cobalt structure. The tungsten carbide hardness is not appreciably affected by the temperatures reached during normal machining operations. Critical hardness losses result when the cobalt binder absorbs sufficient heat to plastically deform [18].

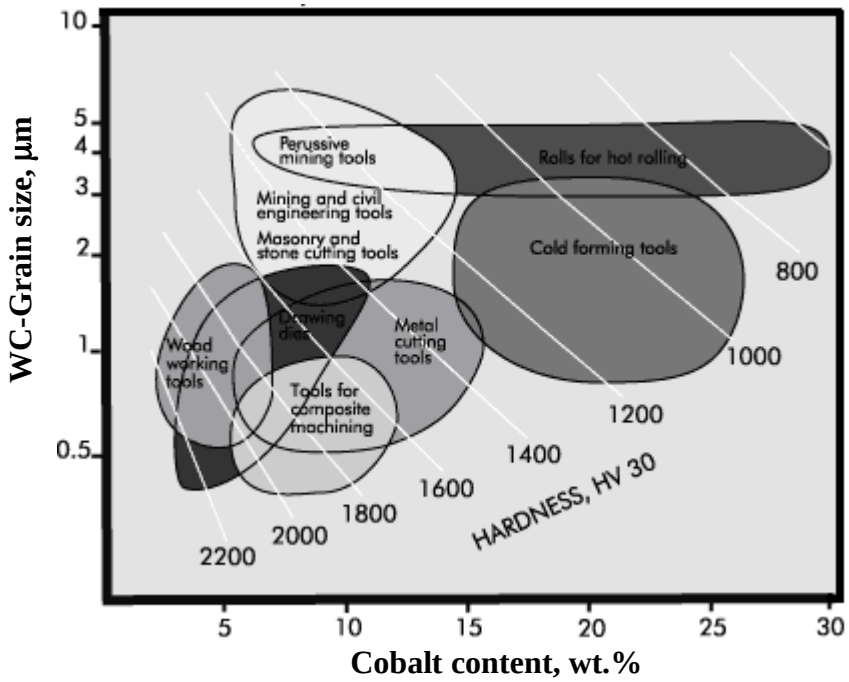

Fig. 1.22. Application range of straight grade cemented carbides [67].

The Hall-Petch relationship or *Hall-Petch Law* is a relation between the grain size, *d*, and the yield point, σ_y, of a material:

$$\sigma_y = \sigma_0 + \frac{k_y}{\sqrt{d}} \tag{1.12}$$

where k_y is the fitting parameter (a material constant), σ_0 is a materials constant for the starting stress for dislocation movement. According to this relation, the magnitude of the applied external stress (hardness) is inversely proportional to the square root of the grain size. For grain sizes in the range 0.5-5 µm the Hall-Petch relation describes the mechanical behaviour quite well for hardmetals with constant binder content [97]. However, at the extreme ends of the grain size range (fine and coarse) the Hall-Petch behaviour becomes apparent.

Several expressions concerning the relationship of hardness of WC cemented carbides with microstructural parameters have been reported. All the expressions are related to the WC-Co system. Lee and Gurland [98] modeled the hardness of cemented carbides as the sum of the in situ hardness of the hardphase times the volume fraction of the contiguous carbide skeleton ($V_{WC}C$) and the hardness of the remaining binder times the rest of the volume (Eq. 1.13). The two in situ hardness values (Eq.s 1.14 and 1.15) were assumed to

obey the Hall–Petch relations based on the grain size (d), and the mean free binder path (λ), respectively. The hardness values are in Vickers units and both d and λ in mm. The agreement between theory and experiments was found to be good for cemented carbides with contiguities in the interval $0.2<C<0.8$, corresponding to hardness values from about 1000–1700 HV [98]. The satisfying quantitative agreement has made the Lee and Gurland model the most widely accepted.

A theoretical model has been also proposed by Gille et al. [88] in order to find a relationship between hardness HV30, and the microstructure parameters, WC mean grain size, d_{WC}, and Co volume fraction, V_{Co} (Eq.s 1.16 and 1.17 in Table 1.7). According to this model one straight line correlates hardness HV30, d_{WC} and V_{Co} for 120 hardmetal samples within a wide spread range of parameters values (d_{WC}=0.10-7.80 μm, V_{Co}=0.10-0.38). A semi-empirical formula between hardness and microstructural parameters, proposed by Makhele [99] (Eq. 1.18) is also reported to fit well experimental results in spite of other factors that affect hardness, like the binder composition and grain size distribution, are not considered.

Table 1.7.

Expressions for the relationship between hardness and microstructural parameters.

Expressions	**Eq.**	**Parameters**	**Author, Year**	**Ref.**
$H_C = H_{WC}V_{WC}C + H_{Co}(1-V_{WC}C)$	(1.13)	C - contiguity V_{WC}- volume fraction of WC H_C – hardmetal hardness H_{WC} –hardness of WC phase H_{Co} – hardness of Co phase d_{WC} – WC grain size (mm) d_{Co} – Co grain size (mm)	Lee and Gurland, 1978	[98]
$H_{WC} = 1382 + 23.1\ d_{WC}^{-1/2}$ (kg.mm^{-2})	(1.14)			
$H_{Co} = 304 + 12.7\ d_{Co}^{-1/2}$ (kg.mm^{-2})	(1.15)			
HV30 = $f(V_{Co})(d_{WC})^{-1/m}$	(1.16)			
HV30 = 1824 (1 - 1.65V_{Co} + 0.92V^2_{Co}) (d_{WC})$^{-0.194}$	(1.17)	V_{Co} -volume fraction of Co	Gille, 2000	[88]
$H_{WC-Co} = \dfrac{4100}{k'\sqrt{\dfrac{\lambda}{2\sqrt{d_{WC}}}+1}} - 130$	(1.18)	H_{WC-Co} - hardness of WC-Co λ -mean free path in Co k' – constant (= 22.3 mm$^{-1/4}$)	Makhele, 2001	[99]
6% Co HV30 = 970 + 540 $d_{WC}^{-1/2}$	(1.19)		Roebuck, 2006	[97]
10% Co HV30 = 850 + 485 $d_{WC}^{-1/2}$	(1.20)			
6% Co HV30 = 1538 + 742log$_{10}$ d_{WC}	(1.21)			
10% Co HV30 = 1391+ 598log$_{10}$ d_{WC}	(1.22)			

Roebuck [97] proposed empirical expressions for the dependence of HV30 on d_{WC} in WC composites with 6 and 10 wt.% Co. Eq.s 1.19 and 1.20 based on the Hall-Petch relation, whereas Eq.s 1.21 and 1.22 supposed a logarithmic dependence. The logarithmic expressions tended to give a better fit at fine and coarse WC grain sizes, although all expressions were reasonable in fit for the middle of the grain size range [97].

1.4.3. **E**lastic **m**odulus

Many theoretical models have been developed to describe and predict the elastic properties of two-phase materials. All these models assume that the two-phase materials are homogeneous on a scale much larger than the size of inclusions, and that the displacements and stresses at the interface between the two phases are continuous. Most models can predict the elastic properties of two-phase materials simply by knowing the elastic properties of each constituent. Under an uniform strain assumption, as proposed long ago by Voigt [100], the elastic modulus, *E,* of the two-phase material can be estimated by Eq. 1.23 (Table 1.8). The effect of pores on the estimated elastic constants is ignored, when the porosity amount in the composites is lower than 1.5%. Under an uniform stress assumption as proposed by Reuss [101], the elastic modulus of the two-phase material can be expressed by Eq. 1.24 (Table 1.8). The values predicted by Eqs. (1.23) and (1.24) are frequently treated as the upper bound and lower bound of the elastic modulus of two-phase materials, respectively [102,103]. For dense materials these expressions do not present any dependence on microstructural parameters, besides the volume fraction of each phase (Table 1.6 and 1.8).

Table 1.8.

Expressions for estimating the Young's modulus of two-phase materials.

Expressions	**Eq.**	**Parameters**	**Ref.**
$E_c^u = E_a V_a + E_b V_b$	(1.23)	V_a – volume fraction of phase a V_b - volume fraction of phase b E_a – Young's modulus of phase a	[100,101]
$E_c^l = \frac{E_a E_b}{E_a V_b + E_b V_a}$	(1.24)	E_b - Young's modulus of phase b E_c^u – upper bound Young's modulus	[102,103]
$V_a + V_b = 1$	(1.25)	E_c^l – lower bound Young's modulus	

1.4.4. **T**ransverse **r**upture **s**trength

Transverse rupture strength (TRS) is another important mechanical property of tungsten carbide. Because of its extreme hardness, carbide does not respond well to the tensile test used to determine the strength of molten metal products. The transverse rupture strength can be regarded as the mechanical shock resistance of specimens during machining. In the transverse rupture test a rectangular test bar is placed across two sintered carbide support cylinders, and a gradually increasing load is applied by a third carbide cylinder at the midpoint between the supports. Transverse rupture strength is determined from the dimensions of the test bar, the distance between the supports, and the fracture load. The strength of cemented carbides is influenced by the binder phase content, carbide grain size distribution, contiguity and mean binder free path, as qualitatively represented in Table 1.6 [18]. Unreacted free carbon and porosity also influence strength [18].

Strength has been reported [12] as an inadequately defined property because it is related to the size of the fracture-initiating crack which is affected by local inhomogeneities, processing defects and foreign particles, resulting in a large scatter of experimental data. The fracture toughness is in this case more indicative of the potential strength of the composite.

1.4.5. **C**ompressive **s**trength

One of the unique properties of cemented carbides is their high compressive strength. Uniaxial compression tests can be performed on straight cylindrical samples or on cylinders having reduced diameters in the middle to localize the fracture. The ductility of cemented carbides is generally low at room temperature and so there is little difference between their yield strength and fracture strength. At higher temperatures, however, these materials exhibit a small but finite amount of ductility. Measurement of yield strength is therefore more appropriate at elevated temperatures.

Like hardness, the compressive yield strengths of cemented carbides decrease monotonically with increasing temperature; the rate of decrease depends on the composition and microstructure [5].

1.4.6. Fracture **t**oughness

Fracture toughness is less sensitive than transverse rupture strength to extrinsic factors such as specimen size, geometry and surface finish. Fracture toughness is measured by the critical stress intensity factor (normally named K_{IC}), which indicates the resistance of a material to fracture in the presence of a sharp crack and thus provides a better measure of the intrinsic strength of the cemented carbide than transverse rupture strength.

The parameter K_{IC} permits a comparison with many other materials and is checked fairly readily with a commercial microhardness tester and optical microscope [95]. This method is particularly useful when applied to brittle materials with low K_{IC}, since it is simple, fast and requires small testing areas.

The calculation of toughness, which is based on values of load (P) and crack length (c or l) depends on the shape of the crack. When the crack is developed only at the corners of the indent, called a Palmqvist type of crack (type Pq), the expressions for toughness link the applied load to the half diagonal, a, of the indent and the crack length, *l,* measured from the edge of the indent, Fig. 1.23 (3). However, when the indentation process generates a crack under the indent, called a median type of crack (type M), Fig. 1.23 (2), the relationships shows a dependence between the ratio of the applied load and crack length *c*, measured at the middle of the indent. The two types of crack are schematically shown in Fig. 1.23.

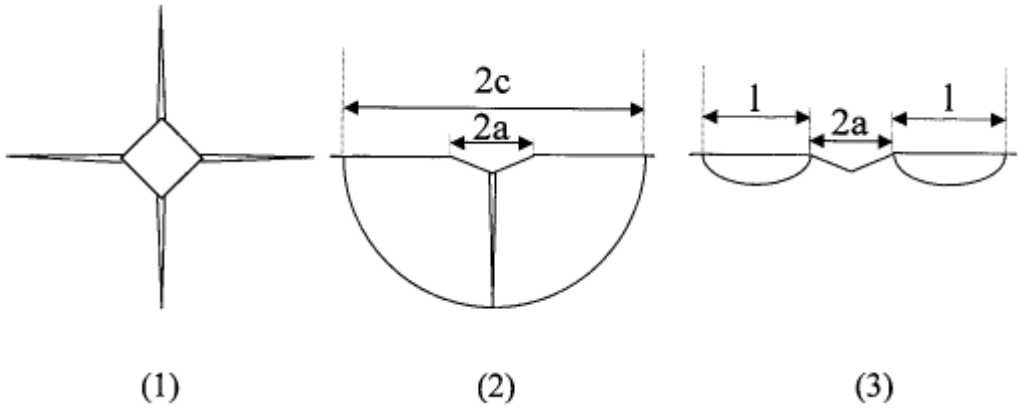

Fig. 1.23. Schematic of Vickers indentation cracks. (1) appearance of indented surface; (2) cross-sectional view of median/radial cracks; (3) Palmqvist cracks [104].

In general, the median crack type of failure is encountered in materials that present low toughness values; high toughness materials generally exhibit a Palmqvist type of failure. Equations for fracture toughness calculation were obtained in three different ways. The first way considers median cracks, the second way considers Palmqvist cracks as semi-elliptical cracks and the third way is based on empirical curve-fitting technique (Table 1.9).

Table 1.9.

Expressions for fracture toughness (K_{IC}) calculation from Vickers indentation crack systems.

Expression	**Eq.**	**Parameters**	**Author, Year**	**Ref.**
Median crack system		K_{IC} –Fracture toughness E – Young's modulus HV – Vickers Hardness P – applied load c – median crack length		
$K_{IC} = 0.016\sqrt{\frac{E}{Hv}} \times \frac{P}{c^{3/2}}$	(1.26)		Anstis, 1981	[105]
$K_{IC} = 0.0725\frac{P}{c^{3/2}}$	(1.27)		Tanaka,1987	[106]
Palmqvist crack system		a – indent half diagonal l – Palmqvist crack length		
$K_{IC} = 0.0089\left(\frac{E}{Hv}\right)^{2/5}\frac{P}{a\sqrt{l}}$	(1.28)		Niihara,1983	[107]
$K_{IC} = 0.015\left(\frac{E}{Hv}\right)^{2/3}\frac{P}{a\sqrt{l}}$	(1.29)		Laugier, 1987	[108]
Curve fitting technique				
$K_{IC} = 0.0889\sqrt{\frac{Hv \times P}{4l}}$	(1.30)		Shetty, 1985	[109]
$K_{IC} = 0.087\ \sqrt{HW}$	(1.31)	$W = P/L_T$, L_T - total length of cracks	Ponton, 1989	[110]

Anstis et al. [105] employed a simplified two-dimensional fracture mechanics model (Eq. 1.26), with *P* in Newtons, *c* in meters, *E* and *H* in GPa. Tanaka [106] also developed a simplified expression based in the median crack system (Eq. 1.27 in Table 1.9). Niihara et al. [107] and Laugier [108] developed expressions for Palmqvist crack configurations, Eq.s 1.28 and 1.29, respectively. Simplified expressions were developed by Shetty and Ponton (Eq.s 1.30 and 1.31) using the curve fitting technique (Table 1.9).

Crack length measurement and surface preparation are the most important contributions to the uncertainty in the measure of K_{IC} using the Palmqvist method. It is important to generate a crack long enough to sample a significant volume of microstructure, and the definition of "total crack length" may be difficult where cracking neighbourhood either is discontinuous, or multiple cracking occurs [111]. The scatter in the measurement of total crack length diminishes for lower binder content, smaller grain size and higher hardness [111]. Another feature of the Palmqvist method is the assumption of an absence of residual stress at the surface [111].

There are four different types of fracture in WC-Co composites [11,112]:

- transgranular fracture of the carbide crystals (W/C),
- interfacial fracture of the carbide crystals (WC/WC);
- fracture following the interface carbide-cobalt (WC/Co);
- transgranular fracture of the cobalt phase (Co/Co).

In WC-Co systems with high Co contents the fracture has been found to occur mainly by the ductile rupture Co/Co, while the first three mechanisms occur essentially at low volume fractions of Co binder because the contiguity of WC is higher [60]. Fracture toughness is strongly controlled by the contiguity of the carbide phase, which is supported by the role played in fracture by the joints between tungsten carbide crystals [11]. Regarding the relative proportion of each type of fracture for low binder amounts, the most important mode is the fracture following the interface WC/WC [11].

The values reported by Chermant et al. [11] for K_{IC} using three-point bending test show the dependence on the volume fraction of cobalt (Fig. 1.24). For a given grain size a steady increase of K_{IC} with increasing volume fraction of cobalt is observed. This is expected if the critical stress intensity factor represents the resistance to crack propagation; its value must increase with the ductility of the material. The influence of the mean diameter of the carbide crystals appears to be more marked when the volume fraction of cobalt increases, and it is the material with the coarsest grain sizes which are the toughest [11,113]. In addition, higher toughness has been suggested to result from the increased contiguity of Co binder, which minimizes the fracture along weak WC/WC boundaries [2]. For a given volume fraction, geometrical arrangement of the ductile binder as a continuous thin matrix phase is beneficial for high toughness while retaining high strength.

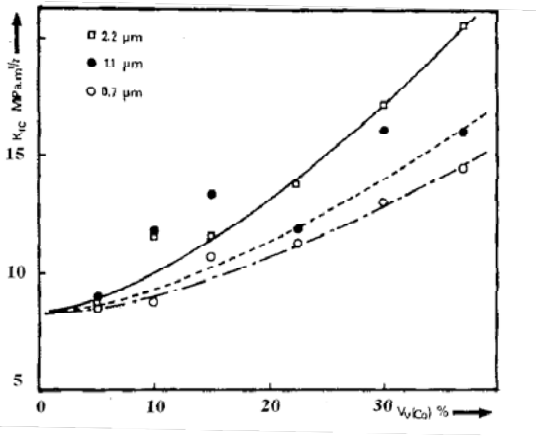

Fig. 1.24. Variation of K_{IC} with the volume fraction of cobalt and carbide grain size [11].

The qualitative dependence of the toughness on the main microstructural parameters is presented in Table 1.6. The correlation between K_{IC} and other mechanical properties was investigated by Chermant et al. and Richter et al. [11,113]. The decrease of K_{IC} with hardness increase was foreseeable: the harder a material the more brittle it is. It can be stated, however, that the hardness is still sensitive to the mean diameter of the tungsten carbide crystals. For a given hardness it is the material with the smallest grain sizes which is the toughest. The material exhibiting most wear is that with the highest volume fraction of cobalt. This is in agreement with the fact that the harder the material, the smaller is K_{IC} and consequently the wear resistance [11].

1.4.7. **A**brasion **r**esistance

Abrasion resistance is a standard test and does not correspond directly to wear resistance in machining operations. Abrasion resistance is directly related to hardness in tungsten carbide/ cobalt systems and is a function of the cobalt binder metal content and the tungsten carbide grain size. The lower the binder content and the finer the WC grain size, the harder and more abrasion resistant is the final product [114]. The abrasion resistance can also be improved by strengthening the binder by alloying and by heat treatments [114,45]. Nickel binder grades have lower abrasion resistance than comparable cobalt binder grades [18,5]. However, iron-nickel bonded tungsten carbide materials (iron rich binders) have superior abrasion resistance when compared with WC-Co compositions [45].

1.4.8. **C**orrosion and **o**xidation **r**esistance

In corrosive attack of cemented carbides, the tungsten carbide component is not usually affected. The binder metal corrodes, exposing the angular tungsten carbide grades and resulting in a roughened surface, which may cause tool wear or work material galling. To increase the corrosion resistance, less binder metal should be exposed to attack. This can be accomplished by using a finer tungsten carbide grain size and lower binder metal content [115]. Finer tungsten carbide grain size also yields more tungsten carbide surface area and results in a higher dissolved tungsten content in the binder metal, with improved corrosion resistance [115]. Frequently, nickel binder grades exhibit higher corrosion resistance than comparable cobalt binder grades. Small additions of chromium to both nickel and cobalt increase corrosion resistance, but cause embrittlement of the cemented carbide [18,5,115,116]. The metallic binders (Co, Ni) decrease oxidation rate of WC-based hardmetals compared to pure tungsten carbide in the temperature range of 500-800 ºC [15,117]. WC-Co is more oxidation resistant due to a fast formation of the protective complex oxide $CoWO_4$. WC-Ni is less oxidation-resistant since WO_3 is the main oxidation product, while NiO and $NiWO_4$ form to a lesser degree [15].

1.4.9. **M**agnetic **p**roperties

As WC is non-magnetic and cobalt is magnetic, measurements of magnetic saturation can be related to composition, and therefore used for quality control. Both carbon and tungsten go into solution in the cobalt. Carbon was found to have no effect on the magnetic saturation but increasing tungsten levels progressively reduced it [118]. At very low carbon levels, carbon is removed from the binder and is dissolved in non-magnetic eta-phase, which causes a sharp drop in the magnetic saturation [118].

The replacement of cobalt by nickel changes the testing philosophy. Cobalt has a Curie temperature of 1123 ºC and nickel has a much lower value of 358 ºC, which is rapidly depressed to 200 ºC by the solution of 12% tungsten [19]. The magnetic saturation will, therefore, be decreased by both the solution of tungsten the rapid decline of this property close to the Curie temperature [19]. Unlike cobalt, solution of carbon in nickel or Fe,Ni binders also causes a fall in the magnetic saturation [55].

1.4.10. **T**ypical **m**echanical **p**roperties **d**ata

In this section the values reported in the bibliography for the main mechanical properties (hardness, transverse rupture strength and fracture toughness) of cemented carbides with different binder compositions are compiled and analysed.

1.4.10.1. **C**obal**t b**inder

The first results presented in Table 1.10 concern the most frequent binder used in cemented carbides, the cobalt. Properties such as the high hardness, yield stress, toughness and strength of Co with its two allotropic modifications, a close-packed hexagonal (CPH) structure, ε, stable at temperatures below approximately 400 ºC, and a face centred cubic (FCC) form, α, stable at higher temperatures are behind the dominating use of Co in hardmetals [88,43]. The values of mechanical properties for different grain size (see Table 1.10) confirm that improved properties, namely hardness, TRS and compressive strength are obtained with decreasing grain size. The increase of the amount of binder decreases hardness, Young's modulus and abrasion resistance, but imparts the TRS of the hard metal. The lower the binder content and the finer the tungsten carbide grain size, the harder and more abrasion resistant is the final product.

Nowadays, the tendency to produce finer and finer hardmetals derives from the understanding that hardness and wear resistance both increase with decreasing grain size. To meet the requirements of the hardmetal industry and to follow the trend towards finer grain sized tools, very fine WC powders classified as nanopowder were developed by Gille et al. [88] using a new synthesis process. The properties of the composites obtained from those powders are listed in Table 1.10. Extremely high hardness values superior to HV 2000 were obtained in these composites for contents of binder lower than 10 wt.% Co.

Table 1.10.

Properties of representative cobalt-bonded cemented carbides [5,88].

Nominal composition	Average grain size (μm)	Density (g/cm^3)	Hardness HV	TRS (MPa)	CS[(a)] (MPa)	E (GPa)	K_c (N/mm)	Relative abrasion resistance[(b)]
97WC-3Co	Medium	15.3	1700	1590	5860	641	–	100
94WC-6Co	Fine	15.0	1700	1790	5930	614	–	100
	Medium	15.0	1650	2000	5450	648	–	58
	Coarse	15.0	1600	2210	5170	641	–	25
90WC-10Co	Fine	14.6	1600	3100	5170	620	–	22
	Coarse	14.5	1300	2760	4000	552	–	7
84WC-16Co	Fine	13.9	1350	3380	4070	524	–	5
	Coarse	13.9	1250	2900	3860	524	–	5
75WC-25Co	Medium	13.0	1000	2550	3100	483	–	3
94WC-6Co	0.1	14.83	2280	–	–	–	370	–
90WC-10Co	0.1	14.46	2043	–	–	–	530	–
88WC-12Co	0.1	14.30	1910	–	–	–	570	–
85WC-15Co	0.1	13.95	1700	–	–	–	725	–

[(a)]Compressive strength; [(b)]Based on a value of 100 for the most abrasion-resistant WC cemented carbide.

1.4.10.2. **I**ron, **N**ickel **b**ased **b**inders

Ni binders are used in special hardmetal applications, requiring high corrosion or oxidation resistance and in some wear applications. Because of the improved corrosion resistance of nickel and the enhanced erosion resistance to chemical attack over cobalt in wet environments, grades containing this binder are finding increasing usage [117].

The replacement of cobalt with increasing amounts of nickel resulted in a continuous linear fall in hardness (Table 1.11). The complete replacement has been reported to cause a decrease of 100-200 HV in the initial hardness values [119,120,38]. The lower hardness does, however, correspond to an increase in fracture toughness at any given volume fraction of WC [34]. The TRS is generally lower than WC-Co alloys of similar composition [38,34] (Table 1.11) though some authors reported that TRS values are not altered by the complete and partial replacement of cobalt with nickel [33,120]. The replacement of cobalt with nickel also leads to a considerable improvement in corrosion resistance. Minor additions of Cr_3C_2 (<0.6 wt.%) to WC-Ni were reported to raised the modulus of elasticity, hardness and TRS to values near that of WC-Co [19,38]. Additions of aluminium to nickel have also been reported to strength the WC-Ni hard metals [121].

Table 1.11.

Mechanical properties of Fe/Co/Ni and stainless steel (AISI 316) bonded cemented carbides.

Nominal composition	Average grain size (μm)	Density (g/cm^3)	Hardness HV	TRS (MPa)	K_c ($MPa.m^{1/2}$)	Ref.
80WC-20Co	1.20	—	1000	3380	16.8	[38]
80WC-20Ni	1.20	—	820	2600	—	[38]
80WC-20Fe	1.20	—	910	2190	—	[38]
80WC-16Fe,4Ni	1.20	—	980	2630	—	[38]
80WC-13Fe,4Ni,3Co	1.20	—	1020	3000	17.2	[38]
80WC-11Fe,3Ni,6Co	1.20	—	1100	3500	17.8	[38]
91WC-9Co	0.8	14.7	1608	—	—	[88]
91WC-6.8Fe,1.3Ni,0.9Co	0.8	14.6	1817	—	—	[88]
80WC-12Fe,4Ni,4Co	2.5	13.5	900	3510	—	[88]
90WC-8.7Fe,1Ni,0.3C	1.0	14.3	1603	—	10	[36]
90WC-8.7Fe,1Ni,0.3C*	1.0	14.3	1580	—	15	[36]
90WC-8.7Fe,1Ni,0.3C	4.0	14.3	1380	—	12	[36]
90WC-7.5Fe,2.3Ni,0.2C**	3.0	14.0	1340	—	23	[122]
90WC-7.7Fe,2.2Ni,0.1C**	3.0	___	1200	—	17	[56]
94WC-6SS	4.1	14.8	1700	1210	9.3	[123]
91WC-9SS	4.5	14.5	1625	1330	10.5	[123]
88WC-12SS	5.1	14.0	1421	1650	12.1	[123]
85WC-15SS	5.4	13.6	1301	1990	14.9	[123]

*Heat treated at 800ºC; **Martensitic Transformation

The complete replacement of Co for a Fe binder also results in a decrease of hardness as well as TRS (Table 1.11), due to the formation of ferritic BCC structures and an increased risk of forming η-phase double carbides [57,30]. Besides that, it is not attractive from the aesthetic point of view because of possible rusting [38,30]. However, the abrasive wear resistance of the iron bonded hardmetal is better than that of WC-Co [38]. Attention has been made on iron plus nickel which results in binder structures varying from BCC/martensite to FCC/austenite, thus giving a range of properties from high strength/high hardness to high ductility [122,56]. According to Moskowitz et al. [30] the Fe-Ni binders have hardness values comparable to that of WC-Co and better abrasion resistance, even though the TRS is smaller, as shown in Table 1.11. Fe-Ni bonded WC materials have not yet been commercially applied, despite the fact that they are superior to the cobalt-bonded variety in resistance to abrasive wear [30]. The Fe-Ni binder phase is mainly austenitic

with restricted mechanical properties. However, additions of carbon to the binder Fe-Ni can improve the hardness and wear resistance, due to the formation of martensite phase [45].

Alloying the Fe-Ni binder with Co allows structural changes in the binder phase leading to hardmetals with better properties (Table 1.11). In the late 1970's, Prakash [38] made the first, well-founded investigations on a broad range of WC hard metals containing a 20 wt.% Fe-Co-Ni alloy as binder. The results show that properties of the WC-Fe/Co/Ni can be varied in a wide range, since the binder phase can exist in the BCC -structures or structures near to the BCC/FCC-phase transformation depending on the composition and heat treatment. These hard materials were reported to be superior to conventional WC-Co hard metals in hardness and abrasion resistance, with slightly inferior transverse rupture strengths (TRSs) (see Table 1.11). Gille et al. [88] developed prealloyed (Fe/Co/Ni) powders to bond WC particles. Two compositions have been prepared, a Co-rich binder (60Co/20Ni/20Fe) and a Fe-rich binder (75Fe/15Ni/10Co). Using WC-Co as reference material, hardmetals with Fe-rich binder are higher in hardness, while Co-rich bound hardmetals are lower in hardness but higher in toughness (Table 1.11). This is due to the dominating FCC lattice structure of these binder types which have a more ductile behaviour with lower yield stress and reduced work hardening.

The carbon was found to exert a critical influence on properties. The control of carbon content is very important in these binders, because changes in carbon content not only influence the BCC-to-FCC ratio but also the strength characteristics of each individual phase [34]. In order to understand the effect of Fe:Ni ratio and carbon content in mechanical properties Suzuki et al. [37] investigated fine (1.0 μm) WC-10 wt.% (Ni-Fe) compositions with different Ni:Fe ratios and carbon amounts. These authors [38] noticed that hardness of the alloys increased with increasing Fe content and reached a maximum at the binder composition of about 90 wt.% Fe in binder (see Fig. 1.25). TRS decreased with a small amount of Fe addition and did not change mostly in the range from 10 to 75 wt.% Fe. Thus, they concluded that the alloy with 75 wt.%Fe of binder composition exhibited the best combination of mechanical properties. However, the strength was much lower than that of WC-Co alloys.

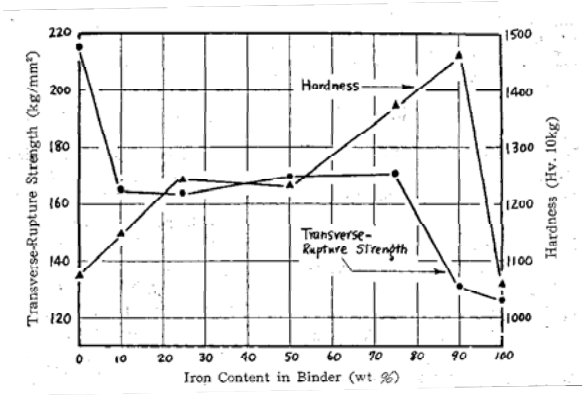

Fig. 1.25. Transverse rupture strength and hardness vs. binder content of iron-bonded WC in high carbon alloys [37].

More recently, Updhyaya et al. [29] investigated the sintering of submicron (0.78 μm) WC-10 wt.% Co hard metals, after partial or complete substitution of binder by nickel or iron. These authors [29] reported similar conclusions, namely:

- the densification and mechanical properties of submicron WC-10wt.% Co hard metals deteriorate on increase in the substitution level of binder by nickel (Fig. 1.26);
- complete cobalt substitution in WC-10 wt.%Co hard metal by Ni-Fe binder imparts better properties compared with substitution by either iron or nickel;
- the grain size of the carbide phase increases with increasing the nickel content in the binder. In contrast, the grain size remains almost the same for the WC-10 wt.% (Ni-Fe) hard metals over the whole composition range (Fig. 1.26);
- the oxidation resistance of WC-10 wt.% Co hard metal decreases on substitution of the cobalt binder by nickel.

González et al. [36] also studied the influence of carbon additions during liquid phase sintering of WC-(Fe,Ni,C). The metallic binder under study represents 10 wt.% of the hardmetal itself, and contains 10 wt.% of Ni and C amounts up to 3.5 wt.%. The relationship between hardness and toughness and WC grain size in these hardmetals has shown to be similar to that in the traditional WC-Co system. The effect of isothermal heat treatments which bring about a modification of the microstructure of the metallic binder was also explored. The results proved that these treatments could be beneficial to increase toughness without an appreciable influence on hardness (see Table 1.11). Others studies [122,56,55] also pointed to the fracture toughness increase without significant difference in hardness (Table 1.11) caused by martensitic transformation.

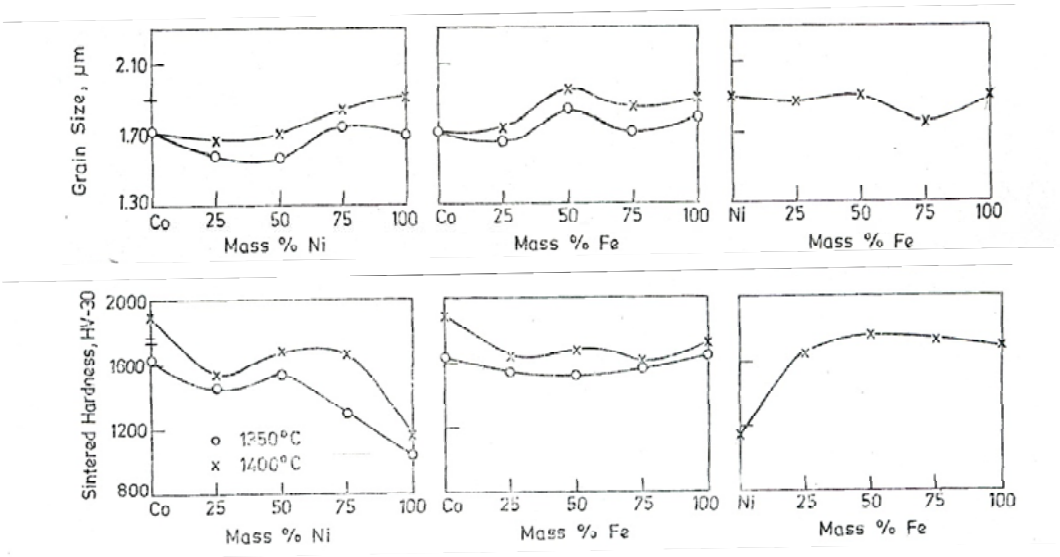

Fig. 1.26. Vickers' hardness plots and variations in grain size of WC-10 wt.%(Co-Ni-Fe) hard metals, sintered at 1350 and 1400 ºC, for 1h in dry hydrogen [29].

Stainless steel (AISI 316) in various compositions (between 6 and 15 wt.%) were chosen by Farroq et al. [123] as the binder phase for the cemented carbides based on tungsten carbide. The excellent bonding achieved with this binder was related to the macrohardness of the densified products which was found to be in the range 1300 to 1700 Hv (kg/mm^2) (Table 1.11). The increasing of binder content increases the transverse rupture strength values and the fracture toughness (K_{Ic}). The fracture toughness, calculated using the Palmqvist indentation method, is in the range 9-15 MPa.m$^{1/2}$ which is within the normal range of WC-Co hardmetals (see Fig. 1.26).

1.4.10.3. **S**econdary **C**arbides

Secondary carbides are added to the WC-base composite primarily to inhibit grain growth during sintering without substantial recrystallization. They also increase hardness, fracture toughness and wear resistance and enhance corrosion resistance. To achieve the optimum benefit of secondary carbides, they must be added as oxides before the carburization process, must be in solid solution and must be evenly distributed around grain boundaries [35,4].

Cemented carbides can contain relatively large amounts of TiC, TaC, NbC in addition to cobalt and WC. At sintering temperatures these carbides dissolve tungsten to a great

extent, forming solid solutions most often referred to as γ phase [43,23]. The predominant carbides in these cemented carbides, i.e. the hexagonal WC and the cubic γ phase, dissolve very little cobalt, iron and nickel. Thus the equilibrium conditions prevailing are not very much influenced by the addition of these elements unless new phases, for instance the η carbides, $(Co,Fe,Ni,W)_6C$ are formed.

The most significant contribution of titanium carbide in a carbide cutting tool is the reduction of the tendency of welding to machined or adhere to the cutting edge [76]. The increase of titanium carbide content in alloyed tungsten carbide grades also results in greater resistance to cratering, higher hot hardness, higher wear resistance and lower strength, in spite of the reduction of transverse rupture strength [4].

The additions of tantalum in carbide cutting tool applications prolong tool life in cutting operations of materials such as steel, which yield long, continuous chips. Small additions of tantalum carbide to tungsten carbide/ cobalt alloys (up to 2%) inhibit recrystallization of the carbide phase; therefore, the resulting alloys generally have a finer grain size and higher hardness than the corresponding compositions that do not contain tantalum carbide. Such alloys also permit wider sintering ranges and are less sensitive to oversintering [18]. The increase of tantalum carbide content in alloyed tungsten carbide grades, over 4%, results in greater resistance to thermal deformation and cratering, higher hot hardness, lower strength and lower wear resistance [4]. Tantalum carbide is often added as (Ta, Nb)C because the chemical similarity between TaC and NbC makes their separation expensive. Fortunally, NbC has an effect similar to TaC in most cases [76].

Many commercial grade carbides contain titanium carbide and tantalum carbide. As described above, addition of titanium carbide has an adverse effect on transverse-rupture strength, but additions of tantalum carbide to tungsten carbide/ titanium carbide/ cobalt alloys result in higher transverse-rupture strength at cutting temperature. This improvement is attributed to the ability of tantalum carbide to form pure solid solutions and to inhibit the grain growth of the carbide phase.

The carbide Cr_3C_2, besides a grain growth inhibitor also increases the corrosion resistance and the transverse rupture strength at high temperature. This is because Cr_3C_2 prevents the transformation from α-cobalt (FCC) to ε-cobalt (HCP), thus improving the ductility of the hard alloys [76].

1.5. **E**merging **t**echnologies for **c**emented **c**arbide **p**roduction

Currently, research is aimed at developing grades having improved wear, corrosion and oxidation resistance by developing new cemented carbides and new production processes. Furthermore, future technology aims the attainment of more reliable, economic and environment friendly processes.

The research in new cemented carbide materials includes nanocrystalline (≤100 nm) composites; WC-aluminides and matrix free carbides that will be below briefly described.

Nanocrystalline composites: Composites of nanosized WC-Co and WC-Ni particles are currently synthesized using sol-gel, rapid carbothermal reduction, spray-conversion and inert-gas condensation [35]. Benefits of this approach include shorter sintering cycles, ultrahigh purity, a final composition that can be tailored even in the precursor stage and precise control of composition.

Nanostructured cemented carbides present higher hardness than the conventional ones that result not only from the ultra fine microstructure, but also from the alloy-strengthening of the binder phase [27,2]. The increase of hardness in nanostructured composites does not decrease their bulk fracture toughness, while in conventional composites the toughness decreases with increasing hardness [27,2].There is a significant difference in the binder phase of conventional and nanostructured composites. Nanostructured composites have a higher tungsten content in the binder phase than conventional ones. This not only increases the volume fraction of the binder phase in the nanostructured composite but also raises the ratio of FCC/HCP cobalt. The small size of the WC grains in the nanostructured composite promotes the solubility of WC in both liquid and solid cobalt, which stabilizes the FCC phase of cobalt during cooling from sintering [27].

In spite of these benefits, high cost and grain growth during sintering are delaying the rapid transition of nanocrystalline WC-base composites from the laboratory to commercial production. These materials are expected to become more competitive as production processes are further improved and larger quantities of nanosized constituents become commercially available.

WC-aluminide matrix composites: Nickel aluminides (Ni_3Al) and NiAl) and iron aluminides (Fe_3Al and FeAl) are being considered as binder materials for WC composites in high-temperature, extremely corrosive applications. The yield strength of Ni_3Al increases with increasing temperature. This property could be beneficial for cutting tool applications in which tools experience rapid temperature increases that weaken conventional WC-Co composites. WC-nickel aluminide composites (maximum of 90 wt.% WC) also have good tensile ductility, an order of magnitude better resistance to corrosion in sulphuric and nitric acids and fracture toughness comparable to both WC-Co and WC-Ni composites. WC-iron aluminide composites (maximum of 81 wt.% WC) provide excellent resistance to sulfidation and oxidation and would be useful in applications in the gas/oil and coal industries. Further research is aimed at increasing the WC content in these materials and improving creep strength and low-temperature ductility in air.

Matrix-free carbide composites: A matrix-free or binderless-carbide composite consists of ultrafine WC and secondary carbides [124]. It takes advantage of the very good corrosion resistance of monolithic WC, which is somewhat compromised with the addition of lower melting-point cobalt and nickel matrix material. These composites are extremely hard and brittle and resist abrasion, wear and corrosion. Because they cannot tolerate even the slightest shock loads, binderless carbides can be used in parts having very little or no impact.

On the other hand, new processes under research for future hardmetal technology include powder coating techniques, near-net-shaping processes (hot extrusion and powder injection molding) and new sintering technologies. From these, powder coating techniques will be reviewed ahead, in a separated section, due to the importance of this topic in the present research.

Hot extrusion: Fully dense complex shapes can be made by hot-extruding powder, a process that eliminates both the need to sinter green compacts to full density and the need for subsequent HIP. Hot-extrusion of powder could be useful in fabricating composite rolls consisting of a steel core (80%) and metallurgically bonded carbide sleeve (20%).

Powder Injection Moulding: Powder injection moulding (PIM) is a relatively new but increasingly popular technique for shaping hardmetals into complex, near-net-shape parts. The process of PIM has some similarities with plastic injection moulding, but also major

differences [125]. It starts with the mixing of an organic binder with the desired grade of powder to form a relatively homogeneous feedstock. This can be moulded into complex shapes by forcing it into a carefully designed oversized die cavity, producing green compacts which, during later sintering, will shrink to the dimensions of the final part [125]. Some major advantages of the PIM process over the performing approach were said to be [126,125]: (i) PIM typically provides better yields, depending on the size and shape complexity of the part; (ii) it can eliminate such secondary operations as milling and reduce set-up time for machine operations; (iii) PIM can provide net shape or closer near-net shapes when compared to performing, reducing the amount of stock to be removed by grinding; (iv) PIM is the best process for creating intricate internal geometries.

In spite of all these advantages, the job-shop manufacture of complex shaped cemented tungsten carbides by PIM has been extremely limited, with only a handful number of companies being involved [126]. Reports [127] have surfaced that PIM makes up about 1% of all the carbide production. The causes are related with a relatively small market for highly complex shaped carbides and the low volume requirements of this industry [126]. Therefore, PIM of hardmetals remained a small niche market segment with few companies being major players.

New sintering technologies: The current trend in the hardmetal industry to finer and finer-grained alloys require high demands on the manufacturing process [128]. Therefore, rapid densification technologies which consolidate the composite to near theoretical densities in minutes versus the traditional processes that takes hours have been developed. Accelerated densification has been reported in spark plasma sintering (SPS) [128] and plasma activated sintering (PAS) [2] which are in principle similar to plasma pressure compaction (P^2C) [129]. The SPS is similar to hot-pressing to the extent that graphite dies are used, but the heating is accomplished by spark discharges in voids between the particles, generated by an instantaneous pulsed direct current which is applied through electrodes at the top and bottom punches of the graphite die. Due to these discharges, the particle surface is activated and purified, and a self-heating phenomenon is generated between the particles, as a result of which heat-transfer and mass transfer can be completed instantaneously [128,130]. The PAS and P^2C achieved densification by a combination of

resistance heating with external pressure application and plasma generation among the powder particles [2,131,96].

Selective laser sintering (SLS) is a rapid prototyping process that allows generating complex 3D parts by consolidating successive layers of powder material on top of each other [132,133,134].The solidification is obtained by fusing or sintering selected areas of the successive powder layers using thermal energy supplied through a laser beam. Successful results have been obtained in the production of sintered carbide or hard metal parts through SLS [135,136]. Due to the low powder density and short sintering time, the most important difference between classic liquid phase sintering and the bonding in SLS is that only the rearrangement stage occurs during the laser heating. This results in a large degree of porosity and hence poor mechanical properties of the "green part". Therefore, a post treatment consisting of a furnace post-sintering, hot isostatic pressing (HIP) or an infiltration with a low melting point metal (e.g. copper or bronze) is usually necessary [135].

Other fast consolidation technique of hardmetals, that start to be investigated 10 years ago, is the microwave sintering [137,138]. Microwave heating is fundamentally different from conventional heating. The source of the heating in the microwave oven is oscillations of the free electrons at high frequency microwave (2.45 GHz) in binder and in free carbon, and of ions in WC [139,138]. The heating is very rapid (> 400ºC/min) as the material is heated by energy conversion rather than by energy transfer, which occurs in conventional techniques. Microwave heating has many advantages over conventional heating methods; some of these advantages include, time and energy saving, considerably shorter processing times and lower sintering temperatures, fine microstructures with reduced grain growth and hence improved mechanical properties and additionally it is an environmental friendly process [137,139,138].

1.5.1. WC **p**owder **c**oating **p**rocesses

Coated powders offer a variety of interesting characteristics, where the essential properties of the powder or the final product can be influenced by a specific coating layer. The coating of the matrix particles by a second component may be used for protection of the core material towards a reactive environment, intentional arrangement of electrically conductive or non conductive outer-layers, hydrophilic or hydrophobic behaviour, colour effects, or design of controlled microstructures [140].

Enhanced processing and final properties have been reported for many systems, such as Ni coated Al_2O_3 [141] and Al_2O_3 coating silicon based powders [142,143]. Improvement of handling characteristics, green density and sintering activity was observed in coated powders, whereas increased mechanical properties were attained in the sintered bodies [141,143,142]. Furthermore, in the specific case of hardmetal powders, the coating of WC with the ductile phase may overcome some of the limitations/disadvantages of the traditional mixing/milling step, namely:

a) fine particulate dust is produced when mixing/milling cobalt, which is a health and environmental hazard;
b) milling takes a long time and much energy to produce an adequate mixture of proper particle size and homogeneity;
c) longer milling times increase impurity levels in the powder blend;
d) there is a limit on the degree of homogeneity which can be attained.

One of the initial experiments on WC particles coating was carried out in fluidised-bed reactors, where the individual particles were suspended in a gas stream with high particle concentrations. This method was not very successful, leading to agglomerated structures and non-uniform coatings and it was not found more detailed information [140]. Other reported coating methods applied to WC powders are summarized in Table 1.12. Chemical processes like electroless nickel were also investigated by Vélez et al. [144], which consists in an auto-catalytic reaction used to deposit a coating of Ni-B on WC powders (1 μm) (Table 1.12). However, the heating of this composites form the carbide (Ni_2W_4C) probably due to decarburization during the deposition process. The chemical precipitation technique, Table 1.12, was reported [129] to produce uniform coating of Co (6 wt.%) on individual WC particles (8 μm) and a better control of the chemical composition.

Table 1.12.

Prior work on coating of tungsten carbide particles.

WC particle size (μm)	Coating	Wt.%	Method	Year	Ref.
1	Ni-B	15	Electroless	1999	[144]
8	Co	6	Chemical precipitation	2002	[129]
6	Co-TiC-Al_2O_3	45	Mechanical coating	2002	[145]
20	Pt	0.01	Ion beam sputter deposition	2003	[146]
__	Co	___	Chemical vapour deposition	2004	[126]

The mechanical coating of WC particles by high-speed rotational impact blending was investigated by Kangwantrakool et al. [130,145]. The coating chamber is surrounded by a jacket in which a coolant is circulating (Fig. 1.27). This processing can be summarized as follows: particles inside the casing of Hybridizer (HYB) are mixed and circulated in a high-speed air stream caused by a rotor, being hit repeatedly among other particles, the wall of a stator and the blades of the rotor. As a result of these mechanical actions, small particles become fixed on the large ones. The authors [130,145] concluded that with the same composition of 55WC-10Co-30TiC-5Al_2O_3 (Table 1.12), the HYB yields a more uniformly dispersed microstructure and higher mechanical properties in comparison with ordinary ball milling.

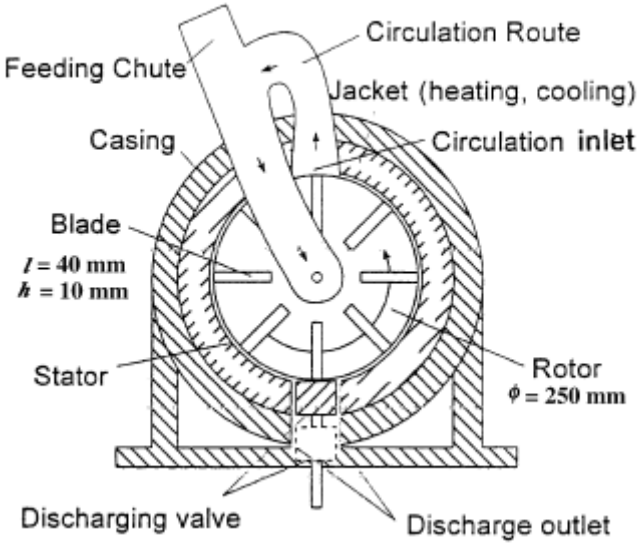

Fig. 1.27. Apparatus for coating particles by rotational impact blending [145,130].

More recently, tungsten carbide powders (20 μm) have been coated with Pt using ion beam sputter deposition for electrocatalytic applications, Table 1.12 [146,147]. The target chamber for ion beam sputter deposition used by Ensinger et al., hosting the sputter target and the powder substrate to be coated, is represented in Fig. 1.28 [146]. The sputter target, either a flat metal strip or a hemisphere, is located at the inner rearside. The powder, typically several hundred mg, was placed in the lower part of the vessel [146]. This system is very limited in terms of quantity of coated powders produced, amount of binder deposited and powder grain size (>20 μm).

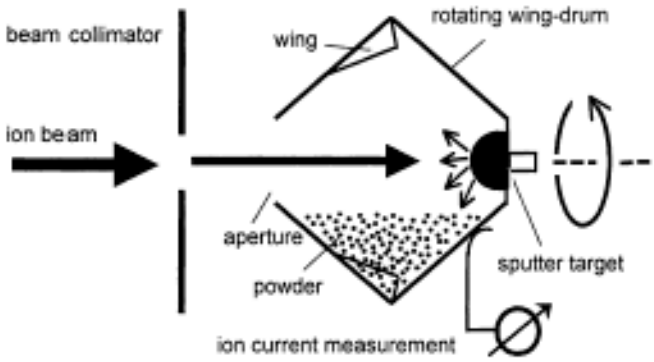

Fig. 1.28. Schematic presentation of set-up for ion beam sputter coating powder [146].

New reactors were developed to produce tough-coated hard powders (TCHP) by chemical vapour deposition (CVD), taking into attention that the coating process depends critically on the ability to separate each particle from its neighbour and the efficiency of maintaining this separation during all the process. These TCHP have already been produced in industrial quantities, and the powders have been consolidated by hot pressing and HIP [126,148]. However, very little information is available and a great deal of field testing is still to be done [126].

The sputter deposition technique is a potential technique for particle surface coating. The usual application of this technique in the coating of monolithic materials showed that a larger variety of materials can be sputtered on different substrates leading to chemically uniform thin coatings with a generally high adhesion, variable coating structures and morphology, largely improving the chemical, thermal and tribological properties [149]. However, the coating of powders requires specific instrumental set-ups to allow the exposition of all the particle surfaces to sputtering, avoiding agglomeration effects. This is

not easy to attain and only few attempts, apart from the one reported before for WC coated with Pt [146] have been recently report for different powder systems [150,151,152]. One of these reports [150] is related to a sputtering equipment (with a hexagonal barrel instead of a cylindrical one) where spherical polymer particles were homogeneously coated with metal films (Au, Ag, Pd, Cu and Ni). Pd coatings were also deposited in a ZrNi powder (500 μm) using a similar Barrel-Sputtering System [152]. An RF sputtering system was also developed to coat Al_2O_3 ceramic particles (20 μm) [151].

In this work, sputtering was used to coat WC powders with steel binders in a modified sputtering equipment, specially developed for this use, as described ahead, in the experimental chapter. Other powders were also successfully coated in the same equipment, such as $Ti_{52}Al_{48}$, $Ti_{80}Al_{20}$, $Ti_{62.5}Si_{37}$ and $Ti_{85}Si_{15}$ with Al and Ti [153] and stainless steel (316L). Reports relatively to the processment and final properties benefits of those powders have been published [153,154,155]. The manufacturing of sputter-deposited powders is already performed for NiB coarse particle powders (>50 μm) in Slovenia.

In the next section the principles of sputtering and the structure and morphology of the sputtered coatings are briefly reviewed.

1.5.1.1 **S**putter **c**oating

Sputtering is the erosion of solid surfaces during ion bombardment [156,157]. In surface analysis, sputtering is used to clean samples and the ions are also used as the "probe" beam for the surface analytical methods known as secondary ion mass spectrometry (SIMS), ion scattering spectroscopy (ISS), direct recoil spectroscopy (DRS) and mass spectroscopy of recoiled ions (MSRI) [156]. Sputtering is also used to deposit thin films for different applications [156].

During sputtering, the bombarding ion transfers energy in collisions to target atoms which recoil with sufficient energy to generate other recoils. Some of these backward recoils will approach the surface with enough energy to escape from the solid. These secondary recoils make up most of the sputtered yield (quantity of material removed per incident ion) [157]. The sputter yield depend on a number of parameters, such as the incident ion flux, background pressure of the sputtering species, gas phase composition and

the raster size. In Fig. 1.29 it is represented the schematic principle of the sputtering deposition technique. In the literature, one can find sputter yield values spanning a range of seven orders of magnitude. For medium mass ion species, the sputtering yield is typically between 0.4 and 20 KeV[156].

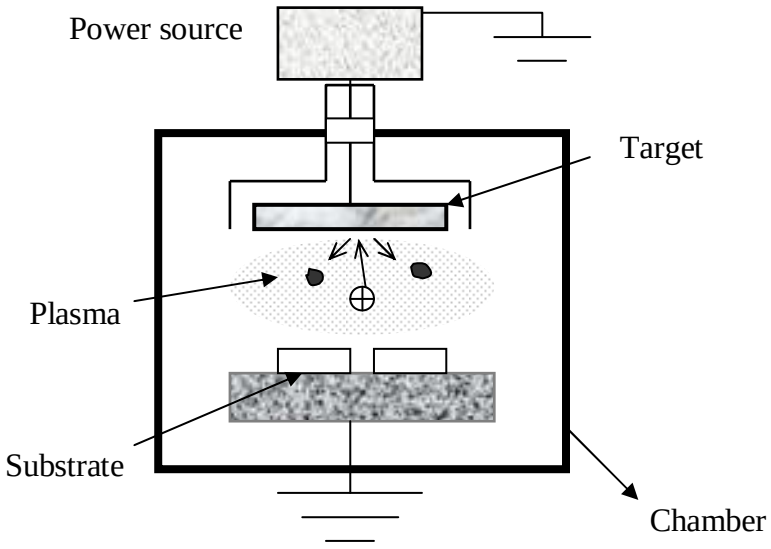

Fig. 1.29. Sputtering principles schematic representation.

A number of trends in sputtering are compiled from the literature by Smentkowski [156] namely these ones:

- As the mass of the sputtering species increases (for sputtering angle and sputtering energy is held constant), the sputtering yield increases.
- As the sputtering energy increases, the sputter yield increases up to ~10-100 eV.
- As the sputtering angle increases (θ increases from zero) the sputtering yield increases up to θ = 70-80º. At higher θ, the sputtering yield decreases towards zero. At grazing incidence, the repulsive action of the surface atoms prevents ions from penetrating into the target.
- The sputtering yield is different for different elements.
- Within a period of the periodic table, the sputtering rate increases as one goes from left to right (i.e., as the d shells fill with electrons).
- Light mass particles are preferentially ejected normal to the surface, while heavy mass particles are ejected (from the surface) at a grazing angle.

- The sputtering yield decreases as the surface damage increases. The sputtering yield of rough surfaces is lower than the sputtering yield of smooth surfaces.
- The temperature of the target affects the sputtering yield. At higher temperatures (~30% of the melting point) the sputter damage decreases and the sputtering yield remains high (surface continuously "anneals" itself). For sputtering at low temperatures, the sputtering yield is lower (the amount of surface damage is greater).
- For multicomponent samples, the lightest weight component is usually preferentially sputtered if the binding energies of the components are similar. The sputtering rate of each component increases as the reciprocal of the binding energy and mass of that component.

The structure of sputter coatings is largely determined by the substrate temperature and deposition rate [158,159,160]. For high substrate temperatures, the resulting structure is consistent with the appropriate equilibrium diagram. As the deposition temperature is lowered, the structure is increasingly subject to kinetic limitations, entering in a regime where two phase mixtures are infeasible and the deposit takes the structure of the most stable single phase which can exist for the particular alloy composition [161]. As the substrate temperature is lowered still further, an increasing proportion of amorphous phase is present in the coating, in accordance with the variation of that phase's stability with composition.

The effect of the deposition conditions on the structures and the properties of the metal films has been explained by structure zone models [162,163,164,165]. The model was first proposed by Movchan and Demchishin [162] for evaporated films of metals and oxides and expanded to sputtered films by Thornton [163,164] and Messier et al. [165]. Thornton [163] based the study in pressure effects, deposition temperature and pressure in a model (Fig. 1.30) that is now well accepted and describes the structures expected when a vapour condenses onto a substrate. It demonstrates how, at low temperatures (<0.3 T/T_m, where T_m is the melting point of the coating), porous, columnar structures are produced. As the temperature is increased, 0.3-0.7 T/T_m, higher density columnar structures are formed and above 0.7 T/T_m fine grained equiaxed structures are produced.

The substrate surface morphology have also a strong influence in the coating morphology, because for example very rough surfaces promote the growth of open columnar structures and this is a problem when depositing a coating onto a porous powder surface [166].

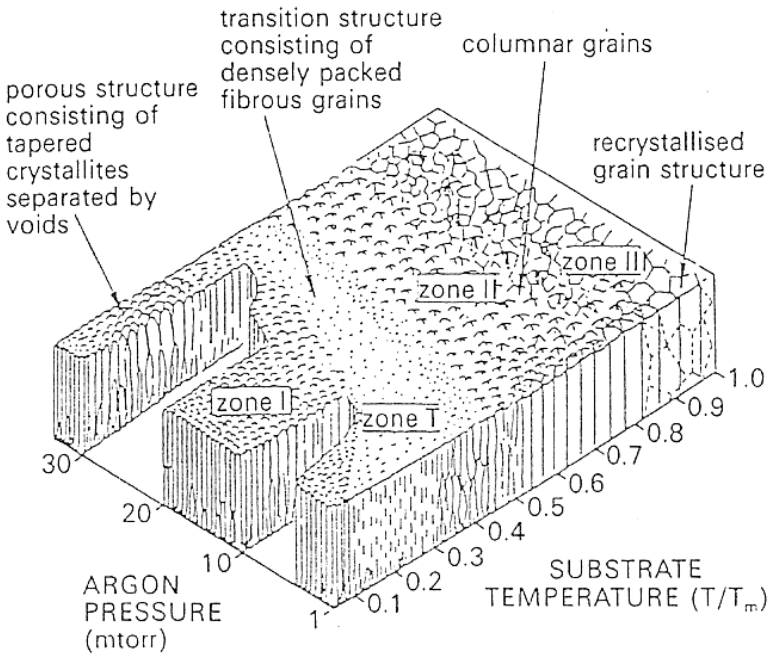

Fig. 1.30. Influence of temperature and pressure on coating structure [163].

1.6. References

[1] Pierson HO. Handbook of Refractory Carbides and Nitrides - Properties, Characteristics, Processing and Applications. *Westwood, New Jersey, U.S.A., Noyes Publications* 1996.

[2] Yao Z, Stiglich JJ and Sudarshan TS. Nano-grained tungsten carbide-cobalt (WC/Co). *Materials Modification* 1999; 1-27.

[3] Friederich KM and Exner HE. Metallographical investigations on tungsten carbide powders. *Praktische-Metallographie* 1984; 21(7): 334-341.

[4] Lardner E. Review of current hardmetal technology. *Hardmetal Technology* 1970; 122-132.

[5] Cermets and Cemented Carbides. 1998; 922-940.

[6] Wang GM and Campbell SJ. Synthesis and structural evolution of tungsten carbide prepared by ball milling. *Journal of Materials Science* 1997; 32: 1461-1467.

[7] Cottrell AH. Cohesion in Tungsten Carbide. *Materials Science and Tecnology* 1995; 11(3): 209-212.

[8] Gusev AI and Kurlov AS. Tungsten carbides and W-C phase diagram. *Inorganic Materials* 2006; 42(2): 121-127.

[9] Gustafson P. A thermodynamic evaluation of the C-Fe-W system. *Metallurgical Transactions* 1987; 18 A: 175-188.

[10] *Information on http://cst-www.nrl.navy.mil/lattice/struk/bh.html.* The tungsten carbide (B_h) structure 2008.

[11] Chermant JL and Osterstock F. Fracture toughness and fracture of WC-Co composites. *Journal of Materials Science* 1976; 11: 1939-1951.

[12] Han DB and Mecholsky Jr.JJ. Fracture-Behavior of Metal Particulate-reinforced WC-Co Composites. *Materials Science and Engineering a-Structural Materials Properties Microstructure and Processing* 1991; 144(Oct.): 293-302.

[13] Leclercq G, Kamal M, Lamonier JF, Feigenbaum L, MalfoyP and Leclercq L. Treatment of Bulk Group-VI Transition-Metal Carbides with Hydrogen and Oxygen. *Applied Catalysis A:General* 1995; 121: 169-190.

[14] Warren A Nylund A and Olefjord I. Oxidation of Tungsten and Tungsten Carbide in Dry and Humid Atmospheres. *International Journal of Refractory Metals & Hard Materials* 1996; 14(5-6): 345-353.

[15] Voitovich VB, Sverdel VV, Voitovich RF and Golovko EI. Oxidation of WC-Co, WC-Ni and WC-Co-Ni Hard Metals in the Temperature Range 500-800ºC. *International Journal of Refractory Metals & Hard Materials* 1996; 14(4): 289-295.

[16] Andersson KM and Bergström L. Oxidation and dissolution of tungsten carbide powder in water. *International Journal of Refractory Metals & Hard Materials* 2000; 18: 121-129.

[17] Janes S and Bonn W. Composites. *A Handbook of Ceramics - Ceramic Monographs* 1979.

[18] Stevenson RW. Cemented Carbides. 1984; ninth edition: 773-783.

[19] Tracey VA. Nickel in Hardmetals. *Refractory Metals & Hard Materials* 1992; 11: 137-149.

[20] Holleck H. Constitutional aspects in the development of new hard materials. 1983; 849-861.

[21] Guillermet AF. Thermodynamic Properties of the Co-W-C System. *Metallurgical Transactions A* 1989; 20A(May): 935-956.

[22] Markström A, Sundman B and Frisk K. A revised thermodynamic description of the Co-W-C system. *Journal of Phase Equilibria and Diffusion* 2005; 26(2): 152-160.

[23] Uhrenius B. Contribution to the Knowledge of Phase Equilibria in Tungsten-Carbon Based Systems. *Scandinavian Journal of Metallurgy* 1991; 20(1): 93-98.

[24] Gruter M. These Undersuchwgen in der systemen Co-C, Co-WC. *Germany: Munster* 1959;

[25] Guillermet AF. The Co-Fe-Ni-W-C Phase Diagram: A Thermodynamic Description and Calculated Sections for (Co-Fe-Ni) Bonded Cemented WC Tools. *Zeitschrift - fur-Metallkunde* 1989; 80(2): 83-94.

[26] Chaporova IN and Shchetlina YeA. Investigations of the carburizing process in tungsten carbide hard alloys with cobalt and nickel. *Hard Metal Production Technology and Research in the USSR* 1964; 196-211.

[27] Jia K, Fischer TE and Gallois B. Microstructure, Hardness and Toughness of nanostructured and conventional WC-Co composites. *NanoStructured Materials* 1998; 10(5): 875-891.

[28] Bergström M. The Eta-carbides in the Ternary System Fe-W-c at 1250ºC. *Materials Science and Engineering* 1977; 27: 257-269.

[29] Upadhyaya GS and Bhaumik SK. Sintering of submicron WC-10 wt.% Co hard metals containing nickel and iron. *Materials Science and Engineering A-(Structural Materials Properties Microstructure and Processing)* 1988; A105-106: 249-256.

[30] Moskowitz D, Ford MJ and Humenik M. High-Strength Tungsten Carbides. *Modern Developments in Powder Metallurgy* 1970; 5: 225-234.

[31] Moskowitz D, Ford MJ and Humenik M. High-Strengh Tungsten Carbides. *International Journal of Powder Metallurgy* 1970; 6(4): 55-64.

[32] Uhrenius B, Forsen K, Haglund BO and Andersson I. Phase-Equilibria and Phase-Diagrams in Carbide Systems. *Journal of Phase Equilibria* 1995; 16(5): 430-440.

[33] Ekemar S, Lindholm L and Hartzell T. Aspects on Nickel as a binder metal in WC-based cemented carbides. *Proc.10th Plansee Seminar - Metallwerk Plansee* 1981; 1: 477-824.

[34] Penrice TW. Alternative binders for hard Metals. *Carbide and Tool Journal* 1988; 20(4): 12-15.

[35] Raghunahan S, Caron R and Sandell P. Tungsten Carbide Tecnologies. *Advanced Materials & Processes* 1996; 4: 21-23.

[36] González R, Echeberría J, Sánchez JM and Castro F. WC–(Fe, Ni, C) hardmetals with improved toughness through isothermal heat treatments. *Journal of Materials Science* 1995; 30(13): 3435-3439.

[37] Suzuki H, Yamamoto T and Chujo N. Properties of WC-10% (Ni-Fe). *Jap.Soc.of Powder and Powder Metallurgy Journal* 1967; 14: 26-31.

[38] Prakash L, Holleck H, Thümmler F and Walter P. The influence of the binder composition on the properties of WC-Fe/Co/Ni. *Modern Developments in Powder Metallurgy* 1981; 14: 255-68.

[39] Chaporova IN, Kudryavtseva VI, Sapronova ZN and Sychkova LV. An investigation of the WC-Fe-Ni System. *Russian Metallurgy* 1981; 4: 211-215.

[40] Chaporova IN, Kudryavtseva VI and Sapronova ZN. Structure and Properties of a hard Alloy Based on Tungsten Carbide with Fe-Ni Binder. *Metal Science and Heat Treatment* 1978; 20(5-6): 402-404.

[41] Guillermet AF. An assessment of the Fe-Ni-W-C Phase Diagram. *Zeitschrift - fur-Metallkunde* 1987; 78(3): 165-171.

[42] Guillermet AF. Use of Phase-Diagram calculations in Selecting the composition of Fe-Ni Bonded WC Tools. *International Journal of Refractory & Hard Metals* 1987; 6(1): 24-27.

[43] Uhrenius B. Phase diagrams as a tool for production and development of cemented carbides and steels. *Powder Metallurgy* 1992; 35(3): 203-210.

[44] Agte C. Development of the tungsten carbide technology in the GDR. *Neue Hütte* 1957; 9(537): 544.

[45] Moskowitz D. Abrasion Resistant Iron-Nickel Bonded Tungsten Carbide. *Modern Developments in Powder Metallurgy* 1977; 10: 543-551.

[46] Uhrenius B, Pastor H and Pauty E. On the Composition of Fe-Ni-Co-WC-Based Cemented Carbides. *International Journal of Refractory Metals & Hard Materials* 1997; 15(1-3): 139-149.

[47] Roebuck B and Bennett EG. Phase size distribution in WC/Co hardmetal. *Metallography* 1986; 19: 27-47.

[48] Rudy E and Chang YA. Plansee Proceedings 1964. 1965; 786-822.

[49] Stecher P, Benesovky F and Nowotny H. Chromium-tungsten-carbon system. *Planseeber Pulvermet* 1964; 12: 89-95.

[50] Gustafson P. A Thermodynamic Evaluation of the C-Cr-Fe-W System. *Metallurgical Transactions A* 1988; 19A: 2547-2554.

[51] Goldschmidt HJ. The Structure of carbides in Alloy Steels Part II-Carbide formation in high-speed steels. *Journal of the Iron and Steel Institute* 1952; 170: 189-204.

[52] Uhrenius B and Frondell S. *Metal Science* 1977; 11: 73-81.

[53] Bergström M. The eta-carbides in the quaternary system Fe-W-C-Cr at 1250ºC. *Materials Science and Engineering* 1977; 27(1): 271-286.

[54] Goldschmidt HJ. Occurrence of the β-manganese structure in transition metal alloys and some observations on x-phase equilibriums. *Metallurgia* 1957; 56: 17-26.

[55] Viswanadham RK and Lindquist PG. Transformation-Toughening in Cemented Carbides: Part I. Binder Composition Control. *Metallurgical Transactions A* 1987; 18A: 2163-2173.

[56] Viswanadham RK and Lindquist PG. Transformation-Toughening in Cemented Carbides: Part II. Thermomechanical Treatments. *Metallurgical Transactions A* 1987; 18A: 2175-2180.

[57] Hanyaloglu C, Aksakal B and Bolton JD. Production and indentation of WC/Fe-Mn as an alternative to cobalt-bonded hardmetals. *Materials Characterization* 2001; 47: 315-322.

[58] Scussel HJ. Friction and Wear of Cemented Carbides. ASM Handbook 1992;(18): 795.

[59] *Information on http://cst-www.nrl.navy.mil/lattice/struk/fscf128.html* The hypothetical cF/28 ferrite structure 2008.

[60] WC-Co enjoys proud history and bright future. *Metall Powder Report* 1998; 32-36.

[61] Pollock CB and Stadelmaier HH. The Eta Carbides in the Fe-W-C and Co-W-C Systems. *Metallurgical Transactions* 1970; 1: 767-770.

[62] Frisk K, Bratberg J and Markström A. Thermodynamic modelling of the M6C carbide in cemented carbides and high-speed steel. *Computer Coupling of Phase Diagrams and Thermochemistry* 2005; 29: 91-96.

[63] *Information on http://cst-www.nrl.navy.mil/lattice/struk/e9_3.html* The F_3W_3C ($E9_3$) structure 2008.

[64] Haller MN. Cemented Carbides. ASM Handbook - Metallographic Techniques 2001; 273-278.

[65] Cho KH, Lee JW and Chung IS. A study on the formation of anomalous large WC grain and the eta phase. *Materials Science and Engineering A* 1996; 209: 298-301.

[66] *Information on http://cst-www.nrl.navy.mil/lattice/struk/a9.html* The hexagonal graphite (A9) crystal structure 2008.

[67] Itia - Cemented Carbides. *Information on http://www.itia.org.uk* 2008.

[68] Spriggs GE. The Importance of Atmosphere Control in Hard-Metal Production. *Powder Metallurgy* 1970; 13(26): 369-393.

[69] Blasko MJ. Vacuum Sintering Trends for Hardmetal Production. *Vacuum Industries* 1970;

[70] Powder Metallurgy - Sintering of Cemented Carbides. *ASM International Handbook* 1992; 385-389.

[71] Bhaumik SK, Upadhyaya GS and Vaidya ML. Full density of complex WC-based cemented carbides. *Journal of Materials Processing Technology* 1996; 58(1): 45-52.

[72] Meredith B and Milner DR. Densification Mechanisms in the Tungsten Carbide-Cobalt system. *Powder Metallurgy* 1976;(1): 38-45.

[73] Exner HE. Aspects of hardmetal sintering. *Max-Plank Institut für Metallforschung* 1980;

[74] Akesson L. Thermodynamic and sintering studies in the Co-W-C system. *Thermochimica Acta* 1979; 29: 327-332.

[75] Missiaen JM and Roure S. Automatic image analysis methods for the determination of stereological parameters-appication to the analysis of densification during solid state sintering of WC-Co compacts. *Journal of Microscopy* 2000; 199(2): 141-148.

[76] Upadhyaya GS. Materials science of cemented carbides - an overview. *Materials and Design* 2001; 22: 483-489.

[77] Wang Y, Heusch M, Lay S and Allibert CH. Microstructure evolution in the cemented carbides WC-Co I. Effect of the C/W ratio on the morphology and defects of the WC grains. *Phys.Stat.Sol.(a)* 2002; 193(2): 271-283.

[78] Chabretou V, Allibert C.H and Missiaen JM. Quantitative analysis of the effect of the binder phase composition on grain growth in WC-Co sintered materials. *Journal of Materials Science* 2003; 38: 2581-2590.

[79] Konyashin I, Senchihin V and Anikeev A. Development, production and application of novel grades of coated hardmetals in Russia. *International Journal of Refractory Metals & Hard Materials* 1996; 14: 41-48.

[80] Brookes KJA. Hard materials at Euro PM 2002-Part 1. *International Journal of Refractory Metals & Hard Materials* 2003; 21: 81-103.

[81] Lardner E. The Control of Grain Size in the Manufacture of Sintered Hard-Metal. *Powder Metallurgy* 1970; 13(26): 394-428.

[82] Rüdiger O, Hirschfeld D, Hoffmann A, Kolaska J, Ostermann G and Willbrand J. Composition and properties of the binder metal in cobalt bonded tungsten-carbide. *International Journal of Powder Metallurgy* 1971; 7(1): 29-38.

[83] Lin C, Kny E, Yuan G and Djuricic B. Microstructure and properties of ultrafine WC-0.6VC-10Co hardmetals densified by pressure-assisted critical liquid phase sintering. *Journal of Alloys and Compounds* 2004; 383: 98-102.

[84] Suzuki H, Hayashi K and Fuke Y. The grain size of binder-phase in WC-Co alloy. *Journal of Japan Society Powder Powder Metallurgy* 1972; 346-354.

[85] Hillert M. On the theory of normal and abnormal grain growth. *Acta Metallurgica* 1965; 13: 227.

[86] Wittmann B, Shubert W-D and Lux B. WC grain growth an grain growth inhibition in nickel and iron binder hardmetals. *International Journal of Refractory Metals & Hard Materials* 2002; 20: 51-60.

[87] Shatov AV, Firstov SA and Shatova IV. The shape of WC crystals in cemented carbides. *Materials Science and Engineering A-(Structural Materials Properties Microstructure and Processing)* 1998; 242(1-2): 7-14.

[88] Gille G, Bredthauer J, Gries B, Mende B and Heinrich W. Advanced and new grades of WC binder powder - their properties and application. *International Journal of Refractory Metals & Hard Materials* 2000; 18: 87-102.

[89] Harmat P, Kotsis I, Laczkó L and Bartha L. Melting and phase transformation of hardmetal powders. *Solid State Ionics* 2001;(141-142).

[90] Sommer M, Schubert W-D, Zobetz E and Warbichler P. On the formation of very large WC crystals during sintering of ultrafine WC-Co alloys. *International Journal of Refractory Metals & Hard Materials* 2002; 20: 41-50.

[91] Shao G-q S, Duan X-l, Xie J-r, Yu X-h, Zhang W-f and Yuan R-z. Sintering of nanocrystalline WC-Co composite powder. *Rev.Advanced Materials Science* 2003; 5: 281-286.

[92] Larson FG, Hong J, Goodson R and Voytek M. Hot isostatic pressing of cemented carbides. *International Journal of Refractory & Hard Metals* 1984; 3(1): 30-34.

[93] Gurland J. *Practical Applications of Quantitative Metallography, ASTM STP* 1984; 839: 65.

[94] Golovchan VT and Litoshenko NV. On the contiguity of carbide phase in WC-Co hardmetals. *International Journal of Refractory Metals & Hard Materials* 2003; 21: 241-244.

[95] Kang KY, Roemer JG and Ghosh D. Microstructural characterization of cemented carbide samples by image analysis techniques. *Powder Technology* 2000; 108: 130-136.

[96] Srivatsan TS, Woods R, Petraroli M and Sudarshan TS. An investigation of the influence of powder particle size on microstructure and hardness of bulk samples of tungsten carbide. *Powder Technology* 2002; 122: 54-60.

[97] Roebuck B. Extrapolating hardness-structure property maps in WC-Co hardmetals. *International Journal of Refractory Metals & Hard Materials* 2006; 24: 101-108.

[98] Lee HC and Gurland J. Hardness and deformation of cemented carbide. *Materials Science and Engineering* 1978; 33(1): 125-133.

[99] Makhele-Lekala L, Luyckx S and Nabarro FRN. Semi-empirical relationship between the hardness, grain size and mean free path of WC-Co. *International Journal of Refractory Metals & Hard Materials* 2001; 19: 245-249.

[100] Voigt W. Lehrbuch der Kristallphysik, *Teubner, Leipzig* 1928.

[101] Reuss A. Brechnung der fliessgrense von mischkristallen auf grund der plastizitatsbedingung für einkristalle. *Zeitschrift für Angewandte Mathematik ung Mechanik* 1929; 9: 49-58.

[102] Hsieh CL, Tuan WH and Wu TT. Elastic behaviour of a model two-phase material. *Journal of European Ceramic Society* 2004; 24: 3789-3793.

[103] Uygur-Mustafa E. Modeling tungsten carbide/cobalt composites. *Advanced Materials & Processes* 1997; 3: 35-37.

[104] Chicot D, Pertuz A, Roudet F, Staia MH and Lesage J. New developments for fracture toughness determination by Vickers indentation. *Materials Science and Technology* 2004; 20: 877-884.

[105] Anstis GR, Chantikul P, Lawn BR and Marshall DB. A critical evalution of indentation techniques for measuring fracture toughness. I. Direct crack measurement. *Journal of the American Ceramic Society* 1981; 64(9): 533-538.

[106] Tanaka K. Elastic/plastic indentation hardness and indentation fracture toughness: the inclusion core model. *J.Mater.Sci* 1987; 22: 1501-1508.

[107] Niihara K, Morena R and Hasselman DPH. A fracture mechanics analysis of indentation-induced. Palmqvist crack in ceramics. *Journal of Materials Science Letters* 1983; 2: 221-223.

[108] Laugier MT. Palmqvist indentation toughness in WC-Co composites. *Journal of Materials Science Letters* 1987; 6(8): 897-900.

[109] Shetty DK, Wright IG, Mincer PN and Claner AH. Indentation fracture of WC-Co cermets. *Journal of Materials Science* 1985; 20: 1873-1882.

[110] Ponton CB and Rawlings RD. Vickers indentation fracture toughness test, Part 1, Review of literature and formulation of standardised indentation toughness equations. *Materials Science and Technology* 1989; 5: 865-872.

[111] EHMG WINTEREV Toughness testing of hardmetals. *Powder Metallurgy* 2004; 47(4): 15-16.

[112] Ravichandran KS. Fracture Toughness of Two Phase WC-Co Cermets. *Acta Metallurgy Materials* 1994; 42(1): 143-150.

[113] Richter V and Ruthendorf Mv. On hardness and toughness of ultrafine and nanocrystalline hard materials. *International Journal of Refractory Metals & Hard Materials* 1999; 17: 141-152.

[114] Reshetnyak H and Kübarsepp J. Structure Sensitivity of Wear Resistance of Hardmetals. *International Journal of Refractory Metals & Hard Materials* 1997; 15(1-3): 89-95.

[115] Wentzel EJ and Allen C. The Erosion-Corrosion Resistance of Tungsten-Carbide Hard Metals. *International Journal of Refractory Metals & Hard Materials* 1997; 15(1-3): 81-87.

[116] Mori G, Sutthiruangwong S, Schaffer B, Grogger W and Koesters R. The role of binder on corrosion properties of cemented carbides. *Proceedings of the PM2004, EPMA, Wien* 2004; 3: 581-588.

[117] Basu SN and Sarin VK. Oxidation behavior of WC-Co. *Materials Science and Engineering A* 1996; A209: 206-212.

[118] Roebuck B, Bennett EG and Almond EA. Infiltartion as a method for producing WC hardmetals with Co and Ni alloy binder-phase. *International Journal of Refractory Metals & Hard Materials* 1984; 3: 35-40.

[119] Eun KY, Kim DY and Yoon DN. Variation of mechanical properties with Ni/Co ratio in WC-(Co-Ni) hardmetals. *Powder Metallurgy* 1984; 27(2): 112-114.

[120] Peters CT and Brabyn SM. Properties of nickel substituted hardmetals and their performance in hard rock drill bits. *Metal Powder Report* 1987; 42(12): 863-865.

[121] Almond EA and Roebuck B. Identification of optimum binder phase compositions for improved WC hard metals. *Materials Science and Engineering* 1988; A105/106: 237-248.

[122] Kakeshita T and Wayman CM. Martensitic transformations in Cermets with a Metastable Austenitic Binder, I: WC-(Fe-Ni-C). *Materials Science and Engineering* 1991; A141: 209-219.

[123] Farooq T and Davies TJ. Tungsten Carbide Hard Metals Cemented with Ferroalloys. *International Journal of Powder Metallurgy* 1991; 27(4): 347-355.

[124] Arenas F, Montoya E, Cabezas M and Lira J. Influence of powder granulometry on the sintering of binderless tungsten carbide. *Key Engineering Materials* 2002; 206-213: 179-182.

[125] Lange E and Müller N. P/M Injection Molding Technique for Ceramic and Metal Parts. *Powder Metallurgy International* 1986; 18(6): 416-421.

[126] Complex shapes and hard-coated powders get over limit factors. *Metal Powder Report* 2005; 60(1): 32-37.

[127] Cornwall RG and German RM. Think bigger! the future is bright for MIM. *Metal Powder Report* 2004; 59(11): 8-11.

[128] Shi XL, Shao GQ, Duan XL, Yuan RZh and Lin HH. Mechanical properties, phases and microstructure of ultrafine hardmetals prepared by WC-6.29 Co nanocrystalline composite powder. *Materials Science and Engineering A* 2005; 392: 335-339.

[129] Sampath A, Stiglich J J, Sudarshan T S, Singh R and Choi KS. Fast Consolidation of WC-Co. *Powder Metallurgy* 2002; 45(1): 25-27.

[130] Kangwantrakool S and Shinohara K. Sintering behavior of mechanically coated WC-Co/TiC-Al_2O_3 particles by high-speed rotational impact blending. *International Journal of Refractory Metals & Hard Materials* 2003; 21: 171-182.

[131] El-Eskandarany MS. Fabrication of nanocrystalline WC and nanocomposite WC-MgO refractory materials at room temperature. *Journal of Alloys and Compounds* 2000; 296: 175-182.

[132] Fischer P, Romano V, Weber HP, Karapatis NP, Boillat E and Glardon R. Sintering of commercially pure titanium powder with a Nd:YAG laser source. *Acta Materialia* 2003; 51: 1651-1662.

[133] Kruth JP, Mercelis P and Van Vaerenbergh J. Binding mechanisms in selective laser sintering and selective laser melting. *Rapid Prototyping Journal* 2005; 11(1): 26-36.

[134] Kruth JP, Wang X, Laoui T and Froyen L. Lasers and materials in selective laser sintering. *Assembly Automation* 2003; 23(4): 357-371.

[135] Wang XC, Laoui T, Bonse J, Kruth JP, Lauwers B and Froyen L. Direct Selective Laser Sintering of hard metal powders: experimental study and simulation. *International Journal of Advanced Manufacturing Technology* 2002; 19: 351-357.

[136] Maeda K and Childs THC. Laser sintering (SLS) of hard metal powders for abrasion resistant coatings. *Journal of Materials Processing Technology* 2004; 149: 609-615.

[137] Rödiger K, Dreyer K, Gerdes T and Willert-Porada M. Microwave sintering of hardmetals. *International Journal of Refractory Metals & Hard Materials* 1998; 16: 409-416.

[138] Agrawal DK. Microwave processing of ceramics. *Current Opinion in Solid State & Materials Science* 1998; 3(5): 480-485.

[139] Breval E, Cheng JP, Agrawal DK, Gigl P, Dennis M, Roy R and Papworth AJ. Comparison between microwave and conventional sintering of WC/Co composites. *Materials Science and Engineering A* 2005; 391: 285-295.

[140] Giesche H. Preparation and applications of coated powders in ceramics and related fields. *Jounal of Dispersion Science and Technology* 1998; 19(2-3): 249-265.

[141] Li G-j, Huang X-x, Guo J-k and Chen D-m. Ni-coated Al_2O_3 powders. *Ceramics International* 2002; 28: 623-626.

[142] Wang C-M and Riley FL. Alumina-coating of silicon nitride powder. *Journal of the European Ceramic Society* 1992; 10: 83-93.

[143] Jr Mitchell TD and De Jonghe LC. Processing and properties of particulate composites from coated powders. *Journal of the American Ceramic Society* 1995; 78(1): 199-204.

[144] Vélez M, Quiñones H, Di Giampaolo AR, Lira J and Grigorescu IC. Electroless Ni-B coated WC and VC powders as precursors for liquid phase sintering. *International Journal of Refractory Metals & Hard Materials* 1999; 17: 99-102.

[145] Kangwantrakool S and Shinohara K. New design of microstructure of WC-Co/TiC-Al_2O_3 composite materials by mechanical coating of particles. *Journal of the Japan Society of Powder and Powder Metallurgy* 2002; 49(12): 1070-1075.

[146] Ensinger W and Muller HR. Surface treatment of aluminum oxide and tungsten carbide powders by ion beam sputter deposition. *Surface & Coatings Technology* 2003; 163-164: 281-285.

[147] Ensinger W. Processing of powder surfaces by ion beam techniques. *Nuclear Instruments and Methods in Physics Research B* 1999; 148: 17-24.

[148] German RM, Smid I, Campbell LG, Keane J and Toth R. Liquid phase sintering of tough coated hard particles. *International Journal of Refractory Metals & Hard Materials* 2005; 23: 267-272.

[149] Giménez S, Huang SG, Van der Biest O and Vleugels J. Chemical reactivity of PVD-coated WC-Co tools with steel. *Applied Surface Science* 2007; 253: 3547-3556.

[150] Taguchi A, Kitami T, Yamamoto H, Akamaru S, Hara M and Abe T. Surface coating with various metals on spherical polymer particles by using barrel sputtering technique. *Journal of Alloys and Compounds* 2007; 441: 162-167.

[151] Abe T, Akamaru S and Watanabe K. Surface modification of Al_2O_3 ceramic grains using a new RF sputtering system developed for powdery materials. *Jounal of Alloys and Compounds* 2004; 377: 194-201.

[152] Hara M, Hatano Y, Abe T, Watanabe K, Naitoh T, Ikeno S and Honda Y. Hydrogen absorption by Pd-coated ZrNi prepared by using Barrel-Sputtering System. *Journal of Nuclear Materials* 2003; 320: 265-271.

[153] Simões FAG. Consolidação de partículas compósitas de matriz Ti-Al e Ti-Si obtidas por síntese mecânica e modificadas superficialmente por pulverização catódica. *PhD Thesis Engenharia Mecânica na especialidade em Engenharia de Materiais* 2005; Coimbra

[154] Vieira MT, Martins AG, Barreiros FM, Matos M and Castanho JM. Surface modification of stainless steel powders for microfabrication. *Journal of Materials Processing Technology* 2008; in press.

[155] Castanho JM, Vieira MT, Matos M and Trindade B. Nanostructured coated powders for structural net shape components. *Journal of Alloys and Compounds* 2007; 434-435: 383-385.

[156] Smentkowski VS. Trends in sputtering. *Progress in Surface Science* 2000; 64: 1-58.

[157] Posadowski WM. Sustained self sputtering of different materials using dc magnetron. *Vacuum* 1995; 46(8-10): 1017-1020.

[158] Thornton JA. *Journal of Vacuum Science and Technology* 1974; 11(4): 666-670.

[159] Shedden BA, Kaul FN, Samandi-M and Window B. The role of energetic neutrals in reactive magnetron sputtering of nitrogen-doped austenitic stainless steel coatings. *Surface and Coatings Technology* 1997; 102-108.

[160] Billard A and Frantz C. Attempted modelling of thickness and chemical heterogeneity in coatings prepared by d.c. reactive magnetron sputtering. *Surface and Coatings Technology* 1993; 59: 41-47.

[161] Miodownik AP. Means of predicting structure and performance of new materials. *Powder Metallurgy* 1989; 32(4): 269-276.

[162] Movchan BA and Demchishin AV. Investigations of the structure and properties of thick Ni, Ti, W, Al_2O_3 and ZrO_2 vacuum condensates. *Phys.Met.Metallogr.* 1969; 28: 83.

[163] Thornton JA. Influence of apparatus geometry and deposition conditions on the structure and topography of thick sputtered coatings. *Journal of Vacuum Science Technology* 1974; 11(4): 666-670.

[164] Thornton JA. High rate thick film growth. *Ann.Rev.Mater.Sci.* 1977; 7: 239.

[165] Messier R, Giri AP and Roy RA. Revised structure zone model for thin film physical structure. *J.Vac.Sci.Technol.A* 1984; 2: 500.

[166] Downing M, Nicholls JR and Stephenson DJ. Physical vapour deposition coating processes for encapsulation of powder metal components before hot isostatic pressing. *Materials Science and Technology* 1991; 7: 1138-1142.

Chapter

II

Experimental Details

Les découvertes scientifiques. . .n'ont pas l'habitude des sortir à l'improviste et tout armées du cerveau d'un penseur.

H. Le Chatelier, Paris 1908.

In this chapter the experimental details concerning the composite powder preparation, including the process of powder deposition, the materials involved and the subsequent processing stages, namely pressing and sintering will be presented. The main characterization techniques including the chemical, microstructural and mechanical ones are also presented.

2.1. **C**omposite **p**owders **p**reparation

2.1.1. **M**aterials

The starting tungsten carbide powder had a mean particle size of 9.0 μm and was gently provided by the company denominated Durit, manufacturers of hardmetal, and located in Albergaria a Velha, Portugal.

The target used for sputtering is made of stainless steel (AISI 304) with the characteristics presented in Table 2.1. The composition of the target was confirmed by ICP and EPMA. In order to increase the nickel content in the binder, small pieces of this metallic material have been attached to the stainless steel target.

Table 2.1.

Characteristics of stainless steel 304 (AISI) at room temperature.

Chemical composition (wt.%)	17.0-19.5 Cr; 8.0-10.5 Ni; 2.00 Mn; 1.00 Si; 0.045 P; 0.03 S; 0.07 C♣
	71.5 Fe; 19.1 Cr; 8.1 Ni; 1.7 Mn (ICP)
	71.3 Fe; 18.3 Cr; 8.0 Ni; 1.7 Mn; 0.31 Si; 0.03 P (EPMA)
Theoretical density♣ (gcm^{-3})	7.9
Melting temperature♣ (ºC)	1400-1450
Tensile strength♣ (MPa)	500-700
Elasticity modulus♣ (GPa)	200
Hardness♣ HB 30	215

♣Wegst-C.W. STAHLSCHLÜSSEL – Key Steels, German, 2001.

2.1.2. Powder Coating

An innovative approach to cover WC powder particles was investigated in this work. A new sputtering equipment at the laboratorial scale was developed specifically for powder coating at the Mechanical Engineering Department of University of Coimbra (Fig 2.1).

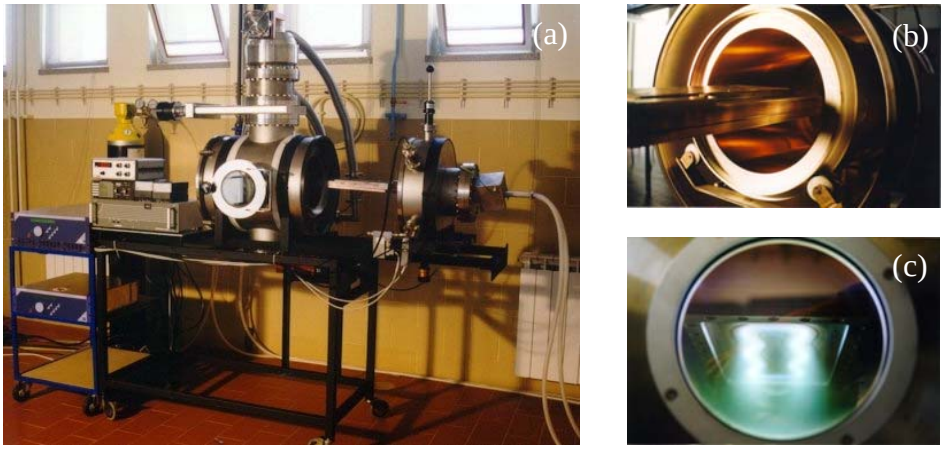

Fig. 2.1. **(a)** Equipment developed to coat the WC powders. **(b)** Drum and target. **(c)** Plasma inside the chamber.

The WC powder was placed in a chamber with vibrational and rotational movement in order to homogeneously cover the particles surface. The main parameters common to all the depositions are listed in Table 2.2. These parameters were established in a previous work [1]. The deposition time has been variable since the binder amount depends directly on this factor. Several coated tungsten carbide powders were prepared with different binder amounts and in some cases the binder composition was also changed (increase of the Ni content). The coated powder compositions will be presented in the corresponding papers.

Table 2.2.
Deposition parameters.

Target area (m^2)	54×10^{-3}
Substrate mass (g)	100
Target to substrate distance (mm)	150
Base pressure (Pa)	1×10^{-4}
Sputter gas composition	99.99% Ar
Sputtering pressure (Pa)	0.5
Magnetron power (W)	700
Rotational speed of the drum (r.p.m.)	3
Frequency vibration of the drum (Hz)	1.6

2.1.3. **C**onventional **m**ixing

Some compositions have also been prepared using conventional powder mixture and milling. The different powder mixtures engage the same tungsten carbide, iron (Goodfellow FE006020, <60 μm), chromium (Goodfellow CR006021/22, <38 μm), nickel (Goodfellow NI006021/11, 3-7 μm) and graphite powders (Panreac 1221, <20 μm) in different proportions, as exposed in the experimental subchapter of each presented paper. Mixtures with WC and stainless steel AISI 304 (Goodfellow, Fe226010/4, <45 μm) were also performed. These powder compositions were mixed and ball milled in stainless steel mills using WC-Co balls and isopropyl alcohol, for 6 h. Typical weight of the powder batches was 50 g. Approximately 1.5 wt.% of paraffin wax was used as a pressing aid. The powder slurry was then dried at 80ºC in a drier. Subsequently, the dried powders were deagglomerated and sieved (325 mesh, i.e. 45 μm mean size).

2.2. **F**orming and **S**intering

Before sintering, the composite powders were uniaxially pressed in a 10 mm diameter die using a hydraulic press (CARVER *Laboratory Press – Model C*). In some cases cold isostatic pressing (CIP) at 330 MPa was also applied to uniaxial pressed compacts in order to attain higher green densities.

The compact materials were dewaxed (only the conventional powder mixtures) and sintered in a vacuum furnace of KANTHAL-SUPER heating elements (maximum temperature of 1650 ºC) with a PID *Eurotherm* controller. The samples were placed in a graphite crucible in order to control the carbon degassing. The furnace was pumped to a vacuum of 10 Pa before sintering and the heating rate was typically 5 ºC/min. The temperature control was performed with a thermocouple Pt/Pt 13% Rh put in contact with the graphite crucible. Fig. 2.2 shows a schematic representation of the furnace with all the attached elements.

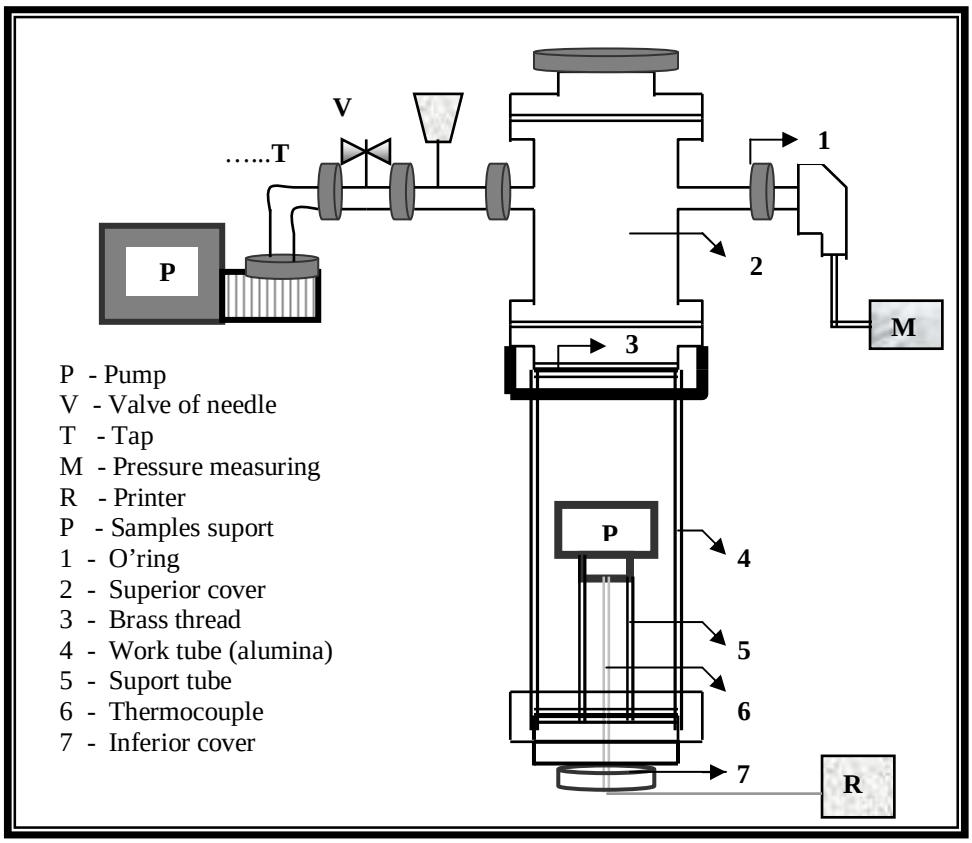

Fig. 2.2. Schematic representation of the furnace used to sinter the samples.

The samples with nickel richer binders (relatively to stainless steel composition) did not achieve enough densification after vacuum sintering in order to allow mechanical characterization. Therefore, these samples have been hot isostatically pressed (HIP) to achieve full density. Hipping was done in argon atmosphere at a pressure of 30 MPa at 1550 ºC. The samples with high amounts of Ni have been hot isostatically pressed at 1400 ºC, for 90 min, at 135 MPa.

2.3. **P**owder **C**haracterization

In order to determine the powder characteristics, namely specific surface area, powder particle size distribution and flowability, the Brunauer-Emmett-Teller (BET) method (Micromeritcs Gemini 2370 V5), the laser diffraction (Coulter LS 130) and the Flodex apparatus, were respectively used.

The zeta potential (ξ) was also determined as a function of pH using a Coulter Delsa 440 SX. More details about the electrokinetic measurements can be found in the paper II.2. The uncoated and coated WC powders were also submitted to differential thermal-thermogravimetric analysis (DTA-TG) in a SETARAM LABSYS equipment, in order to study the air oxidation behaviour.

2.4. **D**ensity **C**ontrol

The real powder density was determined by helium pycnometry (Accupyc 1330). The percentage of binder weight amount, $\%W_{binder}$, deposited on the WC powder can be estimated using the rule of the mixtures of binary composites [2]:

$$\%W_{binder} = \frac{D_{binder} \times (D_{WC} - D_{WC+binder})}{D_{WC+binder} \times (D_{WC} - D_{binder})} \quad (2.1)$$

where D_{WC} and $D_{WC+binder}$ represent the real powder density of WC and coated WC, respectively, while D_{binder} is the coating density.

The apparent density of sintered samples was measured by the immersion method in etilenoglycol, using the Archimedes' method. The green density was geometrically measured. The samples weight was also controlled after and before sintering, in order to evaluate the binder losses.

2.5. Chemical Characterization

The chemical composition of WC coated powders and selected sintered samples was analysed by inductively coupled plasma-atomic emission spectroscopy (ICP). In sintered samples the electron probe microanalysis (EPMA) and the energy dispersive spectroscopy (EDS) were also utilized to perform chemical characterization. More details are described in the papers. The carbon content of WC powder and sintered samples was determined by automatic direct combustion (LECO CS 200 IH).

2.6. Crystallographic Characterization

X-ray diffraction was the principal method used to determine the various crystalline phases present in unsintered and sintered compositions. All the diffraction patterns were taken using CuKα radiation with a graphite crystal monochromator. The relative small volume of the binder, and the shallow depth of penetration of the X-rays, resulted in low intensities for the binder peaks. In addition, the residual stress in the binder resulted in considerable peak broadening. This effect is more pronounced in coated powders were the intrinsic stresses are high due to the deposition conditions.

The phases of the sintered samples have been qualitative and semi-quantitative determined. For the last approach, a general system of analyse structure, named GSAS [3], that is based on the Rietveld method, was used. This method starts with the powder diffraction results, then the parameterized structure factors of each phase are introduced and, finally, the difference between the observed and calculated intensities is obtained through the minimum chi-squared method calculation. The quantification was performed assuming that the minority phases are vestigial, being therefore neglected. Information available in the bibliography was used to get the structure parameters of WC and M_6C phases [4,5].

2.7. **M**icrostructure **C**haracterization

Scanning electron microscopy (SEM) was the technique utilized to perform the microstructural characterization of both powders and sintered samples. The SEM equipment used is a HITACHI-S4100, with a maximum acceleration potential of 30 KV and a resolution of 15 Å. Some sintered samples have been also observed by optical microscopy (Zeiss, Jenaphot 2000).

Some samples have been mounted in thermosetting resin and dried in air atmosphere. After mounting, the samples were ground with abrasives in order to remove scratches and work-hardened regions until the desired surface finish is obtained. After that, the fine polishing is performed using 6, 3 and 1 μm diamond paste.

Chemical etching with Murakami's (10 g $K_3Fe(CN)_6$, 10 g NaOH, 100 ml distilled water) was used in order to reveal η-phase (Fe_3W_3C) and WC phase, during 3 s and 120 s, respectively. Nital (20% vol. NH_3+alcohol) was also used to reveal the iron-rich binder phase.

The method used to measure the grain size of polished and etched cross-sections of metallographic specimens is the linear intercept method, or Heyn's method, established in 1903 [6]. By measuring the length of random intercepts an average grain size can be calculated, using the equation:

$$\overline{l} = L/N \tag{2.2}$$

where $\overline{l}$ is the arithmetic mean linear intercept, or Heyn grain size, L is the length of line across WC and N is the number of WC grains traversed (a minimum of 300 intercepts per sample were considered). The method also gives a distribution of intercepts. The method is proposed to be used as a standard for cemented carbides [6]. The grain shape is assumed to be spherical in order to transform the results of 2D to 3D, using the correction factors given by Fullman [6]:

$$G = 1.5 \times \overline{l} \tag{2.3}$$

where G is the calculated 3D grain size and 1.5 the transformation factor.

The contiguity, C, was also determined, using nearly 100 measurements from the optical micrographs, and applying the equation 1.9 in Table 1.5 [7].

2.8. Mechanical Characterization

2.8.1. Hardness, Young's modulus and yield strength

Depth-sensing indentation was applied to obtain different mechanical characteristics in samples without geometric restrictions (size or shape) in a non-destructive testing way. This method is particularly interesting to characterize materials prepared at a laboratorial scale with equipments that often limit the amount and the size of the samples, as is here the case.

The development of depth-sensing indentation equipment has allowed the easy and reliable determination of two of the most commonly measured mechanical properties, the hardness, *H*, and the Young's modulus, *E* [8,9,10]. The following equations were used to calculate the above-mentioned parameters:

$$H = P_{max}/A_c \tag{2.4}$$

where *H* is defined as the maximum applied load during the indentation test, P_{max}, divided by the contact area of the indentation immediately before unloading, A_c, and for the *E* determination [8,10]:

$$E_r = \frac{\sqrt{\pi}}{2}\frac{1}{\sqrt{A_c}(C_t - C_f)} \tag{2.5}$$

where C_t and C_f are the total compliance of the system and the frame compliance, respectively. In this equation, E_r, is the reduced Young's modulus, which is a function of the Young's modulus and the Poisson's ratio, ν, of the specimen (*s*) and the indenter (*i*):

$$\frac{1}{E_r} = \frac{1-\nu_s^2}{E_s} + \frac{1-\nu_i^2}{E_i} \tag{2.6}$$

In latest years, efforts have been made to establish a reverse analysis algorithm for the evaluation of the plastic mechanical properties of materials. The principal developments in this investigation area are related to the application of the finite element method, to obtain dimensionless functions that relate the characteristic parameters of indentation load-unloading curves to the mechanical properties obtained from the stress-strain curves [11]. Recently, a straightforward reverse analysis approach was proposed [12], which avoids the use of dimensionless functions. In a simplified description, this approach, which was used

in the present work, consists of a direct comparison between experimental and numerical simulation indentation curves, in order to determine the yield stress, σ_y, and the strain hardening coefficient, n, of the material. The Swift law was used in numerical simulations, to describe the plastic behaviour:

$$\sigma_y = K (\varepsilon + \varepsilon_0)^n \quad (2.7)$$

where ε is the plastic strain and K is a material parameter: $K = \sigma_y / \varepsilon_0^n$ (ε_0 is a constant, assumed as 0.005).

The hard metal samples were mechanically characterized using depth-sensing indentation equipment (Fischerscope H100). In order to obtain representative average values for the evaluated properties, 75 tests were performed in different surface points of each sample. In each test the load is increased in steps, since the first load of 0.4 mN until a nominal load of 500 mN. The number of steps used for loading and unloading was 60 and the time between steps was 0.5 s. Two creep periods of 30 s were performed during the tests: at the maximum load and at the lowest load. The average value of the 75 tests made in each sample was used for the direct determination of the hardness, H, and calculation of the Young's modulus, E, and of the yield stress, σ_y.

The Vickers hardness (HV) was also measured using a hardness tester, in order to compare the determined values with others from the literature. The machine makes an indent or impression whose diagonal size(s) is measured with an attached optical microscope. The indentation load used was 294 N.

2.8.2. **F**racture **t**oughness

The traditional methods to measure the K_{IC} use the three-point bending test [13]. However, the preparation of the specimen requires long time, because it is necessary to square off and pre-notched with a "V" or "U". New methods have been developed to measure the fracture toughness, namely the crack indentation method. Indentation is a traditional method used to determine the toughness in brittle materials. Different models may be used for the calculation depending on the shape of the cracks that are initiated and

developed as a result of the indentation. Compared with conventional toughness evaluation methods, such as indentation strength beam, chevron notch beam, double cantilever beam and single edge notch beam [14,13,15], the indentation technique presents many advantages, among them the fact that it is a much simpler experimental technique.

The calculation of toughness, which is based on values of load (P) and crack length (c or l) depends on the shape of the crack. When the crack is developed only at the corners of the indent, called a Palmqvist type of crack (type Pq), the expression 1.31 presented in Table 1.9 was applied [16]. The measurements were performed with 10 kgf of applied load (98 N) and the crack length was measured by optical microscopy. The use of this relatively low load was sufficient to obtain measurable crack lengths, due to the lower binder contents used.

2.9. References

[1] Fernandes CM. Caracterização e Processamento de pós de carboneto de tungsténio revestidos com aço inoxidável. *Master Thesis* 2002; Departamento de Engenharia Cerâmica e do Vidro, Universidade de Aveiro.

[2] Uygur-Mustafa E. Modeling tungsten carbide/cobalt composites. *Advanced Materials & Processes* 1997; 3: 35-37.

[3] Larson AC and Von Dreele RB. LAUR 86-748 Report. *Los Alamos National Laboratory* 1990.

[4] Leciejewicz J. A note on the structure of tungsten carbide. *Acta Crystallographia* 1961; 14: 200-200.

[5] Yang Q and Anderson S. Application of Coincidence Site Lattices for Crystal Structure Description. Part I:=3. *Acta Crystallographia - Sec.B: Structural Science* 1987; 43: 1-14.

[6] Engqvist H and Uhrenius B. Determination of the average grain size of cemented carbides. *International Journal of Refractory Metals & Hard Materials* 2003; 21: 31-35.

[7] Golovchan VT and Litoshenko NV. On the contiguity of carbide phase in WC-Co hardmetals. *International Journal of Refractory Metals & Hard Materials* 2003; 21: 241-244.

[8] Newey D, Wilkins MA and Pollock HM. An ultra-low-load penetration hardness tester. *Journal of Physics Science Instruments* 1982; 15: 119-122.

[9] Loubet JL, Georges JM and Meille G. Vickers indentation curves of elastoplastic materials. 1986; 72.

[10] Oliver WC and Pharr GM. An improved technique for determining hardness and elastic modulus using load displacement sensing indentation experiments. *Jouranl of Materials Research* 1992; 7(6): 1564-1583.

[11] Dao M, Chollacoop N, Van Vliet KJ, Venkatesh TA and Suresh S. Computational modeling of the forward and reverse problems in instrumented sharp indentation. *Acta Materialia* 2001; 49(19): 3899-3918.

[12] Antunes JM, Cavaleiro A, Menezes LF, Simões MI and Fernandes JV. Ultra-microhardness testing procedure with Vickers indenter. *Surface & Coatings Tecnology* 2002; 149: 27-35.

[13] Chermant JL and Osterstock F. Fracture toughness and fracture of WC-Co composites. *Journal of Materials Science* 1976; 11: 1939-1951.

[14] Chicot D, Pertuz A, Roudet F, Staia MH and Lesage J. New developments for fracture toughness determination by Vickers indentation. *Materials Science and Technology* 2004; 20: 877-884.

[15] EHMG WINTEREV Toughness testing of hardmetals. *Powder Metallurgy* 2004; 47(4): 15-16.

[16] Ponton CB and Rawlings RD. Vickers indentation fracture toughness test, Part 1, Review of literature and formulation of standardised indentation toughness equations. *Materials Science and Technology* 1989; 5: 865-872.

Chapter

III

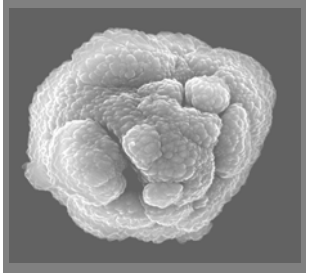

Powder Characterization

Magnetron sputtering offers new possibilities and more flexibility for producing coatings on various substrates at low temperatures.

G. Terwagne et al., Thin Solid Films 377 (2000)

III.1. **I**ntroduction

This chapter is constituted by three papers concerning the characterization of coated powders. The first one is related to the physical and chemical characterization of WC powder coated with stainless steel. The characterization was performed in order to evaluate the feasibility of the sputtering technique to produce composite powders in alternative to conventional powder mixtures. The pressing behaviour and the sinterability were also explored.

The following paper concerns the evaluation of the surface properties in air and aqueous environments. This study was performed in order to explore the effect of processing stainless steel-coated WC powders in aqueous suspensions and in air atmospheres. For such purpose, the thermal reactivity in air of stainless steel coated powders was analysed by DTA-TG. The aqueous behaviour was characterized by electrophoretic measurements at different pH. The effect of pH on the coating adhesion was also determined.

The last paper presents results for the flowability behaviour of coated powders. Three WC coated powders having similar binder contents, ~8-9 wt.%, but different coatings, i.e., stainless steel, stainless steel enriched with nickel and a first layer of nickel followed by a second one of stainless steel, were characterized. The effect of the binder composition and the inherent surface modification on the powder flowabilty was explored in order to evaluate the consequences during the compaction stage. This investigation was performed in co-authorship, but the presentation of these results is relevant for this thesis.

III.2. Stainless steel coatings sputter-deposited on tungsten carbide powder particles

C. M. Fernandes[1], V. M. Ferreira[1], A. M. R. Senos[1] and M. T. Vieira[2]

[1]Department of Ceramics and Glass Engineering, CICECO, University of Aveiro, 3810-193 Aveiro, Portugal
[2]ICEMS, Mechanical Engineering Department, University of Coimbra, 3030-201 Coimbra, Portugal

Surface and Coatings Technology 176 (2003) 103-108

Abstract

The aim of this work was to study the feasibility of a sputtering technique to coat WC powder particles, regarding it as an alternative to the conventional mixture of powders. For such purpose, a stainless steel AISI 304 coating was sputter deposited on WC powder particles using a magnetron sputtering equipment specially developed to coat powder particles. The morphology of the coated powder was characterized by scanning electron microscopy observations, Brunauer-Emmett-Teller and laser diffraction measurements. The crystallographic structure was determined by X-ray diffraction. Inductively coupled plasma–atomic emission spectrometer and electron microprobe analysis were used to characterise the amount, chemical composition and distribution of the sputtered coating. The characterization results indicated that all WC particles were coated and that all the steel constituent elements were deposited in the same original proportion. The coating had a ferrite b.c.c. structure and presented a columnar growth with some porosity. The compaction behaviour of the coated powders was characterized by unidirectional pressing using pressures between 60 and 250 MPa. The maximum of relative density was attained for P≥190 MPa, with values of 57-58% of relative density, comparable to that of non-coated powders, and without the need of any pressing binder to obtain green compacts resistant to handling. High sintered densities, of approximately 95%, were obtained at a relatively low temperature of 1325 ºC with only ~6 wt.% of binder phase in the coated powders.

Keywords: Sputtering; Tungsten carbide; Stainless steel; Pressing behavior

1. Introduction

An extensive work has been performed in the past on WC/Co hard metals, due to their importance for mining tools, tool inserts and other components where wear strength is important. It is well established that tungsten carbide maintains its hardness at high temperatures, but the value of this property is very dependent on the cobalt content. However, some constraints regarding corrosion behavior have been observed in some specific applications. Moreover, some recent research works have investigated the change of cobalt by other metallic elements, to provide lower-cost hard metals and to offer a non-toxic solution [1-7]. Iron alloyed with other elements is one of the solutions envisaged to replace cobalt in hard metals. Mechanical properties evaluation showed that these iron alloy binders may have higher hardness and slightly lower fracture toughness than hard metals with a similar content of cobalt [1-13].

The improvement in processing and properties of metal-bonded tungsten carbide could be attained if the binder was uniformly distributed among the WC grains. In the literature on powder technology of WC, only one reference related to the deposition of Co on WC powders using a chemical precipitation technique was obtained [14]. The as-coated WC powder presented very good uniformity of the Co coating, which led to rapid consolidation near the theoretical density and to an improvement in mechanical properties. Sputtering deposition is one technique broadly used to coat bulk substrates due to its versatility and ability to produce homogeneous coatings of different materials. Sputtering is used here, in an innovative way, to coat WC powders with the appropriate binders for liquid phase sintering. A potential benefit of using this method in composite powder preparation comes directly from a higher chemical homogeneity, which can result from the suitable distribution of the binders. Moreover, this technique allows the production of an extensive range of iron alloys, using a suitable technology for doping the targets. If the deposition conditions are adequate (high deposition pressure, type of inert gas, substrate bias, substrate temperature), it is possible to produce iron-based coatings with a nanocrystalline structure [15]. These coatings could contribute to a more rapid densification process due to both its extremely small grain size and uniform distribution in the matrix.

The aim of the present research work is to obtain, by a sputtering deposition process, WC powders coated with stainless steel and to characterize the morphology, structure and

chemical composition of the coating and to evaluate the uniformity of the binder distribution. The compactibility and sinterability of the coated powder will also be investigated.

2. Experimental

WC powder particles were coated with stainless steel by d.c. magnetron sputtering. The d.c. magnetron sputtering equipment was adapted for powder coating by introducing a chamber with rotational and vibrational movement, favoring the homogeneous coating of the particles (Fig. 1).

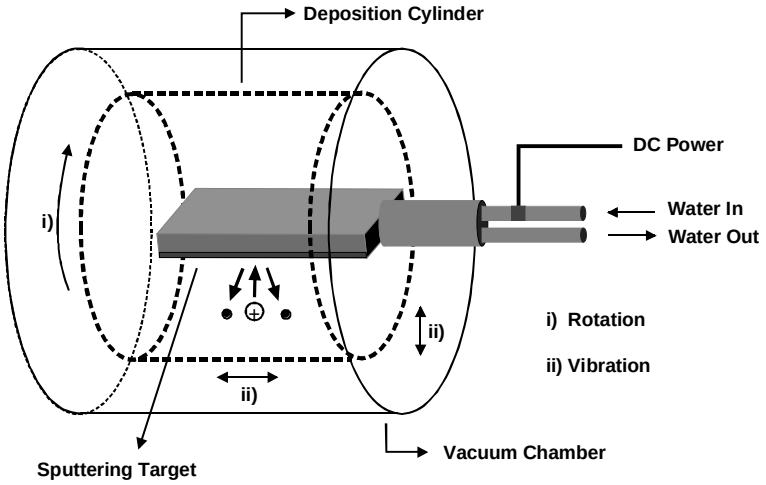

Fig. 1. Sputtering equipment chamber.

The starting powder is a fully carburized WC (9-10 μm) (H.C. Starck, HCST, Germany), which contains, besides the WC phase, traces of W_2C phase. The deposition parameters used are listed in Table 1. Additionally, a rotation speed of 3 r.p.m. and a frequency vibration of 1.6 Hz were used. The targets are made of austenitic stainless steel AISI 304.

For preliminary characterization of the coatings, stainless steel was also deposited in glass substrates with the same deposition parameters listed in Table 1. The morphology characterization of the coating was characterized by scanning electron microscopy (SEM, Hitachi-S4100). The phase identification was performed by X-ray diffraction (XRD, Rigaku). The chemical characterization was carried out by an inductively coupled plasma–atomic emission spectrometer (ICP, Isa JY70Plus) and by electron microprobe analysis

(EMPA, Cameca, Camebox SX50). To determine the adhesion of the coating a scratch test was performed in the stainless steel coating (700 W, 1 h) deposited on WC-Co substrates, under loads from 50 up to 200 N (device maximum load). The powder specific surface area was measured following the Brunauer-Emmett-Teller (BET) method (Micromeritcs Gemini 2370 V5). Laser diffraction (Coulter LS 130) and helium pycnometry (Accupyc 1330) were used to determine the powder particle size distribution and the real powder density, respectively.

Table 1

Deposition parameters for AISI 304 coatings.

Parameters	**Value**
Target area (m^2)	54×10^{-3}
Substrate mass (g)	100
Target-to-substrate distance (mm)	150
Base pressure (Pa)	1×10^{-4}
Sputter gas composition	99.99% Ar
Sputtering pressure (Pa)	0.5
Magnetron power (W)	700
Deposition time (h)	6

In order to evaluate the pressing behavior, the coated powders were uniaxially pressed in the range 60-250 MPa, resulting in pressed compacts with 10 mm in diameter and aproximately 3 mm thick. For comparison, the non-coated powders were also pressed in the same pressure range, after mixing with 1.5 wt.% of paraffin wax, using isopropyl alcohol as solvent in a stainless steel mill with WC-Co balls. Finally, the compacts of coated powders were sintered in a conventional vacuum furnace inside a graphite crucible. The furnace atmosphere was pumped to a base pressure of 1 Pa before sintering. The firing cycle involved a heating rate of 5 $^{o}Cmin^{-1}$ up to a maximum temperature of 1325 ^{o}C, a dwell time of 3 h, and normal cooling down to room temperature. The density of the cermets was obtained by immersion in mercury using the Archimedes method.

3. Results and discussion

Stainless steel coatings were sputter-deposited on glass substrates for a preliminary chemical, structural and morphological characterization, under the coating conditions

mentioned in Table 1. The EPMA analysis carried out in the coating (Table 2) indicated that iron, chromium, nickel, manganese and silicon contents were within the specifications for AISI 304 stainless steel. This means that the magnetron sputtering could successfully transfer the multi-element composition of the stainless steel targets to the coating without any significant stoichiometric variation, as already observed in the sputtering of other types of stainless steel, namely AISI 310 and AISI 316 coatings [16,17].

Table 2

EMPA characterization of the stainless steel coating on glass substrates.

Sample	Fe (wt.%)	Cr (wt.%)	Ni (wt.%)	Mn (wt.%)	Si (wt.%)
Coating	71.6	17.9	8.1	1.9	0.5
Target	71.6	18.4	8.0	1.7	0.3

The XRD diffraction pattern for the AISI 304 coating (Fig. 2) indicate two peaks corresponding to diffraction from {110} and {211} planes of a ferrite (α) stainless steel structure. The crystallographic structure of these coatings is largely determined by the substrate temperature and deposition rate [18]. In this case, the coating takes the structure of the most stable single phase that can exist for the particular alloy composition, indicating that the deposition rate and the substrate temperature are low. It has long been recognized, in related papers, that coatings sputtered from austenitic stainless steel targets do not usually form an austenitic FCC structure, but rather have a ferrite BCC structure [19].

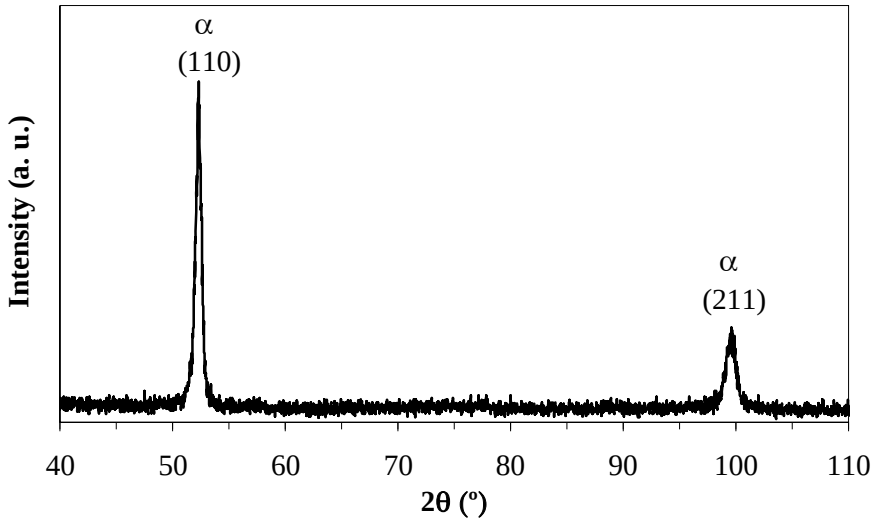

Fig. 2. X-ray diffraction pattern of the coating on a glass substrate.

SEM micrographs obtained from the cross-section and surface of the coating (Fig. 3) revealed a columnar structure. It is possible to observe in Fig. 2(a), a small amount of porosity in the coating which is indicative of a morphology of type 1, according with the model of Thornton [20]. This type of coating morphology is usual for low substrate temperatures and high deposition pressures [20]. The apparent density of the coating was geometrically measured, resulting a value of 6.0 ± 0.5 gcm^{-3}, indicating that the coating is not very dense when compared with the ferrite theoretical density (7.9 gcm^{-3}) [21].

The ICP analysis of the coated powders also confirms that the existing elements in the steel target are all deposited on the powder particles, maintaining the ratios of the initial steel composition (Table 3). The total amount of coating sputtered in the powder was calculated in Table 3 as the addition of all the detected elements by ICP analysis. This is an approximation by defect, since there are minor elements which were not considered, such as C and probably P and S. However, taking the steel composition, the associated error is only ~1.1%, relatively to the coating total values in Table 3.

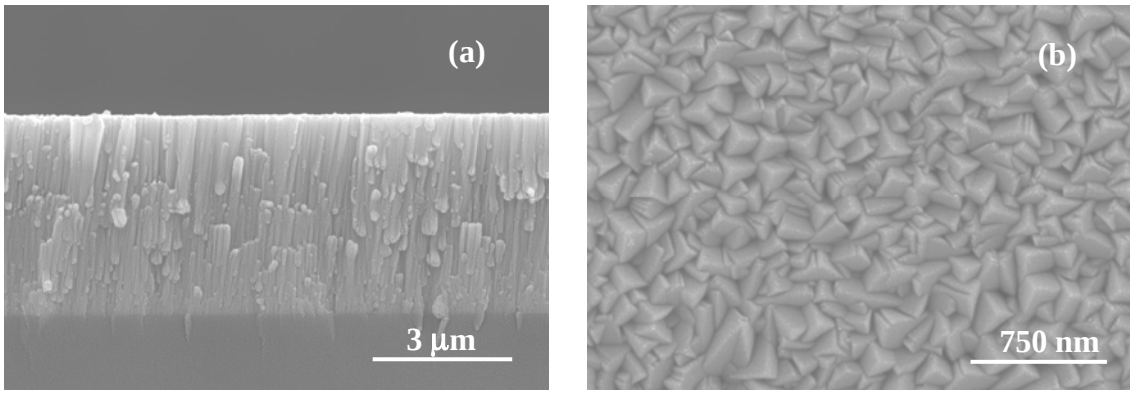

Fig. 3. SEM micrographs of the coating on a glass substrate: (a) cross-section; and (b) surface .

The real density of the coated and non-coated powders was measured with a He pycnometer. The density value for the non-coated powder, d=15.58±0.01 gcm^{-3}, is close to the theoretical density, d_t, of WC (d_t =15.63 gcm^{-3}). For the coated powder the density is reduced, ρ=14.44±0.01 gcm^{-3}, but closely matches the one calculated with the classical law of mixtures [22]:

$$\rho=1/\Sigma(w_i/\rho_i) \qquad \text{(Eq.1)}$$

where ρ is the density of the composite, ρ_i is the density of constituents and w_i is the concentration (weight fraction) of constituents. Using this rule and taking the pre-

determined value for the amount of coverage (5.7%), the measured densities of the coating (6.0 gcm^{-3}) and the WC powder (15.58 gcm^{-3}), the resulting value is 14.3 gcm^{-3}.

Table 3

Chemical characterization of coated and non-coated WC powder by ICP.

Sample	Fe (wt.%)	Cr (wt.%)	Ni (wt.%)	Mn (wt.%)	Total (wt.%)
WC	0.02	<0.009	<0.009	<0.009	0
Coated WC	4.01	1.06	0.48	0.10	5.65

The XRD pattern of the coated powder (Fig. 4) shows, apart from the WC major phase and W_2C vestigial phase in the initial powder, a small peak identified with Fe-α (ferrite), as expected from the XRD pattern of the coating in Fig. 2. The lack of definition of this peak is related to the small amount of coating (~5.7 wt.%), together with internal residual stresses of the coating caused by atomic inadaptation in the interface WC/Fe-α.

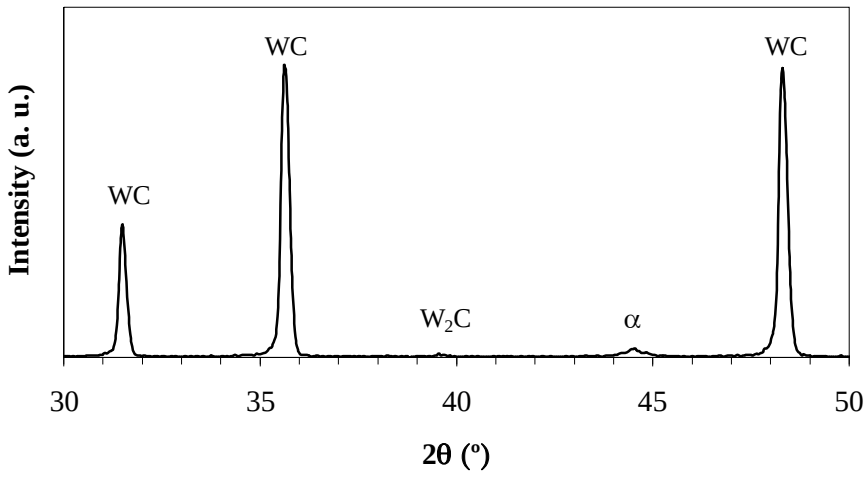

Fig. 4. X-ray diffraction pattern of the coated powder.

The non-coated WC powders are constituted by small particles of less than 3 μm, which form aggregates with a size between 3 and 25 μm with a nodular form (Fig. 5(a) and (b)). These aggregates present a densified appearance with well developed grain boundaries probably formed during the carbonization step, at temperatures between 1400 and 1800ºC. This densified appearance is confirmed by the close matching between the values of real and theoretical density of the powder, quoted above, since the existence of significant amounts of closed porosity inside the aggregates would enlarge the difference

between them. The coated powder also show an identical morphology in the aggregate size distribution (Fig. 5(c) and (d)), but it is possible to observe, in Fig. 5(d), the complete covering of the WC aggregate which shows high roughness originated by the columnar structure of the coating. The EPMA analysis of the coated particles also shows the presence of all the coating elements in each evaluated particle.

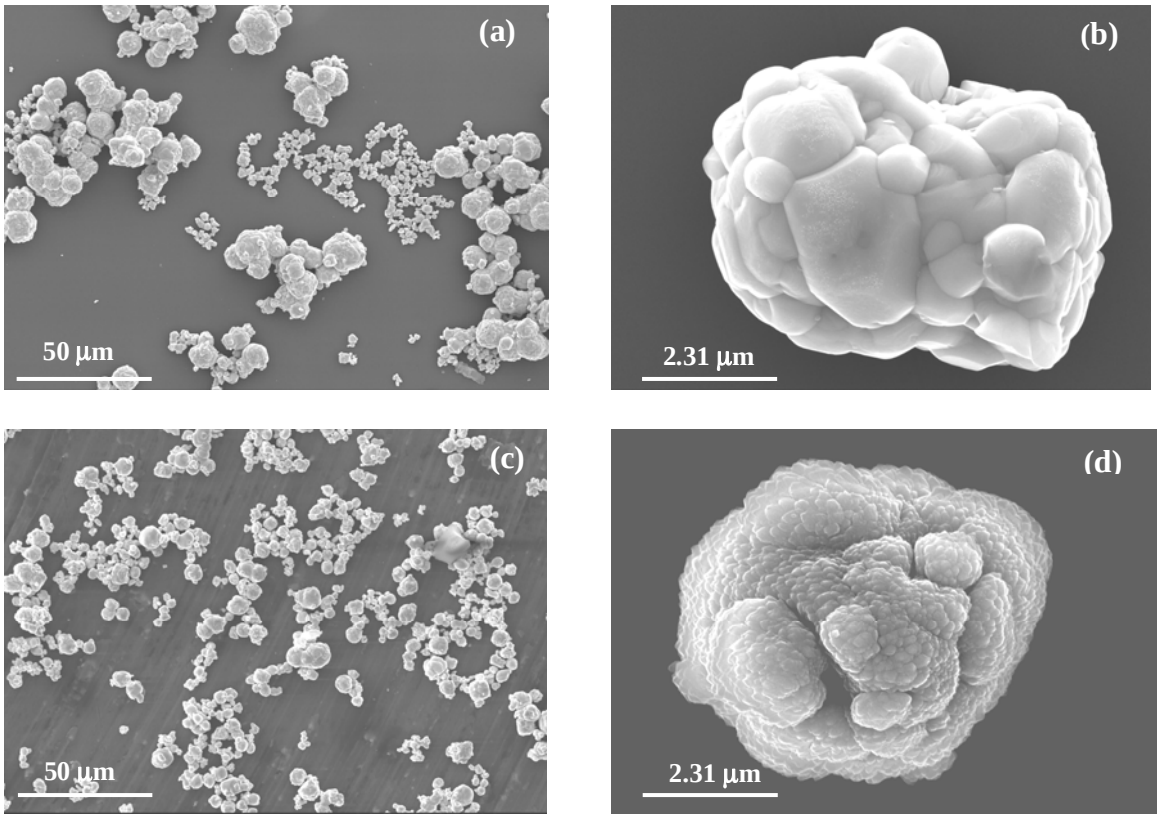

Fig. 5. SEM micrographs taken from: (a) and (b) non-coated WC powder; (c) and (d) coated WC powder.

The particle size distribution of these powders (Fig. 6) shows a small increase in the average particle size in the coated powder. This increase cannot only be attributed to the effect of the coating, since for an amount of ~6 wt.% and considering an uniform distribution, the calculated increase in average particle diameter would be ~0.40 μm and not ~1.5 μm, as presented in Table 4 (G_{LD}). The strong drum rotating movement may result in a slight powder granulation, which may cause this average size increase. However, the calculated values of equivalent spherical diameter from the specific superficial area values (G_{BET}) (Table 4) show a net decrease for the coated powder, apparently contradictory to the G_{LD} values. The G_{BET} values are strongly affected by the increase in specific superficial

area, resulting from the increase in the aggregate roughness in the coated particles surfaces (Fig. 5(b) and (d)).

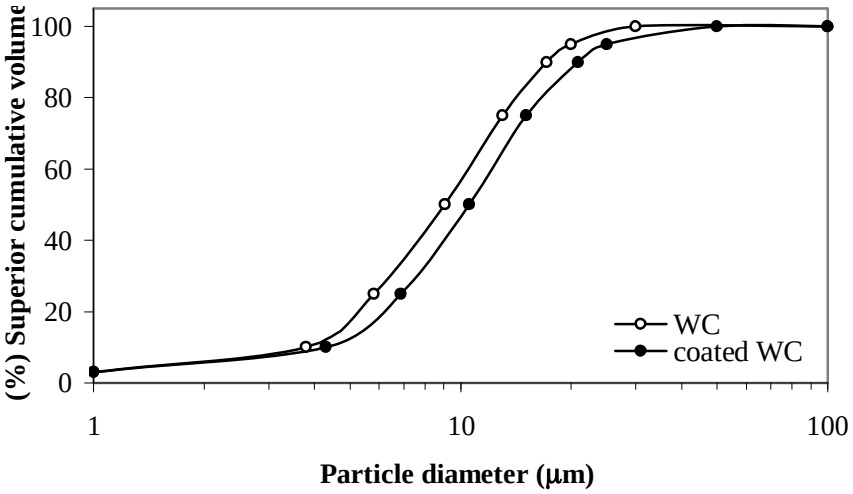

Fig. 6. Particle size distribution of the coated and non-coated WC powder.

The compaction behavior of the coated and non-coated powders was investigated. By directly pressing the powder, it was observed that the coated powder reaches enough resistance to handling without the addition of paraffin wax, while the non-coated one needs the previous paraffin addition as usually done in WC composite processing [2,3,6,8,23]. The possibility of directly press the coated powders is indicative of the good adhesion between the WC particles and the coating, in accordance with the scratch test performed on the stainless steel film deposited on WC-Co substrates, since adhesive imperfections are not detectable by the microscopic examination. The occurrence of plastic deformation of the coating ductile material inside the pores and the high roughness of the particle surfaces can also contribute to the enhanced resistance of the compacts.

Table 4

Physical characterization of coated and non-coated WC powder.

Sample	$S_{w,\,BET}$ [a] (m^2g^{-1})	G_{BET} [b] (μm)	G_{LD} [c] 50% (<) (μm)	Real Density (gcm^{-3})
WC	0.0485	7.9	9.06 ± 0.47	15.58 ± 0.01
Coated WC	0.1336	3.1	10.56 ± 0.40	14.44 ± 0.01

[a] Specific surface area obtained by BET.

[b] Spherical equivalent diameter from BET.

[c] Particle diameter obtained by laser diffraction.

The variation of the relative density as a function of the applied pressure (Fig. 7) shows that close values of green density are obtained in coated and non-coated powders and the maximum density is reached, approximately, for 200 MPa in both powders. The micrograph of the compact of coated WC powder pressed at 190MPa (Fig. 8) also shows that a relatively uniform distribution of the porosity is attained at this pressure values.

The present results show that it is possible to obtain pressed compacts with similar relative densities in coated and non-coated powders, despite the morphological and chemical differences in powders. Furthermore, the powder coating by sputtering may represent an important technological benefit in processing because the removal of pressing binder also eliminates the need for the binder mixing and debinding operations preceding the sintering and therefore, decreases the overall cycle time of conventional processing.

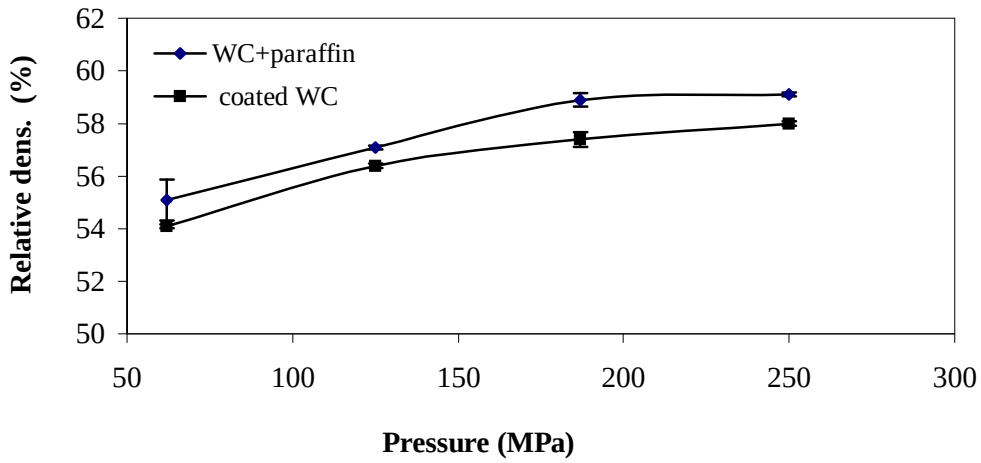

Fig. 7. Variation of the relative green density as a function of the pressing pressure.

The sintering behavior of the coated powder was studied in compacts pressed at 190 MPa in vacuum atmosphere, at 1325 ºC, with a dwell time of 3 h. Previous studies made with 6-7 wt.% of binder have indicated that 95% of theoretical density was reached at this temperature. Such a high value of density obtained at a relatively lower temperature, when compared with similar compositions conventionally processed [3], may be a consequence of a much higher uniformity and higher reactivity of the binder phase in the powder matrix. Forthcoming studies will be made for a better characterization of the sintering behaviour of coated powders.

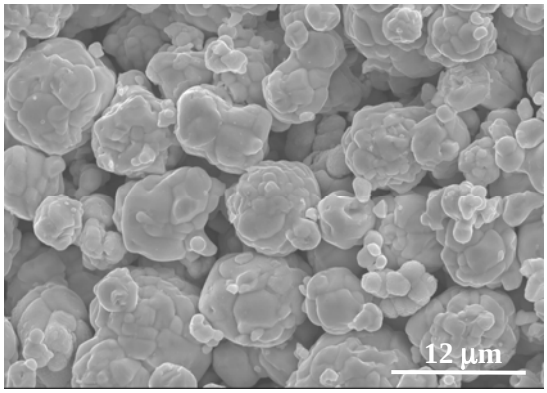

Fig. 8. SEM micrograph of uniaxially pressed coated powder at 190 MPa.

4. Conclusions

The present results demonstrate that the sputtering technique used here, to coat WC powder particles, is very efficient in the promotion of the deposition of all the stainless steel elements in the same stoichiometry as that existent in the target. The powder particles were uniformly coated, which results in a high chemical homogeneity in the distribution of powder constituents.

The compaction behavior of the coated powders showed that it was not necessary to use any type of pressing binder, commonly used in the WC based cemented carbides, to reach an adequate resistance to handling. This observation strengthens the interest of the use of coated powders, because the exclusion of the pressing lubricant leads to the removal of two stages of the conventional WC based cemented carbides processing, namely the milling and removal of the pressing lubricant.

Addition of binder by this sputtering technique is shown to be very efficient in promoting densification, which may also be attributed to the high degree of uniformity in binder distribution and to the high reactivity of the binder phase attained by this process of powder preparation.

References

[1] Hanyaloglu C., Aksakal B., Bolton J.D., Materials Characterization 47 (2001) 315.

[2] Kakeshita T. and Wayman C.M. Materials Science and Engineering A141 (1991) 209.

[3] Farroq T. and Davies T.J. International Journal of Powder Metallurgy 27 (4) (1991) 347.

[4] Uhrenius B. Powder Metallurgy 35 (3) (1992) 203.

[5] Tracey V.A. Refractory Metals & Hard Materials 11 (1992) 137.

[6] González R., Echeberría J., Sánchez JM and Castro F. Journal of Materials Science 30 (1995) 3435.

[7] Uhrenius B., Pastor H. and Pauty E. Int. J. of Refractory Metals & Hard Materials 15 (1997) 139.

[8] Viswanadham R.K and Lindquist P.G. Metallurgical Transactions A 18A (1987) 2163.

[9] Viswanadham R.K and Lindquist P.G. Metallurgical Transactions A 18A (1987) 2175.

[10] Moskowitz D., Ford M.J. and Humenik Jr. M. International Journal of Powder Metallurgy 6 (4) (1970) 55.

[11] Moskowitz D. Mod. Dev. Powder Metall. 10 (1977) 543.

[12] Suzuki H., Yamamoo T and Kawakatsu I. Powder Metallurgy Journal 14 (1967) 26.

[13] Prakash L., Holleck H., Thümmler F. and Walter P. Modern Developments in Powder Metallurgy, 14, MPIF, ed. H. Hausner, H. W. Antes & G. D. Smith, 1981, 255-268.

[14] Sampath A., Stiglich J. J., Sudarshan T. S., Singh R. and Choi K.S. Powder Metallurgy 45 (1) (2002) 25.

[15] Fougere G. EWeertman, J. R. and. Siegel R. W**,** Nanostructered Materials, 5 (1995) 127.

[16] Billard A., Frantz C. Surface and Coatings Technology 59 (1993) 41.

[17] Shedden B.A., Kaul FN, Samandi M, Window B. Surface and Coatings Technology 97 (1997) 102.

[18] Miodownik A.P. Powder Metallurgy 32 (4) (1989) 269.

[19] Dahlgren SD. Metall. Trans. 1 (11) (1970) 3095.

[20] The Materials Science of Thin Films, Milton Ohring, Academic Press, 1991.

[21] JCPDS-International Centre for Diffraction Data, 2000.

[22] Uygur M.E. Advanced Materials & Processes 3 (1997) 35.

[23] Upadhyaya G.S. and Bhaumik S.K. Materials Science and Engineering A A105-106 (1988) 249.

III.3. Particle surface properties of stainless steel-coated tungsten carbide powders

C. M. Fernandes[1], A. M. R. Senos[1] and M. T. Vieira[2]

[1]Department of Ceramics and Glass Engineering, CICECO, University of Aveiro, 3810-193 Aveiro, Portugal
[2]ICEMS, Mechanical Engineering Department, University of Coimbra, 3030-201 Coimbra, Portugal

Powder Technology 164 (2006) 124-129

Abstract

Tungsten carbide powders sputter-deposited with stainless steel were characterized in order to evaluate the surface properties in air and aqueous environments. The scanning electron microscopy with energy dispersive spectroscopy showed that a very high uniformity of the coating distribution on the WC particles was attained by the sputtering technique, enabling a complete surface coverage for low coating contents ($\gtrsim$1 wt.%).

The DTA-TG thermal analysis in air atmosphere revealed that the coating layers increase the oxidation resistance of WC powders, in spite of the coating porosity.

The electrophoretic measurements performed in aqueous solution, for different pH at a constant ionic strength (1 mM KCl), showed that the surface charge until pH$\simeq$8 is essentially determined by the stainless steel coating, while for higher pH becomes closer to that of the WC particles. The coating adhesion measured by a scratch test was found to decrease in the basic pH region. These results were discussed in terms of the effect of the short-range repulsion forces between the coating layer and the particle surface in aqueous suspensions.

Keywords: Sputtering; Zeta potential; Tungsten carbide; Stainless steel

1. Introduction

Hard metal is a metallurgical powder product which generally consists of tungsten carbide (WC) particles bound together with a metal binder, commonly cobalt. It is widely used in a variety of applications that demand wear resistance and high temperature capability, namely cutting tools, drilling and milling equipment. Several studies have been made in order to replace cobalt by other cheaper metals, such as iron rich binders, which result in hard metals with identical mechanical properties [1-9]. In the present work stainless steel AISI 304 was used as a binder material, which was sputter-deposited on tungsten carbide powder particles using a magnetron sputtering technique [10]. This new powder coating technique was successfully employed in the preparation of the composite powder, leading to a very high chemical homogeneity in the distribution of the constituents and to a modification of the particle surface properties [10]. New perspectives for the processing and technological applications of these composites were opened by the use of the sputter deposition which needs to be explored.

Previous investigations of the sputter-deposited WC-stainless steel powders were directed to the chemical, structural and microscopic characterization of the powder coating and showed that it is possible to cover WC particles with thin layers of stainless steel having all the elements of the target in the same stoichiometric proportions [10]. The coating presents a ferrite BCC structure and a high surface roughness originated by a columnar growth [10]. The change of the surface characteristics together with the high uniformity of the binder distribution brings a significant improvement of the powder compactibility and of the densification attained during sintering of these powders, which was also investigated in previous works [10-12].

The reduction of the binder amount is envisaged in these composites due in part to the above mentioned results of the higher sinterability of the sputtered powders. On the other hand, the very high uniformity of the binder distribution attained in coated powder compacts may bring an optimization of the mechanical properties [13-15], enabling the diminution of the additives needed to attain the required technological properties. Moreover, the use of a thin layer of a given element on the particle's surface can be used to appropriately change the surface behaviour before the conventional preparation of the composite powder [16]. In this sense, it will be important to determine the minimum

content of sputtered binder that will be sufficient to complete the particle coverage and consequently change the surface properties.

The possibility of a direct pressing of the sputtered coated powders, without the addition of paraffin wax, is a real benefit of this process [10]. However, this benefit is only observed for contents of stainless steel higher than ~4 wt%, whereas for lower contents the addition of a pressing lubricant is needed to reach adequate resistance to handling. In this case, a wet mixing step with paraffin wax is needed and the study of the behaviour of these coated powders in liquid medium will be of large interest to reach a good homogenization. Furthermore, an additional thermal treatment, before mixing of powder with the pressing lubricant, is convenient to guarantee a high enough adhesion between the coating and the substrate, which must be able to support the attrition forces of the wet mixing step.

In the present work, a complementary particle surface characterization is made focusing the microstructure, the thermal reactivity in air and the electrokinetic properties of the stainless steel coated powders, aiming the characterisation of the surface behaviour for different contents of stainless steel. The adequate choose of experimental conditions in the further processing of these composite powders is also envisaged.

2. Experimental

The starting powder is a fully carburized WC (H.C. Starck, HCST-Germany) which particles were coated with stainless steel by a modified d.c. magnetron sputtering equipment [10]. An austenitic stainless steel (SS) AISI 304 was used as target, and the deposition parameters selected for deposition have already been described elsewhere [10]. These sputter-deposited powders with different contents of deposited stainless steel are here generally designated by C-WC (coated WC) and differentiated by a number corresponding to different amounts of deposited stainless steel (Table 1). An AISI 304 stainless steel (304SS) powder (Fe/Cr18/Ni10 Goodfellow FE226010 powder alloy) was also used for comparative studies.

The morphology of the coated powders were analysed by scanning electron microscopy (SEM, Hitachi-S4100). The coated powders were mounted in an epoxy resin, polished and etched with a 5% nitric acid solution, for 10 s, in order to distinguish the metallic coating. The powder-specific surface area was measured following the Brunauer-Emmett-Teller

(BET) method (Micromeritcs Gemini 2370 V5). Laser diffraction (Coulter LS 130) and helium pycnometry (Accupyc 1330) were used to determine the powder particle size distribution and the real powder density, respectively. The apparent density of the coating was determined from the apparent volume geometrically measured in coatings deposited in glass substrates. The chemical characterization was carried out by inductively coupled plasma–atomic emission spectrometer (ICP, ISA JY70Plus) and energy dispersive spectroscopy (EDS, detector Rontec-EDR288/SPU2). For the ICP analysis, 10 mg of powder were used to prepare 100 ml of solution, under acidic conditions.

Table 1

Coated and uncoated WC powder characterization.

Sample	$S_{W,BET}$ [a] ($m^2 g^{-1}$)	G_{LD} [b] 50% (<) (μm)	Real Density ($g\ cm^{-3}$)	Binder amount [c] (wt.%)
WC	0.049	9.1 ± 0.5	15.58 ± 0.01	0
C-WC1	0.121	10.2 ± 0.2	15.33 ± 0.14	1.0
C-WC2	0.119	10.7 ± 0.3	13.81 ± 0.01	10.0

[a] Specific surface area obtained by BET.

[b] Average particle diameter obtained by laser diffraction.

[c] Total coating amount detected by ICP.

In order to study the air oxidation behaviour of uncoated and coated WC powders differential thermal-thermogravimetric analysis (DTA-TG) measurements were carried out in a SETARAM LABSYS equipment. The powders were heated until 1100 ºC with a heating rate of 5 ºC/min in air atmosphere. X-ray diffraction (XRD, Rigaku), was used to identify the crystalline phases of powders after being heat-treated in air.

The zeta potential (ξ) of the powders was determined as a function of pH using a Coulter Delsa 440 SX. Electrokinetic measurements were carried out on dilute WC, C-WC and 304SS powder suspensions (0.03 wt%) at a constant ionic strength (1 mM KCl). The WC powder was previous oxidized in water for 24 h. The pH of the suspensions was adjusted by adding small amounts of HCl or NaOH solutions, followed by dispersion using an ultrasonic apparatus. During the zeta potential measurements a small decrease of the pH value was observed and corrected when relevant. To achieve more reliable results each sample was analysed ten times at each pH value. The maximum observed deviation of the measured values, relatively to the average value, was ± 5 mV.

A chemical characterization by ICP was performed on C-WC2 powder after been dispersed in an aqueous solution, at constant ionic strength (1 mM KCl) and pH=10, during 24 h. The supernatant liquid obtained by decantation of the previous C-WC2 suspension was also analysed by ICP, together with the supernatant liquid of an equivalent C-WC2 suspension maintained at pH=5, during 24 h.

A stainless steel coating was sputter-deposited in WC-9%Co substrates using the same conditions described elsewhere [10]. The evaluation of the coating adhesion was performed on as-coated surfaces and on coated surfaces which were previous immersed in aqueous solutions of 1 mM KCl, at pH=5 and pH=10 during 24 h, by scratch tests using a commercial scratch-testing equipment (CSEM-Revetest) fitted with an acoustic detector and following the European standard EN1071-3:2005 [17]. In this test three scratches were made on each sample and for all of them the load that gave rise to the first cohesion failure, L_{c1}, and the load that was responsible for the first adhesion failure, L_{c2} were determined. The tests were performed according to the following conditions: a 200 μm diamond tip was used with a scratching speed of 10 mm s^{-1} and a loading rate of 100 N min^{-1}. The load, applied progressively, varied from 0 N to 70 N. The observation of the indentation channels by optical microscopy allowed the determination of the critical loads, L_{c1} and L_{c2}.

3. Results and Discussion

3.1. Chemical and morphological characterization

It is presented in Table 1 the specific surface area, S_W, the average particle diameter, G_{LD} 50%, the real powder density and the sputter-deposited binder amount, calculated as the summation of the main elements content detected by ICP (Fe, Cr, Ni and Mn), for stainless steel coated WC powders. For comparison, the characteristics of the uncoated WC powder are also presented. The coated powders have different binder amounts, 1 wt% for C-WC1 and 10 wt% for C-WC2, which correspond to different real density values. These values are lower than that for WC powder, Table 1, and closely match the calculated ones, using the classic law of mixtures and the experimental value of 6.0±0.5 g cm^{-3} for the apparent coating density. The particle diameter shows an increase for coated powders which comes, as discussed before [10], from the sputter-deposited layer thickness together

with a slight granulation effect caused by the rotation movement during the sputtering process. Considering the experimental determined value of 6.0±0.5 g cm^{-3} for the apparent coating density and the ferrite theoretical density of 7.9 g cm^{-3}, the nanoporosity of the coating [10] can be estimated as being ~20%.

The microstructures presented in Fig. 1(a) and (b) show the surfaces of coated particles for C-WC1 and C-WC2 powders, respectively. A high surface roughness in both powders, characteristic of the columnar growth of the sputter-deposited ferrite (α) stainless steel coating, can be observed [10]. This increase of the surface roughness implies a correspondent increase of the specific surface area, as observed in Table 1. The identical values found for the specific surface area of C-WC1 and C-WC2 powders, mean that the deposition process must be so uniform that even for the low content of 1 wt.% of sputtered elements, in C-WC1 powder, the particle surfaces must be almost completely covered.

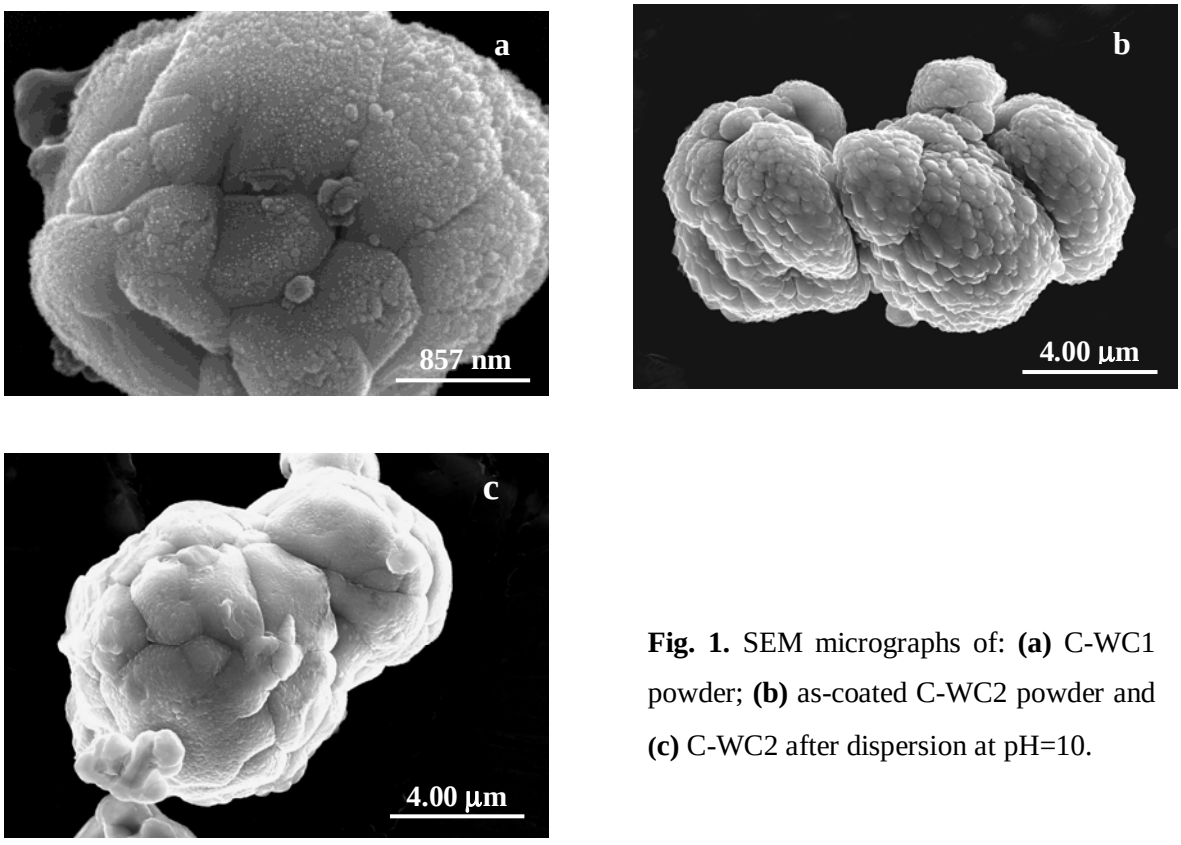

Fig. 1. SEM micrographs of: **(a)** C-WC1 powder; **(b)** as-coated C-WC2 powder and **(c)** C-WC2 after dispersion at pH=10.

For C-WC2, with 10 wt% of binder, the coating thickness can be observed on SEM images of polished samples, Fig. 2(a) and (b) where an inner part (darker) can be distinguished from an external layer (lighter and brilliant). The concentration profiles of Fe

and W clearly show that the inner part corresponds to the original WC particles, while the external layer corresponds to the Fe-rich coating, with all the main components (Fe, Cr and Ni) of the stainless steel target, as given by EDS analysis in Fig 2(a).

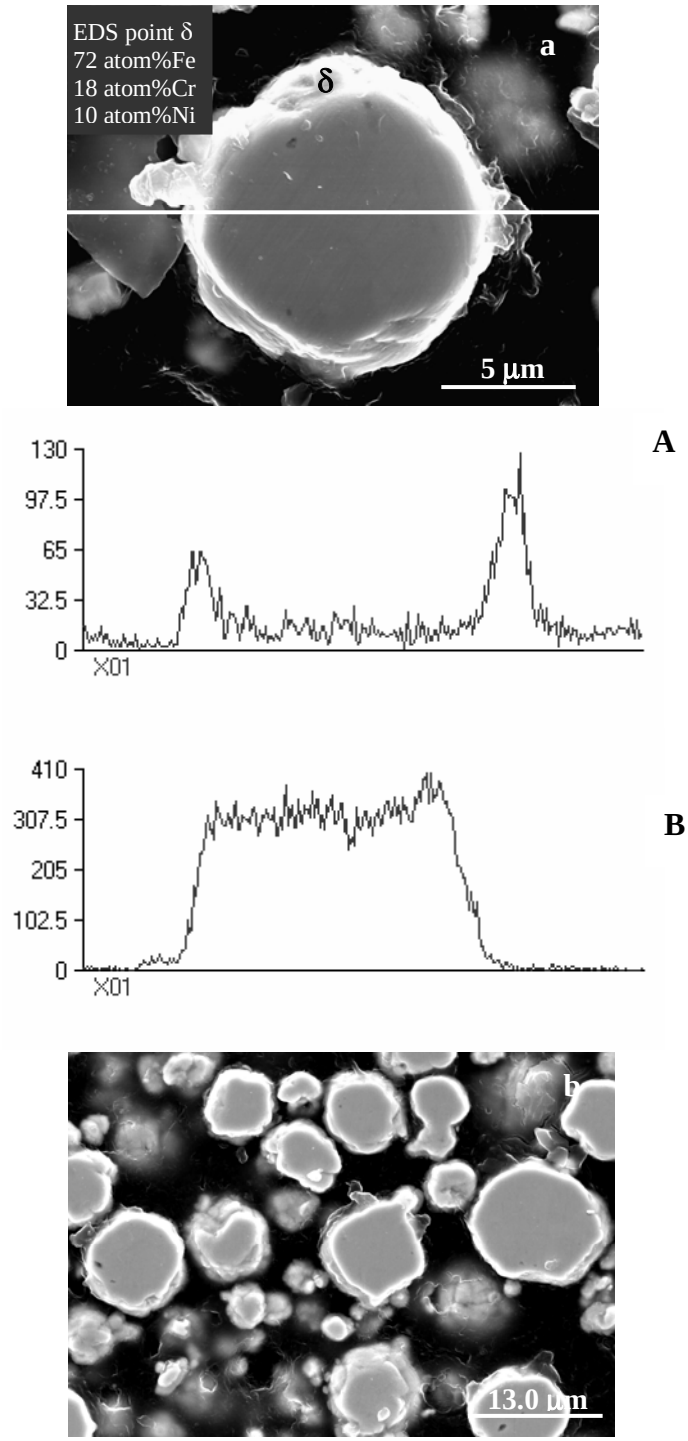

Fig. 2. (a and b) SEM micrographs of C-WC2 and concentration profiles of: (A) iron and (B) tungsten.

All the sectioned particles show a coating layer with a very uniform thickness, in Fig. 2(b). From these photographs, Fig. 2(a) and (b), the estimated average coating thickness is ~0.4 μm, which matches the calculated value assuming an uniform binder distribution on the surface of spherical WC particles 9.1 μm in diameter (G_{LD} 50% in Table 1).

3.2. Thermal analysis

The oxidation resistance of the uncoated and coated C-WC1 and C-WC2 powders was studied by DTA and TG analysis in air until 1100ºC (Fig. 3(a) and (b)). Each of the DTA curves in Fig. 3(a) presents one exothermic peak accompanied by an increase of mass, in Fig. 3(b) which corresponds to the oxidation processes. The oxidation reaction of uncoated WC powder initialises at ~500ºC, presenting a fast increase of weight up to ~650ºC and the maximum of the exothermic peak at ~570ºC. This first stage may correspond to the oxidation of the surface particles. After that, the reaction proceeds with a slower rate of mass gain and without an appreciable exothermic effect. This stage is probably controlled by the oxygen diffusion through the oxide films formed on the surfaces of WC particles. The theoretical calculation of weight gain for the complete oxidation of WC is 18.4 wt. %, according to the most probable oxidation reaction [18]:

$$WC\,(s) + \frac{5}{2}O_2\,(g) \rightarrow WO_3\,(s) + CO_2\,(g) \qquad (1)$$

This weight gain is attained ~1100ºC, Fig. 3(b), which means that the oxidation process must be completed at this temperature. Accordingly, the XRD results of this powder heat treated at 1100ºC, in air, Fig. 4, only present the diffraction peaks of the WO_3 phase.

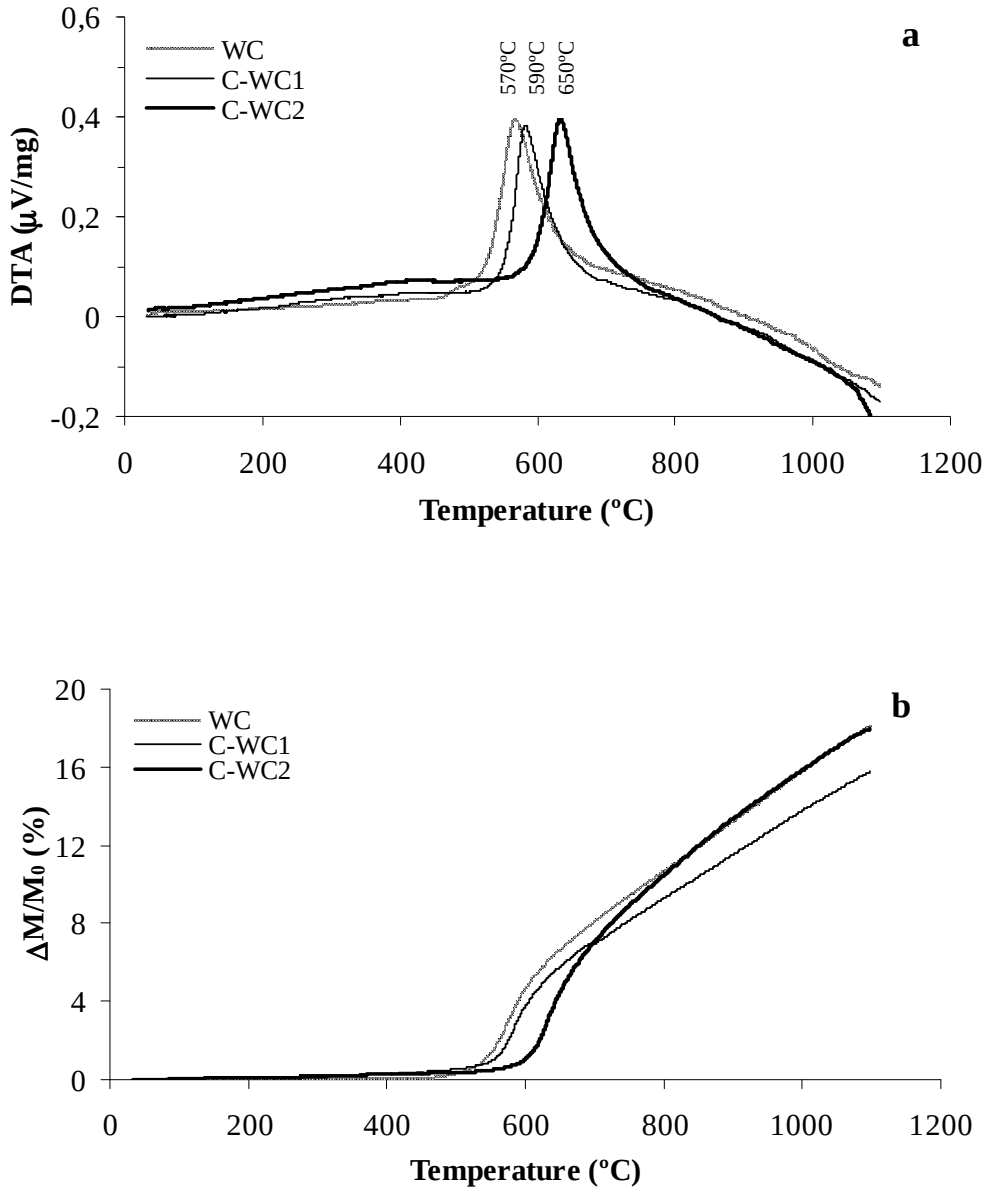

Fig. 3. Thermal analysis in air atmosphere of uncoated and coated WC powders: **(a)** DTA and **(b)** TG.

The DTA-TG curves of coated powders in Fig. 3 show that the oxidation reaction presents two stages, as for uncoated WC powder, but is retarded for slightly higher temperatures. This retardation effect depends on the amount of binder, i.e., increases with the thickness of the coating layers displacing the maximum of the exothermic DTA peak from ~570ºC to 590ºC and 650ºC, for C-WC1 and C-WC2, respectively. The morphological analysis done before indicated that the WC particle surfaces of C-WC2

powder are completely covered, but the coating presents ~20% of nanoporosity and is, therefore, permeable to air. So, the coating layer cannot represent a very effective protection against oxidation, even being its oxidation resistance much higher than that of WC powder (the oxidation reaction of the 304SS powder, with the same composition of the coating layers, occurs for T>900ºC, with an exothermic peak at 1000ºC). However, the oxidation reaction in the coated powders may be controlled during the first stage by the air permeability in the porous coating, which decreases with the increase of the coating thickness and leads to the observed increase of the oxidation temperature.

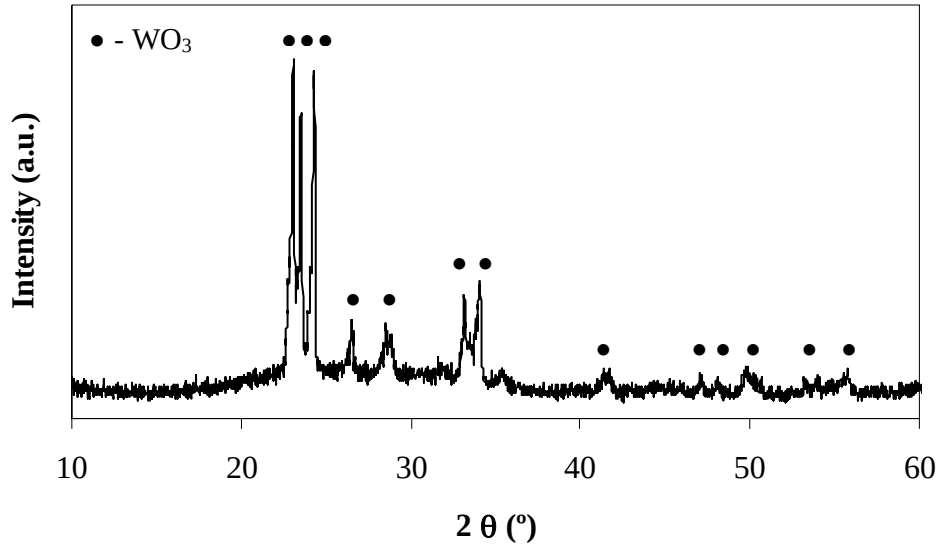

Fig. 4. XRD diffraction profile of WC powder heat treated at 1100ºC, in air.

Taking the present results, thermal treatments of these powders can be done in air atmosphere without presumable oxidation up to 450-550ºC, depending on the binder amount. The limit temperature is slightly increased for larger quantities of binder.

3.3. Electrophoretic measurements

The electrokinetic behaviour of the coated powders was examined in aqueous solution, for different pH at a constant ionic strength (1 mM KCl). For comparative purposes, the electrokinetic behaviour of the WC powder and of the 304SS powder was also investigated.

Fig. 5 shows the zeta potential of the WC powder, the sputter-deposited powders (C-WC), and the 304SS powder in function of pH. The zeta potential for the WC powder

shows a negative value over investigated pH range, between 3 and 10. This behaviour was already found in another study about the electrokinetic behaviour of WO_3 [19], since WC oxidizes in aqueous media and the WO_3 surface layers on the oxidized WC powder controls the surface chemistry and the dissolution [18]. The negative value of the potential is attributed to the high rate of dissociation of the surface hydroxyl groups for the tungsten oxide, even at low pH values, according to

$$\equiv M\text{-}OH \leftrightarrow \equiv M\text{-}O^- + H^+ \quad (2)$$

where M is the metal of the oxide (W). Consequently, the isoelectric point (IEP) of WO_3 is very low, around pH=0.5 [20].

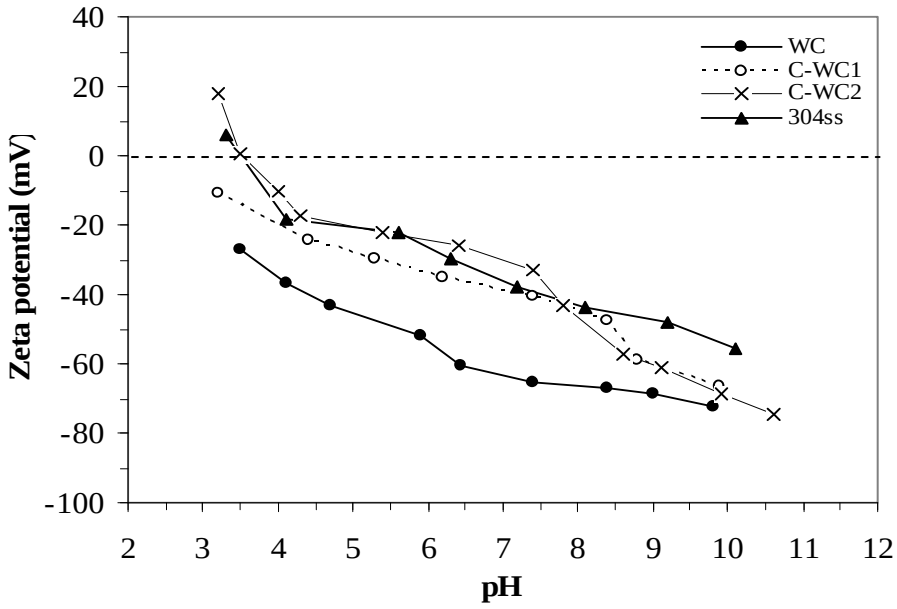

Fig. 5. Zeta potential as a function of pH for powders: WC, C-WC1, C-WC2 and 304SS powders.

It is also shown in Fig. 5 the pH dependence of the surface charge for the 304SS powder. The zero net charge (IEP) is here attained at pH~3.4, resulting in a negative zeta potential for higher pH values. The coated WC powders, C-WC1 and C-WC2, in the same figure, show surface charge values close to the 304SS powder in all the acid range, despite the morphologic and structural differences between the 304SS powder and the coatings. This electrokinetic behaviour also points to the attainment of a very high fraction of coated WC surfaces for a low content of coating (1 wt.% in C-WC1 powder), in consequence of the large uniformity of the coating distribution on the particles, together with the small size of the sputtered stainless steel particles (~200 nm) [10], as previously observed from the

analysis of the BET results, Table 1, and from the SEM micrographs, Fig. 1. A similar electrokinetic behaviour was observed in suspensions of powders coated by colloidal processes, such as Al_2O_3 coating Si_3N_4 [21-23] and Al_2O_3 coating Mo [24]: the surface charges of those coated powders are closer to those of the Al_2O_3 coating phase, approaching it for increasing amounts of coating material, but usually large contents of coating ($\gtrsim$10 wt.%) are needed to attain the IEP of the coating phase [21,24].

For 10 wt.% of coating, in C-WC2, the IEP is attained at the same pH value of the 304SS powder, pH$\simeq$3.4, but for pH$\gtrsim$8 the zeta potential values of both C-WC1 and C-WC2 powders become more negative than the ones of the 304SS powder and closer to those of the WC uncoated powder.

The ICP results of the C-WC2 powder as-coated and after been dispersed at pH$\simeq$10 are presented in Table 2. The results show that in the dispersed powder at pH=10, some coating dissolution occurred, but the total of removed elements only represented ~4.5 wt.% of the original coating amount. The particle surface of this powder in Fig. 1(c) presents a strong decrease of the particle roughness, which may come from the preferential dissolution of the higher chemical potential points on the convex surfaces, but the particle surface remains coated.

Table 2

Chemical characterization of C-WC2 powder by ICP.

Sample	**W (wt.%)**	**Fe (wt.%)**	**Cr (wt.%)**	**Ni (wt.%)**	**Mn (wt.%)**	**Sum**
Powder						
As-coated	—	7.16	1.87	0.81	0.14	9.98
Dispersed at pH=10	—	6.85	1.74	0.79	0.14	9.52
Supernatant liquid						
pH 5	0.31	0.12	0.03	0.06	0.010	0.53
pH 10	4.40	0.03	0.03	0.06	0.006	4.53

The nanoporosity determined for the stainless steel coatings on the WC particles, ~20%, enables the absorption of water and it seems probable the existence of some contact points of the liquid with the WC surface, depending on the contact angle. It can be

observed in Fig. 5 that, due to the negative charges of both WC and stainless steel surfaces from pH>3.4, short-range repulsion forces between these surfaces will be present [22,25] and will increase for higher pH values. In this case, the water may penetrate between the coating and the WC surface and the measured surface charge will approach that of the WC surface. The ICP analysis of the supernatant liquid obtained from the decantation of C-WC2 powder suspensions at pH=5 and 10 (Table 2) shows, in accord, that W do not dissolve significantly in the pH=5 suspension, but an appreciable W dissolution is observed, at pH=10. Since dissolution of WC can occur in all the pH range [18], the much higher dissolved amount found at a pH=10 may be a consequence of the increase of the contact area between the water and the WC surfaces. To better confirm this interpretation, scratch tests were performed on stainless steel coatings sputter-deposited on WC-9%Co substrates. An as-coated surface and other two samples previous immersed in aqueous solutions at pH=5 and pH=10 were characterized. Up to the maximum applied load of 70 N, no flaking off failures were found in the scratch tracks performed on the as-coated surface and on the immersed one at pH=5, which means that the film cohesion is not attained, L_{c1}>70N, and the adhesion is excellent. For the coating immersed at pH=10, the adhesion has a reduction and the coating presents adhesion failures from 52 N of applied load (L_{c1}=52N). These results reinforce the previous interpretation of the effect of short-range repulsion forces in the interface of coated surfaces and point out to the reduction of the adhesion between stainless steel coatings and WC surfaces in basic aqueous suspensions. It should be noted that SEM top and cross section views did not revealed particular aptitude to detect the differences between the samples.

4. Conclusions

The coating of WC powder particles with stainless steel by sputter deposition is an innovative way to change the particle surface properties and to add a very uniform layer of sputtered elements on the surface of WC particles. A complete particle coverage is attained for low sputtered contents, ~1 wt.%.

The coated powders showed a slightly higher resistance to oxidation in air atmosphere, in comparison to the uncoated WC powder, and the resistance increased with the coating thickness. Since the coating presents a high nanoporosity, ~20%, it must be permeable to air, but this permeability will be reduced with the increase of the coating thickness, leading to the observed increase of the oxidation resistance. The limit temperature for thermal treatments in air, without oxidation, changes from ~ 450ºC for non-coated WC powder to ~ 550ºC for the coated powder with 10 wt.% of binder.

The surface charge of coated powders in aqueous suspensions is dominated by the coating layer until pH≃8. For higher values of pH, the surface charge of the coated powders approaches that of the WC particles. It was detected in the basic pH range a net increase of the W solubility and a strong reduction of the coating adhesion. From these observations, it was concluded that the short-range repulsion forces between the coating and the particle surface in basic aqueous suspensions are strong enough to reduce the coating adhesion and increase the wetting of the WC surface. These results also point for the convenience of choosing acid-neutral pH values in the aqueous processing of stainless steel-coated WC because more stable suspensions are obtained in that pH range. Furthermore, the basic region should be avoided because the coating adhesion is strongly reduced.

References

[1] C. Hanyaloglu, B. Aksakal, J.D. Bolton, Mater. Charact. 47 (2001) 315.

[2] T. Kakeshita, C.M. Wayman, Mater. Sci. Eng. A 141 (1991) 209.

[3] T. Farroq, T.J. Davies, Int. J. Powder Metallurgy 27 (4) (1991) 347.

[4] B. Uhrenius, Powder Metall. 35 (3) (1992) 203.

[5] R. González, J. Echeberría, J.M. Sánchez, F. Castro, J. Mater. Sci. 30 (1995) 3435.

[6] B. Uhrenius, H. Pastor, E. Pauty, Int. J. Refract. Met. Hard Mat. 15 (1997) 139.

[7] R.K Viswanadham, P.G. Lindquist, Metall. Trans. A 18A (1987) 2163.

[8] D. Moskowitz, Mod. Dev. Powder Metall. 10 (1977) 543.

[9] H. Suzuki, T. Yamamoo, I. Kawakatsu, Powder Metall. J. 14 (1967) 26.

[10] C.M. Fernandes, V.M. Ferreira, A.M.R. Senos, M.T. Vieira, Surf. Coat. Technol. 176 (1) (2003) 103.

[11] C.M. Fernandes, A.M.R. Senos, M.T. Vieira, Int. J. Refract. Met. Hard Mat. 21 (2003) 147.

[12] C.M. Fernandes, A.M.R. Senos, M.T. Vieira, Mater. Sci. Forum 455-456 (2004) 295.

[13] C.-M. Wang, Ceram. Int. 22 (1996) 113.

[14] J. Michalski, K. Konopka, M. Trzaska, Mater. Chem. Phys. 81 (2003) 407.

[15] T.D. Mitchell, Jr., L. C. De Jonghe, J. Am. Ceram. Soc. 78 (1) (1995) 199.

[16] C.M. Fernandes, A.M.R. Senos, M.T. Vieira, Mater. Sci. Forum 514-516 (2006) 633.

[17] European Standard EN1071-3:2005. Advanced technical ceramics- Methods of test for ceramic coatings – Part 3: Determination of adhesion and other mechanical failure modes by a scratch test. CEN Management Centre, Stassartstraat 36, Brussels, Belgium.

[18] K.M. Andersson, L. Bergström, Int. J. Refract. Met. Hard Mat. 18 (2000) 121.

[19] K.M. Andersson, L. Bergström, J Colloid Interface Sci. 246 (2002) 309.

[20] G.A. Parks, Chem. Rev. 65 (1964) 177.

[21] C.-M. Wang, F.L. Riley, J. European Ceram. Soc. 10 (1992) 83.

[22] E.P. Luther, F.F. Lange, D.S. Pearson, J. Am. Ceram. Soc. 78 (8) (1995) 2009.

[23] W.-H. Shih, D. Kisailus, W. Y. Shih, J. Am. Ceram. Soc. 79 (5) (1996) 1155.

[24] J. Lu, L. Gao, J. Guo, K. Niihara, Mater. Res. Bull. 35 (2000) 2387.

[25] N. Kallay, E. Matijevic, J. Colloid Interface Sci. 83 (1) (1981) 289.

*III.4. Coated **WC p**owders by **s**puttered **n**anostructured **N**i and **s**tainless **s**teel*

J. M. Castanho[1], M. T. Vieira[1], C. M. Fernandes[2], A. M. R. Senos[2] and M. Matos[1]

[1]ICEMS, Mechanical Engineering Department, University of Coimbra, 3030-201 Coimbra, Portugal
[2]Department of Ceramics and Glass Engineering, CICECO, University of Aveiro, 3810-193 Aveiro, Portugal

Vacuum (2008) in press

Abstract

In P/M processes, powder flowability and sinterability are crucial for compaction stage and are mainly influenced by particle shape, size distribution, surface texture and energy, crystallite size, chemical composition and other minor factors of powder particles. Among them, the surface properties play the major role and their improvement is welcome by the industry. The coating of the powders surface by a thin nanostructured film can decrease the cohesion or cohesive strength of conditioned or poured powders, and eliminate some previous traditional surface treatments, also decreasing the quantity of binder and the temperature of sintering. The efficiency of the powder surface modification depends on the coating process selected. Sputtering has been revealing an important skill for coating powders with metals, polymers or ceramics. However, some modifications in the holder of this particulate substrate have obliged to adopt some changes in a non-conventional sputtering system. The aim of the present work is to demonstrate the efficiency of the prototype developed and the influence of deposition parameters in the quality of coated powders; tungsten carbide powders and different coatings have been selected. Concerning the thin films, austenitic stainless steel and nickel targets were sputtered. These types of coatings are used in P/M of tungsten carbide as binders and they will allow a decrease in the inter-particles friction.

Keywords: Thin film, Steel, Tungsten carbide, Powder

Introduction

The worldwide cemented carbide industry is estimated to be more than $10 billion. In 2004, the PIM market was about $850 million even with the negative impact of the downfall world economy. Moreover, in spite of the world economic conditions the PIM will be expected to have a growth rate between 10% and 25% in the next few years, which make PIM a trustful technology, able to provide traditional and emergent industries [1]. However, the success of PIM manufacturers must fulfil several conditions, such as flexibility of the process, optimization of the equipment and especially the continuous research in new materials with enhanced properties [1-2].

The tooling industry is now using newer technologies such as micro-PIM, especially in the areas of micro-tooling.

WC/Co hard metals have been extensively used on tooling industry due to the stability of their hardness at high temperatures, but this property is strongly dependent on the cobalt content. In order to replace cobalt in the WC hard metals, some research work have pointed out to other metallic elements such as iron and/or nickel [3-4], which can lower the manufacturing cost as well as decrease the degree of toxicity.

The major reason to develop the present research work is to demonstrate the possibility to coat uniformly powders with thin films, whose properties can be tailored to specific application, as well as to demonstrate that the modification of the powders surface, by deposition of a thin film, can decrease significantly the interparticulate friction with a strong increase in the flowability of the powders.

Experimental

WC powders with an average particle diameter of 8-9 μm were coated with three different thin films by a home-manufactured d.c. magnetron sputtering equipment. Three types of coatings were deposited on WC powders. Thin films of stainless steel (SS 304 AISI) with increased nickel content (stainless steel sputtering target with nickel discs attached), nickel thin films and dual coatings of nickel and stainless steel. The main sputtering conditions are as follows: powders weight–50g; target-to-substrate distance–150 mm; deposition pressure–0.5 Pa; deposition power–16.7 kW/m^2.

In order to determine the morphology of the coatings, glass substrates were used and the deposited coating was removed to proper scanning electron microscopy (SEM) visualization. The coated powder density and the particle size distribution were evaluated by using helium pycnometry Accupic 1330 and by Laser diffraction Coulter LS 130, respectively. Finally, the flowability of the powders was determined by using a Flodex apparatus.

Results and Discussion

The morphologies of stainless steel and stainless steel with increased nickel content coatings deposited on flat glass substrates are similar (Fig. 1(a)) with a columnar growth matching the zone 1 of the Thornton model [5-6]. The presence of intercolumnar voids allied with the surface roughness point to a coating density lower than the theoretical stainless steel density (7.96 g/cm^3). In fact, the evaluation of the density of the coatings (6.69 g/cm^3) suggests a porosity of approximately 16%, which can be attributed to intercolumnar porosity. In order to evaluate the growth of the coating on the surface of the powders and to compare its morphology with the one deposited on a flat substrate, spherical-shaped copper powders were coated with stainless steel followed by electrochemical polishing. The SEM observation of the coatings deposited on powders shows a perfect coverage of their surfaces by a columnar and rough coating similar to the coatings deposited on flat substrates (Fig. 1(b)).

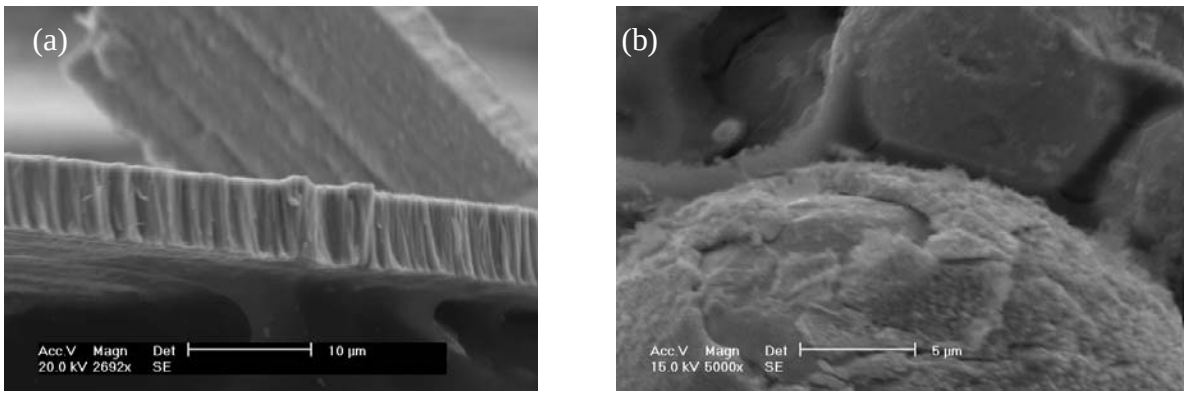

Fig. 1 – Cross section morphology of sputtered stainless steel coatings deposited on (a) glass and (b) copper powders.

The shape of the coated powders differs only slightly from the uncoated WC powders (Fig. 2), especially the agglomeration of the particles due to the deposition process. The electromagnetic fields existing in the deposition chamber during sputtering must promote a slight agglomeration of the powders. However, a strong increase in the particles surface roughness due to the presence of the thin film can be observed.

The deposition rate of the stainless steel coatings on flat substrates is about 0.7 nm/s, and is significantly higher than the stainless steel coatings deposited on the surface of the powders, which is approximately 0.05 nm/s (Table 1). The lower sputtering rate of the coatings deposited on powders is due to their vibration movement in order to attain a uniform surface coverage.

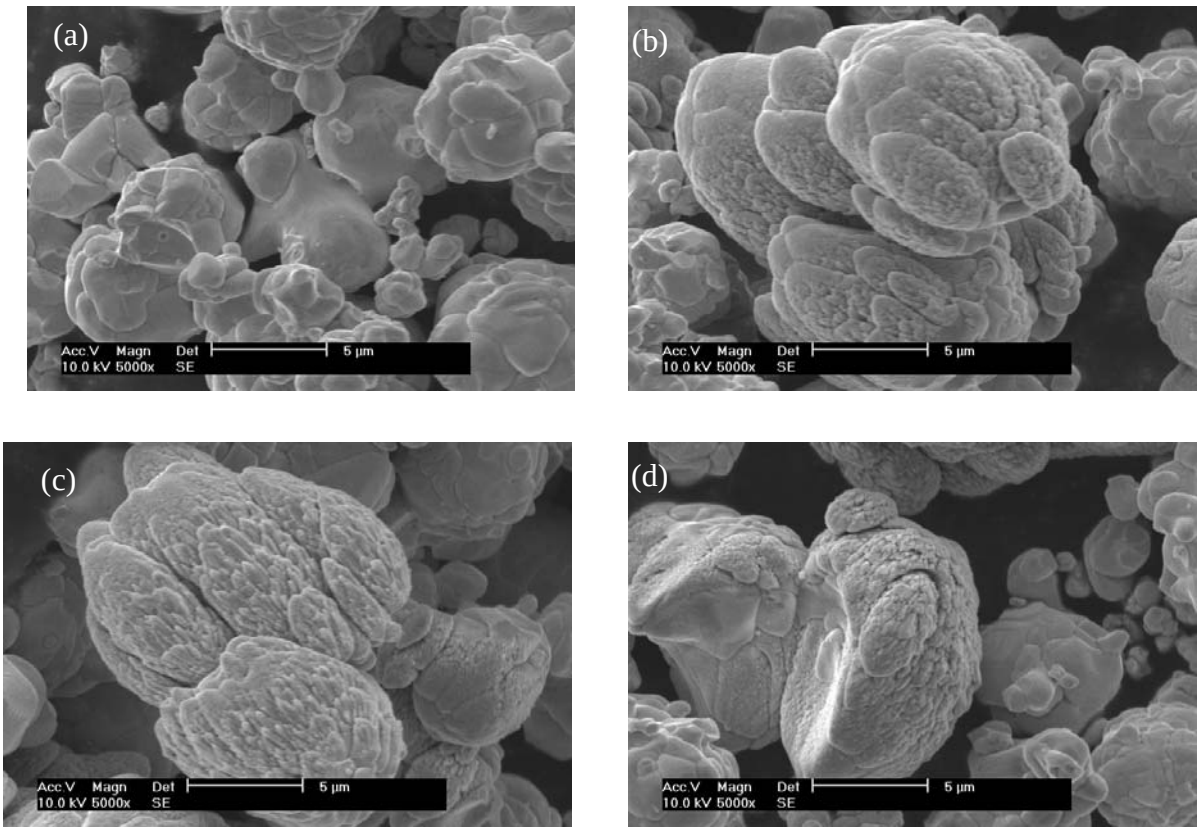

Fig. 2 – Morphology of WC powders. (a) uncoated powders, (b) coated with stainless steel doped with nickel, (c) coated with nickel and (d) coated with a first layer of nickel and a second layer of stainless steel.

The real density of the powders (*d*) agrees with the presence and thickness of the coatings and the decrease of this characteristic can be related with coating content in the powders, i.e., the lower is the density of the coated powders the higher is the coating's thickness. On the other hand, the poured density (d_{pour}) of the coatings does not follow any rule that clearly indicates the presence of a coating.

The flowability of the coatings plays a major rule in near net shape processes, such as micro-PIM, was evaluated by using a Flodex apparatus, in which the powders are allowed to fall freely from a cylindrical cup with a variable circular hole in the bottom. The diameter of the hole that allows powders to fall is called the critical diameter and will be used in the equation 1 to determine the interparticulate friction *k*,

$$k = \frac{g.r.d_{pour}}{2} \quad (1)$$

where g is the gravity acceleration, r is the radius of the hole.

Table 1

Characteristics of the coated and uncoated powders.

	Coating	**Deposition time [hour]**	**D_{50} [μm]**	**d [g/cm^3]**	**d_{pour} [g/cm^3]**	**Friction *k* [Pa]**	**SSA [m^2/g]**
	Uncoated	-	8.22	15.39	5.29	233	0.0485
WC	SS 304 + Ni	10	12.09	14.19	5.61	124	0.0853
powders	Ni	6	11.37	14.74	5.08	224	0.0801
	Ni/SS 304	3/7	14.73	13.94	4.75	163	0.0977

The internal friction of the powders is strongly influenced by the condition of the surface of the powders. In fact, the presence of a stainless steel coating improves strongly the flowability of the WC powders by reducing their internal friction. On the other hand, a nickel thin film does not give any advantage in the flowability relatively to the uncoated powders. The pernicious effect of the nickel layer on the flowability can also be noticed in the powders coated with two layers, an inner layer of nickel and an outer layer of stainless steel, which promotes higher internal friction than the powders coated only with a single stainless steel layer.

In addition, the presence of a thin film on the surface of the powders strongly increases its specific surface area (SSA) (Table 1). However, this increase does not influence the flowability of the powders.

Moreover, taking in consideration the surface morphology of the coated powders, this characteristic appears to have no significant effect on the flowability of the powders, and happens to be more relevant the chemical composition of the powders surface in the interacting forces between particles.

Conclusions

The developed sputtering system fulfills the principal condition of the process, which is the uniform and total coverage of the surface of the powders.

The metal (Ni) and metal alloy (SS 304) thin films had a columnar morphology with intercolumnar voids. The porosity of the coatings, which is approximately 16%, is due to the intercolumnar voids.

The shape of the powders is only slightly modified by the existence of a coating, although an agglomeration of the particles can be noticed, resulting from the deposition process itself. The coatings increase the surface roughness of the powders due to the columnar morphology.

Finally, the flowability of the powders, which is related with the interparticulate friction, is more dependent on the chemical composition rather than the morphology of the thin films. Nickel coatings deposited on WC powders do not improve the flowability of the powders, and in the opposite the surface covered with stainless steel enhances very significantly the flowability by decreasing the powders internal friction.

References

[1] Cornwall RG and. German RM. Metal Powder Reports Dec 2004; 59 (11): 8-11.

[2] Cornwall RG and German RM. Metal Powder Report J-A 1998; 53 (7-8): 32-33.

[3] Fernandes CM, Ferreira VM, Senos AMR and Vieira MT. Surface & Coatings Technology, 2003; 176 (1): 103-108.

[4] Fernandes CM, Senos AMR, Vieira MT. International Journal of Refractory Metals & Hard Materials 2003; 21: 147-154.

[5] Thornton JA. Journal of Vacuum Science & Technology 1986; A 4 (6): 3029.

[6] Ohring M. *"The Materials Science of Thin Films"*, Academic Press 199: 223-232.

Chapter

IV

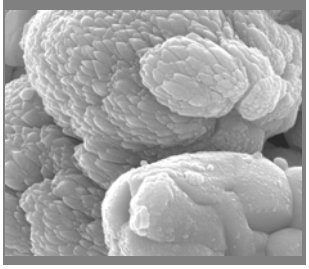

Sintering & Reactivity

Only the Fe-group metals exerted a major effect on densification of WC hardmetals.

Meredith and Milner, Powder Metallurgy 38 (1976)

IV.1. Introduction

In this chapter the study of the reactive sintering behaviour of coated powders is presented. The results of this topic are discussed along three papers which constitute this chapter. The first one presents the results of sintering stainless steel coated WC powder, using a conventional vacuum furnace. The effect of binder amount, in the range between 6 and 10 wt.%, and sintering variables (temperature, time and pressure) are presented.

In the second paper the sintering behaviour of stainless steel coated powders is compared with the sintering of conventionally prepared powders of identical composition. The effect of the thermal cycle on the sintering of coated powders is further evaluated.

Finally, the investigation of the thermal reactivity of coated powders is presented in the third paper. The effect of the initial stainless steel binder amount, between 1 and 15 wt.%, heating temperature and holding time on the phases formation process is reported. The comparison with conventional mixtures containing similar binder amounts was also performed. The altering of the binder composition, nickel increase and carbon addition, to reduce or even eliminate the M_6C phase, is yet analysed.

IV.2. Sintering of tungsten carbide particles sputter-deposited with sainless steel

C. M. Fernandes[1], A. M. R. Senos[1] and M. T. Vieira[2]

[1]Department of Ceramics and Glass Engineering, CICECO, University of Aveiro, 3810-193 Aveiro, Portugal
[2]ICEMS, Mechanical Engineering Department, University of Coimbra, 3030-201 Coimbra, Portugal

International Journal of Refractory Metals & Hard Materials 21 (2003) 147-154

Abstract

The purpose of this work was to study the sintering process of WC-stainless steel AISI 304 composite powders prepared by an innovative process, which consists in the use of a magnetron sputtering to coat WC powder particles with the stainless steel elements. The sintering of pressed compacts was performed in a conventional vacuum furnace using a heating rate of 5 ºCmin^{-1} until the selected maximum temperature, a holding time of 50-173 min and a sintering pressure of 2-20 Pa. For comparison, a conventional prepared WC powder with 6.5 wt.% of stainless steel AISI 304 was also studied.

During the sintering of the coated powders, three different sintering stages were identified: an initial one due to solid state matter transport until ~1150ºC, followed by two other stages where liquid phase may be already present. Very high weight losses occurred during the sintering of coated powder which was diminished by the shortening of the holding time, the increase of the pressure in the sintering furnace and the appropriate control of the sintering atmosphere. Despite the high values of weight loss, 96% of densification can be obtained at a relatively low sintering temperature, T = 1325ºC, for an initial content of ~10 wt.% of binder phase.

Keywords: Sputtering; Tungsten carbide; Stainless steel; Sintering; Hard metals

1. Introduction

WC-based hard metals are mainly manufactured with cobalt as the binder phase due to the excellent wetting of WC by Co at the sintering temperatures and to the special good combination of final mechanical properties obtained in these composites. Despite these well recognised advantages in the use of Co, its high cost and toxicity, together with the need to improve some properties as the oxidation and corrosion resistance, dictated the need to find alternative binders for WC based hard metals [1-9].

The efforts made to replace cobalt by iron or nickel [7-12] have revealed that it is possible to promote the densification of WC-(Fe/Ni) at temperatures near to those used to sinter WC-Co cemented carbides. When the composition of Fe-rich binders is adjusted so that neither free carbon nor eta carbide phase (M_6C) are formed, the mechanical properties such as hardness, toughness and transverse rupture strength (TRS) show similar or even superior values than those found in the WC-Co system [7-13]. Chromium additions to the binder composition have also been studied, because it acts as a strong grain growth inhibitor and improves oxidation and corrosion resistance [13].

Based on these studies, the investigation of WC composites with Fe-Ni-Cr binders reveals interesting and excluding one report [6], it was not been explored yet. So, in the present investigation, a stainless steel composition with Fe, Ni and Cr as the main components was chosen for binder phase of tungsten carbide.

In a previous work it was investigated a new method for the preparation of composite powders, using a magnetron sputtering technique [14]. This technique was used to sputter stainless steel AISI 304 on tungsten carbide powder particles and the results showed that it was possible to cover uniformly all the WC particles with all the stainless steel elements, in the same stoichiometric proportions as those existent in the target [14]. The coating had a ferrite bcc structure and presented a columnar growth with high roughness which led to a strong increase of the specific surface area of the coated powder. The modification of the surface characteristics of the sputter-deposited particles resulted in an improvement of the compact behaviour without any type of pressing binder, commonly used in the WC based cemented carbide powders conventionally processed.

In the continuation of that study [14], the sintering of the as-coated WC powder with stainless steel is now investigated to evaluate the feasibility of the stainless steel as a

sintering binder for WC composites and the effect of the modification of surface properties on the sputter-deposited particles.

2. Experimental

The starting powder is a fully carburized WC (H.C. Starck, HCST-Germany) with a specific surface area of 0.0485 m^2/g and a particle diameter of 9.06 ± 0.47 μm (Table 1), which contains, besides the WC phase, traces of W_2C phase.

WC powder particles were coated with stainless steel by a modified d.c. magnetron sputtering equipment [14]. The targets used are made of austenitic stainless steel AISI 304. The deposition parameters used for deposition have already been described elsewhere [14], with exception of the deposition time that was here changed from 6 to 12 hours, leading to different contents of deposited stainless steel. These sputter-deposited powders are here generally designated by C-WC and are differentiated among them by a number, corresponding to different amounts of deposited stainless steel. For comparison, a conventional mixture was also performed with the same WC powder and with an AISI 304 stainless steel powder (Fe/Cr18/Ni10 Goodfellow FE226010 powder alloy) with a maximum particle size of 45 μm. The mixing was performed with 1.5 wt.% of paraffin wax, using isopropyl alcohol as solvent in a stainless steel mill with WC-Co balls during 6 hours, subsequently dried at 60ºC, granulated and sieved. This powder is noted as M-WC.

Powders were uniaxially pressed at 190 MPa, resulting in pellets with 10 mm in diameter and about 3 mm thick. Finally, the pressed compacts were sintered in a vacuum furnace inside a graphite crucible. The furnace atmosphere was pumped to a pressure less than 10 Pa before sintering, which is stabilised at 2 Pa for T≥1000 ºC. The firing cycle involved a heating rate of 5 ºCmin^{-1} until the selected maximum temperature, a holding time of ~3 h and furnace cooling until room temperature. To study the effect of sintering conditions on the powder densification the holding time was varied from 50 to 173 min and the sintering pressure was increased up to 20 Pa. Finally, some samples were sintered within a small graphite box involved with M-WC powder.

Laser diffraction (Coulter LS 130) and helium pycnometry (Accupyc 1330) were used to determine the powder particle size distribution and the real powder density, respectively. The chemical characterization was carried out by inductively coupled plasma–atomic

emission spectrometer (ICP, Isa JY70Plus). The density of the sintered samples was determined using the Archimedes' method.

The microstructural characterization was done with scanning electron microscopy (SEM, Hitachi-S4100) with energy dispersive spectroscopy (EDS) in fracture sections for more porous samples and polished surfaces for the denser ones. X-ray diffraction (XRD, Rigaku) was performed for structural characterization.

3. Results and Discussion

Some physical and chemical characteristics of the powders under study are presented in Tables 1 and 2. The experimental values of average diameter and real density are presented in Table 1 for non-coated WC powder (WC), WC-stainless steel composite powder conventionally prepared (M-WC) and for powders coated by sputtering (C-WC1 to C-WC5). The binder amount, estimated as the total content of elements detected by ICP, in Table 2, varied from 5.2 to 10.0 wt.% in the coated powders. In the powder prepared by conventional mixture, 6.5 wt.% of binder was used (Table 2).

Table 1

Average particle diameter and real density of powders.

Sample	G_{LD}[a] 50% (μm)	Real density (g cm^{-3})
WC	9.1 ± 0.5	15.58 ± 0.01
M-WC	8.9 ± 0.3	—
C-WC1	10.7 ± 0.4	14.42 ± 0.32
C-WC2	10.6 ± 0.4	14.44 ± 0.01
C-WC3	15.5 ± 0.6	—
C-WC4	13.1 ± 0.5	14.36 ± 0.01
C-WC5	10.7 ± 0.3	13.81 ± 0.01

[a]Average particle diameter obtained by laser diffraction.

In a previous work [14] the morphological and chemical characterization of the coated powders was already presented. Those results showed that all the WC particles were coated and that all the steel constituent elements were deposited in the same original proportion as that of the stainless steel target, forming a coating with a ferrite bcc structure (Fe-α) [14]. The non-coated WC powder is constituted by small particles of less than 3 μm, forming dense aggregates with a size between 3 and 25 μm [14]. These aggregates are prevalent in

the coated powders (Fig.1) but it can be observed a much higher roughness on the surface of the coated aggregates originated by the columnar growth of the coating. A slight increase in the average aggregate size was observed after the coating process (Table 1), coming from the coating thickness together with a small granulation effect, due to the rotating movement of the sputtering chamber. This effect was more pronounced in powder C-WC3, in consequence of a longer rotating time used in this case.

Table 2

Chemical characterization of the powder coating elements by ICP.

Sample	% Fe	%Cr	%Ni	%Mn	Sum (%)
WC	0.02	<0.009	<0.009	<0.009	0
M-WC	4.56	1.21	0.69	<0.020	6.5
C-WC1	3.70	0.96	0.42	0.09	5.2
C-WC2	4.01	1.06	0.48	0.10	5.7
C-WC3	4.78	1.21	0.60	0.12	6.7
C-WC4	5.65	1.49	0.64	0.12	7.9
C-WC5	7.16	1.87	0.81	0.14	10.0

The compacts obtained from coated powders by uniaxial pressing, at 190 MPa, show a regular distribution of the porosity among agglomerates, in Fig. 1(a). The relative density of green compacts is 57 ± 1% without a significant effect of the binder amount. For the conventional prepared powder compacts the green density is 59 ± 1%.

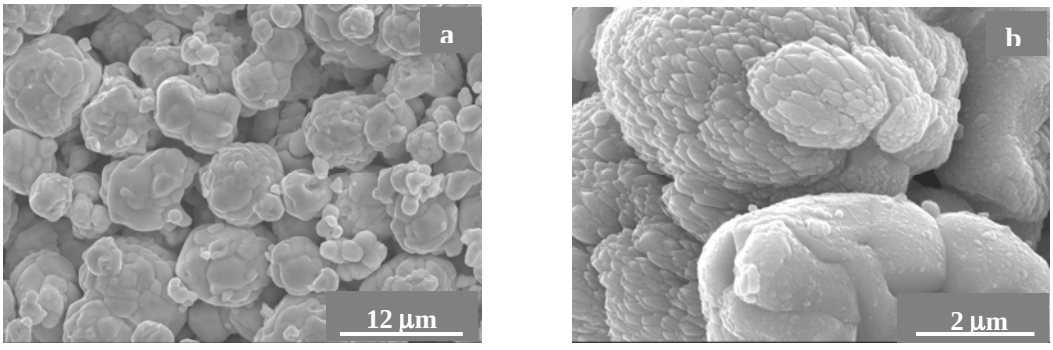

Fig. 1. (a) and **(b)** Microstructures of fracture sections of pressed compacts made from coated powders.

The densification results of C-WC2 powder compacts sintered, for ~3 h at temperatures ranging from 960 to 1425 ºC (sintering pressure, P = 2 Pa) are presented in Fig. 2. The analysis of the densification curve indicates that, until approximately 1150ºC (region I of Fig. 2), the increment in densification is reduced (~3%). This slow increase in densification can be attributed to the solid state sintering. The SEM micrographs taken in fracture sections show, at 960ºC (Fig. 3(a) and (b)) and 1080ºC (Fig 3(c) and (d)), the formation of necks between WC aggregates with wide voids between them. The initial formation of necks during the sintering of WC with iron and nickel binders, was also notified by others authors [15].

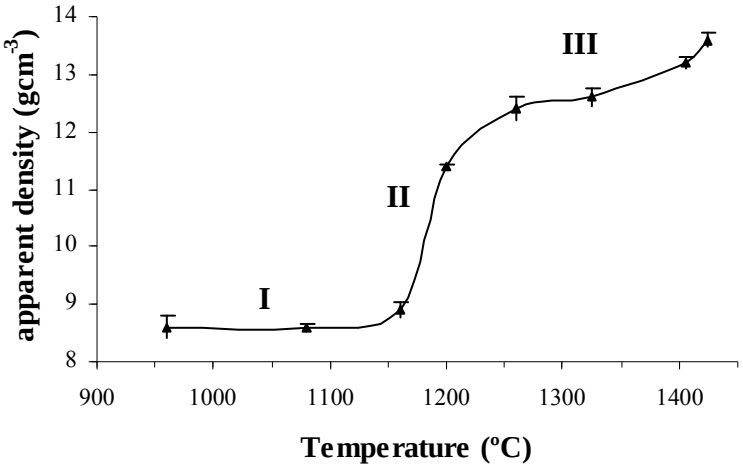

Fig. 2. Densification curve obtained for C-WC2 compacts (holding time of 173 min and P = 2 Pa).

For temperatures higher than 1150 ºC (region II in Fig. 2) an abrupt increase in the densification is observed that may indicate the formation of a liquid phase, although some authors report the existence of shrinkage and considerable densification in the solid state sintering of WC based composites, such as WC-10 wt.% (Fe-Ni) [7,16], WC-10 wt.% Co [15,17] and WC-10 wt.% Ni [11].

For the present composition it does not existing calculated phases diagrams, due to the high number of involved elements. In spite of this, the supposition of the appearance of a liquid phase at temperatures around 1150ºC does not seem misadjusted with the formation of a ternary eutectic at 1143 ºC in the phase diagrams of the system Fe-W-C [16,18]. However, even being Fe the element present in higher percentage in the coverage, (Table 2) these ternary diagrams are not at all conclusive, because the other components (Table 2) may affect the eutectic temperature of the system under study.

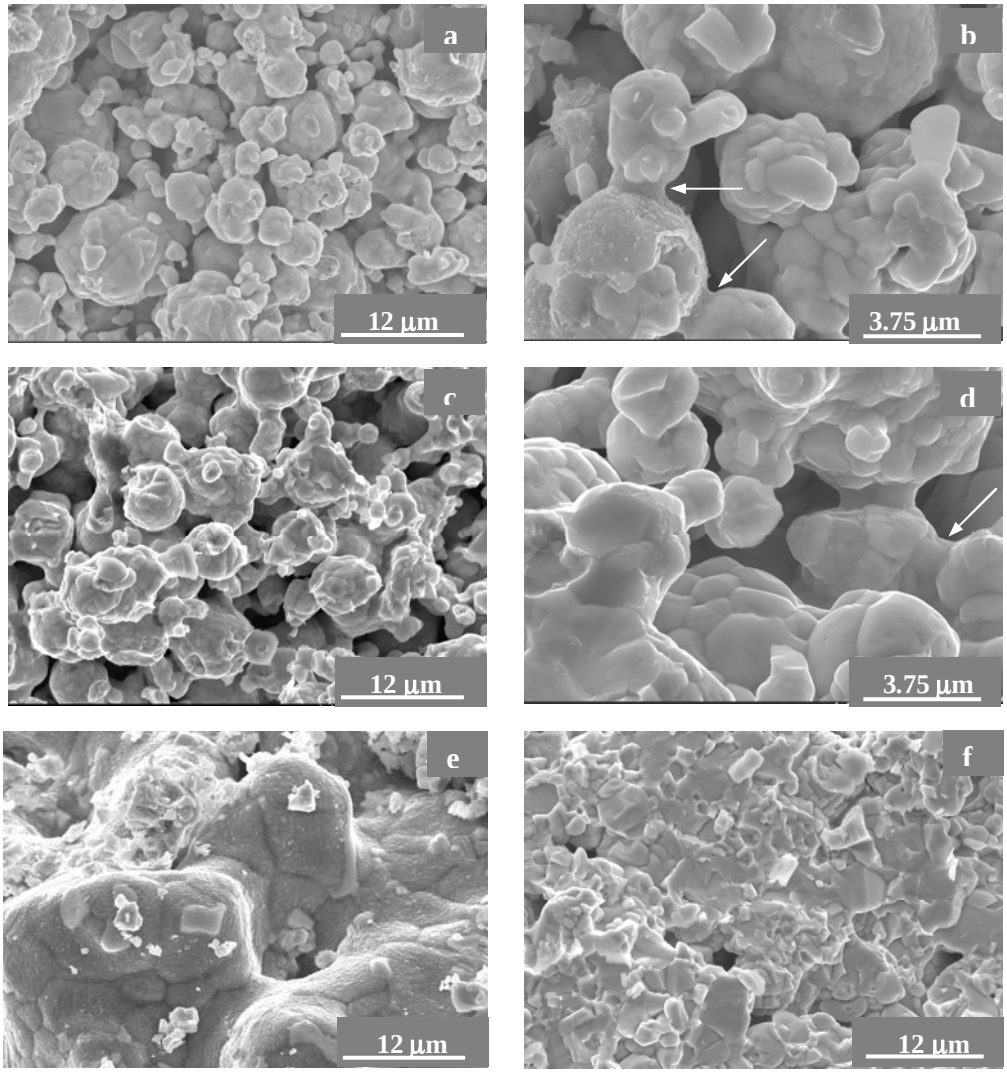

Fig. 3. Microstructural observation of fracture sections of C-WC2 compacts sintered at various temperatures: (a) and (b) 960ºC; (c) and (d) 1080ºC: (e) 1200ºC and (f) 1425ºC. The arrows indicate the formation of necks.

The characterization of the morphological evolution of the covering can also help us to interpret the densification results in Fig. 2. It can be observed in Fig. 4(a) and (b) that the morphology of the covering changes a lot between 1080 and 1200 ºC, showing, at 1200 ºC, the appearance of a film involving the WC aggregates which may result from the formation of a wetting liquid phase at the sintering temperature. The microstructures of Fig. 4(c) and (d), obtained on polished surfaces of samples sintered at 1200 and 1260 ºC, also show a second phase (darker) very well adapted to the contours of the WC grains and well infiltrated in the junctions between aggregates. This second phase is remaining of the liquid phase formed at sintering temperatures, which may promote the densification.

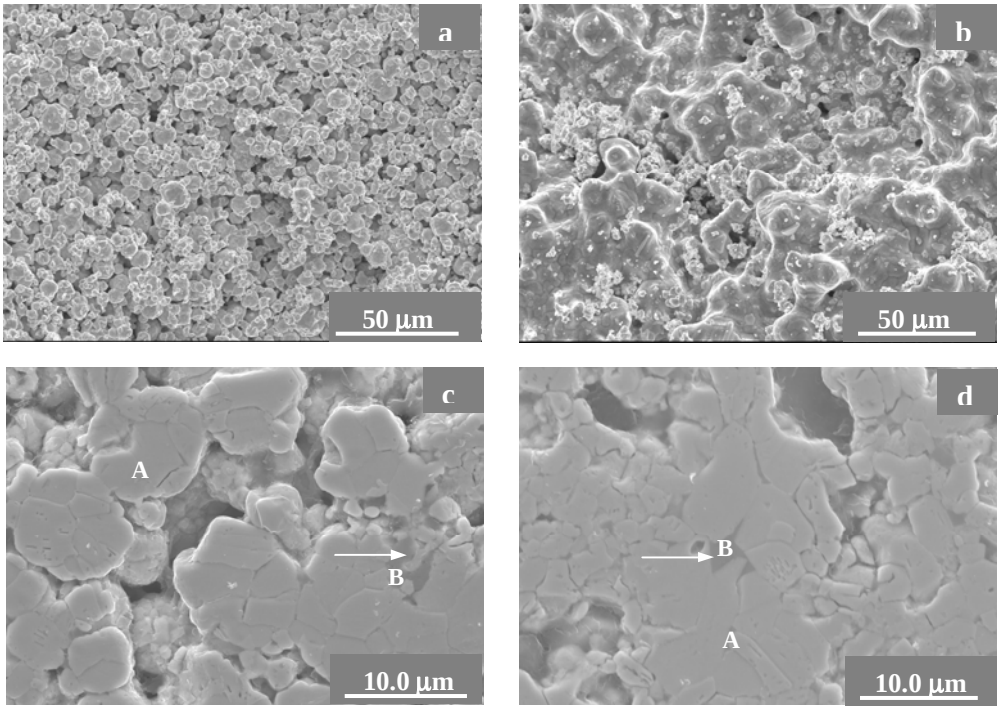

Fig. 4. Microstructures of sintered C-WC2 compacts. Fracture sections at (a) 1080 ºC and (b) 1200 ºC; polished sections at (c) 1200 ºC and (d) 1260 ºC.

So, taking $T \geq 1150$ ºC as the eutectic temperature in the system under study, if the formed liquid has good wettability, as observed by the infiltration of grain boundaries in Fig. 4(c) and (d), a high-speed densification by viscous draining of the liquid phase and particle rearrangement may occur. This first stage of liquid phase sintering, identified in Fig. 2 with the densification in region II, is normally followed by a second stage with a slower densification rate by mechanisms of solution and precipitation of solid particles in the liquid phase. Grain growth by an Ostwald ripening process may also occur. In Fig. 2, the region III, for $T > 1260$ ºC, may correspond to solution-precipitation mechanisms of matter transport.

The microstructural evolution presented in Fig. 3 for C-WC2 compacts, shows that the densification proceeds for temperatures higher than 1200 ºC but no significative grain growth between aggregates is observed even at the higher temperature, $T = 1425$ ºC. The control of grain growth is facilitated when the morphological and chemical scale of homogeneity of the compacts is high [19]. In the present case, the highly uniform distribution of the binder among the WC aggregates, which is attained by the sputter-coating process, may certainly improve the grain growth control during sintering. This

grain growth control can be valuable for mechanical properties, since finer WC grain sizes originate higher values of hardness, transverse rupture strength and compression resistance [20,21].

The results of apparent density for coated powders, with different amounts of binder (Table 3) also show that up to temperatures of 1160 ºC, the improvement in density is very small, even for the highest content of binder deposited (10 wt.%). On the other hand, for sintering temperatures of 1200 ºC and 1325 ºC the densification strongly increases and presents a marked dependence on the binder percentage (Table 3 and Fig. 5). In accordance with the interpretation of the densification curve of Fig. 2 and with the microstructural observations in Fig. 3, the results also point out that a liquid phase must be formed before 1200 ºC and that this Fe alloy presents a very good efficiency as a sintering binder in WC composites.

Very high weight losses occurred during the sintering of powder compacts at temperatures higher than 1200 ºC, as presented in Table 3. The final contents of binder elements, as determined by ICP, are shown in Table 4 for C-WC2 sintered compacts at temperatures between 1200 and 1405 ºC. From these results and from the initial powder characterization by ICP in Table 2, it can be stated that appreciable amounts of covering volatilised during sintering at $T > 1200$ ºC, in such a way that in a compact of C-WC2 only ~50% of the initial binder content remains after sintering at 1405 ºC, during 173 min. The results of Table 4 also show that the rate of volatilisation is almost equivalent for the binder elements, i.e., the binder composition does not significantly change during sintering.

The samples made from conventionally prepared powder (M-WC) and sintered under the same conditions used in the sintering of coated powders compacts also show, in Table 3, significant weight losses, but, in this case, part of those weight losses are due to the burning of the paraffin wax, used in the powder preparation as pressing aid (1.5 wt.%). Analysing the results of ICP for M-WC samples, in Table 4, it can be said that a loss of the binder elements also occurs at the sintering temperatures, but the estimated binder loss (~1 wt.%) for the sintering temperature of 1325 ºC is much smaller than that correspondent to C-WC2 powder compacts (~2.5 wt.%). The higher weight losses of compacts made from coated powders may be related with the higher homogeneity of the binder distribution together with the higher reactivity of the sputtered coating [14].

Table 3.

Sintering results obtained in compacts with different binder contents and sintered for 173 min at selected temperatures (sintering pressure, P = 2 Pa).

Sample	Initial binder content (%)	Green density (g cm^{-3})	Temperature (ºC)	Density (g cm^{-3})	Weight loss (%)
M-WC	6.5	8.7	1160	9.7	1.8
		8.6	1200	11.8	2.1
		8.6	1325	13.2	3.0
C-WC1	5.2	8.0	1200	10.4	0.8
C-WC2	5.7	8.1	1160	8.9	0.5
		8.2	1200	11.4	1.0
		8.2	1325	12.1	3.7
C-WC3	6.7	8.1	1200	12.1	1.2
		7.7	1325	13.5	4.6
C-WC5	10.0	7.8	1160	8.6	1.0
		7.7	1200	13.2	2.1
		7.8	1325	14.3	7.4

The weight losses during sintering certainly restrict the final densification and affect the final properties. In order to control the weight losses, the sintering variables of holding time, sintering pressure and sintering atmosphere were studied. The effect of these variables on the apparent density, weight loss and relative density of compacts sintered at 1325 ºC is summarised in Table 5. The values of relative density, D_{rel}, here presented for an easier comparison of the degree of densification attained during sintering are not related with the initial real powder density (Table 2) because the preferential binder loss at sintering temperatures alters the composite composition and, so, the theoretical density, d_t. The theoretical density was estimated using the classical law of mixtures [22] and considering the final binder content given by ICP. It was also assumed that Fe-α (d_t = 7.9 g cm^{-3}) and WC (d_t = 15.6 g cm^{-3}) were the unique phases present in sintered samples, although as will be discussed ahead, eta phase was formed (Fig. 6).

From the analysis of the results of Table 5, it can be concluded that the weight losses increase with the holding time at the sintering temperatures. So, the reduction of the holding time from 173 to 50 min reduces the losses in ~30%, relatively to the values

obtained at 173 min, with a small improvement (~1%) in the relative density, both in compacts of C-WC2 and C-WC5, sintered at 1325 ºC (P = 2 Pa).

Table 4.

Chemical characterization of the binder elements by ICP in samples sintered at different temperatures, during 173 min, at P = 2 Pa.

Sample	Temp. (ºC)	Fe (wt.%)	Cr (wt.%)	Ni (wt.%)	Mn (wt.%)	Sum (wt.%)
C-WC2	1200	3.94	0.91	0.49	0.03	5.4
	1260	3.20	0.85	0.30	0.03	4.4
	1325	2.41	0.44	0.30	<0.009	3.2
	1405	2.28	0.42	0.25	<0.008	3.0
M-WC	1160	4.23	0.99	0.65	<0.02	5.9
	1200	4.08	0.97	0.62	<0.02	5.7
	1325	3.94	0.86	0.59	<0.02	5.4

Increasing the pressure in the sintering chamber, from 2 to 20 Pa, lower values of weight loss are observed for C-WC2 and C-WC4 compacts sintered at 1325 ºC, in Table 5, without detected surface oxidation. A net increase of 3-5% in the relative density is also observed. Finally, by using a small graphite crucible covering the sample during the sintering and surrounded by powder with a composition close of that of the sample, resulted in a more controlled sintering atmosphere with a net reduction effect on the weight loss, but without appreciable effect on the densification of C-WC4 compacts.

The simultaneous effect of increasing the sintering pressure (2-20 Pa) and of controlling the atmosphere in C-WC4 compacts sintered at 1325 ºC during 115 min, shows, in Table 5, that losses are reduced from 3.4 to 1.6 wt.%, which represents a net improvement in the weight loss control with a concomitant benefit in densification. This study as others in WC hard metals [7,10,12,18,23] pointed out to the importance of optimization of the sintering conditions in reactive systems with volatile components in order to obtain controlled processes and properties.

Table 5.

Sintering results for compacts sintered at 1325 ºC with different holding time (t) and sintering pressure (P) conditions.

Sample (initial binder content %)	Sintering Conditions		Density (g cm^{-3})	Weight loss (%)	D_{rel} (%)
	t (min)	P (Pa)			
C-WC2 (5.7)	50	2	12.2	2.7	81
	115	2	12.1	2.6	81
	173	2	12.1	3.7	80
	173	20	12.7	2.6	85
C-WC4 (7.9)		2	12.5	3.4	84
	115	20	12.7	2.5	87
		20[a]	12.6	1.6	87
C-WC5 (10.0)	50	2	14.2	5.6	96
	115	2	14.3	6.3	96
	173	2	14.3	7.4	95

[a]controlled sintering atmosphere

When the sintering results of the sputter-deposited powders with an initial binder amount of 6-7 wt.% are compared with the conventional-prepared powder (6.5 wt.% of binder) it is something surprising, that there is not a significant improvement in the densification (see Fig. 5), coming from the very high uniformity of the initial binder distribution in the sputter-deposited powders [14]. The high weight losses observed in the sintering of coated powders difficult the sintering process, but besides this, other reaction effects may probably disturb the initial homogeneity of the binder distribution. Effectively, eta-phase was formed during heating by local reactions between WC and some covering elements, as Fe, Cr and Ni and the XRD pattern of Fig. 6 shows that this phase is already present at 960 ºC. The amount of this phase, estimated by the Rietveld method, was found to vary between 8-10 wt.% for C-WC2 compacts sintered at temperatures from 960 up to 1425 ºC. An equivalent phase amount was also found in M-WC samples sintered at $T \geq$ 1060 ºC. The formation of eta-phase in regions of WC grains poor in carbon may disrupt the initial coverage uniformity. One of the main objectives of forthcoming studies will be the elimination of this undesirable eta-phase which may be pernicious both in sintering and in properties [24,25].

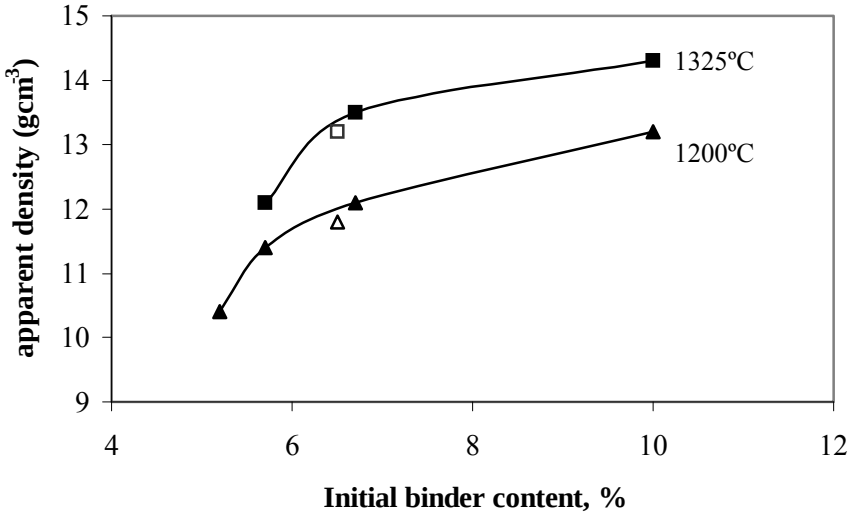

Fig. 5. Effect of the initial binder content and sintering temperature on the apparent density of compacts. The closed points are used for coated powders and the open points for the conventional mixed powder.

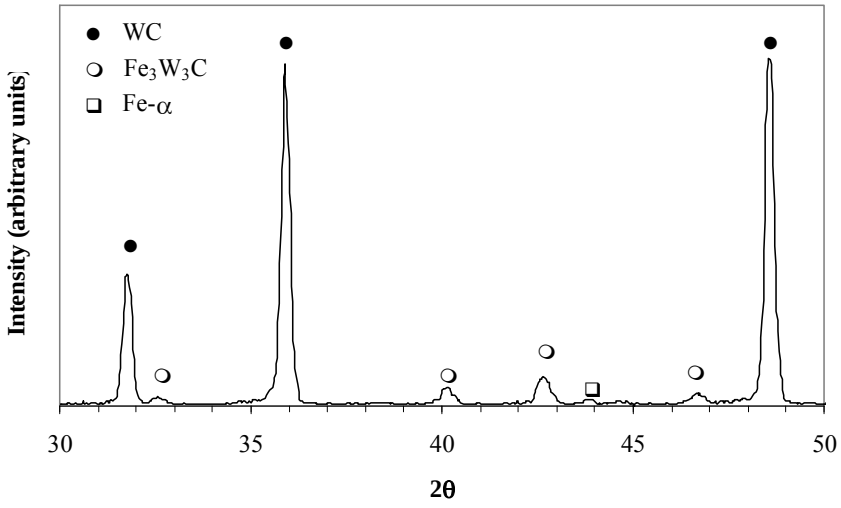

Fig. 6. XRD pattern of a C-WC2 compact sintered at 960 ºC, during 173 min.

On other hand, the formation of eta-phase implies a reduction of the binder content available to form a liquid phase during sintering, even at the lower sintering temperatures ($T \leq 1200$ ºC), where the binder loss by volatilisation is still negligible. Effectively, the results of phase quantification by the Rietveld method in C-WC2 and C-WC5 compacts pointed, respectively, to a maximum amount of ~3 and ~5 wt.% of binder available to form

liquid phase at the sintering temperatures. Even with such limited quantities of binder available to form liquid phase, due to the formation of eta-phase, which is strongly aggravated by the additional binder loss due to the observed volatilisation during sintering, high relative densities of ~96% were obtained at 1325 ºC for C-WC5 powder compacts (Table 5). In WC-Co and WC-Ni compacts with ~6 wt.% of binder, without detected eta-phases, equivalent relative densities are only obtained for temperatures $T \geq 1400$ ºC [12,26] which is indicative of the high efficiency of the stainless steel AISI 304 as a sintering aid in WC. The appearance of a liquid phase at a relatively low temperature of $T \simeq 1150$ ºC, together with the good wettability of the surfaces and interfaces by the formed liquid phase may be responsible for this appreciable sintering promotion.

Conclusions

The use of stainless steel sputter-deposited on WC particles promotes an appreciable densification of these composites at reasonable temperatures and times. The sintering takes place in three stages: (I) small increase of density until 1150 ºC, attributed to solid state sintering; (II) sharp increase in densification endorsed to particle rearrangement characteristic of the first stage of liquid phase sintering; (III) slower densification due to mechanisms of solution and precipitation of solid particles in the liquid phase. Accordingly with the kinectical results, it was observed in SEM micrographs the existence of a viscous phase, for temperatures higher than 1150 ºC, very well adapted to the contours of grains and well infiltrated in the junctions between aggregates.

High weight losses occurs during the sintering of sputter-deposited powder compacts, from 1200 ºC, leading to a net decrease of the binder components. These weight losses are strongly reduced, with a concomitant benefit in the densification, by decreasing the holding time, increasing the sintering pressure and by an adequate control of the sintering atmosphere.

The sputter-deposited powders do not show a significant improvement in the densification when compared with the conventional-prepared powder, which probably arises from the high weight losses observed during the sintering of coated powders and from the formation of eta-phase. The formation of eta-phase, at low temperatures, $T < 960$

ºC, may disturb the very high initial homogeneity of binder distribution attained in the sputtering process of powder preparation. Both the formation of eta-phase and the volatilisation at the sintering temperatures strongly reduce the content of binder components available to form liquid phase during sintering. Even so, high relative densities of ~96% were obtained at a relatively low temperature of 1325 ºC for sputter-deposited powder compacts with an initial content of 10 wt.% of stainless steel, in consequence of the low eutectic temperature found in this system, $T \simeq 1150$ ºC, and the good wettability of the liquid phase.

References

[1] Suzuki H, Yamamoo T and Kawakatsu I, Properties of WC-10% (Ni-Fe). Powder Metall. J. 1967; 14: 26-31.

[2] Moskowitz D, Ford M J and Humenik Jr. M, High-strength tungsten carbides. Int. J. Powder Metall. 1970; 6 (4): 55-64.

[3] Moskowitz D, Abrasion resistant iron-nickel bonded tungsten carbide. Mod. Dev. Powder Metall. 1977; 10: 543-551.

[4] Moskowitz D, Ford M J and Humenik Jr. M, High-strength tungsten carbides. Mod. Dev. Powder Metall. 1971; 5: 225-234.

[5] Miodownik A P, Means of predicting structure and performance of new materials. Powder Metall. 1989; 32 (4): 269-276.

[6] Farroq T and Davies T J, Tungsten carbide hard metals cemented with ferroalloys. Int. J. Powder Metall. 1991; 27 (4): 347-355.

[7] Viswanadham R K and Lindquist P G, Transformation-toughening in cemented carbides: Part I. Binder composition control. Metall. Trans. A 1987; 18A: 2163-2173.

[8] Kakeshita T. and Wayman C M, Martensitic transformations in cermets with a metastable austenitic binder. Mater. Sci. Eng. 1991; A141: 209-219.

[9] Uhrenius B, Phase diagrams as a tool for production and development of cemented carbides ans steels. Powder Metall. 1992; 35 (3): 203-210.

[10] González R, Echeberría J, Sánchez J M, and Castro F, WC-(Fe, Ni, C) hardmetals with improved toughness through isothermal heat treatments. J. Mater. Sci. 1995; 30 (13): 3435-3439.

[11] Cooper R, Manktelow S A, Wong F and Collins L E, The sintering characteristics and properties of hard metal with Ni-Cr binders. Mater. Sci. Eng. A 1988; A105-106: 269-273.

[12] Tracey V A, Nickel in hardmetals. Refr. Metals & Hard Mater. 1992; 11: 137-149.

[13] Penrice T W, Alternative binders for hard metals. Carbide and Tool J. 1988; 20 (4): 12-15.

[14] Fernandes C M, Ferreira V M, Senos A M R and Vieira M T, Stainless steel coatings sputter-deposited on tungsten carbide powder particles. Surf. Coat. Technol. 2003; 176: 103-108.

[15] Meredith B, and Milner D R, Densification mechanisms in the tungsten carbide-cobalt system. Powder Metall. 1976; 1: 38-45.

[16] Viswanadham R K and Lindquist P G, Transformation-toughening in cemented carbides: Part II. Thermomechanical treatments. Metall. Trans. 1987; 18A: 2175-2180.

[17] Åkesson L, Thermodynamic and sintering studies in the Co-W-C system. Thermochimica Acta 1979; 29: 327-332.

[18] Upadhyaya G S and Bhaumik S K, Sintering of submicron WC-10 wt.% Co hard metals containing nickel and iron. Mater. Sci. Eng. 1988; A105-106: 249-256.

[19] Cho K H, Lee J W and Chung I S, A study on the formation of anomalous large WC grain and the eta phase. Mater. Sci. Eng. A 1996; 209: 298-301.

[20] Gille G, Bredthauer J, Gries B, Mende B and Heinrich W, Advanced and new grades of WC binder powder – their properties and application. Int. J. Refr. Metals & Hard Mater. 2000; 18: 87-102.

[21] Harmat P, Kotsis I, Laczkó L and Bartha L, Melting and phase transformation of hardmetal powders. Solid State Ionics 2001; 141-142: 157-161.

[22] Uygur M E, Modeling tungsten carbide/cobalt composites. Adv. Mater. & Processes 1997; 3: 35-37.

[23] Hanyaloglu C, Aksakal B, Bolton J D, Production and indentation of WC/Fe-Mn as an alternative to cobalt-bonded hardmetals. Mater. Charact. 2001; 47: 315-322.

[24] Guillermet A F, An assessment of the Fe-Ni-W-C phase diagram. Metallkd. 1987; 78 (3): 165-71.

[25] Uhrenius B, Contribution to the knowledge of phase equilibria in tungsten-carbon based systems. Scand. J. Metallurgy 1991; 20: 93-98.

[26] Janes S, editor. *Ceramic Monographs – A handbook of Ceramics*, Bonn: research institute of the refractory –industry, 1979.

IV.3. Study of sintering variables of tungsten carbide particles sputter-deposited with stainless steel

C. M. Fernandes[1], A. M. R. Senos[1] and M. T. Vieira[2]

[1]Department of Ceramics and Glass Engineering, CICECO, University of Aveiro, 3810-193 Aveiro, Portugal
[2]ICEMS, Mechanical Engineering Department, University of Coimbra, 3030-201 Coimbra, Portugal

Materials Science Forum Vols. 455-456 (2004) 295-298

Abstract

WC-stainless steel AISI 304 composite powders have been prepared by an innovative process, which consists in the use of a magnetron sputtering to coat WC powder particles with the stainless steel elements. The characteristics of the particle surfaces are strongly changed by the sputtering process, leading to rough surfaces with increased reactivity. The objective of this work was to study the sintering variables of these tungsten carbide-stainless steel powders. For such, powder compacts were sintered using different conditions of thermal cycle. Samples were characterised by inductively coupled plasma-atomic emission spectroscopy, X-ray diffraction and scanning electron microscopy with chemical analysis. The experimental results are analysed and the sintering conditions leading to densified compacts with a controlled composition, microstructure and crystallographic structure are discussed.

Keywords: Sputtering; Tungsten carbide; Stainless steel; Sintering; Hard metals.

Introduction

Hard metals or cemented carbides are powder-metallurgical products consisting of hard, wear resistant carbide particles, bound together with a metal binder. The most common carbide is tungsten carbide, WC, and the usual binder metal is cobalt. The iron alloyed with other elements is one of the solutions investigated to replace cobalt in hard metals in order to provide lower cost materials [1-4]. Several studies show that these iron alloys binders may have higher hardness and slightly lower fracture toughness than the hard metals with similar content of cobalt [1-9]. In the present investigation, a stainless steel with Fe, Ni and Cr as the main components was chosen as binder phase of tungsten carbide.

In a previous work [10] composites of tungsten carbide and stainless steel have been prepared by an innovative way, using a magnetron sputter equipment to coat tungsten carbide particles with stainless steel 304 AISI. All the tungsten carbide particles were coated with the stainless steel components in the same original proportion as that existent in the target, resulting in a much higher chemical homogeneity than that ever attained in a conventional process of powder preparation [10]. Furthermore, the compaction behaviour of the coated powders indicated that it was not necessary to use any type of pressing binder, commonly used in the WC based cemented carbides, to reach an adequate resistance to handling [10].

In order to evaluate the effect of the surface modification on the sputter-deposited particles, the sintering of the as-coated WC powder with stainless steel is now investigated. For such, different conditions of thermal cycle have been investigated and the results were compared with those obtained in conventional prepared powders.

Experimental

The starting powder is a fully carburized WC (H.C. Starck, HCST-Germany) with an average particle diameter of 9.06 ± 0.47 μm, which contains, besides the WC phase, traces of W_2C phase. WC powder particles were coated with stainless steel AISI 304 by a modified d.c. magnetron sputtering process [10]. The deposition parameters used here are the same as used before in previous work [10], with exception for the deposition time,

which was fixed in 6 and 12 hours. These powders are here designated by C-WC1 and C-WC2, respectively for 6 h and 12 h of deposition time. The binder amount, estimated as the total content of elements detected by ICP, was 6.7 wt.% for C-WC1 and 10.0 wt.% for C-WC2. For comparison, two powders with close compositions (M-WC1 with 6,5 wt.% and M-WC2 with 10.0 wt.% of binder) were also prepared using the same WC powder and an AISI 304 stainless steel powder, maximum particle size of 45 μm (Goodfellow FE226010 powder alloy). The mixing of WC and stainless steel powders was performed with 1.5 wt.% of paraffin wax, using isopropyl alcohol as solvent in a stainless steel mill with WC-Co balls during 6 hours, subsequently dried at 60ºC, granulated and sieved.

Powders were uniaxially pressed at 190 MPa, resulting in pellets with 10 mm in diameter and about 3 mm thick. Finally, the pressed compacts were sintered in a vacuum furnace inside a graphite crucible. The furnace atmosphere was pumped to a pressure less than 10 Pa before sintering, which is stabilised at 2 Pa, for T≥1000ºC. The firing cycle involved a heating rate of 5 ºCmin^{-1} until the selected maximum temperature of 1325 ºC and furnace cooling until room temperature. To study the effect of sintering conditions on the powder densification the holding time was varied from 50 to 173 min.

The chemical characterization of the coated powders and conventional mixtures was carried out by inductively coupled plasma–atomic emission spectrometer (ICP, Isa JY70Plus). The density of the sintered samples was determined using the Archimedes' method. X-ray diffraction (XRD, Rigaku) was performed for structural characterization. The microstructural characterization of green and sintered samples was done with a scanning electron microscopy with energy dispersive spectroscopy (SEM/EDS, Hitachi-S4100).

Results and Discussion

The sputter-deposited powder particles are completely coated with stainless steel as shown in Fig. 1, being visible the high roughness originated by the columnar structure of the coating in Fig. 1(a) and the coating thickness in Fig. 1(b), estimated as approximately 0.4 μm for an amount of 10 wt.% of binder. The morphological and chemical characterization of the coated powders was already been reported [10]. Those results showed that all the steel constituent elements were deposited in the same original

proportion as those of the stainless steel target, forming a coating with a ferrite bcc structure (Fe-α) [10].

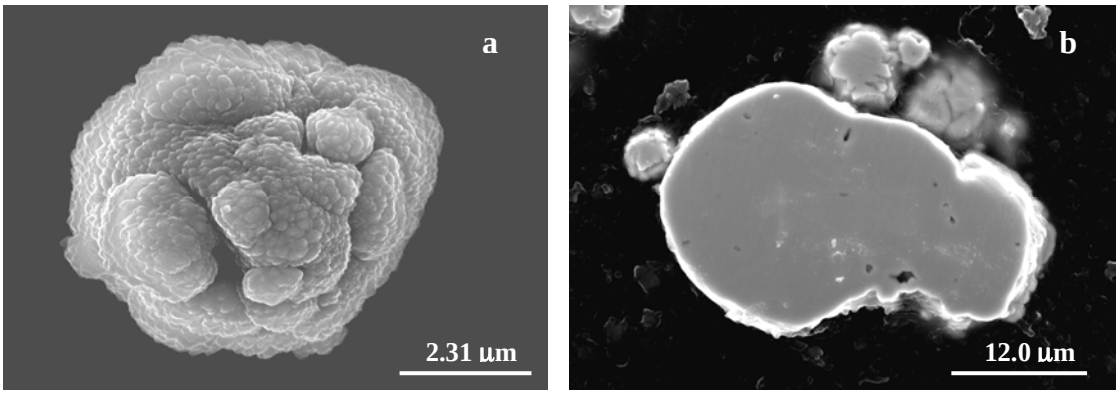

Fig. 1. SEM micrographs taken from coated powders: (a) particle surface of C-WC1 and (b) polished section of C-WC2.

The results of densification of these powder compacts in a previous work [11] showed that the densification process becomes important for temperatures, T≥1150ºC, when an iron rich liquid phase forms. It was also observed that the particle surfaces of the coated powders are very reactive, leading to high weight losses, for T≥1200ºC, identified with the volatilisation of appreciable amounts of binder. Besides those high weight losses, the favourable formation of eta-phase in these composite systems [11], at T<960ºC, reduces the content of binder components available to form liquid phase during sintering, both in coated and in conventionally prepared powders [11]. It is believed that the formation of eta-phase during the heating period disturbs the initial homogeneity of binder distribution in the coated powders, strongly reducing the potential benefits for the sintering process. It is expected that this effect will be more critical for low binder contents, because the thinner the coating thickness more probable will be its local disruption with the formation of eta-phase. Accordingly, the sintering results, presented in Table 1, show that the densification obtained during sintering at 1325 ºC for 173 min is comparable for coated and conventionally prepared powders with ~6.5 wt.% of binder, while for powders with a higher binder content, i.e. 10 wt.%, the benefits of the very high homogeneity attained in densification of coated powders become visible by the reasons pointed before.

Table 1

Sintering results obtained at 1325 ºC.

Sample	initial binder content [wt.%][a]	Sintering time [min]	Density [g cm^{-3}]	Weight Loss [%]	D_{rel} [%]
C-WC1	6.7	173	13.5	4.6	89
M-WC1	6.5	173	13.2	3.0	89
C-WC2	10.0	50	14.2	5.6	96
		173	14.3	7.4	95
		173*	14.2	5.5	96
M-WC2	10.0	173	13.1	4.1	90

[a]Chemical analysis by ICP. *Intermediate holding time of 115 min at 1000ºC.

The SEM micrographs of polished sections of M-WC2 and C-WC2, sintered at 1325 ºC during 173 min, are presented in Fig.2(a) and (b), respectively. The comparison of both micrographs (Fig.2) shows that the sintered compact of C-WC2 is denser (Fig. 2(b)) than the M-WC2 one. The grain size of M-WC2 (Fig. 2(a)) is smaller in consequence of the milling step.

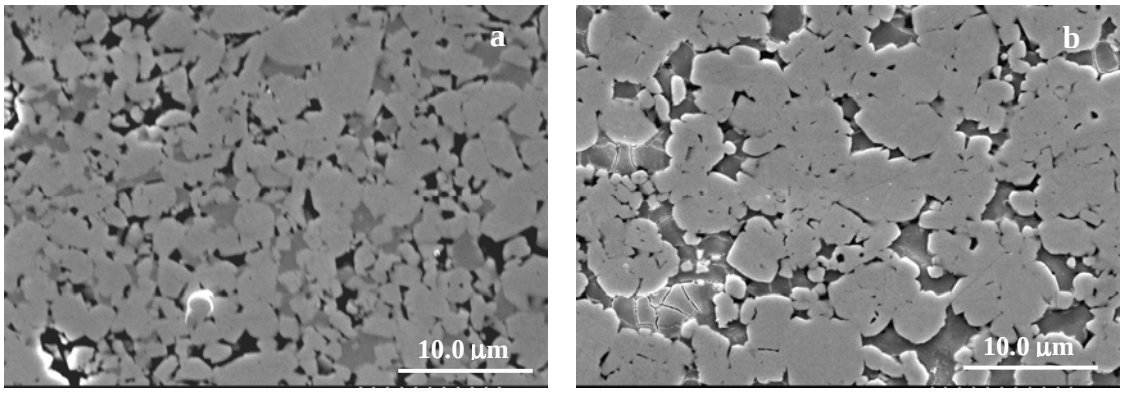

Fig. 2. SEM micrographs taken from sintered compacts at 1325ºC during 173 min: (a) M-WC2; (b) C-WC2.

In previous studies the reduction of weight losses in coated powders were attained by altering the sintering atmosphere, i.e., increasing the sintering pressure and saturating the sintering atmosphere with the binder elements [11]. In this work, another approach was tried which comes from the analysis of the effect of the sintering time variation, from 173 to 50 min, in Table 1, for C-WC2 powder compacts. It can be observed an appreciable reduction of the weight loss with the sintering time which claims for a time dependent volatilisation process, probably controlled by the solubilization of the eta-phase in the

liquid phase. In this sense, it was tested the reduction of the system reactivity by performing an intermediate holding time of 115 min at 1000 ºC, where eta-phase is already formed, during the sintering cycle. As expected, the weight loss is effectively decreased with a slight increase of the relative density. So, by an adequate control of sintering variables, such as the sintering cycle duration, it is possible to obtain sintered compacts with controlled stoichiometric deviations, together with high densities at relatively low temperatures.

Conclusions

A much higher homogeneity in binder distribution is attained for sputter-deposited WC powders, when compared with powders conventionally prepared. The initial high homogeneity of binder distribution is disturbed by the formation of eta-phase during the heating period of sintering. Large weight losses are also observed at sintering temperatures, difficulting the attainment of high densities. Even so, for a sputter-deposited binder content of 10 wt.%, the density attained at 1325 ºC (d_{rel} = 96%) is higher than that obtained in conventional prepared composites with the same composition, evidencing the benefits of the sputter-coating on the processing of composite powders.

By an adequate control of the sintering variables, such as the sintering cycle duration, it is possible to obtain, from sputter-deposited powders, sintered compacts with controlled stoichiometric deviations together with high densities at relatively low temperatures.

References

[1] C. Hanyaloglu, B. Aksakal and J.D. Bolton: Mater. Charact. 47 (2001), p. 315.

[2] T. Kakeshita and C.M. Wayman: Mater. Sci. and Eng. A141 (1991), p. 209.

[3] T. Farroq and T.J. Davies: Int. J. Powder Metall. 27 (4) (1991) p. 347.

[4] B. Uhrenius: Powder Metall. 35 (3) (1992), p. 203.

[5] R. González, J. Echeberría, J.M. Sánchez and F. Castro: J. Mater. Sci. 30 (1995), p. 3435.

[6] B. Uhrenius, H. Pastor and E. Pauty: Int. J. Refr. Metals & Hard Mater. 15 (1997), p. 139.

[7] R.K Viswanadham and P.G. Lindquist: Metall. Trans. A 18A (1987), p. 2163.

[8] D. Moskowitz: Mod. Dev. Powder Metall. 10 (1977), p. 543.

[9] H. Suzuki, T. Yamamoo and I. Kawakatsu: Powder Metall. J. 14 (1967), p. 26.

[10] C.M. Fernandes, V.M. Ferreira, A.M.R. Senos and M.T. Vieira: Surf. Coat. Technol. 176 (2003) p. 103.

[11] C.M. Fernandes, A.M.R. Senos and M.T. Vieira: Int. J. Refr. Metals & Hard Mater. 21 (2003) p.147.

IV.4. Control of eta carbide formation in tungsten carbide powders sputter-coated with (Fe/Ni/Cr)

C. M. Fernandes, A. M. R. Senos and M. T. Vieira

[1]Department of Ceramics and Glass Engineering, CICECO, University of Aveiro, 3810-193 Aveiro, Portugal
[2]ICEMS, Mechanical Engineering Department, University of Coimbra, 3030-201 Coimbra, Portugal

International Journal of Refractory Metals & Hard Materials 25 (2007) 310-317

Abstract

Composite powders of tungsten carbide with variable coating contents of Fe/Ni/Cr based alloys (1-15 wt.%) were prepared by sputtering. The coated powders have revealed a good performance to shape-forming and sintering. However, the presence of nanocrystalline coatings could enhance the formation of a brittle phase during sintering, named η-phase, $(M,W)_6C$. To investigate this effect, the powders were heat-treated at variable temperatures, up to 1400 ºC. For comparison, conventionally prepared powders were studied, too, and the content of η-phase was found to be higher for the sputter-coated ones. This result is attributed to the content of binder elements with affinity to carbon, like chromium, enhanced by the difference on binder characteristics, such as nanocrystallinity and morphology. It was concluded that an effective control of the reaction can be achieved by increasing in the binder composition the ratio between the elements without affinity and those with affinity to carbon and/or enlarging the carbon content.

Keywords: Tungsten carbide, Coated powders, Fe/Ni/Cr, η-phase, M_6C

1. Introduction

The constant increase in the use of WC-based cemented carbides in new applications, where cobalt is not welcome, and the threat from the depleting resources of cobalt led to a great deal of research into the development of alternative cemented carbides compatible with the WC-Co based ones.

Early attempts have been made [1-9] to find a satisfactory alternative binder phase to cobalt in WC hard metals with similar mechanical properties. The efforts made in the replacement of cobalt by other transition metals of VIII group, as iron or nickel [7-12], revealed that it is possible to promote the densification of WC-(Fe/Ni) at temperatures near those used for WC-Co cemented carbides. However, it might be more difficult to obtain competitive mechanical properties and to find the optimum choice of carbon content for such alloys. The most suitable compositions, from a carbon control point of view, are those where neither η-phase $(M,W)_6C$ nor graphite are formed during the thermal cycle needed to sinter the material [13,14]. A vertical section of the phase diagram W-C-Fe, calculated to 10 wt% Fe (Fig. 1(a)), shows that only very close compositions, between the points *a* and *b*, fulfill these conditions [15]. Moreover, in the present system, this range of compositions corresponds to carbon contents higher than the stoichiometric. The addition of Ni to the W-C-Fe system can enlarge the suitable composition range and move this region to more favourable carbon contents, closer to the stoichiometric, depending on the Ni:Fe ratio, as illustrated in Fig. 1(b) [12,16,17].

When the composition of Fe-rich binders is adjusted there are no occurrences of free carbon or of brittle η-phase in the WC composites and the mechanical properties, such as hardness, toughness and transverse rupture strength (TRS), indicate similar or even superior values to the WC-Co system [7-13]. The role of chromium in the binder has also been investigated, because it acts as a strong grain growth inhibitor and improves oxidation and corrosion resistance [13]. However, the presence of this element, which has more affinity to the carbon than the iron, obliges to an increase of the carbon content to avoid the formation of η-phase [12].

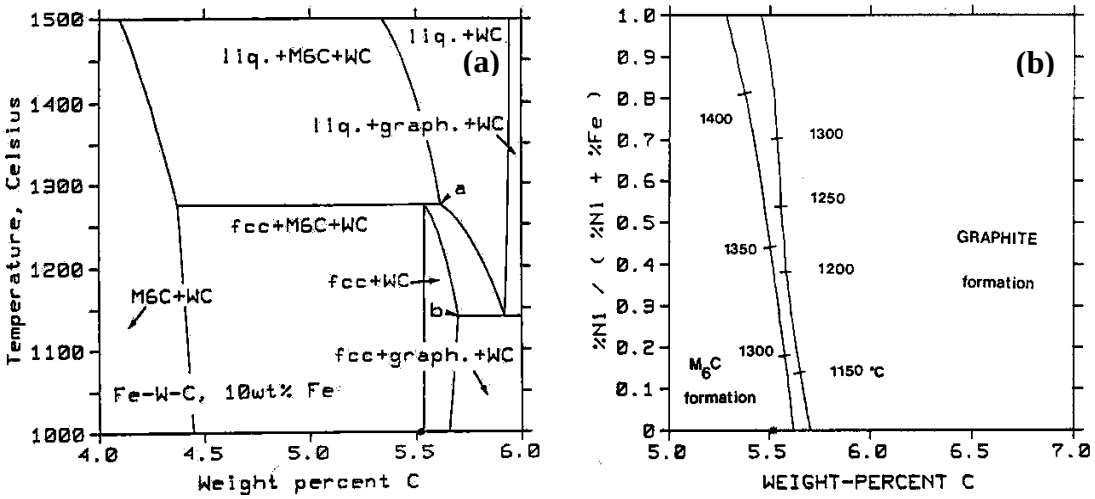

Fig. 1. (a) Vertical section of the Fe-W-C phase diagram, calculated at 10 wt.% Fe (from Ref. [15]). (**b)** Temperature projection of a section of the Fe-Ni-W-C phase diagram calculated at Fe+Ni=10 wt.%. The lines describe the compositions of a mixture of WC and liquid in equilibrium with fcc+M_6C (to the left), and of a mixture of WC+fcc in equilibrium with liquid+graphite (to the right) (from Ref. [16]). The solid symbol on the composition axis on both pictures indicates the stoichiometric composition.

In the authors' own studies [18-21], tungsten carbide powders were sputter-deposited with stainless steel 304 AISI (71%Fe, 8%Ni, 18% Cr, 2%Mn and 0.07%C) by an innovative technique to produce composite powders. The aim of the selection of this binder is to induce two roles: (i) to improve the quality of the powder surfaces and (ii) to establish the optimum composition for the different elements studied. The structure, morphology and chemical distribution of the coated powders have already been investigated [18,19] and revealed that all the WC particles were uniformly coated and show "rough" surfaces, coming from the columnar growth of the thin film deposited [18,19]. The coated powder presents a WC major crystalline phase, traces of W_2C coming from the bulk, and a ferrite b.c.c. structure (Fe-α) for the sputtered layer.

The processing of these coated powders does not need a pressing binder, commonly used in the WC based cemented carbide powders. Sintering performed in a vacuum atmosphere provides high relative densities, ~96%, at a relatively low temperature of 1325 ºC for compacts with an initial content of 10 wt.% of stainless steel [20,21]. This is a consequence of the low *liquidus* temperature, T $\simeq$ 1150 ºC, and good wettability of the liquid phase to the powders to be sintered, together with the nanometer character and the

highly uniform distribution of the coating induced by the sputtering process [18-21]. However, these qualities can enhance the formation of η-phase during the deposition process and sintering.

In this work, an attempt has been made to study η-phase formation with respect to the heating temperature, holding time, binder composition, namely the Ni/(Fe+Cr) ratio, and the carbon content. The optimization of the best ratio between elements with affinity and no-affinity to carbon was envisaged. The conclusions might be applied to coated and uncoated powders.

2. Experimental

WC powder particles were coated with stainless steel by d.c. magnetron sputtering. The deposition chamber was tailored to powder coating by a rotation and vibration of the substrate holder [18].

The powder is a fully carburized WC (9-10 μm) (H.C. Starck, HCST-Germany), which contains, besides the WC phase, traces of W_2C phase. The coatings were sputter-deposited on the WC particles from a target, consisting of a commercial type AISI 304 stainless steel disc (71%Fe, 8%Ni, 18% Cr, 2%Mn and 0.07%C). To increase the Ni/Fe ratio, high purity nickel discs have been bonded to the target. The percentage and the chemical composition of the binder phase in the coated powders (C-WC1 to C-WC6) were characterized by inductively coupled plasma–atomic emission spectrometry (ICP, Isa JY70Plus) in Table 1.

Table 1

Chemical compositions given by ICP of the sputter-deposited coatings on WC powders.

Sample	Fe wt.%	Cr wt.%	Ni wt.%	Mn wt.%	$\frac{Ni}{Fe+Cr}$	Sum (wt.%)
WC*	0.02	<0.009	<0.009	<0.009	___	0.0
C-WC1	0.68	0.18	0.07	0.01	0.1	0.9
C-WC2	3.13	0.81	0.35	0.06	0.1	4.4
C-WC3	4.01	1.06	0.48	0.10	0.1	5.7
C-WC4	7.16	1.87	0.81	0.14	0.1	10.0
C-WC5	10.80	2.92	1.30	0.25	0.1	15.3
C-WC6	2.57	0.65	3.66	0.05	1.1	6.9

*Non-coated WC powder, presented for comparison.

Conventional mixtures have also been prepared with uncoated WC powder and an admixed binder (Fe/Cr18/Ni10 Goodfellow FE226010 powder alloy), with a chemical composition similar to that of the coating of coated powders. Other binder compositions have been also prepared using different contents of iron (Goodfellow FE006020), chromium (Goodfellow CR006021/22) and nickel (Goodfellow NI006021/11) powders (Table 2 and 3). The proportionated powders were milled with 1.5 wt.% of paraffin wax, using isopropyl alcohol as solvent, in a stainless steel mill with WC-Co balls, for 6 h. The mixture was subsequently dried at 60ºC, granulated and sieved. Graphite powder (Panreac 1221) with a maximum particle size of 20 μm has been added to the conventional and coated mixtures, in a dry mixer, for 1 hour.

Table 2

Characteristics of the starting powders used in conventional mixtures, as given by suppliers.

Powder	Maximum particle size (μm)	Purity/Composition (wt.%)
Stainless steel AISI 304	45	/Fe 72; Cr 18; Ni 10
Iron	60	99/
Chromium	38	99/
Nickel	7	99/

Pellets with 10 mm in diameter and about 3 mm thick were prepared by uniaxial pressing, at 190 MPa. The compacts from coated and conventional mixtures were heated in a vacuum furnace inside of a graphite crucible. The furnace atmosphere was pumped to a vacuum of 10 Pa before heating. The heating cycle involved a constant heating rate of 5 ºC min^{-1} up to the maximum temperature, a holding time from 1 to 3 h and a cooling rate of 5 ºC min^{-1} until ~800 ºC, followed by the natural cooling rate of the furnace to room temperature.

Table 3

Chemical formulation of the conventional mixtures.

Sample	Fe wt.%	Cr wt.%	Ni wt.%	$\frac{Ni}{Fe+Cr}$	Sum (wt.%)
M-WC1	2.9	0.7	0.4	0.1	4.0
M-WC2	4.6	1.2	0.7	0.1	6.5
M-WC3	7.2	1.8	1.0	0.1	10.0
M-WC4	10.8	2.7	1.5	0.1	15.0
M-WC5	5.8	1.4	2.8	0.4	10.0
M-WC6	3.6	0.9	5.5	1.2	10.0

The microstructural characterization was done by scanning electron microscopy (SEM, Hitachi-S4100) with energy dispersive spectroscopy (EDS, detector Rontec-EDR288/SPU2) on polished surfaces. An electron microprobe (EMPA-SX50, Cameca) was also used for chemical phase analysis.

The structural characterization of the as-coated and uncoated powders and heat-treated samples was performed by X-ray diffraction (XRD, Rigaku PMG-VH), after desagregation of the heat-treated compacts, using a CuK_α radiation (λ = 1.5418 Å).

The phase quantification was derived from Rietveld analyses of XRD spectra with the aid of the GSAS suite [22]. To achieve better results, each sample was analysed three times and the quantification of WC and η-phase was performed with the structure parameters available in the bibliography for the hexagonal WC crystalline phase [23] and the cubic η-phase Fe_3W_3C [24]. The modifications on the structure parameters, coming from the substitution of some Fe for Ni and Cr in the eta-carbide phase, η-phase, were neglected, as well as the interference of the Fe-α and Fe-γ phases with the quantification. The equivalent amounts of WC and η-phases achieved by stereology, using an areas ratio, on a polished surface of a C-WC3 sample heat-treated at 1200 ºC, are indicative that these assumptions are acceptable in the present Rietveld determinations. On the other hand, the quantification of the Fe-α and Fe-γ crystalline phases in the coated powders were not successful due to a significantly enlarged peak area, caused by the nanometer grain size of the sputtered powders and residual stresses. Moreover, the diminishing quantity of those phases reduces the diffraction spectra to only one quantifiable peak, (110) Miller index for Fe-α and (111) for Fe-γ.

3. Results and Discussion

3.1. Structural evolution during heating

The sputtered powders have different amounts of coating, variable between ~1 and 15 wt.% (C-WC1 to C-WC5, in Table 1). The coated powder C-WC6 has a different binder composition with a higher Ni/(Fe+Cr) ratio, when compared with that of the other coated powders.

As-deposited coated powders do not reveal by X-ray diffraction the presence of η-phase. In order to evaluate the formation of phases during heating, the C-WC3 powder with 5.7 wt.% of binder (Table 1) was heated to different temperatures and the crystallographic phases were analysed by XRD. As reported in Fig. 2, the XRD diffraction profiles show the presence of the WC as major phase and another secondary phase, identified as η-phase $(M,W)_6C$, in all the studied temperatures above 750 ºC. Moreover, a ferrite phase (Fe-α) was detected in the as-coated powder, becoming vestigial for temperatures higher than 800 ºC. The reduction of the ferrite phase content was caused by its reaction with the WC grains to form $(M,W)_6C$ and, additionally, by the transition for an austenitic form, Fe-γ, more stable at high temperatures, Fig. 2. The $(M,W)_6C$ is the stable phase, like in W-C-Fe systems [17,25].

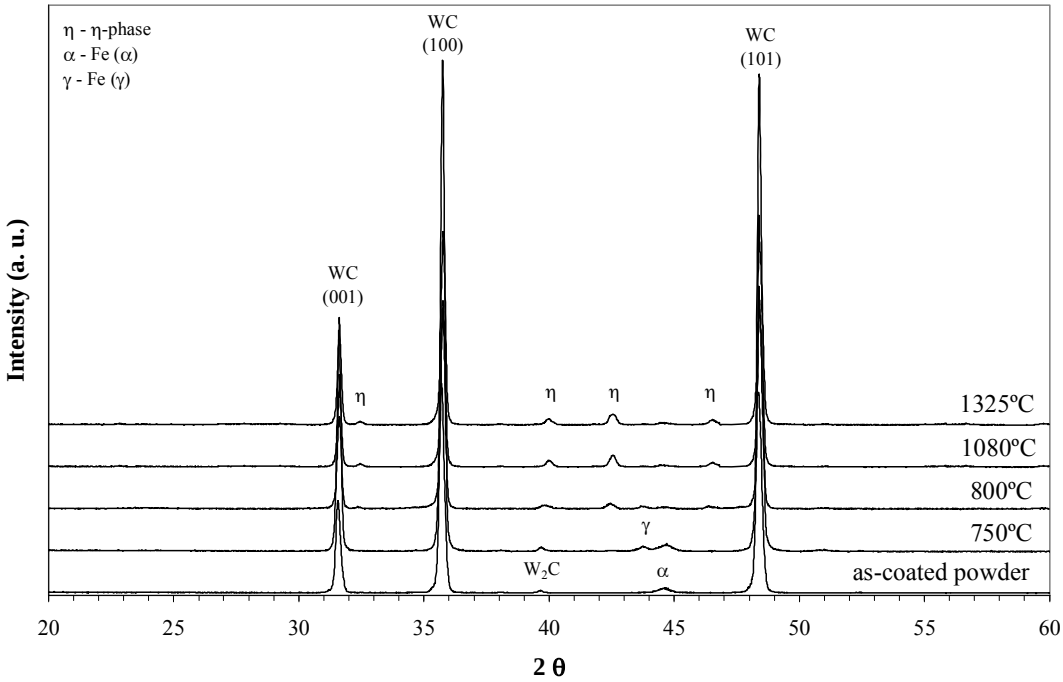

Fig. 2. XRD diffraction profiles of C-WC3 samples heated at different temperatures, for 3 h.

The microstructure of a polished C-WC3 surface, sintered for 3 h at 1200 ºC, in Fig. 3, shows near dense WC grains and an intergranular phase, darker than the matrix. The points identified in Fig. 3 with α, β, χ, indicate the places were EMPA analyse have been performed. The analysis in point α, inside a WC grain, presents an excess of carbon, caused by the impregnation with resin, needed for the sample polishing. The detection of other elements, besides W and C, in the analysis of point α has been related to the width

of the electronic beam, catching the interference of other phases, namely the η-phase, since the solubility of Fe, Ni and Cr in WC is very low [12,26]. The EMPA analysis at the points β and χ, inside the darker phase, shows that this phase is richer in Fe, Cr and Ni, and also contains an appreciable amount of W, as expected for the $(M,W)_6C$ phase. Taking the EMPA analysis done in several points (5 determinations), the stoichiometry of this phase is $(Fe_{2.3}\ Ni_{0.3})(Cr_{0.6}W_{2.8})C$. This composition of the $(M,W)_6C$ phase remains constant, within the experimental error, with the increase in temperature from 1200-1325 ºC, or with the increase of the binder amount (5.7-10 wt%) in the WC-stainless steel AISI 304 composites. The main binder elements, Fe, Ni and Cr, are systematically detected in the $(M,W)_6C$ phase within atomic proportions close to that found in the binder (see table inserted in Fig. 3). The easy accommodation of metal elements (Ti, V, Ta, Cr, Mo) in the M_6C structure was already observed in the WC-Co system, where both W and Co could be partially substituted by other metal additives [27,28].

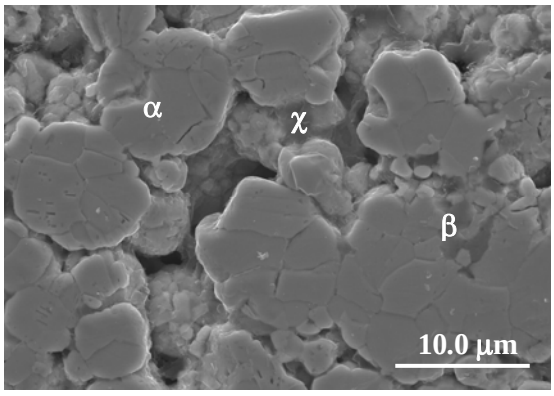

EMPA Analysis (Atomic percentages)

Point	W	Fe	Cr	Ni	C
α	32.1	4.4	0.8	0.4	62.3
β	23.3	24.2	5.0	2.3	45.2
χ	23.8	26.3	5.7	2.0	42.2

Fig. 3. SEM micrograph and EMPA analysis of a C-WC3 (5.7%) compact heat-treated at 1200ºC, for 3 h.

3.2. Eta carbide formation: effect of temperature, time and binder amount

The percentage of η-phase, relative to the total amount of the main crystalline phases, η and WC, calculated from the XRD data, vs. the heating temperature, for a holding time of 3 h, is shown in Fig. 4 for the C-WC3 powder. The figure shows that the η-phase formation starts at low temperatures, near 750 ºC, and its amount gradually increases until ~1100 ºC. The densification results of this composite powder indicate that the liquid phase

appears only at temperatures ~1150 ºC [20]. So, the $(M,W)_6C$ phase is formed by a solid state reaction at temperatures significantly lower than those of the liquid phase formation. When the liquid phase forms, ~1150 ºC, some dissolution of the η-phase is observed to occur in Fig. 4. It must also be pointed that as a consequence of the high content of η-phase formed at low temperatures in these systems, the amount of binder elements available for the liquid phase formation, at higher temperatures, is significantly reduced.

The variation of the relative amount of $(M,W)_6C$ phase with the initial binder content is shown in Fig. 5, for powders with a constant binder composition (C-WC1 to C-WC5 powders, Table 1) heated at 1325 ºC, for 3 h. A near-linear relation with a positive slope of ~1.7 was found. This relation means that increasing the binder content both increases the amount of η-phase and the amount of binder elements available to form a liquid phase.

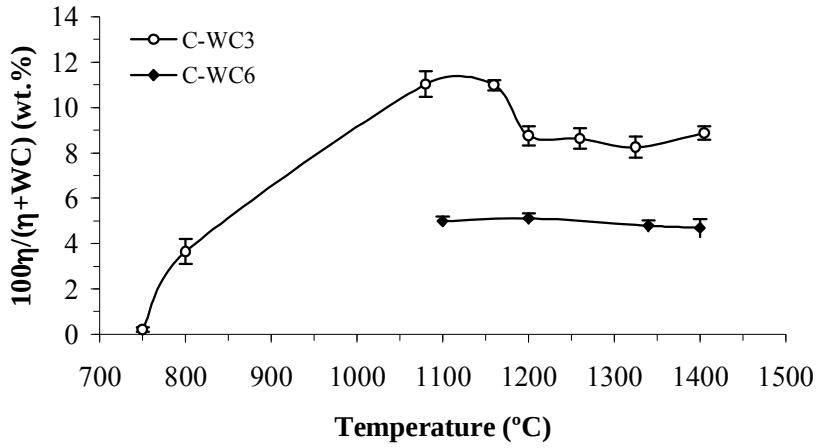

Fig. 4. Amount of M_6C phase vs. heating temperature (holding time of 3 h) for C-WC3 and C-WC6 samples.

Also represented in Fig. 5 are data for conventionally prepared composites powders with compositions equivalent to those of the coated powders and using the same heating schedule. It can be observed that a near-linear relation between the η-phase percentage and the binder amount was also obtained but, in this case, the slope is smaller, ~0.8. So, comparing the results of coated and conventionally prepared powders, it is verified that in the coated powders the formation of η-phase is much more extended, being formed in the double amount than in admixed powders with the same composition. The differences between coated and conventionally prepared powders are related to the much higher uniformity of the binder distribution attained in the sputtered powders, together with the

nanometer particle size in the sputtered coating. In consequence, a larger increase of the contact area between the WC and the binder phases with a strong decrease of the diffusion distances needed to transport the species for $(M,W)_6C$ formation would be expected. If this is the case, the formation of this phase must be controlled by the species diffusion, after an initial fast nucleation step.

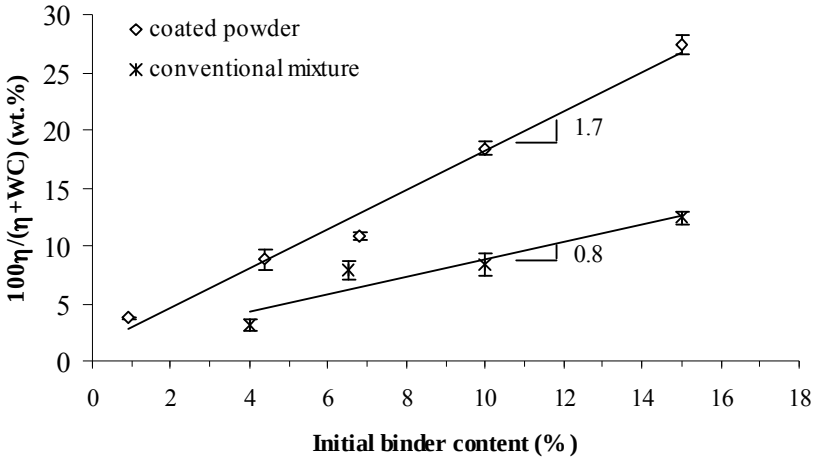

Fig. 5. Amount of M_6C phase vs. initial binder content for coated and admixed powder compacts heated at 1325ºC (3 h hold time).

The kinetic of the $(M,W)_6C$ phase formation was studied at 800 ºC, both in sputtered and conventional prepared powders with 10 wt % of binder (Fig. 6). It can be observed in Fig. 6(a) that, as expected, an equivalent amount of $(M,W)_6C$ is rapidly formed in both powders, within the first 5 min. After, the rate of formation is reduced and this reduction is more pronounced for the conventional mixture. The representation of Avrami for these data is presented in Fig 6(b). A slope of $n = 0.6$ was determined for the coated powder, identified by the Avrami law with a growth process of the η-phase effectively controlled by diffusion. The slope found for the conventionally prepared powder, $n = 0.2$, is lower than the theoretical range of predicted values, but a diffusion controlled mechanism is yet the most probable.

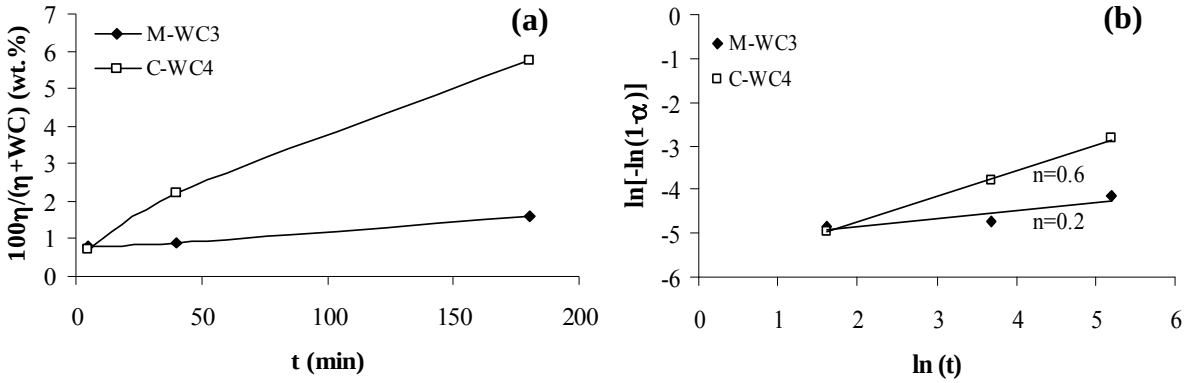

Fig. 6. Relative amount of M_6C vs. time at 800 ºC for M-WC3 and C-WC4 powder compacts: **(a)** linear representation; **(b)** Avrami representation.

3.3. Control of eta carbide formation

The occurrence of η-phase is related to a carbon deficit, caused by decarburisation during sintering, or to a carbon content in the initial composition below the necessary to prevent the formation of η-phase. This phase being formed at relatively low temperatures, before the formation of any liquid phase, decarburisation is not expected to be significant. Other relevant phase diagrams, namely for the W-C-Fe [15,29] and for W-C-Fe-Ni [16,17] systems, show that the carbon content needed to avoid the precipitation of η-phase could be higher than the stoichiometric one (as shown in Fig. 1). The effect of Cr on the favourable carbon content is not established but it is known that Cr is a carbide former [11,13,30], suggesting that the carbon content must be increased further to avoid η-phase formation. Therefore, in a WC-Fe-Cr-Ni system with a low Ni/(Fe+Cr) ratio and a stoichiometric carbon content the formation of η-phase would be unavoidable. These conditions are met in the present system, with an AISI 304 stainless steel binder (~72 wt% Fe, ~18 wt% Cr, ~10 wt% Ni as the main elements) and a near stoichiometric WC powder (actually, a slight carbon deficiency of ~0.3 wt% was experimentally determined).

The formation of the η-phase being thermodynamically favoured in these compositions and kinetically accelerated by the morphology and the nanocristallinity in the sputtered coated powders, significant amounts may be formed, as shown in Figs. 4 and 5. One approach to reduce the amount of η-phase is the adjustment of the binder composition in order to move the limits of the two-phase region to lower carbon contents. As previously

noted, the enrichment of the binder composition with Ni could have the desired effect and this was first tested in conventional mixtures (M-WC), where it is easier to control both the composition and the content of binder. The impact of the Ni/(Fe+Cr) ratio between 0.1 (for AISI 304 stainless steel) and 1.2 in powders with 10 wt% binder, sintered at 1100ºC, is shown in Fig. 7. The percentage of η-phase was effectively reduced from ~12 to ~4 wt%. For coated powders (C-WC) with 6-7 wt% binder, the increase of the Ni content from 0.1 to 1.1 also brought an equivalent reduction of the η-phase from ~11 to ~4.5 wt%, see Fig. 7. This amount of $(M,W)_6C$ does not significantly change within the sintering temperature range, 1100-1400 ºC, as is shown in Fig. 4.

Although an effective reduction of the η-phase was achieved by the Ni enrichment of the initial binder composition, the elimination of that phase will require yet a larger Ni content. For the conventional prepared powders with 10 wt% binder, this content can be estimated to Ni/(Fe+Cr) ratio ≈1.8 (Fig. 7) and even larger amounts would be needed for equivalent binder amounts in the sputter-coated powders. Such an increase of the Ni content would also increase the sintering temperatures [13,26]. As a consequence, during conventional sintering, densification and weight losses are difficult to control, as experimentally tested by our team, and production costs increase. In this sense, an adjustment of the carbon content in powders has been tried as a complementary way to further reduce the η-phase amount.

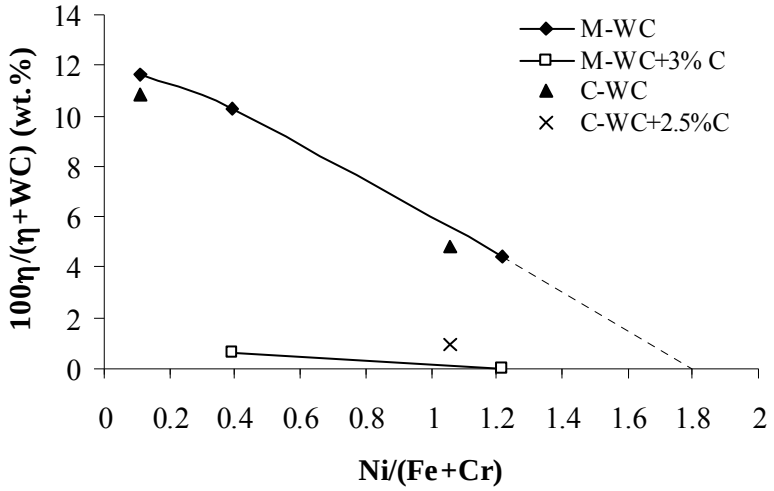

Fig. 7. Binder composition vs. relative amount of M_6C formed at 1100ºC, 1h, in admixed powders (M-WC) with 10 wt.% of binder and in coated powders (C-WC) with 6-7 wt.% of binder.

Carbon additions were performed in conventionally admixed as well as in coated powders. For the conventional powders, M-WC5 and M-WC6, with 10 wt.% of binder, 3 wt.% carbon in excess, relative to the stoichiometric carbon, were added, and for the coated powder, C-WC6, with 6 wt.% of binder, an excess of 2.5 wt.% was applied. The XRD profiles for M-WC6 and C-WC6 powders heated at 1100ºC, 1 h, are presented in Fig. 8. For the C-WC6 powder the M_6C phase became residual. For the M-WC6 powder, only the WC phase and Fe-γ phases are observed. No graphite phase was detected in any case. The corresponding amount of η-phase, calculated from the XRD data, are also represented in Fig. 7, confirming that none or very low amounts of η-phase are formed in these powders with a higher Ni content and excess carbon. So, by an adequate Ni enrichment of the binder composition and the use of excess carbon, it is possible to dramatically reduce, or even eliminate, the $(M,W)_6C$ formation in W-C-Fe-Ni-Cr system. The reactivity control during the heat-treatment necessary to obtain dense samples provided us the technological basis to obtain sintered compacts with similar compositions, but different structural characteristics. In a continuation of this work, the mechanical behaviour of such composites, obtained from sputtered-coated powders is currently under study. Actually, one of the aspects investigated is the effect of the η-phase content, since the higher dispersion of this phase attained in the coated powder samples, compared to conventional powders, can minimize its deleterious role in the mechanical properties.

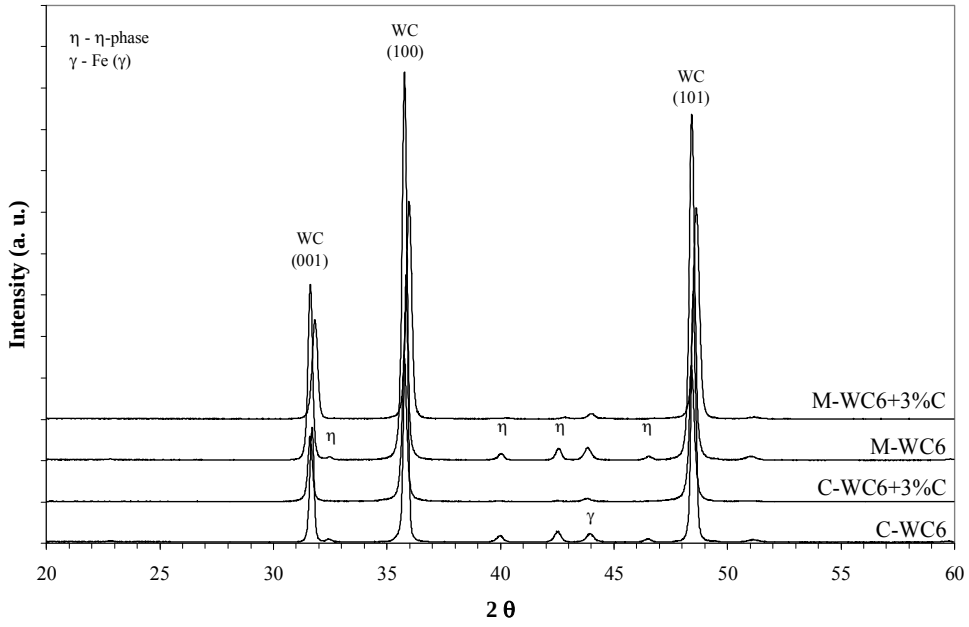

Fig. 8. XRD diffraction profiles of C-WC6 and M-WC6 powders, with and without carbon addition, heated at 1100ºC, for 1 h.

4. Conclusions

The formation of η-phase in composite powders of WC sputter-coated with stainless steel AISI 304 starts at about 750 ºC, increases up to 1100 ºC, and continues until the maximum studied temperature, 1400 ºC. The η-phase, in the temperature range 1200-1325 ºC, can be represented approximately as $(Fe_{2.3}Ni_{0.3})(Cr_{0.6}W_{2.8})C$ ($(M,W)_6C$). The main binder elements (Fe, Ni, Cr) are easily accommodated in the $(M,W)_6C$ structure.

The amount of η-phase is higher in coated than in the admixed powders with similar chemical composition and the same processing conditions. The $(M,W)_6C$ phase is formed by a solid state reaction with the growth process controlled by diffusion. The much higher uniformity of the binder distribution and the nanometric character of the thin film in the sputtered powders lead to an increase in contact area between the WC and the binder phases, and to a decrease of diffusion distances, compared with traditional micrometrics binders.

In both cases the amount of η-phase is reduced by increasing the Ni/(Fe+Cr) ratio from 0.1 to 1.1. Additionally, 2.5~3 wt.% excess carbon can eliminate the $(M,W)_6C$ phase. Thus, by a suitable elemental variation it is possible to control the reaction between the WC particles and the Fe/Ni/Cr binder during the heating process, which is crucial to control selected structural properties.

Acknowledgements

The authors wish to thank Dr. Maxim Avdeev and Dr. Dimitry Khalyavin for the help in the analysis of XRD data.

References

[1] Suzuki H, Yamamoo T, Kawakatsu I. Properties of WC-10% (Ni-Fe). Powder Metall J 1967; 14: 26-31.

[2] Moskowitz D, Ford MJ, Humenik M Jr. High-strength tungsten carbides. Int J Powder Metall 1970; 6 (4): 55-64.

[3] Moskowitz D. Abrasion resistant iron-nickel bonded tungsten carbide. Mod Dev Powder Metall 1977; 10: 543-51.

[4] Moskowitz D, Ford MJ, Humenik M Jr. High-strength tungsten carbides. Mod Dev Powder Metall 1971; 5: 225-34.

[5] Miodownik AP. Means of predicting structure and performance of new materials. Powder Metall 1989; 32 (4): 269-76.

[6] Farroq T, Davies TJ. Tungsten carbide hard metals cemented with ferroalloys. Int J Powder Metall 1991; 27 (4): 347-55.

[7] Viswanadham RK, Lindquist PG. Transformation-toughening in cemented carbides: Part I. Binder composition control. Metall Trans A 1987; 18A: 2163-73.

[8] Kakeshita T, Wayman CM. Martensitic transformations in cements with a metastable austenitic binder. Mater Sci Eng 1991; A141: 209-19.

[9] Uhrenius B. Phase diagrams as a tool for production and development of cemented carbides and steels. Powder Metall 1992; 35 (3): 203-10.

[10] González R, Echeberría J, Sánchez JM, Castro F. WC-(Fe, Ni, C) hardmetals with improved toughness through isothermal heat treatments. J Mater Sci 1995; 30 (13): 3435-9.

[11] Cooper R, Manktelow SA, Wong F, Collins LE. The sintering characteristics and properties of hard metal with Ni-Cr binders. Mater Sci Eng A 1988; A105-106: 269-73.

[12] Tracey VA. Nickel in hardmetals. Int J Refr Metals Hard Mater 1992; 11: 137-49.

[13] Penrice TW. Alternative binders for hard metals. Carbide Tool J 1988; 20 (4): 12-5.

[14] Uhrenius B. On the composition of Fe-Ni-Co-WC-based cemented carbides. Int J Refr Metals Hard Mater 1997; 15: 139-49.

[15] Guillermet AF. The Co-Fe-Ni-W-C phase diagram: A thermodynamic description and calculated sections for (Co-Fe-Ni) bonded cemented WC tools. Metallkd 1989; 80 (2): 83-94.

[16] Guillermet AF. An assessment of the Fe-Ni-W-C phase diagram. Metallkd 1987; 78 (3): 165-71.

[17] Guillermet AF. Use of phase-diagram calculations in selecting the composition of Fe-Ni bonded WC tools. Int J Refr Metals Hard Mater 1987; 6 (1): 24-7.

[18] Fernandes CM, Ferreira VM, Senos AMR, Vieira MT. Stainless steel coatings sputter-deposited on tungsten carbide powder particles. Surf Coat Technol 2003; 176 (1): 103-8.

[19] Fernandes CM, Senos AMR, Vieira MT. Particle surface properties of stainless steel-coated tungsten carbide powders. Powder Technol 2006; 164 (3): 124-9.

[20] Fernandes CM, Senos AMR, Vieira MT. Sintering of tungsten carbide particles sputter-deposited with stainless steel. Int J Refr Metals Hard Mater 2003; 21: 147-54.

[21] Fernandes CM, Senos AMR, Vieira MT. Study of sintering variables of tungsten carbide particles sputter-deposited with stainless steel. Mater Sci Forum 2004; 455-456: 295-8.

[22] Larson AC, Von Dreele RB LAUR 86-748 Report, General Structure Analysis System. Los Alamos National Laboratory; 1990.

[23] Leiciejewicz J. A note on the structure of tungsten carbide. Acta Cryst 1961; 14: 200.

[24] Yang Q, Andersson S. Application of coincidence site lattices for crystal structure description. Part I: Σ=3. Acta Cryst 1987; B43: 1-14.

[25] Åkesson L. Thermodynamic and sintering studies in the Co-W-C system. Thermochim Acta 1979; 29: 327-32.

[26] Upadhyaya GS, Bhaumik SK. Sintering of submicron WC-10 wt.% Co hard metals containing nickel and iron. Mater Sci Eng A 1988; A105-106: 249-56.

[27] Åkesson L. An experimental and thermodynamic study of the Co-W-C system in the temperature range 1470-1700 K. In: Viswanadham RK, Rowcliffe DJ, Gurland J, editors. Science of Hard Materials, New York: Plenum Press; 1983, p. 71-82.

[28] Pollock CB, Stadelmaier HH. The eta carbides in the Fe-W-C and Co-W-C systems. Metall Trans 1970; 1: 767-70.

[29] Bergström M. The eta carbides in the ternary system Fe-W-C at 1250ºC. Mater Sci Eng 1977; 27: 257-69.

[30] Bergström M. The eta carbides in the quaternary system Fe-W-C-Cr at 1250ºC. Mater Sci Eng 1977; 27: 271-86.

Chapter

V

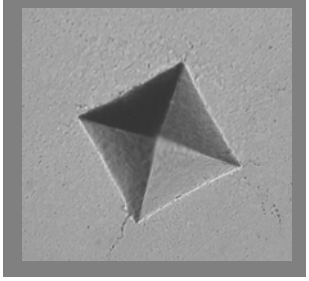

Mechanical Characterization

Fe-rich binders have improved mechanical properties, such as hardness and toughness compared to cobalt bonded hardmetals.

Prakash et al., Morden Dev. Powder Metall. (1981)

V.1. **I**ntroduction

In this chapter the results of the mechanical characterisation of the composites obtained from WC powders coated with Fe/Ni/Cr binders are presented and related to the chemical, structural and microstructural features. Two papers constitute this chapter. The first one is related to the characterization of composites with Ni richer binders and the second one to the properties of composites with iron richer binders. In both papers the mechanical characterization of hardness, Young's modulus and yield strength were performed using a depth-sensing equipment. The fracture toughness was determined by the Pamqvist cracks in the corners of the indent performed with 98 N load. In order to compare with values from literature, the Vickers hardness was also carried out.

*V.2. **M**echanical **c**haracterization of **c**omposites **p**repared from **WC p**owders **c**oated with **N**i **r**ich **b**inders*

C. M. Fernandes[1], A. M .R. Senos[1], M. T. Vieira[2] and J. M. Antunes[3]

[1]Department of Ceramics and Glass Engineering, CICECO, University of Aveiro, 3810-193 Aveiro, Portugal
[2]ICEMS, Mechanical Engineering Department, University of Coimbra, 3030-201 Coimbra, Portugal
[3]CEMUC, Mechanical Engineering Department, University of Coimbra, Rua Luís Reis Santos, Pinhal de Marrocos, 3030-788 Coimbra, Portugal

International Journal of Refractory Metals & Hard Materials 26 (2008) 491-498

Abstract

In this study composite powders of WC and Ni/Fe/Cr were prepared in an innovative way, which consists of the sputter-deposition of the metallic binder onto the tungsten carbide particles. Compacts of coated powders were sintered by conventional vacuum sintering followed by hot isostatic pressing (HIP) to reach almost full densities. In order to evaluate the mechanical properties of reduced specimens size (microcomponents), depth-sensing indentation equipment was used. This method enabled the evaluation of the hardness, H, Young's modulus, E, and the yield stress, σ_y, in a non-destructive way, using only one sample. For the composites of sputter-coated WC-Ni/Fe/Cr the results showed an effective reduction of H and E due to the properties of Ni and the binder characteristics of the coated powders, such as uniform distribution and nanometer structure.

Keywords: Sputtering; Tungsten carbide; Nickel; Coated powders; Mechanical properties

1. Introduction

Hard metal has been industrially produced since the 1920s and nowadays represents more than 40% of the cutting tool market [1]. Due to their technological importance these composites of WC, which are formed using a transition metal binder, usually cobalt but to a lesser extent iron or nickel, have been subject to a great deal of investigation in order to optimize the compositions and the processing leading to the highest mechanical properties [2-7]. During the last few decades, the deployment of cobalt natural resources and the increasing demands on material performance has directed the research mainly towards the search and optimization of new binder compositions and the development of specific coatings to improve the useful properties [8,9]. On the other hand, the industrial processing of these composites has made very little difference, although new emerging technologies for powder metallurgy are currently being researched with a view to industrial implementation [10-12].

In this study, an innovative method of preparing composite powders was used, consisting of the sputtering of the metallic binder onto the WC particles. The coated powders resulting from this technique show a very high uniformity of binder distribution associated with a nanocrystalline structure. The surface properties of the particles are changed, increasing the powder's flowability, pressing behaviour and sinterability in such a way that easier powder processing can be adopted [13-17]. One of the benefits comes from the possibility of shaping without a pressing binder, therefore eliminating the long milling step used in the conventional hard metal processing to add the binder and to prepare the composite powders, and also the subsequent drying of the slurry and the burnout of the pressing binder. Moreover, due to the high uniformity of the binder's distribution and its nanometer structure, liquid phase sintering is more efficient, leading to high density compacts at lower temperatures [15-17]. Additionally, by eliminating the milling and the pressing binder burnout steps, the processing is moving towards a cleaner technology with environmental and health benefits.

Weighing up the benefits of the low binder content needed to coat the particle surfaces using this technique (i.e. for WC particles with 2-10 μm, ~4 wt% of stainless steel AISI 304, will be enough for a complete particle coverage [13-18]) together with the high sinterability of the sputtered powders against the relatively high cost of the sputtering step,

points to the benefits of this methodology: an innovative technological process with interesting prospects in the production of powders with low binder content for high hardness applications.

Previous studies were dedicated to the study and optimization of the surface characteristics in sputtered powders and consequences on the powder processing [13-18]. In this study, composites of WC and low Ni/Fe/Cr binder content (4-7 wt%) were prepared using both the sputtering technique and the standard conventional mixture, in order to highlight the role of sputter coating powders on the mechanical properties.

A novel method was used in order to get the best possible measurements of mechanical characteristics using only one test – depth-sensing indentation. This methodology is particularly appropriate for the characterization of materials prepared on a laboratorial scale with equipment that often limits the amount and the size of the samples, as was the case here. This is a problem that researchers have to face frequently. The reverse analysis method has been successfully applied to characterize single phase materials [19] but had not previously been tested in multi-phase, composite materials. This method was therefore first applied to a commercial WC-Co sample, whose mechanical characteristics had been characterised in previous studies, before it was used to measure the mechanical properties of the coated and conventionally prepared WC-Ni rich binder samples.

2. Experimental Procedure

The starting powder was fully carburized WC (H.C. Starck, HCST-Germany) with a particle size of 2-10μm. The WC powder particles were coated with Ni/Fe/Cr binders using modified d.c. magnetron sputtering equipment and previously selected deposition parameters, which are described elsewhere [14]. Two coated powders, C-WC1 and C-WC2, with different binder contents (< 8 wt.%) were investigated. For comparison a conventional mixture of nickel (Goodfellow NI006021/11), iron (Goodfellow FE006020) and chromium (Goodfellow CR006021/22) powders was performed with the uncoated WC powder and 1.5 wt.% of paraffin wax, named M-WC.

Pellets of ~10 mm diameter were subjected to cold isostatic pressing (CIP), at a maximum pressure of ~330 MPa. The compacts underwent conventional vacuum sintering to a maximum temperature of 1510ºC, for 1 h, at a pressure of 20 Pa. To simplify the

experimental procedure, the same sintering cycle was used for coated and conventionally prepared powders, although higher densifications are attained for coated powders, due to their higher reactivity. Finally, to attain almost complete densification, the pre-sintered samples were submitted to hot isostatic pressing (HIP) at 1550ºC, for 2 h at a pressure of 30 MPa. For each composition a set of 4-6 samples were sintered.

The density of the sintered samples was determined using the Archimedes' method. Phase identification was performed by X-ray diffraction (XRD, Rigaku PMG-VH). Optical microscopy (Zeiss, Jenaphot 2000) and scanning electron microscopy (SEM, Hitachi-S4100) were used to characterize the microstructure of polished surfaces chemically etched with Murakami's reagent[1], for 2 min, to reveal the grain boundaries. WC average grain size and size distribution were measured using the linear intercept method [20] on the SEM micrographs. Random straight lines were drawn across the micrographs and the length of the intercepts with the WC grains were measured and averaged (at least 300 intercepts per sample were used). Fullman's formula was applied to transform the two-dimensional mean intercept, l, into a three-dimensional mean grain size, $\overline{G}$, using a transformation factor of 1.5 [20]. The contiguity, C, was also determined using nearly 100 measurements from the optical micrographs, and applying the following equation [21]:

$$C = 1 - \mathbf{V_b}^{0.644} \exp(0.391 \times \mathbf{V}) \quad (1)$$

where V_b is the volume fraction of binder and V is the coefficient of variation of WC grain size distribution ($V = \sigma_{WC} / \overline{G}_{WC}$ where σ_{WC} is the standard deviation and $\overline{G}_{WC}$ is the mean carbide grain size).

The chemical characterization of the sintered samples was obtained using an electron microprobe (EMPA-SX50, Cameca) and the final carbon content was determined by automatic direct combustion (LECO CS 200 IH).

The hard metal samples were mechanically characterized using depth-sensing indentation equipment (Fischerscope H100). In order to obtain representative average values for the evaluated properties, 75 tests were performed on different surface points of each samples per set. In each test the load was increased in steps, from the first load of 0.4 mN until a nominal load of 500 mN. Sixty steps were used for both loading and unloading, with a 0.5 s delay between each step. Two creep periods of 30 s were performed during the

[1] A solution of potassium ferricyanide (10g) and sodium hydroxide (10g) in distilled water (100ml).

tests: at the maximum load and at the lowest load. The values of the 75 tests performed on each sample were used for the direct determination of the hardness, *H*, and calculation of the Young's modulus, *E*, and of the compressive rupture strength, σ_r. In order to evaluate the effectiveness of this method, a commercial sample of WC-Co with 4 wt.% of binder was first characterized. Additionally, the hardness of this standard sample was also measured using Vickers hardness tester (Zwick/Roell ZHU) with a load of 294 N and dwell time of 15 s, and the dynamic Young´s modulus, *E*, was yet determined by the impulse excitation vibration method at room temperature using a sample of dimensions 50 x 12 x 1.5 mm^3.

The fracture toughness, K_C, was determined in WC-Ni/Fe/Cr composites from the measurements of the Palmqvist radial cracks at the corners of Vickers hardness indentations (load, 98 N), using the formula [22]:

$$K_c = 0.087 \sqrt{HW} \quad (2)$$

where, *H* is the hardness and $W = P/L_T$, *P* is the applied load and L_T the total length of cracks.

3. Results and discussion

3.1. Chemical and morphological characterization

The composites of WC-Ni/Fe/Cr prepared by conventional mixing (M-WC) and by sputter-deposition (C-WC) had final metal amounts that varied between 4 and 7 wt % (Table 1). The chemical characterization of the binder was performed by EPMA analysis after sintering (Table 1). Ni is present in the highest percentage for all the compositions, followed by Fe. Cr is a minor composition, not exceeding 7 wt.% of the total binder amount, in any case. Moreover, the Fe and Cr amounts are near constant for the three samples. The final binder amount (Table 1) was calculated as the summation of Ni, Fe and Cr contents in each samples set. No significant carbon losses have been found in final compositions, as described by LECO analysis (Table 1).

Table 1

Final binder elements and carbon percentages.

Sample	Fe[a] (wt.%)	Ni[a] (wt.%)	Cr[a] (wt.%)	Total (wt.%)	C[b] (wt.%)
C-WC1	1.5	2.3	0.1	3.9	—
C-WC2	1.3	4.3	0.4	6.0	5.62
M-WC	1.0	5.9	0.1	7.0	5.60

[a] EPMA analysis; [b] Automatic direct combustion

The XRD patterns in Fig.1 show that hexagonal WC and f.c.c. rich Ni phases are the phases identified in coated and conventionally prepared composites; graphite and η-phases were not discernible. The Fe and Cr elements appeared to be in solid solution in the Ni phase.

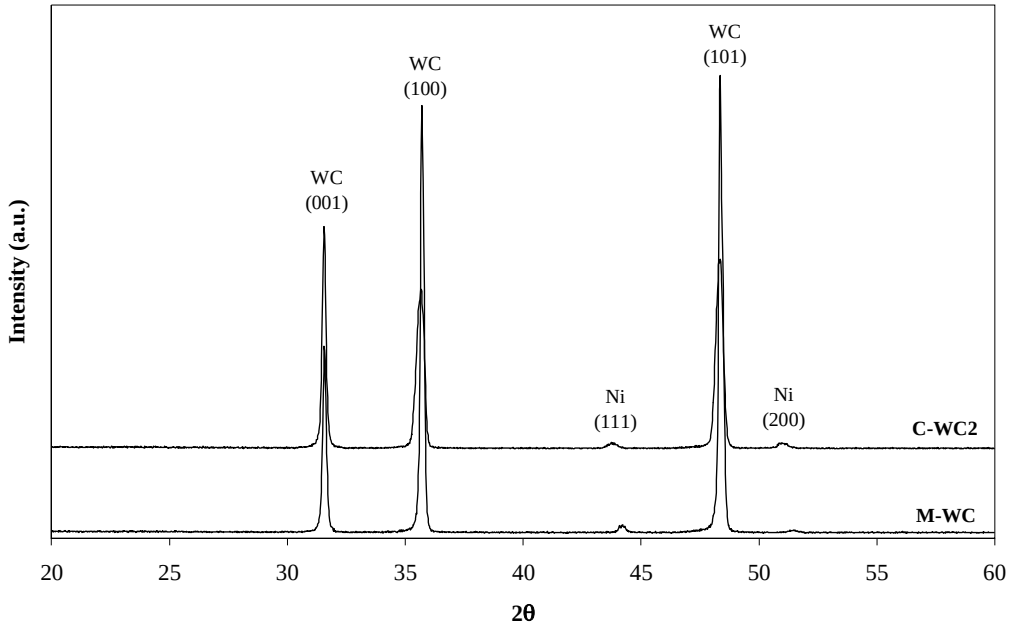

Fig. 1. XRD diffraction patterns of M-WC and C-WC2 composites.

High apparent density values, ρ_{app}, were attained after sintering (Table 2). The correspondent relative densities, ρ_r, vary from ~94 to ~99%, considering the theoretical density, ρ_{th}, calculated by the mixing rule where ρ_{th} = 15.63 g cm^{-3} for WC and ρ_{th} = 8.9 g cm^{-3} for f.c.c. Ni (the effect of Fe and Cr on the density was neglected). The highest ρ_r value (99%) was attained for the coated powder with 6 wt.% of binder (C-WC2), whereas the densification of the conventionally prepared powder (M-WC), with an equivalent amount of binder, showed the lowest value, ρ_r ~94%. For the coated powders, even 4 wt% of binder (C-WC1, Table 2) was enough to attain high densification, ρ_r ~97%. These

results demonstrate the improvement of the sinterability in sputtered-coated powders, already reported in previous studies [14-17], showing that it is possible to achieve higher density materials than those conventionally prepared, using lower binder content.

Table 2.

Physical characteristics of the WC-Ni/Fe/Cr composites.

Sample	ρ_{app} (g cm^{-3})	ρ_{th} (g cm^{-3})	ρ_r (%)	G_0 (μm)	G (μm)	$\overline{G}$ (μm)	C
C-WC1	14.7 ± 0.1	15.17	97	1.7 – 10	2.0 – 9	4.4	—
C-WC2	14.8 ± 0.1	14.95	99	1.7 - 10	2.0 – 10	4.3	0.62
M-WC	13.9 ± 0.1	14.84	94	0.4 – 4.2	1.5 – 8	3.4	0.60

ρ_{app} – apparent density; ρ_{th} – theoretical density; ρ_r – relative density; G_0 – initial grain size; G – grain size; $\overline{G}$ – mean grain size; C - contiguity

The microstructures of the samples were observed by optical and SEM microscopy, in Figs. 2 and 3, respectively. The optical microstructures of the samples C-WC2 and M-WC, presented in Fig. 2, show that the microstructures of WC grains and the binder phase have greater tonal variation under optical observation than under the correspondent SEM analysis (Fig. 3): the WC phase has a darker grey and the binder phase a grey colour. The binder phase is spread between the WC grains since it constituted a viscous phase at the sintering temperatures. In Fig. 2a C-WC2 shows a microstructure without significant heterogeneities of binder distribution, while for the M-WC sample (Fig. 2b), a lower uniformity of the binder distribution is detected, showing an accumulation of the binder phase in some well dispersed regions. They can attain higher dimensions than the WC grains (0.6-6 μm) as shown in Fig. 2b where a large binder area of ~9 x 9 μm^2 can be discernible. The even distribution of the binder phase in the sputter-coated samples is really expected, due to the high initial uniformity of binder distribution, while the lower chemical homogeneity observed in the conventional prepared compacts is commonly observed, as a result of insufficient mixing conditions, powder agglomeration and scale effects [23,24].

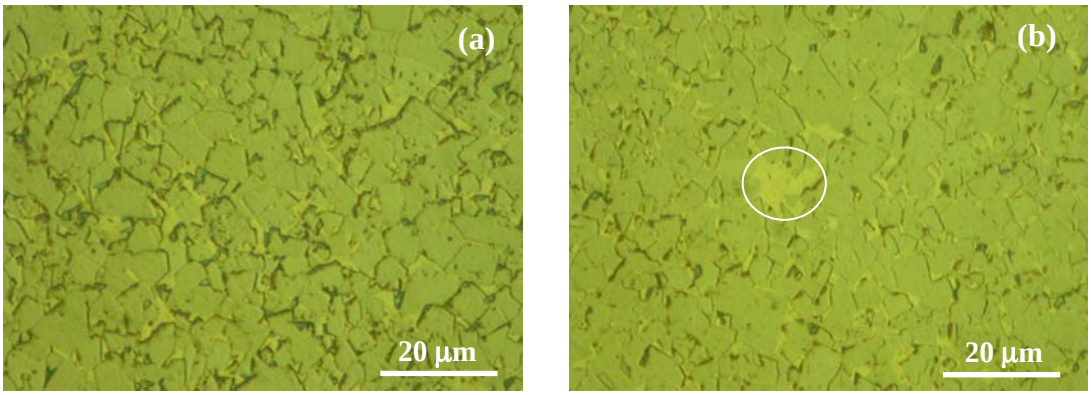

Fig. 2. Optical micrographs: (a) C-WC2 and (b) M-WC. The surrounding area shows the heteregoneity of binder distribution.

The SEM microstructures (Fig. 3) show polyhedral WC grains and a darker intergranular phase, corresponding to the rich Ni phase. The samples prepared from coated powders (C-WC1 and C-WC2), present very similar microstructures with coarser grains that the one prepared from mixed powders (M-WC). The values for the average grain size measured from the SEM micrographs are presented in Table 1, together with the range of particle/grain size before and after sintering. It can be observed that the grain size width in the sintered samples of coated powders is correspondent to the original particle size width, which means that no appreciable growth of the particle size occurred during sintering. The inhibition of particle growth during the sintering of the sputtered-coated powders has previously been reported and attributed to the highly uniform binder distribution attained in the sputtering process [14-17]. The correspondent results for the M-WC compact show that the ranges of initial particle sizes develop to higher values, which is indicative of particle coarsening during sintering. Thus, the larger C-WC grain size did not originate during the sintering process but came from differences in the powder particle size distribution of the coated and mixed powders, as shown in Table 2. Although the same WC powder was used as starting material for both processes, the mixing step used in the conventional preparation tends to desagregate some particles, resulting in a finer powder and a finer sintered compact.

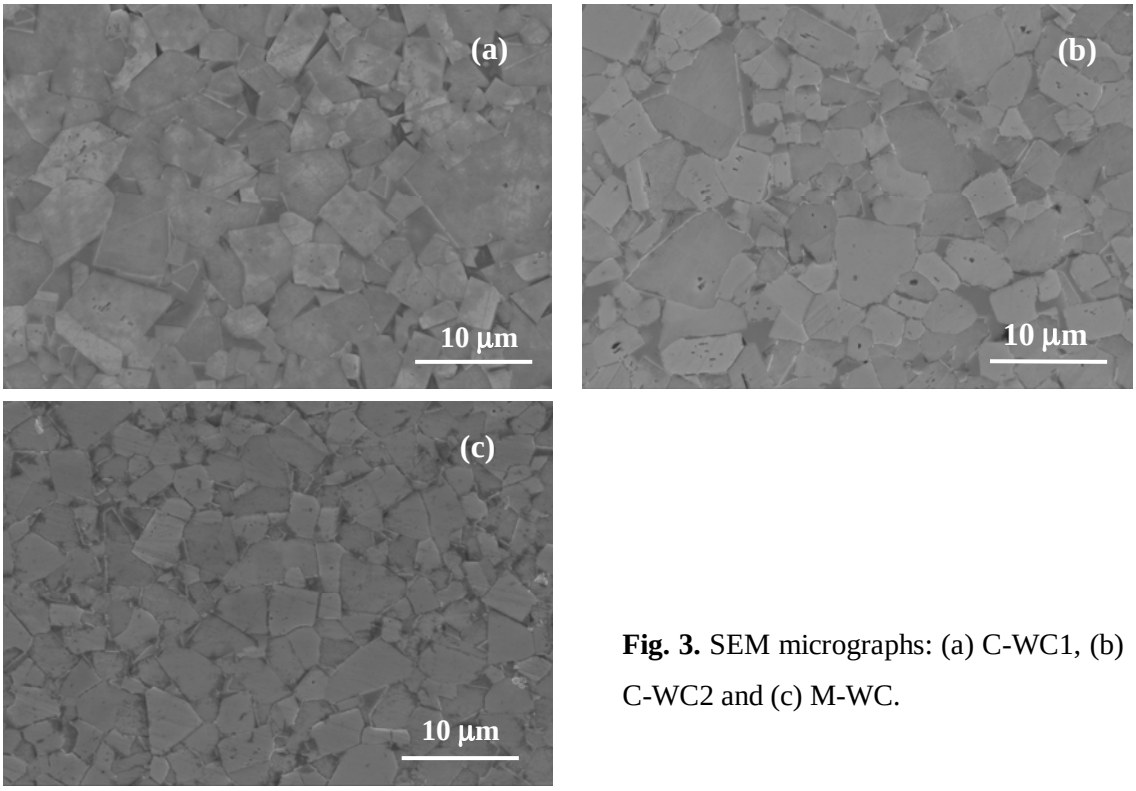

Fig. 3. SEM micrographs: (a) C-WC1, (b) C-WC2 and (c) M-WC.

3.2. Test of the depth-sensing indentation method in a WC-Co composite material

In order to test the values of the mechanical properties determined by the depth-sensing indentation in multi-phase materials, a commercial WC-4%Co sample was used as standard. The optical microstructure of the polished and etched surface is shown in Fig. 4. The standard sample is characterized by a fine microstructure with almost no pores and an average grain size of ~2 μm (Table 3).

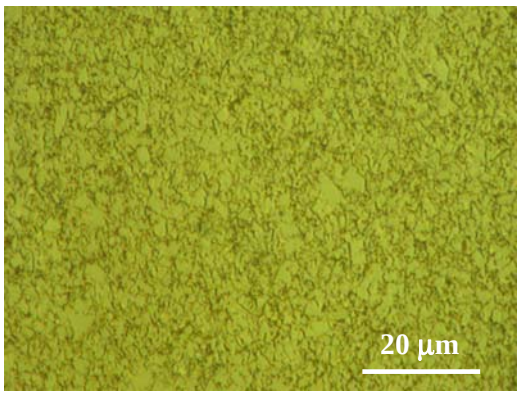

Fig. 4. Optical microstructure of the WC-Co composite.

Ultra-microhardness equipment was used to calculate the hardness and the Young's modulus, E, of the sample, using Eq. (3), taking ν = 0.22 for WC-4wt.%Co [25]. The following equation was proposed for determining the reduced Young's modulus [26,27]:

$$E_r = \frac{\sqrt{\pi}}{2}\frac{1}{\sqrt{A_c}(C_t - C_f)} \tag{3}$$

where C_t and C_f are the total compliance of the system and the frame compliance, respectively, and A_c is the contact area. In this equation, E_r, is the reduced Young's modulus, which is a function of the Young's modulus and the Poisson's ratio, ν, of the specimen (s) and the indenter (i), through:

$$\frac{1}{E_r} = \frac{1-\nu_s^2}{E_s} + \frac{1-\nu_i^2}{E_i} \tag{4}$$

In recent years, efforts have been made to establish a reverse analysis algorithm for the evaluation of the plastic mechanical properties of materials. The principal developments in this area of investigation are related to the application of the finite element method to obtain dimensionless functions that relate the characteristic parameters of indentation loading-unloading curves to the mechanical properties obtained from the stress-strain curves [28]. Recently, a straightforward reverse analysis approach was proposed [19], which avoids the use of dimensionless functions. In a simplified description, this approach, which was used in the current investigation, consists of a direct comparison between experimental and numerical simulation indentation curves, in order to determine the yield stress, σ_y, and the strain hardening coefficient, n, of the material. The Swift law was used in numerical simulations to describe the plastic behaviour:

$$\sigma_y = K(\varepsilon + \varepsilon_0)^n \tag{5}$$

where ε is the plastic strain and K is a material parameter: $K = \sigma_y / \varepsilon_0^n$ (ε_0 is a constant, assumed as 0.005). The calculated values of σ_y can thus be envisaged using this method and considering ε = 0.042 (Fig. 5). The results are shown in Table 3, together with those resulting from conventional tests[2] done in this study and reported in the literature for specimens with similar chemical and physical characteristics [25,29,30]. The value

[2] E is typically determined by dynamic excitation of ultrasonic frequency longitudinal oscillations in a test bar and σ_y by compressive strength tests of a piece between two parallel carbide blocks, until failure occurs [25,29,30].

obtained for the Young's modulus, *E*, by the depth-sensing indentation is equivalent to the one determined by dynamic excitation in this work, Table 3. A very strong agreement is also observed with those reported in the literature in Table 3. The ultra-microhardness value determined by the depth-sensing method is not directly comparable with the HV30 values due to the large difference in the magnitude of the indentation loads, 500 mN in the first method and 294 N in HV30 tests. Even so, it can be said that the determined value (H=22 GPa) concurs with the HV30 ((H=18.3 GPa), being of the same order of magnitude but somewhat higher, as expected from the lower indentation load used. The yield compressive strength, σ_y, using depth-sensing indentation, show very strong agreement with those resulting from conventional tests in the literature, Table 3. The hardening coefficient was very low, n=0.02, characteristic of brittle materials.

Table 3.

Microstructural and mechanical characteristics of WC-Co samples.

Co (wt.%)	**G (μm)**	**Density (g cm^{-3})**	**Hardness HV30**	**Hardness (GPa)**	***E* (GPa)**	**σ_y (GPa)**	***n***	**Ref.**
4	2.5	15.3	1830	22.0 ± 0.2*	662 ± 6* 660	6.52*	0.02*	in this work
4	2 - 4	15.2	1900	—	660	6.00	–	[25]
3	2 - 4	15.3	1950	—	641	5.86	–	[29]
4	2 - 4	—	2000	—	665	7.10	–	[30]

*Values obtained using depth-sensing indentation.

The good match between the previous values of the mechanical parameters determined by local depth sensing tests in the WC-Co sample and those from macroscopic measurements is strongly indicative that the depth sensing test can be used in homogeneous and fine size multiphase materials, since a representative indentation area was analysed overall. The number of tests needed to attain a representative indentation area in multiphase materials is dependent on microstructural characteristics, such as phase distribution and grain size. Increasing the degree of chemical homogeneity of the composite by increasing the uniformity of the phase distribution and the fineness of the microstructure will decrease the size of the representative area and, therefore, the number of measurements needed. In the case of the WC-Co standard, with fine microstructure (G=1.9 μm, smaller than the diagonal of each indentation, ~8.4 μm, load=500 mN), the conditions of a representative area were clearly fulfilled and a good match with the

measurements made by the classical methods of mechanical characterization could be found.

Thus, it can be concluded that the applied method of depth-sensing indentation for the calculation of mechanical properties by depth-sensitive equipment, allows different mechanical characteristics used in material science/mechanical engineering to be evaluated with precision.

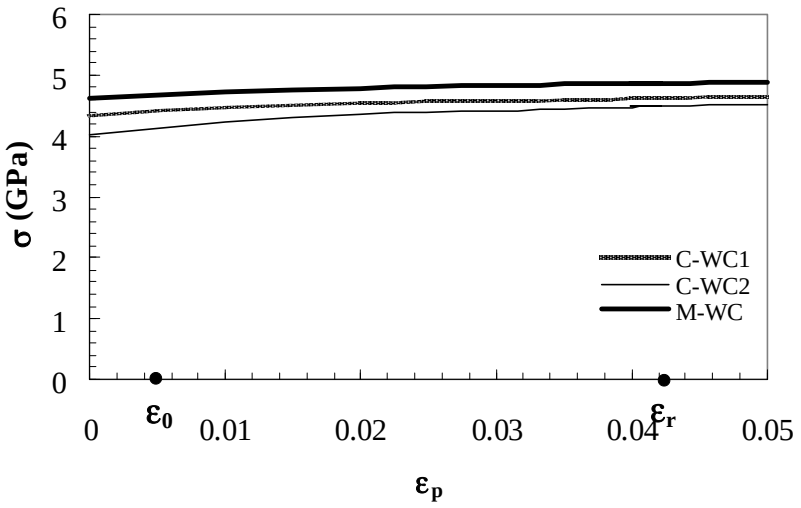

Fig. 5 – Stress-plastic strain curves obtained in the reverse analysis showing the representative plastic strain value (ε_r) and the constant value (ε_0).

3.3. Mechanical characterization

The mechanical characterization was carried out using depth-sensing indentation and Palmqvist toughness tests. Comparing the mechanical properties of the samples prepared by sputter-deposition (C-WC) and conventional wet milling (M-WC), (Table 4), with the correspondent properties of a WC-Co standard sample with equivalent amounts of binder (Table 3), the general trend points to lower values of hardness, *H*, Young's modulus, *E*, and yield strength, σ_y, of the sputter-deposited samples (C-WC). On the other hand, M-WC has only slightly different property values compared to the standard sample, due to similar microstructures but associated with the slight difference in mechanical properties between Ni rich binder and Co.

For the samples prepared from coated powders C-WC1 and C-WC2, the mechanical properties are almost unaffected by the variation of the composition (Table 1), reflecting identical microstructures; high uniformity in the binder distribution and similar relative densities and grain size distributions (Fig. 3a and b and Table 2). In fact, the microstructure of cemented carbide is characterized by various parameters; phase volume fraction of carbide and binder, homogeneity, grain size, and degree of contact between individual grains, i.e. contiguity [31]. The only difference in these parameters for C-WC1 and C-WC2 is the binder content (Ni amount). The property that could be most affected by this difference must be the Young's modulus, but for the samples under analysis, the divergent values are included within the experimental error.

Comparing the properties of the samples prepared from coated powders (C-WC) with those of the conventionally prepared one (M-WC), the most significant deviation is in the Young's modulus values, E, where the M-WC composite has the highest value, despite the fact that it contains the highest Ni and total binder content, Table 1. The difference attained cannot be included in Voigt-Reuss bounds [32], $E_{\text{Reuss}} - E_{\text{Voigt}}$ (calculated assuming the E value of Ni), as shown in Table 4. The differences between the values of C-WC and M-WC Young's modulus cannot be attributed directly to the lower grain size of M-WC, as for the light differences of the other properties evaluated. E is very sensitive to extrinsic factors such as binder distribution. The higher the grain size the lower the specific surface, thus binder distribution may not be so efficient. However, the contiguity values (Table 2) are similar in both cases and the sintered density is favourable to the C-WC samples, also showing a lower tendency for porosity content higher than 1.5%, which could significantly decrease the E values. A possible explanation for the difference observed in E values can be attributed to the chemical composition of WC grains. Diffusion of Ni to WC particles was observed during the high temperature vacuum brazing process (1020-1120ºC, 10^{-3} Pa) of NiCrBSi and WC-17 Co powders on a mild steel substrate [33]. The preparation of nickel-tungsten bimetallic carbides was investigated and the results pointed to the formation of bimetallic carbides, where Ni enters in the tungsten carbide lattice in a metallic state without forming bonds with carbon [34]. Due to the formation of this type of solid solution a decrease of the carbide Young's modulus proportional to the Ni content will be expected. Thus the solid solution effect of Ni in WC and its effect on the Young's modulus could not be ignored in the sintered WC and Ni. Reporting to our results, during

the powders' preparation stage or sintering process the Ni may diffuse more efficiently in coated powders than in traditional prepared ones, due to sputtering deposition conditions and to the nanocrystalline character of the Ni binder. Forthcoming studies will be performed in order to investigate the diffusion of sputtered Ni on WC surfaces. In addition, after sintering the Ni rich binder achieves a preferential orientation (200) that also contributes to a decrease in its Young's modulus bearing in mind the polycrystalline value.

Table 4.

Mechanical characteristics of WC-Ni/Fe/Cr samples.

Sample	Hardness (GPa)	E (GPa)	σ_y (GPa)	n	K_C * (MPa m$^{1/2}$)	E_{Reuss} - E_{Voigt} (GPa)
C-WC1	17.0 ± 0.4	519 ± 7	4.32	0.03	9.6 ± 0.3	581 - 638
C-WC2	16.5 ± 0.4	520 ± 9	4.07	0.05	9.8 ± 0.4	546 - 622
M-WC	17.8 ± 0.2	609 ± 5	4.62	0.02	11.0 ± 0.4	531 - 615

*Fracture toughness determined from measurements of the Palmqvist radial cracks.

Palmqvist toughness testing [22] was performed using the cracks that appeared at the corners of Vickers indentations (load = 98 N). This technique was successfully used because the contents of nickel are low. The values for the fracture toughness, K_C, (Table 4) are very close for the three samples, although a slightly higher value was evaluated for the conventional WC sample (M-WC) as a direct consequence of the grain size differences.

4. Conclusions

Using this method of depth-sensing indentation for the calculation of mechanical properties in compressive strength is an interesting alternative to the conventional methods of mechanical characterization for composite materials, as it enables several properties to be determined from a reduced size sample. The characteristics obtained for a standard WC-Co sample using this method are very close to the published results of macroscopic characterizations for the determined values of hardness, H, Young's modulus, E, and yield stress, σ_y.

The depth-sensing local characterization of sintered WC-Ni/Fe/Cr coated powders showed that lower values of E than those found in similar sintered conventional powders cannot be attributed to differences in grain size as for H and σ_y. The high binder uniformity

and the nanometer-sized coating achieved by the sputter-deposition process is not the principal cause for the lowest values of *E*. The decrease in *E* may have its origin in Ni diffusion into WC powders during the sputtering, which is enhanced during the sintering process. However, a preferential orientation could also have a role in *E* values, contributing to their decrease. It is suggested that lower amounts of ductile binder will be needed to obtain convenient ductile properties in the composites prepared from sputtered powders, than when a conventional mixing process is used.

Acknowledgements

The authors wish to thank Bsc Mariana Matos for the help in the sputter deposition, Prof. Valdemar Fernandes for the guidance of the depth-sensing indentation measurements and Dr. Filipe Oliveira for the assistance in HIP.

References

[1] Cornwall RG, German RM. Think bigger! The future is bright for MIM. Metal Powder Report 2004; 59 (11): 8-11.

[2] Viswanadham RK, Lindquist PG. Transformation-toughening in cemented carbides: Part I. Binder composition control. Metall Trans A 1987; 18A: 2163-73.

[3] Kakeshita T, Wayman CM. Martensitic transformations in cements with a metastable austenitic binder. Mater Sci Eng 1991; A141: 209-19.

[4] Uhrenius B. Phase diagrams as a tool for production and development of cemented carbides and steels. Powder Metall 1992; 35 (3): 203-210.

[5] González R, Echeberría J, Sánchez JM, Castro F. WC-(Fe, Ni, C) hardmetals with improved toughness through isothermal heat treatments. J Mater Sci 1995; 30 (13): 3435-9.

[6] Cooper R, Manktelow SA, Wong F, Collins LE. The sintering characteristics and properties of hard metal with Ni-Cr binders. Mater Sci Eng A 1988; A105-106: 269-73.

[7] Tracey VA. Nickel in hardmetals. Int J Refr Metals Hard Mater 1992; 11: 137-49.

[8] Raghunathan S, Caron R, Friederichs J, Sandell P. Tungsten carbide technologies. Adv Mater Process 1996; 4: 21-3.

[9] Lardner E. Review of current hardmetals technology. Hardmetal Technology 1970; 122-32.

[10] Taheri-Nassaj E, Mirhosseini SH. An in situ WC-Ni composite fabricated by the SHS method. J Mater Process Tech 2003; 142: 422-6.

[11] Kangwantrakool S, Shinohara K. New design of microstructure of WC-Co/TiC-Al_2O_3 composite materials by mechanical coating of particles. J Jap Soc Powder and Powder Metall 2002; 49 (12): 1070-5.

[12] Brookes KJ. Complex shapes and hard-coated powders get over limit factors. Metal Powder Report January 2005; 60 (1): 32-37.

[13] Castanho JM, Vieira MT, Fernandes CM, Senos AMR, Matos M. Coated WC powders by sputtered nanostructured Ni and stainless steel. Vacuum 2008. in press.

[14] Fernandes CM, Ferreira VM, Senos AMR, Vieira MT. Stainless steel coatings sputter-deposited on tungsten carbide powder particles. Surf Coat Technol 2003; 176 (1): 103-8.

[15] Fernandes CM, Senos AMR, Vieira MT. Sintering of tungsten carbide particles sputter-deposited with stainless steel. Int J Refr Metals Hard Mater 2003; 21: 147-54.

[16] Fernandes CM, Senos AMR, Vieira MT. Study of sintering variables of tungsten carbide particles sputter-deposited with stainless steel. Mater Sci Forum 2004; 455-456: 295-8.

[17] Fernandes CM, Senos AMR, Castanho JM, Vieira MT. Effect of the Ni chemical distribution on the reactivity and densification of WC-(Fe/Ni/Cr) composite powders. Mater Sci Forum 2006; 514-516: 633-7.

[18] Fernandes CM, Senos AMR, Vieira MT. Particle surface properties of stainless steel-coated tungsten carbide powders. Powder Technol 2006; 164: 124-9.

[19] Antunes JM, Fernandes JV, Menezes LF, Chaparro BM. A new approach for reverse analyses in depth-sensing indentation using numerical simulation. Acta Mater 2007: 55 (1): 69-87.

[20] Roebuck B, Bennett EG, Gee MG. Grain size measurement methods for WC/Co hardmetals. In: Bildstein H, Eck R, editors. Proc 13th Int Plansee Seminar, Metallwerk Plansee, Reutte; 1993, vol.2, p. 273.

[21] Golovchan VT, Litoshenko NV. On the contiguity of carbide phase in WC-Co hardmetals. Int J Refr Metals Hard Mater 2003; 21: 241-4.

[22] Ponton CB, Rawlings RD. Vickers indentation fracture toughness test, Part 1, review of literature and formulation of standardised indentation toughness equations. Mater Sci Technol 1989, 5: 865-72.

[23] Lin C, Kny E, Yuan G, Djuricic B. Microstructure and properties of ultrafine WC-0.6VC-10Co hardmetals densified by pressure-assisted critical liquid phase sintering. J Alloys Compounds 2004; 383: 98-102.

[24] Lisovskii AF, Vishneskii AS, Sirota KI. An investigation of sintered WC-Ni hard alloys with an uneven distribution of the binder metal. Powder Metallurgical Materials, Parts and Coatings 1977; 16 (5): 345-8.

[25] Brookes KJA. Hardmetals and other Hard Materials. 2nd ed. London: European Powder Metallurgy Association (EPMA), International Carbide Data, 1992.

[26] Newey D, Wilkins MA, Pollock HM. An ultra-low-load penetration hardness tester. J Phys E: Sci Instrum 1982; 15: 119-22.

[27] Oliver WC, Pharr GM. An improved technique for determining hardness and elastic modulus using load and displacement sensing indentation. J Mater Res 1992; 7 (6): 1564-83.

[28] Dao M, Chollacoop N, Van Vliet KJ, Venkatesh TA, Suresh S. Computational modelling of the forward and reverse problems in instrumented sharp indentation. Acta Mater 2001; 49 (19): 3899-918.

[29] Scussel HJ. Friction and wear of cemented carbides. ASM Handbook 1992, Vol. 18, ASM Int, p. 796.

[30] N. Ingelstrom, H. Nordberg. The fracture toughness of cemented tungsten carbides. Engineering Fracture Mechanisms 1974; 6: 597-607.

[31] Roebuck B, Bennett EG. Phase size distribution in WC-Co hardmetal. Metallography 1986; 19: 27-47.

[32] Hsieh CL, Tuan WH, Wu TT. Elastic behaviour of a model two-phase material. J Europ Ceramic Soc 2004; 24 (15-16): 3789-93.

[33] Lu S-P, Know O-Y. Microstructure and bonding strength of WC reinforced Ni-base alloy brazed composite coating. Surf Coat Technol 2002; 153: 40-8.

[34] Xiao T, Wang H, York APE, Williams VC, Green MLH. Preparation of nickel-tungsten bimetallic carbide catalysts. J Catal 2002; 209: 318-330.

*V.3. **C**omposites from **WC** **p**owders **s**putter-**d**eposited with **i**ron **r**ich **b**inders*

C. M. Fernandes[1], A. M .R. Senos[1], M. T. Vieira[2] and J. V. Fernandes[2]

[1]Department of Ceramics and Glass Engineering, CICECO, University of Aveiro, 3810-193 Aveiro, Portugal
[2]CEMUC, Mechanical Engineering Department, University of Coimbra, Rua Luís Reis Santos, Pinhal de Marrocos, 3030-788 Coimbra, Portugal

Submitted to Composites Part B: Engineering

Abstract

In the present work composite powders of WC and iron rich binder were prepared by an innovative approach, which consists in sputtering of a metallic binder on the tungsten carbide particles. The phase composition, microstructure and mechanical behaviour of WC coated powder composites with binder contents from 6 to 9 wt.% were characterized. η-phase is early formed during sintering and its effect on the mechanical behaviour was investigated and related to the microstructure and atomic structure. The results show that the presence of η-phase has not a hazardous role in toughness as is previewed in conventional cemented carbide. Despite the presence of η-phase, a good compromise between toughness and hardness was attained in composites prepared from iron rich binders sputtered on WC powders.

Keywords: Cemented carbide; Coated powders; Sputtering; Hardness; Toughness

1. Introduction

Hard metals are commonly manufactured with tungsten carbide (WC) and cobalt as metallic binder. Due to the unique mechanical properties of this composite it has not been easy to find a good substitute, in spite of the several studies with other transition metals in the neighbourhood of cobalt, as iron or nickel [1-6].

Fe-Cr-Ni-C alloys, as stainless steel, have been studied for cobalt substitution [7-11]. The binder was added to WC by an innovative way, which consists in sputtering austenitic stainless steel on the tungsten carbide particles. The coated powders have a good pressing behaviour, which allows the direct pressing without the need of the usual paraffin wax [7-11]. Moreover, the nanocristallinity of these coatings, together with the good distribution of the binder, increases the reactivity of the powders and consequently decreases the sintering temperature needed to attain dense specimens [9,12]. Nevertheless, binders enriched in iron induce the formation of a brittle η-carbide M_6C, which is generally considered an undesirable phase in tungsten carbide, as it is expected to markedly reduce the toughness, comparatively to cemented carbides free of this phase [13-15]. However, η-carbide was already mentioned in 1950's as a possible raw material to improve hardness in cemented carbide [16], but neither this potential advantage of η-phase was further explored, nor its negative effects in the mechanical properties have been determined and related to the phase composition and microstructure of the composites.

In this work, the feasibility of Fe/Ni/Cr based alloys as binders in cemented carbides and sputtering as an alternative to the conventional powder mixture will be investigated. For such purpose, the effect of binder composition and, consequently, of the η-phase content in the final mechanical properties will be evaluated in composites obtained from sputter coated powders and from a conventional mixture, used as standard.

2. Experimental

The starting powder is a fully carburized WC (H.C. Starck, HCST-Germany) with an average particle diameter of 9.06 ± 0.47 μm. Composite powders were prepared by coating the WC particles with the metallic binder, using a modified d.c. magnetron sputtering deposition chamber with deposition parameters reported elsewhere [7]. Two different targets were used; a stainless steel AISI 304 (SS) and a SS composed with a pathwork of Ni discs (in order to increase the sputtered Ni content of SS). A conventional mixture was also prepared with 1.5 wt.% of paraffin wax, the same WC powder and a SS powder (Goodfellow FE226010, maximum particle size of 45 μm) by wet milling, using isopropyl alcohol in a stainless steel mill with WC-Co balls, during 6 h. After mixing, the mixture was dried, deagglomerated and sieved.

Two coated powders have been prepared. The first one, coated with SS, was designated by C-WC1. After unidirectional pressing at 190 MPa, the compacts were vacuum sintered at a maximum temperature of 1350ºC and pressure of 20 Pa, for 1h. The compacts of the second powder, which was coated with SS enriched in Ni (C-WC2), were sintered at the same pressure and holding time, but at a higher temperature, 1500ºC. The compacts of the conventional mixture (M-WC) were also vacuum sintered at 1320ºC, during 3 h, at 20 Pa, and then hot isostatic pressed at 1400ºC, for 90 min, at 135 MPa, in order to reach almost full density. Between three to five sintered samples per composition were prepared. The chemical characterization of sintered specimens was carried out by energy dispersive spectroscopy (EDS, detector Rontec-EDR288/SPU2) and electron microprobe analysis (EPMA-SX50, Cameca) was complementary used. The final carbon content of sintered specimens was evaluated by an automatic direct combustion (LECO CS 200 IH). The density was determined by the Archimedes' method, using ethilenoglycol.

The phase identification was performed by X-ray diffraction (XRD, Rigaku PMG-VH) and the average size of η-phase crystallites, D_C, was estimated from the Scherrer equation, $D_C = K\lambda / (\beta \cos\theta)$, where λ represents the X-ray wavelength, θ the Bragg angle, β the peak width at half-maximum corrected for instrumental broadening, and K = 0.9. The phase quantification results from the Rietveld analysis of XRD spectra with the aid of the GSAS suite [17]. The WC and η-phase quantification was performed with the structure

parameters available in the bibliography for the hexagonal WC crystalline phase [18] and the cubic η-phase Fe_3W_3C [19] and neglecting the other minor phases.

The microstructure characterization was performed with scanning electron microscopy (SEM, Hitachi-S4100) on polished and chemically etched surfaces with Murakami's reagent (a solution of potassium ferricyanide (10g) and sodium hydroxide (10g) in distilled water (100ml)). The WC average grain size was measured using the linear intercept method [20] on the micrographs and at least 300 intercepts per sample were used. The Fullman relation was applied to transform the two-dimensional mean intercept in a three-dimensional mean grain size, G [21].

The composites were mechanically characterized using depth-sensing indentation equipment (Fischerscope H100) [22-24]. In order to have representative average values for the evaluated properties, 100 tests were performed in each sample. In testing, the load is increased in steps until a nominal load of 500 mN is reached. The number of steps used for loading and unloading was 60 and the time between steps was 0.5 s. The first load step is always equal to 0.4 mN; for subsequent steps, the value of the load increment between two consecutive steps, $\Delta P_i = P_i - P_{i-1}$, is such that $\sqrt{P_i} - \sqrt{P_{i-1}}$ is constant. Two creep periods of 30 s were performed during the tests: at maximum load and at the lowest load during unloading (0.4 mN). The values of the 100 tests made in each sample were used for the direct determination of the hardness, *H*, and calculation of the Young's modulus, *E*, and of the yield stress, σ_y, using a reverse analysis approach [25]. For comparison with previously reported results, hardness measurements (HV30) were also made using a Vickers diamond indentor (293 N load). An average of ten measurements from randomly selected areas of the sample was taken as the average hardness value of the sample. The fracture toughness, K_C, was also determined from the measurements of the Palmqvist radial cracks at the corners of Vickers hardness indentations (load, 98 N), using the formula [26]:

$$K_c = 0.087 \sqrt{HW} \quad (1)$$

where $W = P/L_T$, P is the applied load and L_T the total length of cracks. The total crack length formed on the four corners of the diamond indent was measured using an optical microscope (Zeiss, Jenaphot 2000) at 400× magnification. The average of ten indentation values was used for calculation.

3. Results and Discussion

3.1 Chemical composition, Atomic structure and Microstructure

The chemical composition of the sintered composites, concerning Fe, Ni, Cr and C, was evaluated by EPMA and Leco and is presented in Table 1. The composites of C-WC1 powder have a binder composition similar to SS and a total binder amount of ~6 wt.% (Table 1), assuming for the total binder amount the addition of Fe, Ni and Cr contents, the main constituents of the binder phase and neglecting other minor elements, such as Mn, Si, P, S and C (representing approximately 2 wt.% of the SS composition). The composites of C-WC2 powder possess higher binder amount (~9 wt.%) and Ni content (~7 times superior to C-WC1). Another composites from coated powders (C-WC3) were also considered, in spite of their microstructure and mechanical properties had been already reported elsewhere [10]. C-WC3 composites have the same binder amount than C-WC1 (~6 wt.%), but a much higher Ni content, Table 1. The variation of the ratio between the elements with and without affinity to carbon in the binder composition of hard metal was proved to strongly limit the final phases [11]. Therefore, in the present study, the suitable variation of the ratio Ni/(Fe+Cr), from 0.1 until 2.5, Table 1, was used to obtain differences in the composite phase structure, namely in what concerns the percentage of η-phase. Samples of conventional powder mixture, with ~12 wt.% of SS (Table 1) were also investigated.

Table 1

Final binder elements and carbon contents.

Sample	Fe[a] (wt.%)	Ni[a] (wt.%)	Cr[a] (wt.%)	Total (wt.%)	C[b] (wt.%)	$\frac{Ni}{Fe + Cr}$
C-WC1	4.3	0.6	1.0	5.9	5.09	0.1
C-WC2	3.9	4.4	1.0	9.3	5.27	0.9
C-WC3	1.3	4.3	0.4	6.0	5.40	2.5
M-WC	7.8	2.0	2.5	12.3	___	0.2

[a]EPMA [b]LECO analysis

The reactive sintering of the WC powders coated with SS was already systematically investigated [9,12], highlighting the higher sinterability and reactivity of the coated powders when compared with conventional mixed ones. The higher sinterability enables the achievement of near full densification in coated powders vacuum sintered, ensuring that weight losses are controlled [12]. Therefore, C-WC1 reached ~99% of relative density at 1350ºC, 1h, whereas an equivalent densification was also attained for C-WC2, at a higher temperature of 1500 ºC. The increase of Ni in the binder composition of C-WC2 obliges to increase the sintering temperature, related to the highest eutectic temperature and to the reported lower solubility of W/C in Ni rich binders [27]. After sintering, the conventional powder mixture reached only a relative density of 90% during vacuum sintering and it was requested to be subsequently hot isostatic pressed for further densification. This was also the case of the C-WC3 compacts, due to the high Ni percentage in the binder [10].

The XRD spectra of the C-WC1, C-WC2 and M-WC sintered samples, Fig. 1, show three different phases: WC, η-phase (M_6C) and an austenite enriched in Cr and Ni. A vestigial ferrite phase is yet detectable for C-WC1 and M-WC samples, Table 2, which is not visible in the low magnification spectra of Fig. 1. Both austenite and ferrite phases are present in very small amounts in these compacts, due to the significant η-phase formation during sintering [10]. Therefore, in the quantification of the η-phase amount by the Reitveld method [17], they could be neglected. The C-WC3 composite does not present η-phase, only WC and metallic phase (Me) were detected [10].

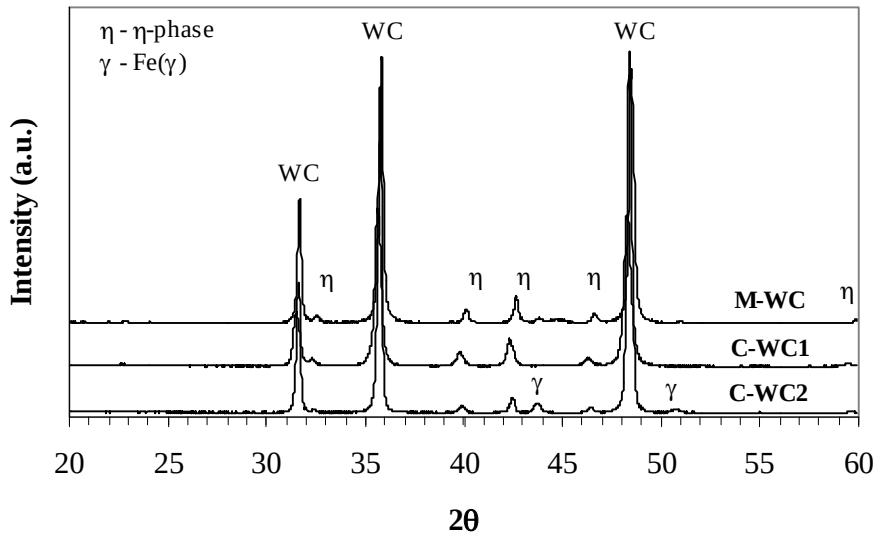

Fig. 1. XRD diffraction profiles of C-WC1, C-WC2 and M-WC samples.

The results of the η-phase quantification are presented in Table 2. The C-WC1 composite has the highest amount, 17 wt.%, which is significantly reduced for C-WC2, 5 wt.%, and not detectable for C-WC3 (Table 2). This decrease of η-phase, relatively to C-WC1, is related, as previously refereed, to the increase of the Ni/(Fe+Cr) ratio in the binder composition [11]. This increase displaces and enlarges the favourable region of WC+Me to carbon amounts close to the WC stoichiometric carbon [28]. Although some decarburization has occurred during sintering, (as it is highlighted by the final carbon content of C-WC1 (Table 1), that is smaller than the estimated one (5.7 wt.%), assuming only the WC and binder phases) the C-WC3 sample has a high enough Ni/(Fe+Cr) ratio to place the final composition in the WC+Me region. M-WC also presents ~12 wt.% of η-phase (Table 2). In spite of the low SS binder amount in C-WC1, the M_6C content is higher than in M-WC due to the increased reactivity of coated powders, comparatively with conventional mixed powders [9,11]. For this reason, the influence of comparable η-phase contents on the final mechanical properties could not be achieved with similar binder content in coated powders and conventional mixtures.

Table 2

XRD data of sintered powders.

Sample	$\frac{\eta}{\eta + WC}$ **(wt.%)**	**fcc (γ)**	**bcc (α)**	D_C^{a} **(nm)**
C-WC1	17	vestigial (+)	vestigial	26
C-WC2	5	small (++)	not detected	__
C-WC3	0	~6 wt.%	not detected	__
M-WC	12	vestigial (+)	vestigial	40

[a]average size of η-phase crystallites

The microstructure of C-WC1 sintered sample is presented in Fig. 2(a), where, after a short etching with Murakami's, two different phases are distinguished. The major gray phase is attributed to WC and the other phase is mainly η-phase. However, a darker gray colour is observed around the contours of WC grains, which may correspond to the binder phase. The η-phase seems well adapted to the WC grains because the vestigial binder phase, that is viscous at sintering temperatures, spreads between WC and η-phase. This observation was already reported by Jia et al. [29] that also detected a binder film between

WC and η grains in the three-phase region of WC-Co system. A preliminary EDS analysis was performed in the points indicated in Fig. 2(a) and is listed in Table 3. The elements detected and the atomic content confirm the presence of the $(M,W)_6C$ phase with a stoichiometry $(Fe_{2.3}Ni_{0.3})(Cr_{0.6}W_{2.8})C$. The chemical composition of this phase was also confirmed by EPMA and remains constant, within the experimental error, for different sintering temperatures and SS binder contents, as already reported [11].

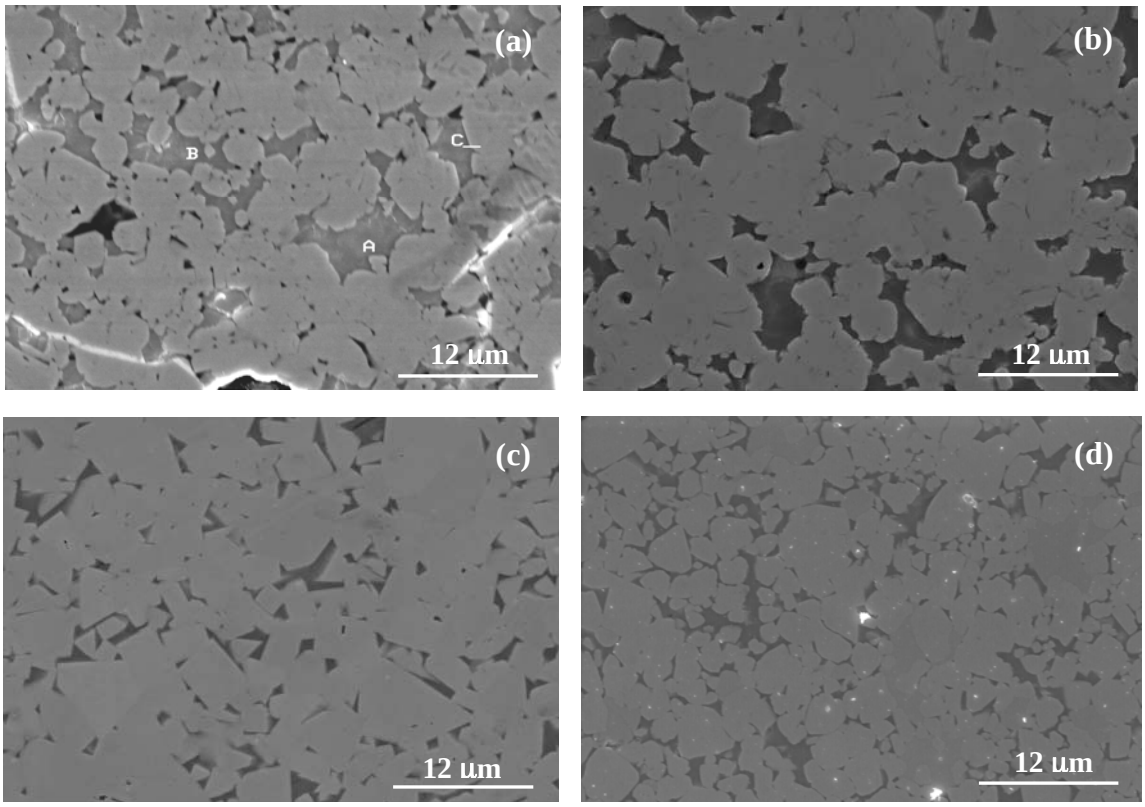

Fig. 2. SEM micrographs of (a) C-WC1; (b) C-WC2; (c) C-WC3 and (d) M-WC samples.

The microstructure of the sample C-WC2 is presented in Fig. 2(b). Among the WC grains the two secondary phases can be distinguished: a darker phase surrounding the WC grains (binder phase) and whiter areas (η-phase). For comparison, the microstructure without η-phase (C-WC3) is also shown in Fig. 2(c), where it can be observed that the WC grain morphology is quite different from the others (C-WC1 and C-WC2): rounded for C-WC1 and C-WC2 and angular for the enriched Ni binder composite (C-WC3). Several authors [30,31] have already reported that the growth rate and the morphology of the WC interfaces change with the binder composition. Accordingly, the WC grains appear slightly

rounded when the binder is enriched in W. The solubility of W in Ni and Fe at 1350 ºC was reported to be 5 and 9 wt.%, respectively [27]. Therefore, rounded WC grains are expected for iron rich binders, as in C-WC1 and C-WC2. The microstructure of M-WC is similar to C-WC1 and C-WC2 (Fig. 2(d)). The average grain size, presented in Table 4, is similar for the different composites showing a slight trend to increase for the Ni enriched compositions that were sintered at higher temperatures.

Table 3

EDS analysis performed on C-WC 1 sample (atomic percentages).

Point	W	Fe	Cr	Ni
A	43.0	40.1	10.6	6.3
B	44.6	39.1	11.0	5.3
C	49.2	35.7	9.7	5.4

The X-ray maps of elements are shown in Fig. 3, for the C-WC1 composite. Fe and Cr are concentrated around the WC grains, in the regions correspondent to the η-phase and to the vestigial Me phase. Ni is present in lower quantity than Fe and Cr (see Table 1) and seems to be well dispersed either in the secondary phases or in the WC matrix grains (the solubilization of some Ni in the WC grains was already suggested in relation with the mechanical properties, in a previous work [10]). Moreover, the W X-ray map shows a marked reduction of intensity in the $(M,W)_6$ regions, where taking the EDS/EPMA analysis, Table 3, a significant fraction of this element must be present. This effect suggests that the η-phase must be finely divided to give a weaker signal for W, than the presumed one. The average size of η-phase crystallites, D_C, estimated from the Scherrer equation, is very small for the sample C-WC1, ~26 nm, comparatively with the sample M-WC with ~40 nm (Table 2), a value near of the measurable limits. The D_C value of C-WC2 can not be properly calculated due to the small peak intensity of η-phase.

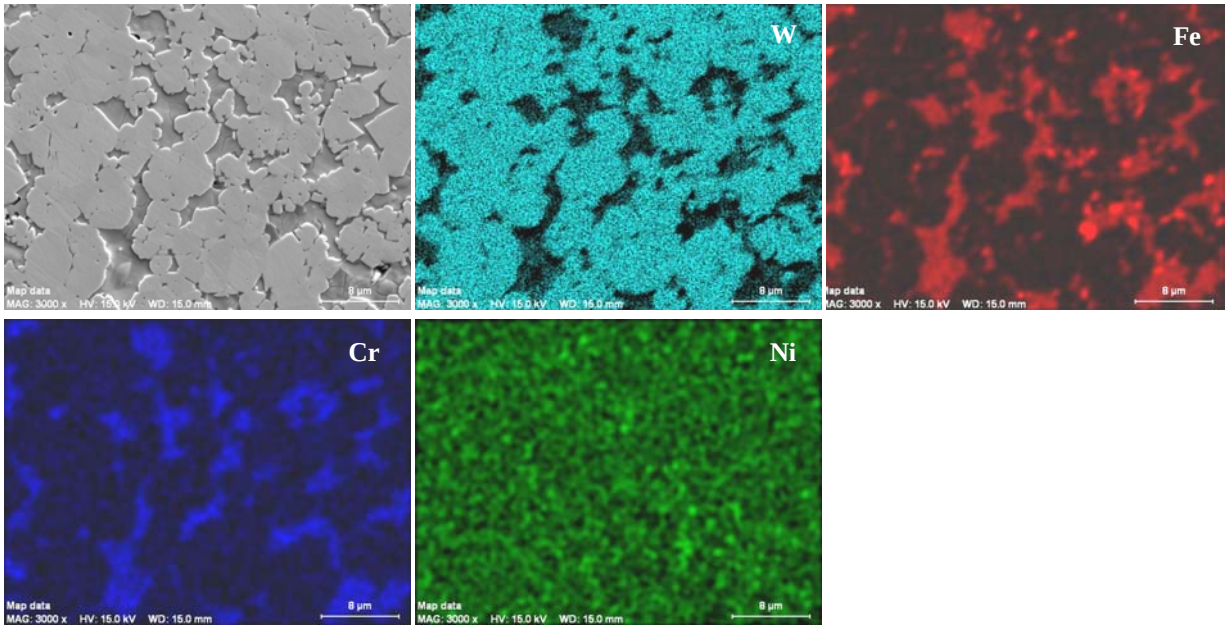

Fig. 3. SEM-SE micrograph of C-WC1 sample and respective X-ray maps of elements.

3.2. Mechanical Characterization

The mechanical characteristics of the composites are presented in Table 4. The Young's modulus, *E*, follows the expected trend, decreasing with the increase of the binder content for all the tested samples. The yield strength, σ_y, is lower for the samples with higher Ni content, C-WC2 and C-WC3. As previously reported [10], enhanced Ni diffusion to WC in sputtered powders can be responsible for the observed decrease of the mechanical properties.

Table 4.

Physical and mechanical characteristics of composites prepared from coated powders and conventional mixture.

Samples	Density (g cm^{-3})	$\bar{G}$ (μm)	*E* (GPa)	σ_y (GPa)	*H* (GPa)	HV30	K_C * (MPa m$^{1/2}$)
C-WC1	14.0	3.0	545 ± 6	6.07	21.3 ± 0.4	1840 ± 70	9.7 ± 1.1
C-WC2	13.5	3.5	495 ± 11	4.07	15.0 ± 0.5	1400 ± 80	12.8 ± 1.2
C-WC3	14.8	4.3	520 ± 9	4.01	16.5 ± 0.4	1570 ± 90	9.8 ± 0.4
M-WC	12.8	3.0	___	___	___	1330 ± 50	12.5 ± 1.8

*Fracture toughness determined from measurements of the Palmqvist radial cracks.

The hardness determined by depth-sensing, *H*, (Table 4) shows decreasing values with the increase of the binder and Ni amount in the composition, Table 1. Therefore, the lowest value is observed for C-WC2 with simultaneously high Ni, 4.4 wt.%, and binder amount, 9.3 wt.%. The values of HV30, Table 4, are not comparable with those of *H*, due to the very different testing loads (see the experimental section) but the same trend is observed. Toughness measurements show higher values related to increasing binder amounts (Table 4). The values for C-WC2 and M-WC are similar, within the experimental error, although the conventionally prepared sample, M-WC, possesses a larger binder percentage, without presenting significant difference on the average WC grain size, Table 4.

In figures 4(a) and (b) the representation of fracture toughness, K_C, vs HV30 was chosen to further analyse the effect of the composition and processing conditions on the mechanical behaviour of the tungsten carbide composites here developed and to compare the measured values with results for WC-Co and WC-SS composites, reported in the bibliography [32,33] and compiled in Table 5. In Fig. 4(a) three groups of cemented carbide, within medium/coarse range, were distinguished: WC-Co composites (from 6 until 15 wt.% Co) with the lowest values of K_C for the same hardness [32]; WC-SS composites from the bibliography [33] together with M-WC, all conventionally prepared, with intermediate values of K_C for equivalent hardness; finally, the results for composites from coated powders, presenting the highest relation between K_C and HV30, were grouped, despite the differences in their binder compositions. The decrease of K_C with hardness was foreseeable for the three groups of composites: the harder a material more brittle it is. However, the relation between hardness and toughness is higher for the composites with SS binder when compared with the ones with Co, all using conventionally prepared powders. Therefore, in terms of the considered properties, the already reported advantages of SS for Co substitution [33,34], is here reinforced. It may also be noted that the point correspondent to M-WC support very well those from literature, despite the fact that this composite possesses a very significant amount of η-phase, ~12 wt.%, whereas those from literature are reported to be free of η-phase [33]. Moreover, the composites from coated powders show yet higher values of K_C for the same hardness, when compared with the conventionally prepared composites, in Fig. 4-a). A higher uniformity of the binder distribution was already shown to persist, even after sintering, in the composites from coated powders [10]. Additionally, the smaller crystallite size of the second phases formed

from the sputtered binder during sintering, Table 2, contributes also for the higher toughness. The grain size should be reduced to a range of submicron size to attain K_C and HV30 values similar to C-WC1 in WC/Co cemented carbides, as shown in Fig. 4(b).

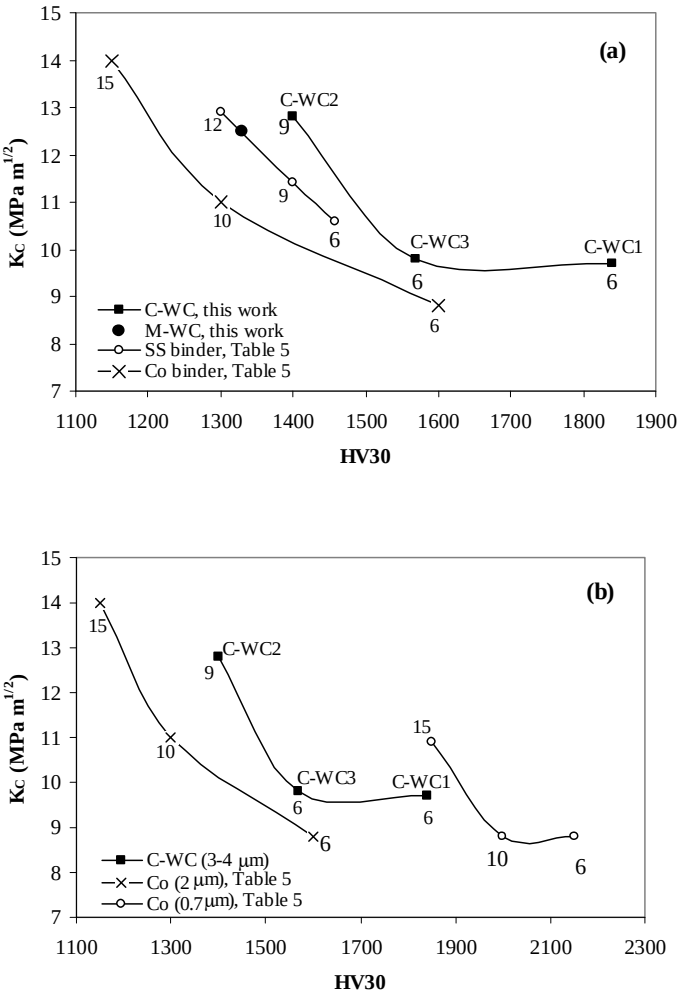

Fig. 4. Variation of K_c with Vickers hardness for hardmetals with different binder compositions (the numbers indicate the binder amount (wt.%)): **(a)** effect of composition and processing method for medium/coarse grain sizes ($\overline{G}$>2 μm); **(b)** effect of composition and grain size.

Regarding the effect of the η-phase on the reported mechanical properties of the coated powders, the reduction of the M_6C phase from ~17 wt.% in C-WC1 to non detectable values (<2 wt.%) in C-WC3, with the total binder content constant, had a clear reduction of hardness without any benefit of toughness, Fig. 4(a) and Table 2. Some authors [34,35] have already stated that η-phase enhances hardness and abrasion resistance in WC composites with ultrafine grains. In fact, the binder phase of C-WC1 sample is vestigial, so

the most representative region is WC+M_6C phases, which could explain the high hardness. Furthermore, a high toughness (K_C) was attained in the C-WC2 composite, although it was estimated to have ~5 wt.% of η-phase. However, the toughness was expected to degrade with the substitution of the ductile binder phase by the brittle η-phase [14,15], but this effect was not here observed. Phase composition and microstructure suggested that the studied composites have different contributions, resulting from the presence of the previous coating on powders, such as: (i) spreading of the ductile binder phase into the WC and M_6C junctions, Fig. 2, due to its good wettability at the sintering temperatures, and favoured by the high uniform distribution in the coated powders; (ii) the nanocrystalline size of η-phase, Table 2, and the fine dispersion of the η-phase, Fig. 3. These aspects need, however, further investigation to be confirmed, namely using TEM analysis in forthcoming studies.

Table 5.

Literature results for WC composites using stainless steel (SS) and cobalt (Co) binders.

Binder (wt.%)	$\bar{G}$ **(μm)**	**HV30**	K_C **(MPa m$^{1/2}$)**	**Ref.**
6 Co	2.2	1600	8.8	[32]
10 Co	2.2	1300	11	[32]
15 Co	2.2	1150	14	[32]
6 Co	0.7	2150	8.8	[32]
10 Co	0.7	2000	8.8	[32]
15 Co	0.7	1850	10.9	[32]
6 SS	4.1	1458	10.6	[33]
9 SS	4.5	1398	11.4	[33]
12 SS	5.1	1300	12.9	[33]

Therefore, the WC coated powders with iron-rich binders are interesting to prepare cemented carbide that requires high hardness, using small amounts of coating binder. Besides, the relative high cost of the coated powders production can be balanced with the manufacturing cost reduction, coming from the elimination of the milling and dewaxed steps and the decreasing of sintering temperatures, without the need of HIP to obtain complete dense compacts. The use of coarse grain sizes is also an economical benefit, since equivalent properties to the ultrafines ones were obtained, reducing the milling time and energy.

Conclusions

The composites of WC powders coated by sputtering with SS or Ni enriched SS binders show a good compromise between toughness and hardness, better than composites of similar composition and grain size, conventionally prepared.

The η-phase formed in these composites increases the hardness without loss of toughness, which was attributed to specific microstructural and structural characteristics, as the spreading of the ductile binder phase in the WC/η-phase junctions and the nanocrystalline structure and fine dispersion of the formed η-phase.

SS binders are promising substitutes for Co, taking into account the relation between toughness and hardness. Superior values for these properties were found mainly in composites prepared from coating powders with nanocristalline iron enriched coatings, making these composites attractive for applications where high hardness and moderate toughness are the targets.

Acknowledgements

The authors wish to thank Bsc A.M. Jesus for the help in the toughness measurements.

References

[1] Viswanadham RK, Lindquist PG. Transformation-toughening in cemented carbides: Part I. Binder composition control. Metall Trans A 1987; 18A: 2163-73.

[2] Kakeshita T, Wayman CM. Martensitic transformations in cements with a metastable austenitic binder. Mater Sci Eng 1991; A141 209-19.

[3] Uhrenius B. Phase diagrams as a tool for production and development of cemented carbides and steels. Powder Metall 1992; 35 (3): 203-210.

[4] González R, Echeberría J, Sánchez JM, Castro F. WC-(Fe, Ni, C) hardmetals with improved toughness through isothermal heat treatments. J Mater Sci 1995; 30 (13): 3435-9.

[5] Cooper R, Manktelow SA, Wong F, Collins LE. The sintering characteristics and properties of hard metal with Ni-Cr binders. Mater Sci Eng A 1988; A105-106: 269-73.

[6] Tracey VA. Nickel in hardmetals. Int J Refr Metals Hard Mater 1992; 11: 137-49.

[7] Fernandes CM, Ferreira VM, Senos AMR, Vieira MT. Stainless steel coatings sputter-deposited on tungsten carbide powder particles. Surf Coat Technol 2003; 176 (1): 103-8.

[8] Fernandes CM, Senos AMR, Vieira MT. Particle surface properties of stainless steel-coated tungsten carbide powders. Powder Technol 2006; 164: 124-9.

[9] Fernandes CM, Senos AMR, Vieira MT. Sintering of tungsten carbide particles sputter-deposited with stainless steel. Int J Refr Metals Hard Mater 2003; 21: 147-54.

[10] Fernandes CM, Senos AMR, Vieira MT, Antunes JM. Mechanical characterization of composites prepared from WC powders coated with Ni rich binders. Int. J. Refract. Met. Hard Mat. 2008; in press.

[11] Fernandes CM, Senos AMR, Vieira MT. Control of eta carbide formation in tungsten carbide powders sputter-coated with (Fe/Ni/Cr). Int. J. Refract. Met. Hard Mat. 2007; 25: 310-7.

[12] Fernandes CM, Senos AMR, Vieira MT. Study of sintering variables of tungsten carbide particles sputter-deposited with stainless steel. Mater Sci Forum 2004; 455-456: 295-8.

[13] Miodownik AP. Means of predicting structure and performance of new materials. Powder Metallurgy 1989; 32 (4): 269-76.

[14] Moskowitz D, Ford MJ, Humenik M. High-strength tungsten carbides. Modern Developments in Powder Metallurgy 1970; 5: 225-234.

[15] Moskowitz D, Ford MJ, Humenik M.. High-strength tungsten carbides. International Journal of Powder Metallurgy 1970; 6 (4): 55-64.

[16] Goldschmidt HJ. The structure of carbides in alloy steels Part II – carbide formation in high-speed steels. Journal of the Iron and Steel Institute 1952; 170: 189-204.

[17] Larson AC, Von Dreele RB LAUR 86-748 Report, General Structure Analysis System. Los Alamos National Laboratory; 1990.

[18] Leiciejewicz J. A note on the structure of tungsten carbide. Acta Cryst 1961; 14: 200.

[19] Yang Q, Andersson S. Application of coincidence site lattices for crystal structure description. Part I: Σ=3. Acta Cryst 1987; B43: 1-14.

[20] Antunes JM, Menezes LF, Fernandes JV. Ultra-microhardness testing procedure with Vickers indenter. Surf. Coat. Technol. 2002; 149 (1): 27-35.

[21] Roebuck B. Bennett EG, Gee MG. Grain size measurement methods for WC/Co hardmetals. In: H Bildstein, R Eck, editors. Proc 13th Int Plansee Seminar, Metallwerk Plansee, Reutte, vol.2, (1993) 273.

[22] Newey D, Wilkins MA, Pollock HM. An ultra-low-load penetration hardness tester. J Phys E: Sci Instrum 1982; 15: 119-22.

[23] Loubet JL, Georges JM, Meille G. Vickers indentation curves of elastoplastic materials, in: P.J. Blau, B.R. Lawn (Eds.), Microindentation Techniques in Materials Science and Engineering, ASTM STP 889, American Society for Testing and Materials, Philadelphia, PA, 1986, 72.

[24] Oliver WC, Pharr GM. An improved technique for determining hardness and elastic modulus using load and displacement sensing indentation. J Mater Res 1992; 7 (6): 1564-83.

[25] Antunes JM, Fernandes JV, Menezes LF, Chaparro BM. A new approach for reverse analyses in depth-sensing indentation using numerical simulation. Acta Mater 2007; 55 (1): 69-81.

[26] Ponton CB, Rawlings RD. Vickers indentation fracture toughness test, Part 1, review of literature and formulation of standardised indentation toughness equations. Mater Sci Technol 1989; 5: 865-72.

[27] Uhrenius B, Forsen K, Haglund BO, Andersson I. Phase-equilibria and phase-diagrams in carbide systems. Journal of Phase Equilibria 1995; 16 (5): 430-440.

[28] Guillermet AF. An assessment of the Fe-Ni-W-C phase diagram. Metallkund 1987; 78 (3): 165-171.

[29] Jia K, Fisher TE, Gallois B. Microstructure, Hardness and Toughness of nanostructured and conventional WC-Co composites. Nanostructured Materials 1998; 10 (5): 875-891.

[30] Chabretou V, Allibert CH, Missiaen JM. Quantitative analysis of the effect of the binder phase composition on grain growth in WC-Co sintered materials. Journal of Materials Science 2003; 38: 2581-90.

[31] Wang Y, Heusch M, Lay S, Allibert CH. Microstructure evolution in the cemented carbides WC-Co I. effect of the C/W ratio on the morphology and defects of the WC grains. Phys Stat Sol (a) 2002; 193 (2): 271-283.

[32] . Chermant JL, Osterstock F. Fracture toughness and fracture of WC-Co composites. Journal of Materials Science 1976; 11: 1939-51.

[33] Farooq T, Davies TJ. Tungsten Carbide hard metals cemented with ferroalloys. The International Journal of Powder Metallurgy, 1991; 27 (4): 347-55.

[34] Upadhyaya GS, Bhaumik SK. Sintering of submicron WC-10%Co hard metals containing nickel and iron. Materials Science and Engineering 1988; A105-106: 249-256.

[35] Bergström M. The eta-carbides in the quaternary system Fe-W-C-Cr at 1250ºC. Materials Science and Engineering 1977; 27: 271-86.

Chapter

VI

Final Conclusions

Powder Characterization

The sputtering technique is an innovative way to change the particle surface properties and to add a very uniform layer of sputtered elements on the surface of WC particles. Particles coated with thin films of controlled composition and thickness can be achieved by the developed sputtering technique. The sputtered coating brings relevant chemical and physical powder surface modifications, such as different chemical nature and structure, high roughness and nanometric grain size, inducing particular changes in the particle properties.

The coated powders showed a slightly higher resistance to oxidation in air atmosphere, in comparison to the uncoated WC powder, and the resistance increased with the coating thickness. The behavior of coated powders in aqueous suspensions is dominated by the coating layer until pH≈8, whereas, for higher values of pH, the coating adhesion is strongly reduced, and, consequently, the surface charge approaches that of the WC particles. Therefore, in the aqueous processing of stainless steel-coated WC acid-neutral pH values should be chosen.

The flowability of the coated powders is more dependent on the chemical composition rather than the morphology of the thin films. Nickel coatings deposited on WC powders do not improve the flowability, whereas the coating with stainless steel enhances it very significantly, by decreasing the powder internal friction.

The pressing of WC sputter-coated powder can be directly performed, without the need of pressing binder, commonly used in the WC based cemented carbides to reach an adequate resistance to handling. This feature is interesting from a technological point of view, since two stages of the conventional WC based cemented carbides processing, namely milling and dewaxing, can be excluded.

Sintering & Reactivity

The binder addition by this sputtering technique reveals to be very efficient in the promotion of the densification, which may be attributed to the high degree of uniformity in the binder distribution and to the high reactivity of the binder phase attained by this coating powder process. Additionally, the stainless steel binder forms a viscous phase during sintering that wets very well the matrix grains.

The volatilisation of binder components, together with the formation of eta-phase during sintering, are the main factors responsible for some limitation in the attained densification in coated powders. However, by an adequate control of the sintering variables, such as the sintering cycle and sintering pressure, it is possible to obtain, from sputter-deposited powders, sintered compacts with controlled stoichiometric deviations, together with high densities at relatively low temperatures. Comparatively, the admixed powders show a generally poor sinterability.

The formation of η-phase in powders of WC sputter-coated with stainless steel AISI 304 starts ~750 ºC by a solid state reaction with the growth process controlled by diffusion. The η-phase structure accommodates the main binder elements (Fe, Ni, Cr) and can be represented approximately as $(Fe_{2.3}Ni_{0.3})(Cr_{0.6}W_{2.8})C$ ($(M,W)_6C$).

The amount of η-phase is higher in coated than in the admixed powders with similar chemical composition and the same processing conditions, due to the increased contact area between the WC and the binder phases and to the reduced diffusion distances in the coated powders. In both cases, the amount of η-phase can be reduced by increasing the Ni/(Fe+Cr) ratio or, even, eliminated with an additional excess of carbon.

Mechanical Characterization

The mechanical properties obtained in composites of WC with sputter-deposited iron rich binders show a very good compromise between toughness and hardness. Furthermore, the presence of η-phase, usually formed with iron rich binders, increased the hardness of the composites, without degradation of the respective toughness. The specific microstructural and structural characteristics of the η-phase formed in coated powders, like nanocrystallinity and fine dispersion, may be responsible for this behaviour.

The increase of the binder nickel content brings a strong decrease in the Young's modulus, *E*, not presumed in the theoretical relations and larger than has been found in composites from conventional powders. This difference can not be attributed to differences in grain size or contiguity, but was supposed to come from the diffusion of Ni into WC in sputtering, which is enhanced during the sintering process. It is suggested that lower amounts of ductile binder will be needed to obtain convenient ductile properties in the composites prepared from sputtered powders, than when a conventional mixing process is used.

The comparison of the mechanical properties of composites prepared from sputter-coated powders with those from conventionally prepared of similar composition and grain size evidences that, for the same hardness, higher toughness values are obtained for the coated powder processing. On the other hand, the iron rich binder composites show superior values of hardness and toughness than those of Co binder composites, found in literature, even when a conventional preparation is used. These results show that the sputtering is effectively a very promising technique as an alternative to the mixing of powders, leading to benefits either in processing, or in the technological properties. Fe/Cr/Ni binders, such as stainless steel, are good substitutes to Co in WC based composites, giving superior values of hardness versus toughness. Composites with low amounts of stainless steel binders prepared by sputtering are especially interesting to applications requiring a very high hardness.